Aegir Satellite Network

Designing a BiSAR Satellite Network for Maritime Monitoring of the North Sea

T. Buijs	1506811	T.D. van den Oever	4145704
D. Ju	4115295	D. Petković	4162722
N.M. de Kogel	4031512	B.T. van Putten	4091000
S.P. van der Linden	4082346	C.W.M. Verhoeven	4038452
A. Melaika	4048210		

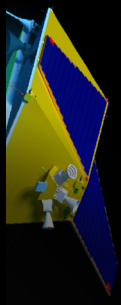

Final Report

Design Synthesis Excercise

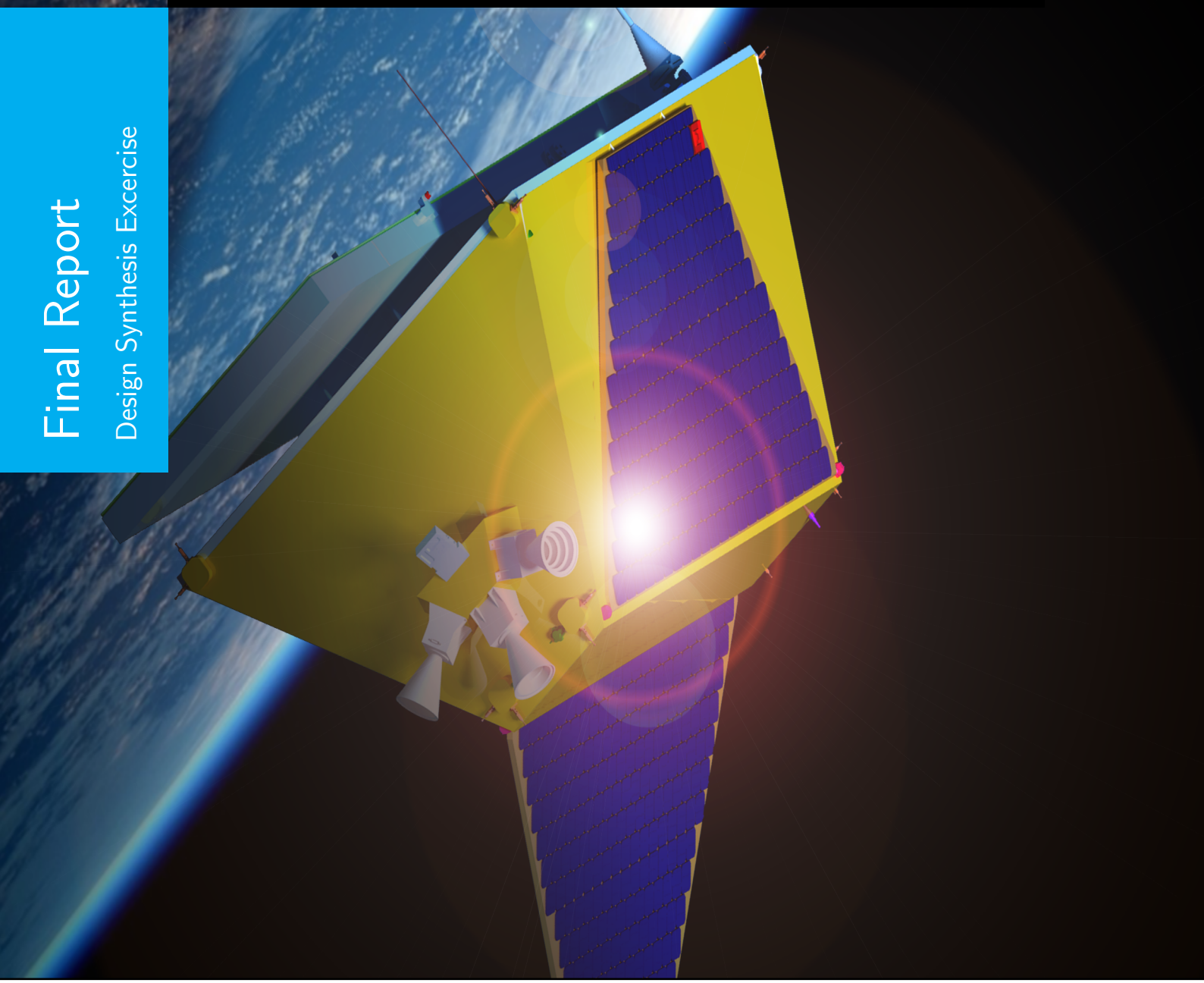

TU Delft Delft University of Technology

Aerospace Engineering

July 1, 2014

Preface

This report is part of the Design Synthesis Exercise, a project organised twice a year by the Faculty of Aerospace Engineering at the Delft University of Technology in the Netherlands. The aim of this exercise is to apply all the knowledge gained from three years of the Aerospace Engineering bachelor programme and design a complete aerospace product with a group of nine people. The detailed design will be presented to the customer during the final review.

The editors of this report, DSE group 19 'Aegir', are designing a satellite constellation to monitor the North Sea traffic for the Dutch company SSBV. This report has been written in order to inform SSBV and other interested parties about the results of the project. We would like to express our appreciation to the two project coaches: Maarten Holtslag and Xinyuan Mao for their advice and their help with the design process. We want to express special gratitude to Max Pastena, Senior Space System Engineer at SSBV, for supplying us with the information about the PanelSAR instrument. Last but not least, we would like to thank our project coordinator, Prem Sundaramoorthy, for setting up this project, coordinating and advising us throughout the DSE.

Contents

List of Symbols

Symbol	Description	Default Unit
α	Right Ascension	rad
α	absorptance	-
α_g	Right Ascension of Greenwich	rad
β	Inertial Flight Path Angle Measured w.r.t. the Radius Vector	rad
β	Pointing Accuracy	rad
δ	Declination	rad
Δe	Relative eccentricity vector	rad
δe	Magnitude of relative eccentricity vector	-
Δi	Relative inclination vector	-
δi	Magnitude of relative inclination vector	-
$\delta(s)$	Jitter angle	rad
ΔT	Time a satellite takes to be in the same position as its predecessor	
ΔT_i	Time a satellite takes to be in the same position as its predecessor	
$\dot{\Omega}_{J2}$	Change in argument of right ascending node due to J_2	
η	Surface Emittance Coefficient	-
γ	Coherence between two image cells	-
λ	Longitude	deg
λ	Wavelength	m
μ	Standard Gravitational Parameter of Earth	km^3/s^2
ω	Argument of Periapsis	rad
Ω	Argument of right ascending node	rad
Ω_0	Starting argument of right ascending node	
ω_e	Rotational Velocity of the Earth	rad/s
Ω_i	Initial argument of right ascending node for i-th satellite	rad
ϕ	Phase of the signal	rad
Φ	Looking Angle	deg
$\rho_\bullet$	Density (note the variable index)	kg/m^3
σ	Boltzmann Constant	m^2kg/s^2K
θ	True Anomaly	rad
θ	Phase angle of relative inclination vector	-
θ	Cosine Loss	-
φ	Latitude	deg
φ	Phase angle of relative eccentricity vector	rad
a	Semi-Major Axis	km
a	Albedo	-
A_{sol}	Area that receives solar radiation	m^2
A_{sur}	Area of the bus that radiates its heat into space	m^2
A_a	Area that receives albedo radiation	m^2
A_p	Area that receives planetary radiation	m^2
$B_\bullet$	Magnetic Field (note the variable index)	T
c	Speed of light	m/s
C_D	Drag coefficient	-
d	Distance between the observation area and the payload	km
D	Distance between the Radar antenna and the target	m
d	Length of antenna	m
D	Diameter	m

Symbol	Description	Default Unit
D_C	Duty Cycle	-
ΔV	Velocity Change	m/s
e	Eccentricity	-
E	Expected value of operation	-
f	Thrust force	N
F	Fraction of fuel	-
F	Visibility Factor	-
F_s	Solar constant	W/m^2
$G_\bullet$	Gain (note the variable index)	-
g_0	Gravitational Acceleration of Earth	m/s^2
h	Altitude of the Spacecraft	km
H	Angular momentum	Nms
I_{sp}	Specific Impulse	s
I_{xx}	Moment of inertia around the x-axis	m^4
I_{yy}	Moment of inertia around the y-axis	m^4
I_{zz}	Moment of inertia around the z-axis	m^4
j	Number of revolutions per repetition	-
J_{sol}	Power flux from solar radiation	W/m^2
J_2	Disturbance effect due to the flattening of the Earth	-
J_a	Power flux from albedo radiation	W/m^2
J_p	Power flux from planetary radiation	W/m^2
k	Number of days	-
k	Boltzmann constant	m^2 kg s^{-2} K^{-1}
L	Radar Antenna Length	m
$l_\bullet$	Length (note the variable index)	m
$L_\bullet$	Loss (note the variable index)	-
$m_\bullet$	Mass (note the variable index)	kg
M	Moment	Nm
n	Mean Motion	1/s
$n_{launcher}$	Number of Launches	-
n_{sats}	Number of satellites	-
N	Filter coefficient	-
O	Fraction of Oxidiser	-
O	Cross sectional area of a beam	m^2
p	Semi-latus rectum	km
p_b	Burst pressure	Pa
$P_\bullet$	Power (note the variable index)	-
$P_\bullet$	Power (note the variable index)	W
q	Reflectance factor	-
Q	Dissipated Power	W
R	Travel Distance of a signal	m
r	Distance between the satellite an the centre of the Earth	
r	Altitude of the spacecraft	km
R	Data Rate	Gb/s
R, R_e	Radius of the Earth	km
$R_{PQW-IJK}$	Transformation matrix of the IJK to PQW coordinates	-
S_r	Slant range	km
T	Temperature	K
t	Time between radar transmission and echo	s
$T_\bullet$	Torque	Nm
$t_\bullet$	Time (note the variable index)	-
T_E	Orbital Period of the Earth	s
T_g	Gravity Gradient Torque	Nm
T_i	Transformation about a specific axis	-
u	Argument of latitude	rad
v	Velocity of spacecraft	km/s
v_1	Complex values in the cell of image 1	-
v_2	Complex values in the cell of image 2	-
w_s	Swath width	km
x_i	x-coordinate	km
y_i	y-coordinate	km
z_i	z-coordinate	km

List of Abbreviations

Abbreviation	Description
ADCS	Attitude Determination and Control System
AIS	Automatic Identification System
ATI	Along Track Interferometry
BER	Bit Error Rate
BiSAR	Bistatic Synthetic Aperture Radar
BOL	Begin of Life
CFAR	Constant False Alarm Rate
CPU	Central Processing Unit
DEM	Digital Elevation Model
DOD	Depth of Discharge
DSE	Design Synthesis Exercise
ECI	Earth Centered Inertial
EMSA	European Maritime Safety Agency
ESA	European Space Agency
EOL	End of Life
FBS	Function Breakdown Structure
FFBD	Functional Flow Block Diagram
FMCW	Frequency Modulated Continuous Wave
GNC	Guidance, Navigation and Control
GNSS	Global Navigational Satellite System
GPS	Global Positioning System
GS	Ground Station
IAGA	International Association of Geomagnetism and Aeronomy
IMU	Inertial Measurement Unit
IUU	Illegal, Unreported and Unregulated
JPL	Jet Propulsion Laboratory
LEO	Low Earth Orbit
LVLH	Local Vertical Local Horizontal
MEOP	Maximum Expected Operating Pressure
MTR	Mid-Term Review
nm	Nautical Mile
OIM	Orbital Insertion Module
OPS	Operations
PCDU	Power Conditioning and Distribution Unit
PV	Photo Voltaic
RADAR	Radio Detection And Ranging
SAR	Synthetic Aperture Radar
SIR	Space-borne Imaging Radar
SLC	Single Look Complex
SNR	Signal to Noise Ratio
STK	Satellite Tool Kit
TAC	Total Allowable Catch
TDX	TanDEM-X
TSX	TerraSAR-X
TT&C	Telemetry, Tracking and Control
UMDH	Unsymmetrical DiMethyl Hydrazine
UTC	Coordinated Universal Time
UTJ	Ultra Triple Junction
XTI	Cross Track Interferometry

Summary

This report presents the final design results of the project. This report was preceded by the Project Plan, Baseline Report and Midterm Report. The North Sea has the highest ship density compared to other seas. The main economic activities being performed in the North Sea are fishing and shipping operations. Overfishing causes depletion of fish population, already leading to a 4 billion [€] loss per year. Illegal dumping of oil in the fuel tanks of ships causes serious environmental damage to the North Sea. Therefore there is a need for a monitoring system.

The mission objective of this project is to present a complete design of a satellite constellation which can monitor the North Sea with a temporal resolution below 100 minutes, using a bi-static SAR configuration. The satellites are especially designed to accommodate the PanelSAR instrument, developed by SSBV. A separate receiver satellite and transmitter satellite are required in a bi-static configuration. An Automatic Identification System (AIS) receiver is included as well. The SAR instrument is capable of detecting ships based on the reflected SAR signal, while the AIS receiver can identify ships based on their AIS signal. A combination of these two instruments will result in a system which can both detect and identify ships.

The PanelSAR has a swath width of approximately 120 [km], but it differs with the side-looking angle. The satellite pairs will be in an Earth repeat orbit at an altitude between 510 [km] and 517 [km]. The satellites will be placed at inclination between 58 [deg] and 63 [deg]. In order to obtain a 100 [min] temporal resolution of the North Sea, 20 satellite pairs are launched using four Soyuz-2b launchers. The entire constellation consists of 40 satellites of which six satellites are redundant with respect to the temporal resolution.

The Soyuz-2b has an off-the-shelf kick stage called the Fregat. The Fregat is capable of providing the inclination changes between separate satellite pairs. Since the satellites will orbit the Earth in satellite pairs, formation flying is required. In order to perform formation flying with an high accuracy, a Septentrio PolaRx2 GPS receiver is used with a position accuracy of 2 [cm] and a velocity accuracy of 1.9 [mm/s]. From simulations it was found that the satellites pairs will have a minimum separation of 200 [m] and a maximum separation of 2 [km]. In order to perform formation flying, as well as orbital maintenance and momentum dumping, the propulsion system is required to provide a total Delta V of 143.07 [m/s]. The propulsion system is able to unload the reaction wheels for the ADCS. The ADCS is required to provide an attitude accuracy of 5 [arcsec]. In order to do so, the ADCS will be equipped with three star trackers. During measuring times, the SAR panels produce 2.4 [Gb/s] of data.

In order to process and transmit all this data to Earth, an data storage of 85 [GB] will be placed on board, as well as two X-band transmitters. The satellite transmitter and receiver require a peak power of 823.3 [W] and 793.3 [W] respectively. In order to provide this power, a total Photo Voltaic cell area of 3.47 [m^2] and 3.68 [m^2] is required respectively for the transmitter and receiver. The solar panels are able to rotate over a range of 150 [deg] to increase the power output. During eclipse and peak power demand, Lithium-ion batteries will provide the necessary power. The thermal control system can maintain the satellites temperature using 12 thermistors and 14 polymide strip heaters. The satellite stiffness comes from the main thruss structure. The total structure has a weight of 95 [kg] for both satellites.

After the last iteration, the mass of the transmitter satellite is equal to 470.85 [kg] and the mass of the receiver satellite is equal to 482.65 [kg], the satellites have a peak power of 823.3 [W] and 793.3 [W] respectively. The costs per satellite pair is equal to 32.5 million [€]. The launch costs are equal to 40 million [€] per launch. The total cost for the system will be equal to 809.2 million [€], excluding operational and payload costs.

The AEGIR constellation can replace current monitoring systems partially and therefore save up to 315.2 million [€]. The temporal resolution and coverage of the space based system will be better than current solutions and therefore the total income is an underestimate.

A carbon footprint estimate is made for this project. A total of four launches are required, which produce a total of 319 ton CO2. Currently, the Dutch coast is being monitored using two Dornier 228's. If one of these aircraft can be replaced by the satellite constellation, the carbon payback will be in 1.86 years. Note that observation planes of other countries can be replaced as well, leading to an even faster carbon payback. Beside reducing the carbon footprint of current systems, the satellites will be able to prevent fishing in illegal areas, detect and identify oil polluters and reduce the amount of accidents in the North Sea using AIS and SAR data. This will lead to a better North Sea environment.

Introduction

A large portion of all goods being transported around the world is transported over sea. The ships carrying these goods vary in size, ranging from small fishing boats to large container ships with a capability to transport thousands of tonnes of goods. While these ships are free to travel across the world, most of the trade is concentrated along two main routes: from (Eastern) Asia to North America and the route between Asia and Northern Europe. The former of these routes crosses the Pacific Ocean where there is enough room for boats to travel freely and safely. For the latter route, however, most of the ships are destined for the ports of Rotterdam, Antwerp or Hamburg, which are all located in close proximity of each other, as well as being connected to the North Sea. Compared to the Pacific Ocean, the North Sea is a lot smaller, meaning that the coordination and monitoring of the traffic across the sea is essential to guarantee the safety and security of the ships. The purpose of this project is to check the feasibility and, if possible, create the design of a space-based bistatic Synthetic Aperture Radar (SAR) monitoring system for the North Sea. This will be done by employing a SAR instrument, designed by SSBV, on a constellation of satellites.

The report will start by introducing the problem and presenting a general overview of the solution in Chapter 1. This will include diagrams describing the functions and the requirements of the system. In Chapter 2, the orbit design of the constellation is presented. This is followed by Chapter 3 which contains a description of the various operations and logistics required for performing the mission as well as the mission modes for the spacecraft. In Chapters 4 through 12, the various subsystems in the spacecraft bus are described. All these subsystems put together form the space segment of the satellite system, its characteristics are described in chapter 13. This is followed by a market analysis in chapter 14. A large system as the one presented in this paper will have environmental implications, hence the approach to sustainability within the project is shown in chapter 15. Chapter 16 looks ahead into the future: the different design and operational phases after the DSE are defined and scheduled. The report finishes by stating conclusions and recommendations in chapter 17.

Chapter 1

Mission and System Analysis

This chapter gives a high level overview of the mission: the problem and the general solution provided by the constellation. The chapter continues by presenting the Functional Flow Block Diagrams (FFBDs), which describe the logical flow between the separate subsystems. Closely related are the Function Block Structures (FBS), showing all the different operations performed during the mission.

1.1 Mission Description

The ship density in the North Sea is the highest in the world. The main cause of this is the high volume of maritime traffic travelling through the North Sea on their way to the big ports in Northwestern Europe such as Rotterdam, Hamburg or Antwerp. As a matter of fact, approximately 34% of the World's shipping trade operates via one of these ports [1]. Between 2007 and 2010, 1861 serious maritime incidents were reported, ranging from collisions, fires and even sinking ships [2]. This indicates that there is a serious need for effective and continuous monitoring of the traffic in the North Sea.

An electronic monitoring system is already in place: the Automatic Identification System or AIS. This system requires a transponder carried on board of the vessels which is mandatory since 2002 [3]. Two problems with the AIS lower its efficiency drastically. Firstly, even though it is mandatory, there are many vessels which still do not have an AIS transponder due to various reasons. Secondly, the range of the receivers for monitoring is limited to about 20 to 40 nautical miles (nm) from the coast [4].

A solution for these problems is provided by the Aegir network. The Aegir network is a constellation of forty bistatic Synthetic Aperture Radar (biSAR) satellites, that is able to detect and monitor vessels in the entire North Sea under all weather conditions. The spacecraft in the constellation are grouped in pairs, each acting as a biSAR system. For this reason, formation flying and attitude control are important for operation of the biSAR instruments.

The spacecraft are inserted into orbit in groups of ten, using a Soyuz launcher with a Fregat upper stage. Pairs of SAR satellites are separated from the launcher at different inclinations, varying from 58 [deg] to 63 [deg]. This provides optimum coverage of the North Sea by the constellation.

The operational lifetime of the constellation is five years. At the end of its lifetime, the spacecraft will enter the end-of-life phase. During this phase, the spacecraft will deorbit within two years.

1.2 Functional Flow Block Diagram

A Functional Flow Block Diagram (FFBD) shows all the functions of a system in chronological order to successfully create an overview of the mission process, separated into individual steps. The FFBD usually contains many levels. Figure 1.1 shows the top level functional flow of this mission while the complete Functional Flow Block Diagram may be found in Appendix D.

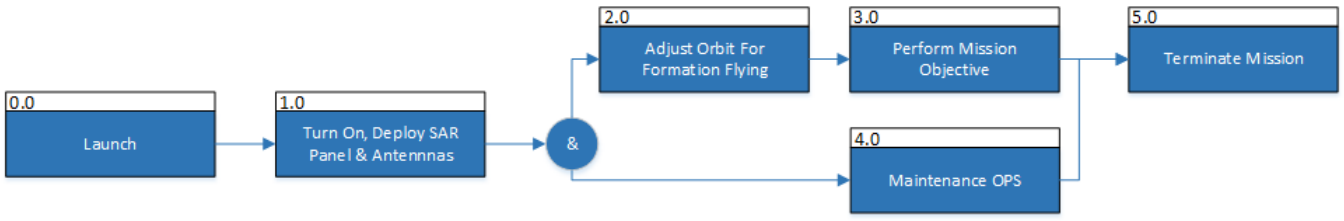

Figure 1.1: Top level of the FFBD

As can be seen in figure 1.1, the mission is split up in 6 top level functions.

1. **Launch** - The satellites are launched and inserted as pairs into the target orbit.
2. **Turn On, Deploy SAR Panel and Antennas** - This phase includes the start up of supporting systems, deployment of the SAR panel, deployement of the antennas and the system checks.
3. **Adjust Orbit For Formation Flying** - The satellites decrease their relative distance to iniate formation flying.
4. **Perform Mission Objective** - This includes collecting and sending data.
5. **Maintenance OPS** - Subsystem activities, monitoring, and keeping the satellite in the correct orbit and/or relative position with regards to other satellites.
6. **Terminate Mission** - Disposal of the satellite.

Every top level function is split up into a second level FFBD and where needed into a third or fourth level. Figure 1.2 shows the second level FFBD for the 'Perform Mission Objective' top level block.

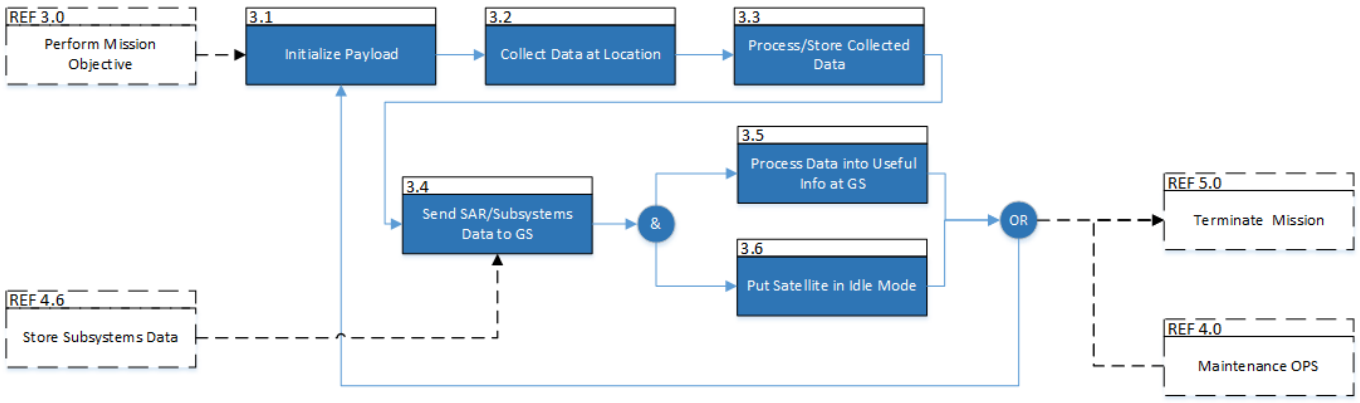

Figure 1.2: Second level 'Perform Mission' FFBD

The dashed lines and blocks are not a part of the second level 'Perform Mission Objective' FFBD, but are used as reference blocks to show how it fits in the big picture. This FFBD is structured as a loop. The satellite initializes its payload, uses that payload to collect data, stores the data and sends the data to the Ground Station. Hereafter, the satellite will go into standby mode while the data is processed at the ground station. All of these functions are repeated or the mission is terminated.

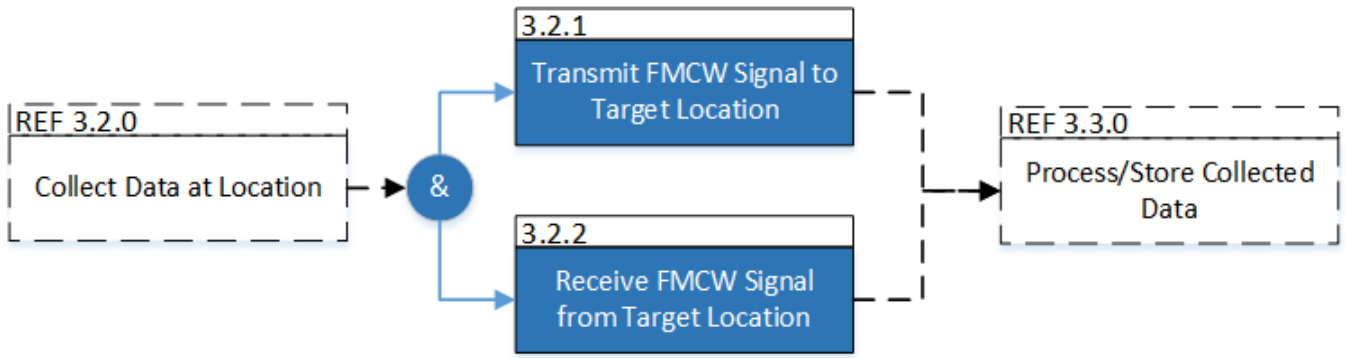

Figure 1.3: Third level 'Collect Data at Location' FFBD

Figure 1.3 shows the third level FFBD for 'Collect Data at Location'. The FMCW signal is a continuous signal, therefore the signal and the reflected signal are simultaneously transmitted and received.

The FFBD helps in designing the mission, because it shows precisely what functions the system must be able to perform. The complete mission's FFBD with all sub-level FFBDs can be found in Appendix D.

1.3 Function Breakdown Structures

The Functional Breakdown Structure (FBS) lists all the elements that are in the FFBD. In the FBS all those elements are listed in a hierarchical order. Every function in the FBS needs to be performed either parallel with the other functions or

independently, but all top level functions need to be conducted fully. This gives a general overview of all functions needed to perform the mission. Firstly, 'Perform Mission Objective' is split up into the same functions that can be found in top

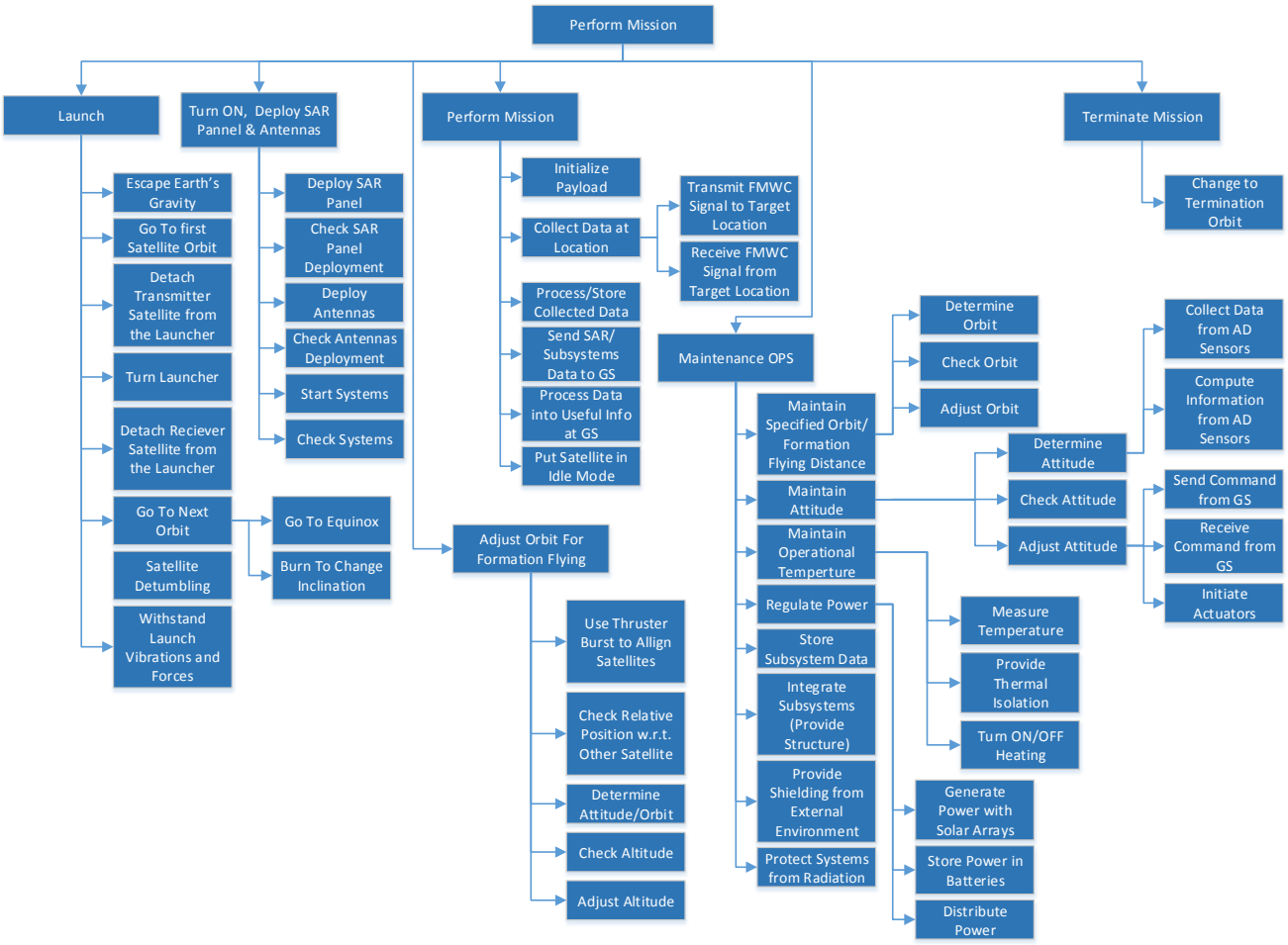

Figure 1.4: The functional breakdown structure for the Aegir mission

level FFBD. Those functions are split up into the functions that are in the second level of FFBDs. The block 'Determine Orbit' is divided further once the orbit determination method is chosen. The block 'Adjust Orbit' is not split up further because the functions under 'Transer to OPS Orbit' are essentialy the same.

1.4 System Requirements

The Baseline Report of this project lists many requirements. During the process of the detailed design, mainly described in this report, the various subsystems were designed with these requirements in mind. Appendix C lists the various tables containing the requirements and whether they have been met by the final design. Each row includes the original designated requirement id and a description of the requirement. Next, the specific values of the final design are compared to the requirements. The requirements for each subsystem are described in the chapters for the corresponding subsystem design.

Chapter 2

Astrodynamic Design

In the Midterm report a preliminary design of the orbit was presented [5]. An Earth repeat orbit has the advantage that the same ground track is repeated after a certain amount of orbits. If this ground track is properly alligned with major shipping routes, fishing areas and the general geometry of the North Sea, the performance of the system can be increased. Therefore, it has been decided that the orbit will be an Earth repeat orbit. In this report, the preliminary design is improved to an orbit which provides a better coverage while keeping the same temporal resolution. During the design, the orbit will be modelled in depth in order to determine the performance for a specific orbit.

2.1 Requirements

The design of the orbit is constrained by a set of requirements. These requirements can be derived from the stakeholder requirements, which are shown below.

- Stakeholder Requirement [BSAR-1a]: At least 90% of the total ship traffic shall be detected.
- Stakeholder Requirement [BSAR-1b]: Continuous monitoring shall be performed.
- Stakeholder Requirement [BSAR-1c]: The North Sea area shall be monitored.
- Stakeholder Requirement [BSAR-1d]: The bistatic PanelSAR instrument designed by SSBV shall be used.

The combination of the stakeholder requirements [BSAR-1a] and [BSAR-1d] result in a maximum achievable swath width which is given in system requirement [BSAR-1bc-Sys3]. [BSAR-1b] is translated to a temporal resolution system requirement given in [BSAR-1b-Sys1]. Similary [BSAR-1c] can be translated into an inclination requirement given in system requirement [BSAR-1c-Sys1]. Stakeholder requirement [BSAR-1d] can be translated into system requirement [BSAR-1d-Sys1], since the PanelSAR instrument has an operational range between 350 km and 650 km [6].

- System Requirement [BSAR-1bc-Sys3]: The bistatic SAR instrument shall have a swath width of 100 [km].
- System Requirement [BSAR-1b-Sys1]: The system shall have a maximum temporal resolution of 100 minutes.
- System Requirement [BSAR-1c-Sys1]: The orbital planes shall have a minimum inclination of 58 [deg].
- System Requirement [BSAR-1d-Sys1]: The operational altitude shall have a minimum altitude of 350 [km] and a maximum altitude of 650 [km].

The four system requirements above should be taken into account during the design of the orbit.

2.2 Orbit Simulation Flowchart

To calculate and simulate the orbits of the satellites, a MATLAB script has been written. The flowchart for the script can be seen in Figure 2.1. The flowchart for simulating the payload and the swath is shown in Figure 2.2. The outputs for the orbit model (position vectors) are used as an input for the payload model.

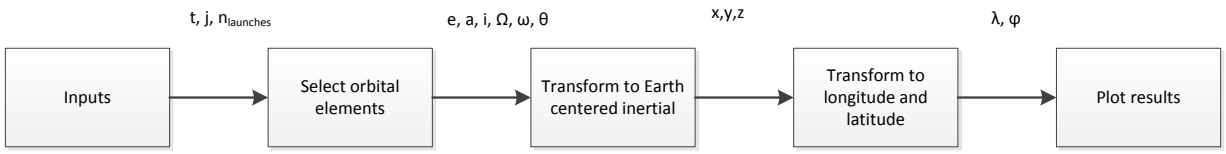

Figure 2.1: Flowchart for the MATLAB code used for orbit modeling

The variable 't' is a vector containing the time. The parameter 'j' is a variable which refers to the number of orbits the satellite needs to complete untill the ground track repeats. '$n_{launches}$' is the total number launchers used to put all satellites in space. The orbital elements are calculated to satisfy the requirements in Section 2.1. The orbital elements are the eccentricity (e), the semi-major axis (a), the inclination (i), the right ascension of ascending node (Ω), the argument of periapsis (ω) and the true anomely (θ). Ω and θ are a function of time, the other orbital elements are constant. The orbital elements are transformed to cartesian position vectors (x,y,z) in the Earth centered inertial reference system (ECI). The position vectors can be translated to longitude(λ) and latitude (φ) which are coordinates which can be plotted on a world map.

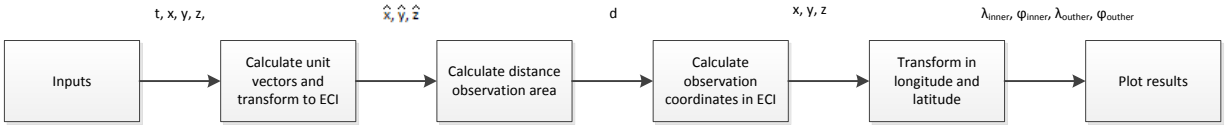

Figure 2.2: Flowchart for the MATLAB code used for payload modeling

The payload model requires the cartesian position vectors (x,y,z) and the time (t) from the orbit model. These are used to calculate pointing unit vectors in the payload frame, and are rotated to the ECI reference frame ($\hat{x}$, $\hat{y}$, $\hat{z}$). These unit vectors are extrapolated to intersect with the surface of the Earth, and combined with the position vectors from the orbital model, the distance to the observation area (d) can be found. Now the position of the observation area can be calculated first in ECI coordinates. These coordinates are transformed to longitude and latitude coordinates of both the inner swath area and the outher swath area (λ_{inner}, φ_{inner}, λ_{outher}, φ_{outher}).

2.3 Assumptions

In order to perform the simulations and to design the orbit, a couple of assumptions have to be made.

- The Earth has an equatorial bulge which is modelled using the J_2 effect.
- All other disturbances can be neglected.
- The orbit is circular (e=0).
- For modelling the payload operations, it is assumed that the payload is side looking, has a nominal looking angle between 25 and 33 [deg] and has a field of view of $\pm$ 5 [deg].
- The J_2 disturbances can be averaged over time.
- The body fixed reference frame is aligned with the flight path reference system.

In order to calculate the latitude of the ground track, another assumption is made.

- The Earth is spherically shaped.

This assumption is only valid when calculating the latitude of the ground track and not during the orbit propagation.

2.4 Orbit Model

In order to simulate the orbits, a MATLAB code has been written which simulates the satellites. This is done by plotting the orbit first in the PQW frame. W points in the direction of the angular momentum vector and the unit vector P points

in the direction of the perigee. The unit vector Q completes the right handed reference system. The frame can be seen in Figure 2.3.

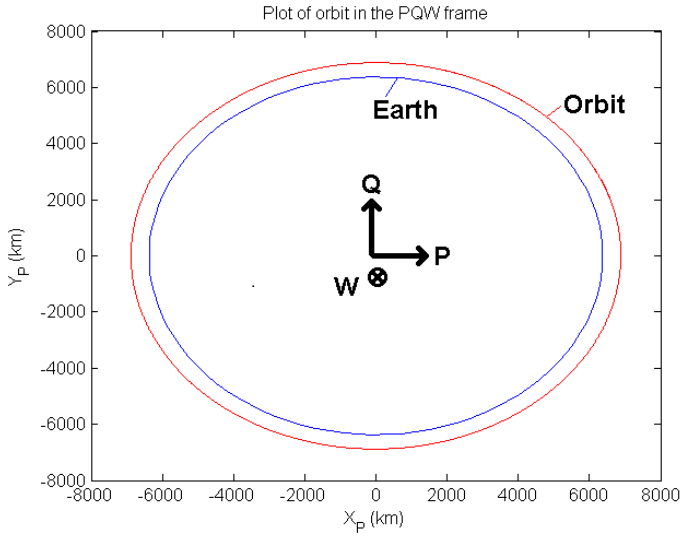

Figure 2.3: Example orbit at 510 [km] in the PQW frame (outer circle) and the Earth (inner circle)

The position vectors can be calculated as a function of the true anomaly using Equation 2.1.

$$\begin{bmatrix} x \\ y \\ z \end{bmatrix}_{PQW} = \frac{p}{1 + ecos(\theta)} \begin{bmatrix} cos(\theta) \\ sin(\theta) \\ 0 \end{bmatrix} \tag{2.1}$$

The position vectors can be rotated to the ECI (Earth Centered Inertial) reference frame in IJK coordinates using a 3-1-3 rotation sequence. This rotation can be caried out if ω (argument of periapsis), i (inclination) and Ω are known and is shown in Equation 2.2 [7].

$$\begin{bmatrix} x \\ y \\ z \end{bmatrix}_{IJK} = T_3(\Omega)T_1(i)T_3(\omega) \begin{bmatrix} x \\ y \\ z \end{bmatrix}_{PQW} = R_{IJK-PQW} \begin{bmatrix} x \\ y \\ z \end{bmatrix}_{PQW} \tag{2.2}$$

Where $R_{IJK-PQW}$ is the resulting transformation matrix and can be calculated by multiplying the three rotation matrices around their specified axis. The result can be seen in Equation 2.3 in which 'c' denotes a cosine function and 's' denotes a sine function.

$$R_{IJK-PQW} = T_3(\Omega)T_1(i)T_3(\omega) = \begin{bmatrix} c(\Omega)c(\omega) - s(\Omega)s(\omega)c(i) & -c(\Omega)c(\omega) - s(\Omega)s(\omega)c(i) & s(\Omega)s(i) \\ s(\Omega)c(\omega) + c(\Omega)s(\omega)c(i) & -s(\Omega)c(\omega) + c(\Omega)s(\omega)c(i) & -c(\Omega)s(i) \\ s(\omega)s(i) & c(\omega)s(i) & c(i) \end{bmatrix} \tag{2.3}$$

Using the IJK position vectors, 3D plots can be generated for an orbit. In order to model the ground track of the satellite, coordinates should be expressed in latitude and longitude. First, the right ascension (α) and the declination (δ) are calculated. This can be performed using Equations 2.4, 2.5, 2.6 and 2.7.

$$sin(\alpha) = [\frac{y}{\sqrt{x^2 + y^2}}]_{IJK} \tag{2.4}$$

$$cos(\alpha) = [\frac{x}{\sqrt{x^2 + y^2}}]_{IJK} \tag{2.5}$$

$$\alpha = tan2^{-1}\frac{sin(\alpha)}{cos(\alpha)} \tag{2.6}$$

$$\delta = [sin^{-1}\frac{z}{r}]_{IJK} \tag{2.7}$$

Before the longitude can be determined, the rotation of the Earth needs to be known. First, using the sidereal time, the right ascension of Greenwich (α_g) is determined. This right ascension can be used to determine longitude as a function of time and right ascension using Equation 2.8. Where α_g is calculated using Equation 2.9 [7].

$$\lambda = \alpha - \alpha_g(t) \tag{2.8}$$

$$\alpha_{g@midnight} = [100.46061838 + d(0.7700537 + 3.88 \cdot 10^{-4} \cdot d) + 360 \cdot frac(100d)] \mod 360deg \tag{2.9}$$

$$\alpha_g(t) = [\alpha_{g@midnight} + \omega_E \cdot t] \mod 360deg \tag{2.10}$$

In Equation 2.10 ω_E is the angular velocity of the Earth and is equal to 15.04 [deg/mean solar hour] or 0.001478 [deg/s] [7] and t is equal to the time since midnight [s]. Since the Earth has been assumed to be a sphere, the latitude is equal to the declination, see Equation 2.11.

$$\varphi = \delta \tag{2.11}$$

An example simulation is executed to show the result of the calculations. An Earth repeat orbit is selected at an inclination of 58 [deg]. A plot of 5 hours is shown in Figure 2.4a. Another plot is generated for 48 hours to show that the orbit is in fact an Earth repeat orbit. This orbit is shown in Figure 2.4b.

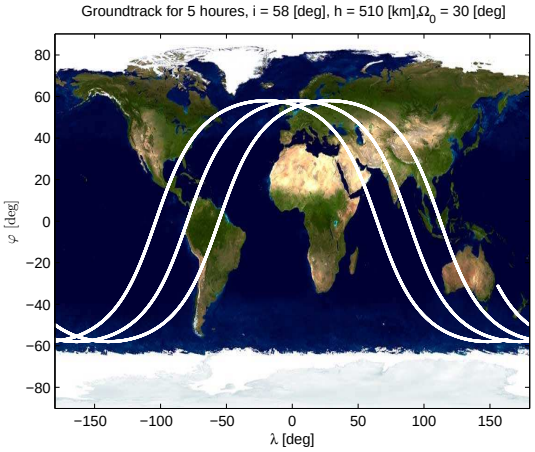

(a) Groundtrack simulation of a satellite for 5 hours

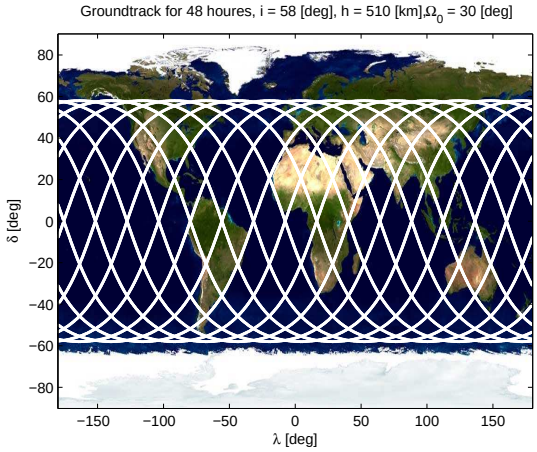

(b) Groundtrack simulation of a satellite for 48 hours

Figure 2.4: Multiple ground track simulations

2.5 Payload model

In order to simulate the performance of a specific orbit, a model has to be constructed which simulates the coverage of the payload. The SAR panels are side-looking at angles between 20 [deg] (Φ_{min}) and 36 [deg] (Φ_{max}) from nadir[6]. The SAR panels are pointed at a nominal looking angle between 25 [deg] and 31 [deg] and can adjust the looking angle over a range of $\pm$ 5 [deg] from the nominal looking angle. First, the field of view vectors in which the payload can perform operations is determined in payload fixed coordinates. This is translated to the ECI frame using rotation matrices. If the field of view of the payload is known in ECI coordinates, it can be used to calculate the intersection with the surface of the Earth. The transformations and related reference systems can be seen in Figure 2.5.

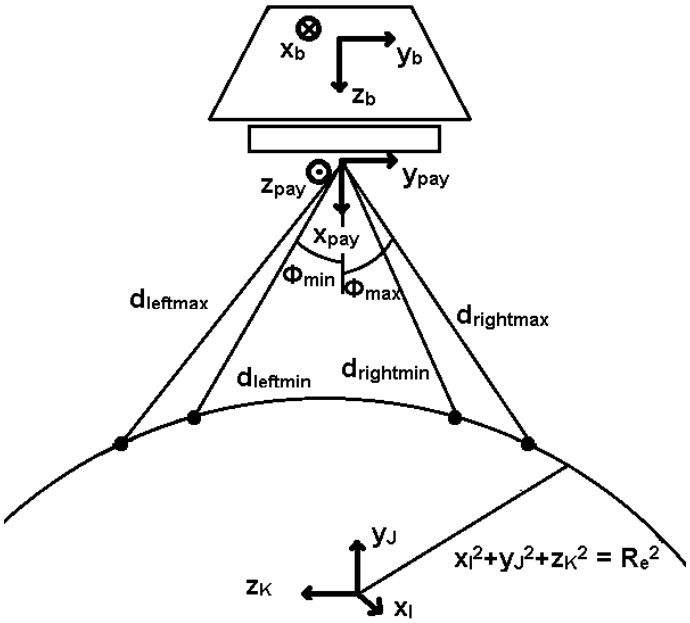

Figure 2.5: Relevant reference systems for payload operations

The field of view vectors in payload fixed coordinates can be calculated using Equations 2.12, 2.13, 2.14 and 2.15.

$$d_{leftmax} \cdot \begin{bmatrix} \hat{x} \\ \hat{y} \\ \hat{z} \end{bmatrix}_{pay} = d_{leftmax} \begin{bmatrix} cos(\Phi_{max}) \\ -sin(\Phi_{max}) \\ 0 \end{bmatrix} \tag{2.12}$$

$$d_{leftmin} \cdot \begin{bmatrix} \hat{x} \\ \hat{y} \\ \hat{z} \end{bmatrix}_{pay} = d_{leftmin} \begin{bmatrix} cos(\Phi_{min}) \\ -sin(\Phi_{min}) \\ 0 \end{bmatrix} \tag{2.13}$$

$$d_{rightmax} \cdot \begin{bmatrix} \hat{x} \\ \hat{y} \\ \hat{z} \end{bmatrix}_{pay} = d_{rightmax} \begin{bmatrix} cos(\Phi_{max}) \\ sin(\Phi_{max}) \\ 0 \end{bmatrix} \tag{2.14}$$

$$d_{rightmin} \cdot \begin{bmatrix} \hat{x} \\ \hat{y} \\ \hat{z} \end{bmatrix}_{pay} = d_{rightmin} \begin{bmatrix} cos(\Phi_{min}) \\ sin(\Phi_{min}) \\ 0 \end{bmatrix} \tag{2.15}$$

In these equations d is the distance between the satellite and the observation area. $\hat{x}$, $\hat{y}$ and $\hat{z}$ are unit vectors which describe the orientation of the beam leaving the spacecraft. These equations have to be solved for d. In order to calculate d, the equations need to be transformed to body fixed coordinates. This rotation is done using a 3← 2← 1 rotation sequence. In the final design, the SAR panels are located under the satellite, so only one positive rotation is required about the y-axis of $\frac{\pi}{2}$ [deg]. Note that it has been assumed that the body fixed coordinates are aligned with the flight path system, and since the orbit is circular, the flight path system is aligned with the Local Vertical Local Horizon (LVLH). See Equation 2.16.

$$d \cdot \begin{bmatrix} \hat{x} \\ \hat{y} \\ \hat{z} \end{bmatrix}_{LVLH} = d \cdot \begin{bmatrix} \hat{x} \\ \hat{y} \\ \hat{z} \end{bmatrix}_{flight} = d \cdot \begin{bmatrix} \hat{x} \\ \hat{y} \\ \hat{z} \end{bmatrix}_{body} = d \cdot T_2(\frac{\pi}{2}) \begin{bmatrix} \hat{x} \\ \hat{y} \\ \hat{z} \end{bmatrix}_{pay} \tag{2.16}$$

The LVLH coordinates can be rotated to the PQW frame. This is done by performing a rotation of $\theta + \frac{\pi}{2}$ around the y-axis and a rotation of $\frac{\pi}{2}$ around the x-axis. The reference frame is translated from the center of the satellite to the centre of the Earth. Therefore, the position vector of the satellite needs to be added to the payload field of view vector. See Equation 2.17.

$$\begin{bmatrix} x \\ y \\ z \end{bmatrix}_{PQW,pay} = d \cdot T_2(\theta + \frac{\pi}{2}) T_1(\frac{\pi}{2}) \begin{bmatrix} \hat{x} \\ \hat{y} \\ \hat{z} \end{bmatrix}_{LVLH} + \begin{bmatrix} x \\ y \\ z \end{bmatrix}_{PQW} \tag{2.17}$$

Now the field of view vectors can be expressed in the PQW frame. The vectors are rotated to the ECI frame silimary as done for the ground track of the satellites. See equation 2.18.

$$\begin{bmatrix} x \\ y \\ z \end{bmatrix}_{IJK,pay} = R_{IJK-PQW} \begin{bmatrix} x \\ y \\ z \end{bmatrix}_{PQW,pay} \tag{2.18}$$

Now, the field of view vectors from the SAR panel can be expressed in the ECI frame. Still there is one variable d. By calculating the intersection with the Earth's surface, d can be found. The Earth is approximated as a sphere using Equation 2.19.

$$[x^2 + y^2 + z^2]_{IJK,e} = R_e^2 \tag{2.19}$$

The field of view vector calculated using Equation 2.18 can be substituted in Equation 2.19 and solved for d. When d is known, the position vectors of the covered points by the payload can be calculated. These points can either be expressed in the ECI frame, or expressed in terms of longitude and latitude, similarly as done for the orbit, using Equations 2.4 up to 2.11. The result can be seen in Figure 2.6.

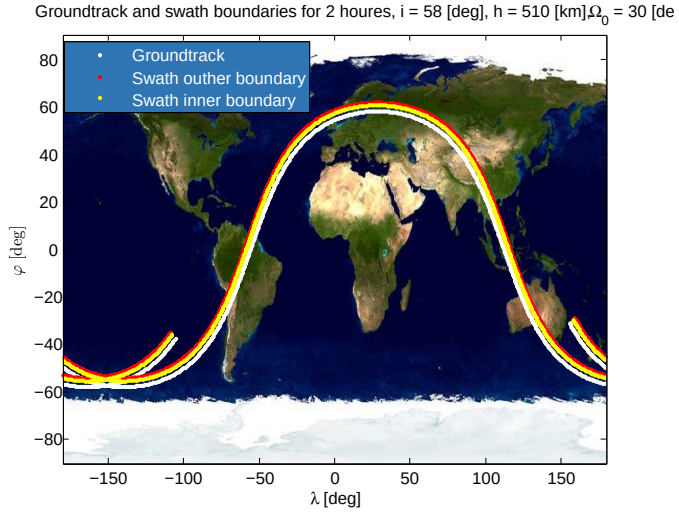

Figure 2.6: Groundtrack with swath for an satellite for 5 hours

2.6 Orbit selection

The orbit that will be designed is an Earth repeat orbit. An Earth repeat orbit should satisfy Equation 2.20 [7].

$$j \left| -2\pi \frac{2\pi\sqrt{a^3/\mu}}{T_E} - \frac{3\pi J_2 R_e^2 cos(i)}{a^2(1-e^2)^2} \right| = k2\pi \tag{2.20}$$

In this equation j refers to the number of revolutions and k refers to the number of days until the ground track repeats. a is the semi-major axis, for this circular orbit it is equal to the radius r. μ is the gravitational parameter of the Earth, equal to 398600 $[km^3/s^2]$ [7]. J_2 is the disturbance effect due to the flattening of the Earth [8] and is given to be $1082 \cdot 10^{-6}$ [-]. R_e is the mean Earth radius and is equal to 6371 [km]. The eccentricity, e, is zero for circular orbits. The inclination i is a variable and should be chosen such that the North Sea is optimally covered. T_E is the orbital period of the Earth and is calculated by Equation 2.21.

$$T_E = \frac{2\pi}{\omega_e} \tag{2.21}$$

In Equation 2.21, ω_e is the rotational velocity of the Earth, equal to 7.2921e-005 [rad/s]. If inclinations between 0^o and 90^o are considered, the disturbance effect of the J_2 will always be negative. This way, the absolute brackets can be removed in Equation 2.20 and the equation can be rewritten as a function of the semi-major axis. See Equation 2.22.

$$2\pi j \frac{2\pi}{T_e\sqrt{\mu}} a^{3.5} - k2\pi a^2 + 3\pi J2R_e^2 cos(i)j = 0 \tag{2.22}$$

This equation can be solved by MATLAB for different values of k, j and i. The semi-major axis should comply with requirement [BSAR-1d-Sys1] and must result in an altitude range between 350 [km] and 650 [km]. The inclination should

comply with requirement [BSAR-1c-Sys1] and must result in a minimal inclination of 58 [deg]. Earth repeat orbits which measure up to the requirements where found using Equation 2.22. The orbits repeat on a daily basis using 15 revolutions. An inclination of 58 [deg] results in an altitude of 510 [km] while at an inclination of 63 [deg] an altitude of 517 [km] is found. When keeping j and k constant, the inclination can be increased which will result in a slightly higher altitude. Therefore, there is some range in which the inclination and altitude can be chosen.

The orbit can be simulated if the orbital elements are known. The semimajor axis and inclination are limited by the altitude and inclination requirement and are dependent upon each other to satisfy Equation 2.22. Since the orbit is circular, the argument of periapsis (ω) is redundant and is set to be equal to 0 [deg]. Furthermore, the eccentricity (e) is equal to zero. The remaining orbital elements are calculated using Equations 2.23 and 2.24.

$$\theta(t) = \theta_0 + \sqrt{\frac{\mu}{a^3}}t \tag{2.23}$$

$$\Omega(t) = \Omega_0 + < \dot{\Omega}_{J2} > t \tag{2.24}$$

$$< \dot{\Omega}_{J2} >= -\frac{3}{2}J2\sqrt{\frac{\mu}{a^3}}\frac{R_e^2}{a^2}cos(i) \tag{2.25}$$

In this equation, $< \dot{\Omega}_{J2} >$ is the disturbance of the J_2 effect on Ω and is calculated using Equation 2.25 [7]. Ω_0 is the starting right ascension of ascending node. Since a single launcher will put multiple satellites into a single orbit, a group of satellites will have the same Ω_0. Other groups launched by another launcher will have chosen a different Ω_0 such that the ground track of the new group will be the same as the ground track of the previous group. Equation 2.26 is used to determine the starting right ascension of ascending node. This equation determines the starting Ω for different launches (k_{launch}) as a function of number of revolutions per repetition (j) and the total number of launches ($n_{launches}$). A constant is added to shift the total ground track such that the North Sea is optimally covered.

$$\Omega_0(j) = \frac{2\pi}{j}round(\frac{j}{n_{launches}}k_{launch}) + C \tag{2.26}$$

In the midterm report, an orbit was selected which had an inclination of 62 [deg]. The global ground track of this orbit can be seen in Figure 2.7. In Figure 2.8a, the North Sea ground track can be seen and it can be concluded that the North Sea is not completely covered yet. In order to improve the coverage of the North Sea, the satellite pairs will be placed at different inclinations. These inclination changes will be provided by a seperate kickphase. A satellite pair on a lower inclination can then cover the area underneath a satellite which is placed at a higher inclination. If 5 satellite pairs are considered at inclinations ranging from 58 [deg] to 63 [deg], the entire North Sea can be covered. The ground track of these orbits can be seen in Figure 2.8b.

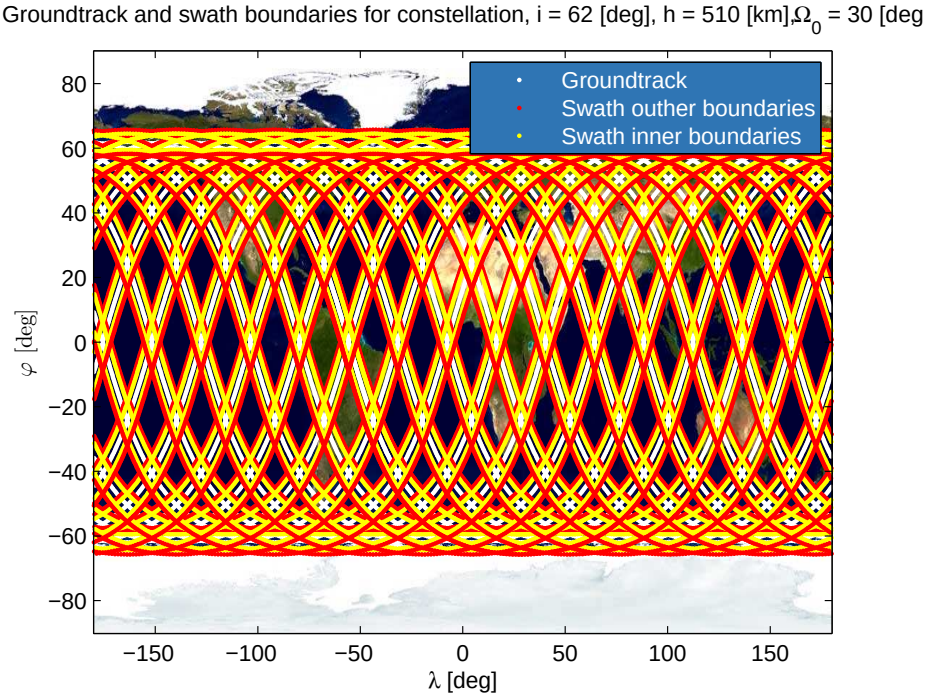

Figure 2.7: Global ground track simulation with swath for the midterm orbit

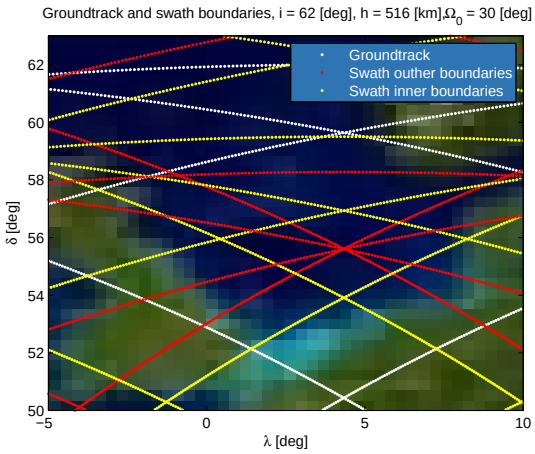

(a) North Sea ground track simulation with swath for the midterm report orbit

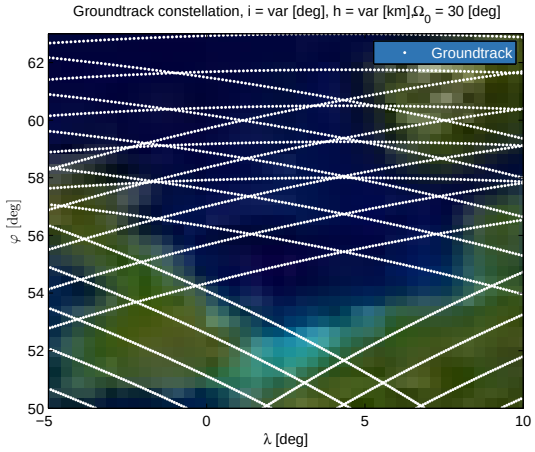

(b) North Sea ground track simulation for the entire constellation for the final report orbit

Figure 2.8: Comparison between the midterm orbit and the final orbit. The final design has orbital planes placed at different inclinations. For convenience, the swath width is not plotted for the final orbit.

2.7 Temporal resolution

The swath width is determined by the variable looking angle of the SAR panel which can be rotated by $\pm$ 5 [deg]. The nominal looking angle can be varied by changing the roll angle of the spacecraft between 33 and 25 [deg]. The looking angles should be selected in such a way that the North Sea can be covered by an as low as possible temporal resolution or with a minimum number of satellites. Per launch, five satellite pairs will be put in orbit. These five pairs are called a group of satellites. The total number of groups required is a trade-off between temporal resolution and cost. To estimate the temporal resolution, a scanning pattern is determined per satellite, per pass. The looking angles are selected manually by observing the ground track and the plots of the payload swath. The selected angles can be seen in Table 2.1.

Table 2.1: Looking angles for the SAR panel

Pass	Satellite pair number	Direction	Nominal looking angle (Φ) [deg]
1	1 (i = 58.00 deg)	left	30
1	2 (i = 59.25 deg)	left	30
1	3 (i = 60.50 deg)	left	30
1	4 (i = 61.75 deg)	left	30
1	5 (i = 63.00 deg)	left	30
2	1 (i = 58.00 deg)	right	33
2	2 (i = 59.25 deg)	right	33
2	3 (i = 60.50 deg)	right	33
2	4 (i = 61.75 deg)	right	33
2	5 (i = 63.00 deg)	right	33
3	1 (i = 58.00 deg)	right	33
3	2 (i = 59.25 deg)	right	33
3	3 (i = 60.50 deg)	right	33
3	4 (i = 61.75 deg)	right	33
3	5 (i = 63.00 deg)	right	33
4	1 (i = 58.00 deg)	left	33
4	2 (i = 59.25 deg)	right	28
4	3 (i = 60.50 deg)	right	27
4	4 (i = 61.75 deg)	right	26
4	5 (i = 63.00 deg)	right	25
5	1 (i = 58.00 deg)	left	33
5	2 (i = 59.25 deg)	left	33
5	3 (i = 60.50 deg)	left	33
5	4 (i = 61.75 deg)	left	33
5	5 (i = 63.00 deg)	left	33

For the first set of passes, the ground track of the constellation can be seen in Figure 2.9a. The looking angles have been chosen in such a way that all swaths are aligned with respect to each other. The temporal resolution per swath in Figure 2.9a differs only in the order of minutes and therefore it is assumed that all the swaths have the same temporal resolution of 1421 minutes. Figure 2.9a can then be simplified to the scanning path shown in Figure 2.9b.

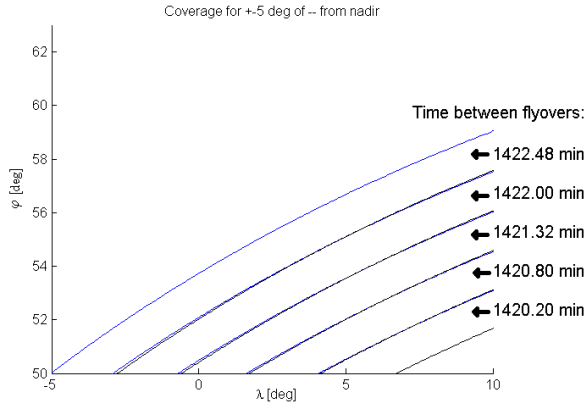

(a) Scanning path for the first pass

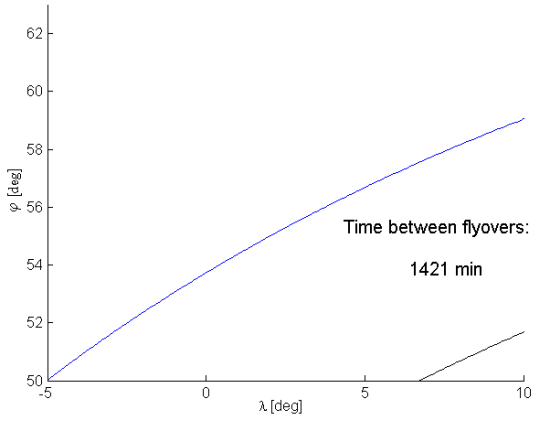

(b) Simplified scanning path for the first flyover

Figure 2.9: Scanning paths and simplified scanning path for the first pass

In total, five different passes are possible, per inclination. The remaining four passes are shown in Figure 2.10a, 2.10b, 2.11a and 2.11b.

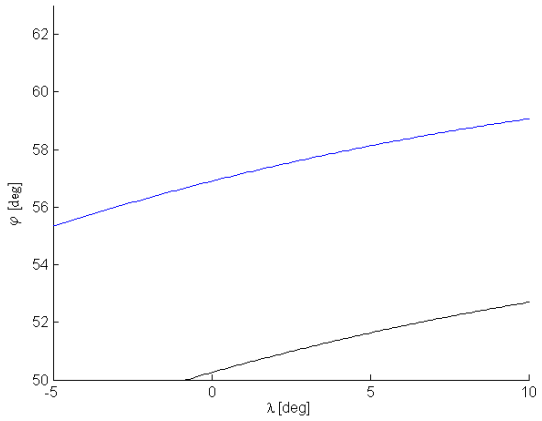

(a) Simplified scanning path for the second pass

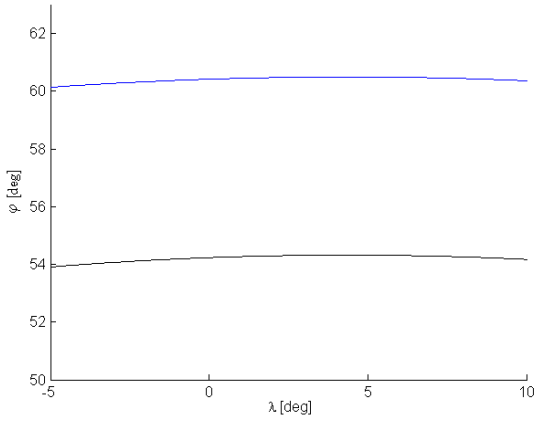

(b) Simplified scanning path for the third pass

Figure 2.10: Simplified scanning paths for the second and third pass

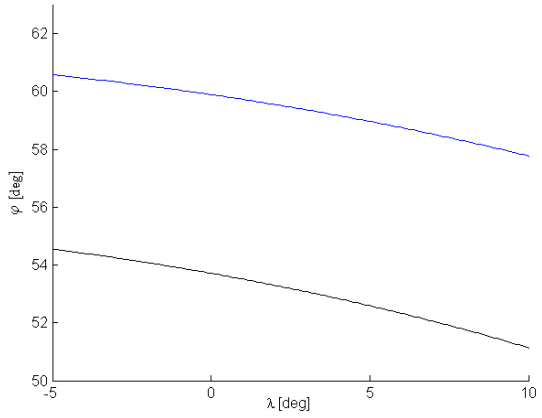

(a) Simplified scanning path for the fourth pass

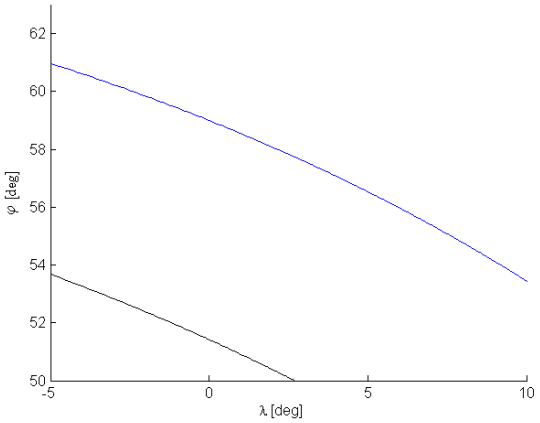

(b) Simplified scanning path for the fifth pass

Figure 2.11: Simplified scanning paths for the fourth and the fifth pass

The figures can be combined together in Figure 2.12. Colors indicate how many different scanning paths overlap. Moreover, the number of overlaps are shown as well as a text reference (x) in the figure. For reference, the map of the North Sea is included on the background.

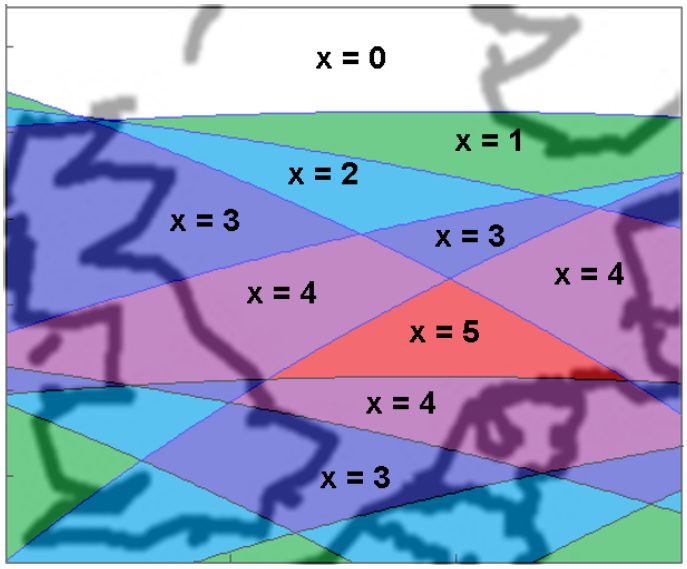

Figure 2.12: Combined coverage of the ground tracks[9]

Areas which are only covered once will be denoted by x = 1, areas that are covered twice will be denoted by x = 2 and so on. As a function of x and the number of groups launched into orbit, the temporal resolution can be calculated using Equation 2.27. The result of this equation can be seen in Table 2.2 and Figure 2.13.

$$\frac{\Delta t}{covered} = \frac{1421 minutes}{\frac{n_{launches} \cdot xpasses}{day}} \tag{2.27}$$

Table 2.2: Temporal resolution per area and number of launches

Color	x (Times covered)	$n_{launch} = 1$	$n_{launch} = 2$	$n_{launch} = 3$	$n_{launch} = 4$	$n_{launch} = 5$
Green	1	1421 minutes	711 minutes	474 minutes	355 minutes	284 minutes
Light blue	2	711 minutes	355 minutes	237 minutes	178 minutes	142 minutes
Blue	3	474 minutes	237 minutes	158 minutes	118 minutes	95 minutes
Purple	4	355 minutes	178 minutes	118 minutes	88 minutes	71 minutes
Red	5	284 minutes	142 minutes	95 minutes	71 minutes	57 minutes

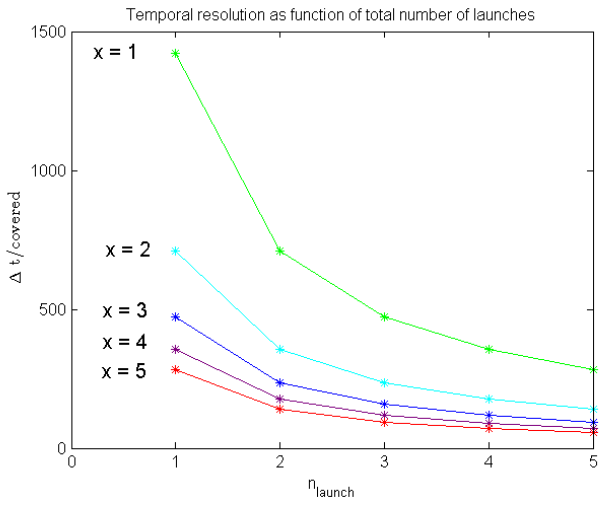

Figure 2.13: Temporal resolution of specific areas as function of number of launches

From Figures 2.12 and 2.13 it can be concluded that most of the North Sea can be covered with an average temporal resolution below 100 minutes if four groups of satellites are launched into orbit. This will result in four launches and a total of 40 satellites. The actual temporal resolution is dependent on how the constellation is phased. However, the phase will

have no effect on the average temporal resolution. Complex scanning algorithms can assure a smoother temporal resolution. Generating these scanning algorithms is beyond the scope of the current design phase.

2.8 Sensitivity Analysis

In order to test the robustness of the design, a sensitivity analysis is performed. Small changes are made in the initial stakeholder requirements and the effect on the design of these changes is measured. Recall the stakeholder requirements.

- Stakeholder Requirement [BSAR-1a]: At least 90% of the total ship traffic shall be detected.
- Stakeholder Requirement [BSAR-1b]: Continuous monitoring shall be performed.
- Stakeholder Requirement [BSAR-1c]: The North Sea area shall be monitored.
- Stakeholder Requirement [BSAR-1d]: The bistatic PanelSAR instrument designed by SSBV shall be used.

Stakeholder requirement [BSAR-1a] can be derived to a requirement stating that all ships longer than 15 meter shall be detected. This influences the azimuth and range resolution. If the resolution is refined, the number of panels increase, nonetheless, the swath width remains the same. Therefore, a change in this requirement does not alter the design of the orbit.

From stakeholder requirement [BSAR-1b] a requirement on the temporal resolution namely [BSAR-1b-Sys1], which states that the area will be monitored with a 100 minute temporal resolution. Assuming that the other requirement remain as the old requirement, a higher or lower temporal resolution is inversely proportional with the required number of launches. The required number of launches for a certain temporal resolution can be seen in Table 2.2.

Stakeholder requirement [BSAR-1c] can be translated to an requirement on the inclination which is system requirement [BSAR-1c-Sys1]. If the area that requires monitoring is located at a higher inclination, for the Barents Sea; 74 [deg] would be required, launching 10 satellits with a single Soyuz 2 launcher will not be possible for that inclination. Besides, at a higher inclination, their would be less overlap of the ground track and how often an area will be covered by a satellite. The size of the area that needs to be covered will be directly proportional to the number of satellites required and such, the number of launches. If the Mediterranean Sea requires coverage, the constellation will be placed at a lower inclination. This will result in a lower fuel weight requirement or a higher payload mass. At an lower inclination there will be more overlap between different ground tracks resulting in a higher temporal resolution with the same amount of satellites. However, since the Mediterranean Sea is larger than the North Sea, still a minimum of four launches would be requirement to cover most of the Mediterranean Sea. The result of such an constellation can be seen in Figure 2.14. The orbits have an altitude ranging from 485 to 488 [km] and an inclination of 38 to 42 [deg].

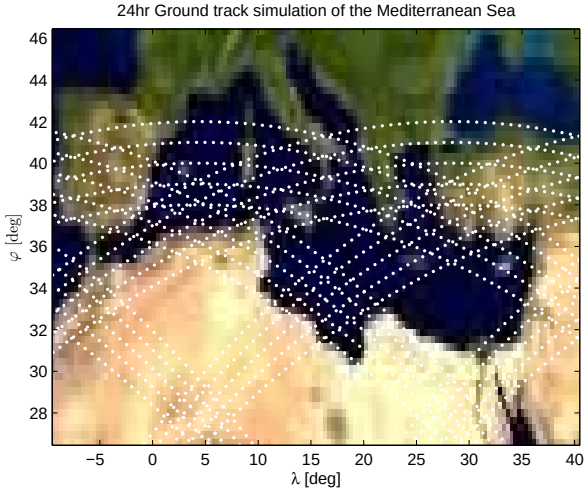

Figure 2.14: 24 hr ground track simulation of the Mediterranean Sea

Changes in stakeholder requirement [BSAR-1d] will have a large impact on the design of the orbit. If the panelSAR will be replaced by an optical instrument, the satellites can perform nadir and forward looking, resulting in a lower required inclination. If the panelSAR will be enhanced resulting in a wider swath width, the number of satellite pairs will be reduced and the spacing in inclination between specific satellite pairs will be increased.

2.9 Verification and Validation

In this section, first the verification tests are shown which are used to verify the MATLAB scripts. After the verification tests, a global validation test is shown which is used to validated the scripts.

Verification 1: Earth repeat orbit

In order to verify the MATLAB scripts, verification test are carried out. One orbit is chosen for which it will be checked whether the orbit satisfies the Earth repeat orbit requirement and if the disturbance effect is modelled correctly. The selected orbit is at an inclination of 58 [deg]. The MATLAB code found a corresponding semi-major axis of 6881.2 [km]. It will be checked whether this value is correct with Equation 2.20 and 2.21. First the period of the Earth is calculated.

$$T_E = \frac{2\pi}{7.2921 \cdot 10^{-5}} = 86164s \tag{2.28}$$

The numerical value found for the period of the Earth is equal to 86164 and is the same value as the analytical value.

$$15 \left| -2 \cdot \pi \frac{2\pi\sqrt{6881.2^3/398600}}{86164} - \frac{2\pi 1082 \times 10^{-6} \cdot 6371^2 \cos(58)}{6881.2^2(1-0^2)^2} \right| = 1 \cdot 2\pi \tag{2.29}$$

This equation solves to:

$$6.2832 = 6.2832 \tag{2.30}$$

It can be concluded that the values satisfy the equation and the orbit is indeed an Earth repeat orbit. This can as well be seen in the geometry of the ground track shown in various figures throughout the chapter.

Verification 2: J2 Disturbance effect

The J_2 disturbance effect on the right ascension of ascending node is verified as well. Recall Equation 2.25, a substitute form of this equation can be seen below.

$$< \dot{\Omega}_{J2} >= -\frac{3}{2} 1082 \cdot 10^{-6} \sqrt{\frac{398600}{6881.2^3}} \frac{6371^2}{6881.2^2} \cos(58) = -8.154 \cdot 10^{-7} \text{ rad/s} \tag{2.31}$$

The numerical model slo found a disturbance of $-8.1544 \cdot 10^{-7}$ rad/s and therefore the J_2 disturbance can be assumed verified.

Verification 3: Payload model

The payload model is verified as well by calculating the value of d analytically. The sketch which can be seen in Figure 2.15 is used to verify the calculations.

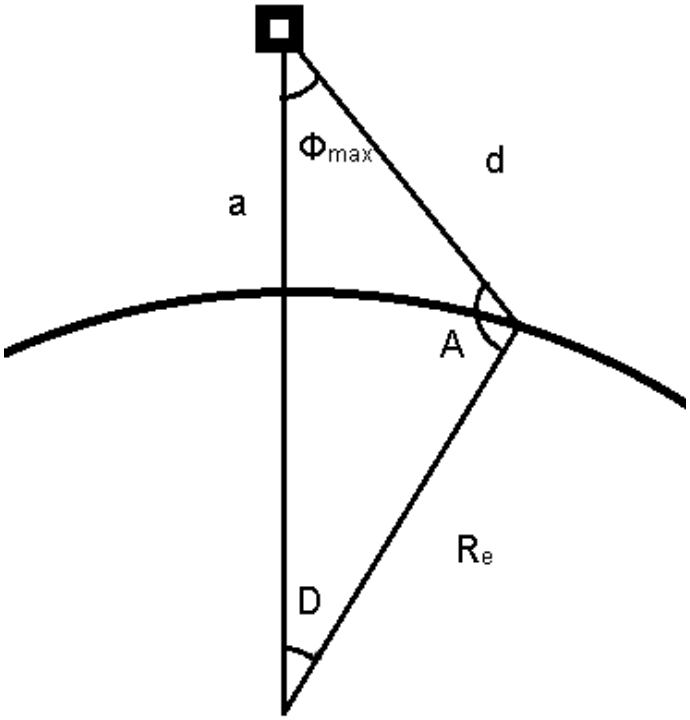

Figure 2.15: Sketch used to verify the calculation of d.

In this figure, a is the semi-major axis, R_e is the radius of the Earth, Φ_{max} is the looking angle, A is the angle between the looking vector and the Earth's radius and D is the angle between the radius of the Earth and the position vector of the satellite. The law of sines is used to solve this problem. See Equation 2.32

$$\frac{d}{\sin D} = \frac{a}{\sin A} = \frac{R_e}{\sin \Phi_{max}} \tag{2.32}$$

This equation can be used to calculate the angle A.

$$A = sin^{-1}(a\frac{sin(\Phi_{max})}{R_e}) = 138.32deg \tag{2.33}$$

Since all angles should add up to 180 [deg], angle D can now be calculated.

$$D = 180 - A - \Phi_{max} = 3.68deg \tag{2.34}$$

By rewriting Equation 2.32, the value of d can be calculated.

$$d = sin(D)\frac{R_e}{sin(\Phi_{max})} = 664.12km \tag{2.35}$$

The numerical found value is equal to 664.12 [km] and therefore the code can be assumed verified.

Validation 1: North Sea coordinates

First the background map which is used in the MATLAB script is validated. The longitude and latitude coordinates of points along the coast of the North Sea are plotted in Figure 2.16. Longitude and latitude data is extracted from Google Maps. It can be seen that the background map is correctly aligned with longitude and latitude axes.

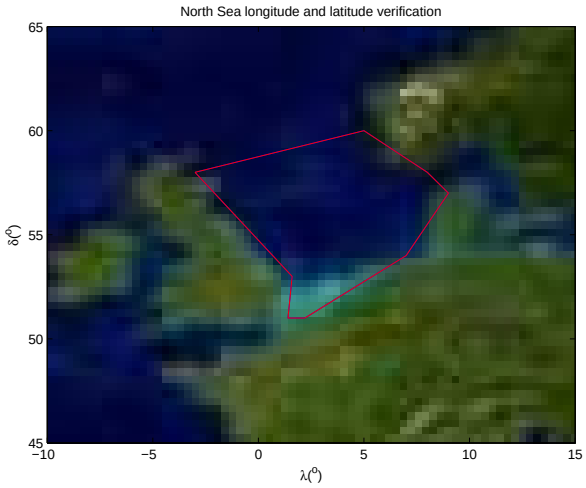

Figure 2.16: Plot containing North Sea coordinates

Validation 2: Groundtrack

In order to validate the script, the orbital elements are substituted in the Systems Tool Kit (STK). STK is an simulation program which can be used to model the ground track of a satellite [10]. The ground track found in STK is compared to the ground track found using the MATLAB script. The result of the two ground tracks can be seen in Figure 2.17 and 2.18.

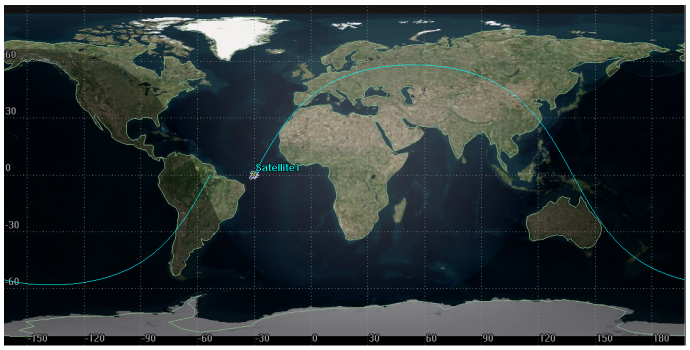

Figure 2.17: Simulation performed in MATLAB: inclination = 58 [deg], a = 6881.2 [km], Ω_0 = 30 [deg]

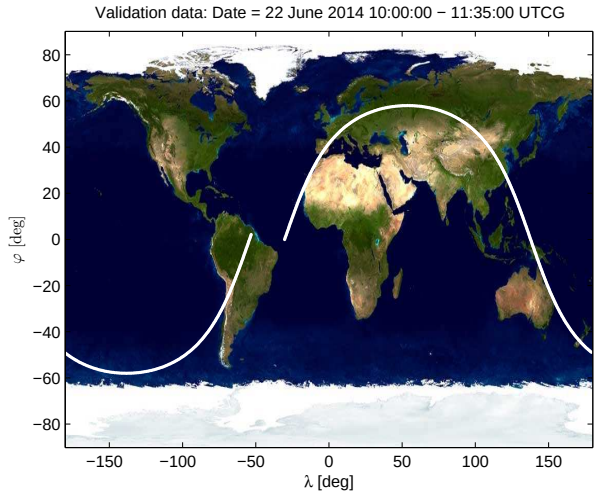

Figure 2.18: Simulation performed in MATLAB: inclination = 58 [deg], a = 6881.2 [km], Ω_0 = 30 [deg]

During the validation process one major difference was found between the time systems. STK used the UTCG time, where midnight is the reference point. The MATLAB script uses a method where 12 o'clock in the noon is set as a reference

point, which is custom in the field of astronomy. This problem was adjusted by translating the MATLAB time system by 12 hours so both simulations use the same time systems. It can be seen that the final result shows two identical ground tracks and therefore it can be assumed that the ground track is validated.

Chapter 3

Operations and Logistics

In this chapter the operations and logistics flow diagram is presented. This diagram will show the relations between different subsystems which are relevant during the operational phase of the mission. Secondly, the effect of redunancy on operations is discussed. Finally, the different modes of operation that the satellites will employ during the mission are explained.

3.1 Operations and Logistics Flow Diagram

The operations and logistics flow diagram shows the flow of information between the system and the surroundings.

The flow diagram, shown in Figure 3.1 is divided into four separate blocks, which each represents a different part of the logistics chain of the mission. The satellite logistics block is divided into two smaller blocks, the TT&C and Payload subsystems, which provide the information that the customer and mission command needs. The other blocks of the diagram show the different entities that interact with the satellite.

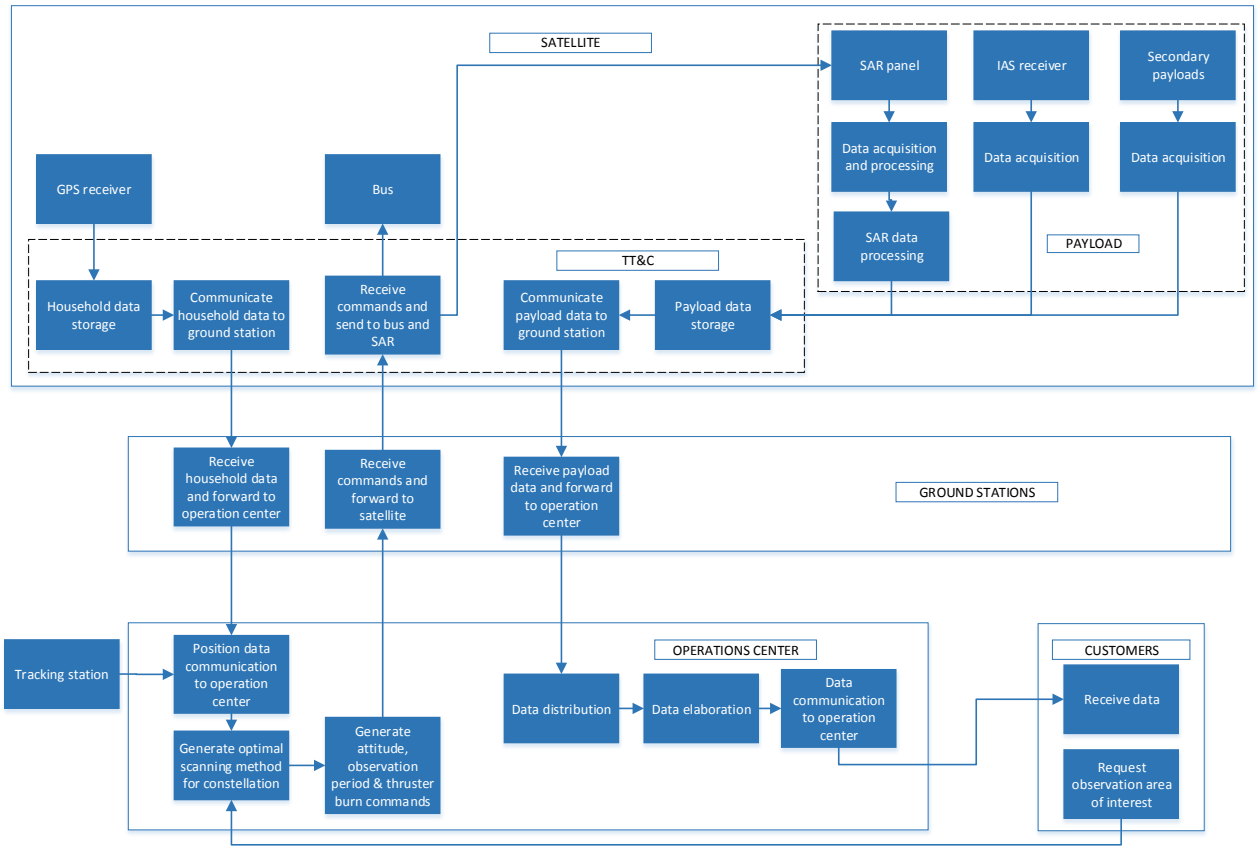

Figure 3.1: The operations and logistics concept description flow diagram

3.2 Redundancy

As mentioned in the astrodynamic section of the report, 17 pairs of satellites are required in order to fulfil the temporal resolution of 100 minutes. Each pair of satellites requires both the transmitter and receiver to be functional. If one of the two satellites in the pair fails, the other wont be able to perform the mission alone, and this will reduce the temporal resolution of the mission.

As it is too costly and time consuming to launch extra satellites whenever one fails, redundancy is created by sending more satellites into orbit than the number that is required to perform the mission. In order to determine the extra number of satellites required to achieve the reliability that is wanted for the mission, the failure rate for the individual satellites needs to be known. As this is not yet possible to determine at this point in the design, an estimation is made by looking at the number of redundant satellites in other constellations.

Three different constellations are looked at in order to determine the required number of spare satellites for the mission, the Iridium, the GPS, and the Galileo constellations.

Table 3.1: Redundancy in reference constellations

Constellation	Number of Satellites	Spares	Percentage
Iridium [11]	66	10	0.152
GPS [12]	24	3	0.125
Galileo [13]	30	3	0.100

As Table 3.1 shows, the number of spare satellites lies between 10 and 15 percent of the total. The satellites are put into orbit in a group of 10 satellites per launch and four launches, resulting in a total of 40 satellites or 20 pairs. Since only 17 pairs are required for the temporal resolution, the redunancy in the system will be 15%. This is comparable with respect to the other constellations.

3.3 Mission Modes

In this section the different modes for the satellite during the mission will be discussed. There are 3 different phases that the satellites will encounter, these are the Begin Of Life (BOL), Operating Life and the End Of Life (EOL). The first section discusses the modes during the BOL which is from launch until the satellite is in the operating orbit with all systems deployed. The modes included are the Standby mode, the De-tumbling mode, the Deployment mode and the Start-up mode. The next section discusses the Operating life of the satellite, this includes the Scanning mode, the Communication mode, the Idle mode, the Safe mode and the Manoeuvring mode. In the last section the modes during EOL are discussed.

3.3.1 Begin Of Life

Standby Mode

The standby mode occurs when the satellite is stored in the launcher, there is no need to control or manoeuvre the satellite at this point in time. Most of the subsystems are turned off, only the main computer is working at minimal power, so that the critical systems can be monitored while the satellite is in the launcher.

De-tumbling Mode

After the satellite is expelled from the launcher, it will start rotating due to misalignment of the force that expels the satellite from the launcher. In order to damp this rotation the satellite goes into de-tumbling mode.

In order to de-tumble, the ADCS is the most vital system on-board of the satellite. However, due to the fact that the satellite is tumbling, the solar cells will be unable to point correctly at the sun, and the satellite is unable to generate adequate power. Therefore the de-tumbling mode will be performed completely on the battery power. Using on-ground tracking, the initial position of the satellite is determined, however the orbit determination is not critical.

Start-up Mode

In Start-up Mode, all subsystems are set up such that the satellite can start performing the mission. Firstly using the GNC system, the position of the satellite is determined. Secondly the solar cells from the satellite are deployed in order to charge the batteries after the de-tumbling mode. Then the initial separation between the two satellites in the formation is determined. Finally a manoeuvre is performed using the propulsion system, in order to set the required distance between the two satellites for operations.

3.3.2 Operating Life

The operating phase starts when the satellite pair is in the correct orbit, the separation between the pair is stable, all antennas are deployed, and all systems are operational. In the following paragraphs, the different modes that occur during this phase of the satellite life are explained.

Scanning Mode

The scanning mode is the most important mode of the operational lifetime, since it is the mode where the satellites are actually performing their mission. Since the two satellites perform different functions during this mode, the mode is explained separately for each of the satellites.

Transmitter: For the transmitter the PanelSAR is in transmitting mode, this requires a lot of power. If the scanning is performed while the satellite is in sunlight, part of this power can be generated by the solar cells, however if the scanning occurs during an eclipse all the power must be extracted from the batteries. The GNC will perform measurements as often as possible (multiple times per second), in order to provide the highest position and velocity accuracy possible, which are required for the SAR data.

Receiver: The SAR payload on-board of the receiver satellite requires less power than that on-board of the transmitter, since it is only receiving and processing the data. However, on the receiving satellite the communications system is required to work at full force in order to transmit all the generated SAR data down to Earth.

Communication Mode

The communication mode is a mode specific for the receiver satellite. After the scanning is completed, there is still a part of the data that needs to be transmitted to Earth. However, the SAR payload is turned off, and only the communication system is operational.

Idle Mode

The satellite will be in idle mode when it is not scanning using the SAR payload or transmitting the payload data using the X-band antenna. In this mode the satellite is focussed on charging the batteries by pointing the solar arrays at the sun. There is no need for high accuracy on the position of the satellite, so the GNC only operates once or twice per orbit.

Safe Mode

The satellite will go into safe mode if any failure occurs on-board of the satellite. The safe mode is characterised by a shut-down of all non-essential systems on-board of the satellite. The main purpose of this mode is to preserve the satellite in the event of any error. The first action to be taken is to point the satellite towards the sun in order to satisfy the thermal and power management on-board of the satellite.

Manoeuvring Mode

The manoeuvring mode will be used when the satellite needs to perform large manoeuvres such as a plane change. In this mode the solar cells are positioned close to the body in order to increase structural integrity, however they will be moved if the plume from the propulsion is directed at the array in order to avoid damage. Communication with the ground station is necessary in order to oversee the manoeuvre and to assure that both satellites perform the same manoeuvre in order to maintain the same separation.

3.3.3 End Of Life

The End Of Life phase of the satellite is initialized when the satellite is no longer able to perform the mission. There is only a single mode in this phase of the satellite.

EOL Mode

In this mode all the subsystems on the satellite are shut off, and the solar panels are fully deployed to increase drag. The satellite will stay in this mode until it burns up in the atmosphere.

Chapter 4

Payload Instruments

This chapter looks into the operations of the Synthetic Aperture Radar instrument which is the primary payload on board of each satellite in the constellation. Furthermore, the sizing and operations of the Automatic Identification System is discussed.

4.1 Synthetic Aperture Radar

Radar, or RAdio Detection And Ranging, is a technology for finding the direction and range to a target. A common misconception is that development of this technology started during the Second World War. However, it already started in the early 1920s. In 1922, Albert H. Taylor demonstrated the first radar system using a continuous wave [14]. With these types of radar, the velocity of the target can be measured by analysing the Doppler shift of the between the transmitted and received signal. In 1934 the first pulse radar was created, which makes it possible to transmit and receive radar with only one antenna [15]. The pulse radars were optimized by the British, Americans and Germans during the Second World War.

Standard radar, for example the type used by air traffic controllers, consists of one pulsed beam. Thus, the process starts with the antenna transmitting a beam in a specific direction. This pulse will keep on travelling in the same direction until it hits a target. Depending on the geometrical shape of the target, part or all of the pulse will be reflected back towards the antenna that now acts as a receiver. By measuring the time between the transmission of the pulse and the receiving of the echo, the distance towards the target can be determined with [16].

$$R = \frac{ct}{2} \tag{4.1}$$

where R is the distance to the target, c the speed of light (approx. 3×10^8 [m/s]) and t the time between the transmission and the echo. By rotating the radar around its vertical axis, a 360 [deg] flat image can be created of the radar's surroundings.

Synthetic Aperture Radar (SAR) is the technique of mounting a radar on a moving platform. The motion of the platform causes the radar to behave as having one very long antenna. It is shown in [16] that the resolution of a radar depends on its signal wavelength λ, the antenna length L and the distance to the target D:

$$r = \frac{\lambda}{L} D \tag{4.2}$$

Thus, a longer (synthetic) radar antenna means a higher resolution r. In nearly all cases, SAR is installed on an aircraft or satellite and used to create an image of a piece of terrain. Because each pixel in the resulting image is formed out of multiple radar from different angles, no single range for that pixel exists. The only two pieces of information that form the pixel are the phase and amplitude of the returned signals.

The radar is usually installed in a side-looking configuration to avoid so-called image folding. This is because of the symmetry in the beam when it is installed nadir-looking, which causes two points to be at the same distance that can not be distinguished in post-processing [16]. The latter situation is shown in Figure 4.1a and the side-looking configuration is sketched in Figure 4.1b.

Two conventions for naming the two main axes of a radar image exists. The British designate the axis in the direction of motion the *along-track* axis (just as with spacecraft) and the perpendicular axis the *cross-track*. Continental European and American engineers usually call them *azimuth* and *range* respectively [16]. These terms are used interchangeably in literature.

The PanelSAR instrument designed by SSBV that is used by the Aegir project is a continuous wave SAR. This means that the signal emitted by the instrument is not pulsed but a continuous wave radar, like the first radar developed by Taylor. To still be able to measure the time between the transmission and the echo, the wave is modulated in a wave pattern. Because targets are illuminated constantly instead of in pulses, the required peak power of the instrument is much lower [17]. A frequency modulated continuous wave SAR (FMCW SAR) requires a bistatic configuration and therefore a transmitting

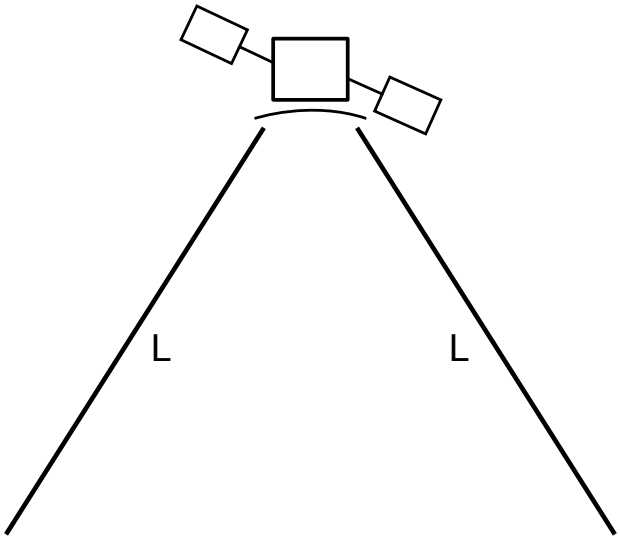

(a) A fully nadir looking configuration, which causes the beam to be symmetric. This results in many equal beam distances, which can not be distinguished from each other

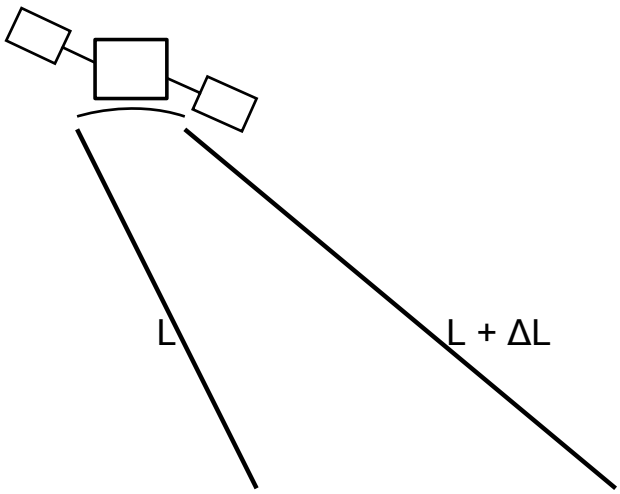

(b) A common side-looking configuration which does not have the folding problem that the nadir-looking radar has

Figure 4.1: Two different configurations of the SAR instrument

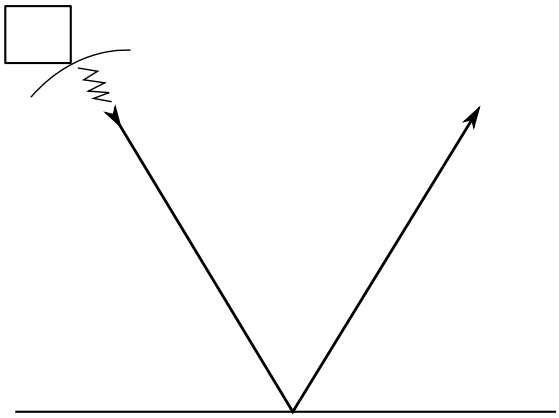

(a) In this case, the radar signal is transmitted towards a flat surface such as a flat sea. The signal reflects away from the transmitter, resulting in a low signal intensity at that spot

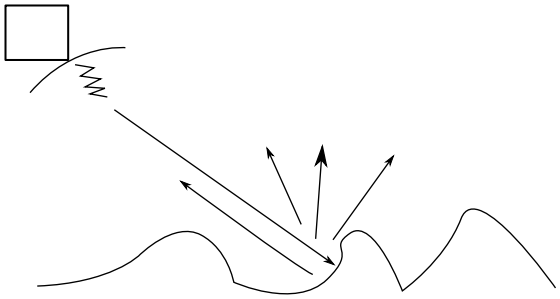

(b) When a signal encounters a rough surface such as a rough sea, the signal is partially reflected back to the SAR receiver, while most of the signals scatters in nearly all directions.

Figure 4.2: Two different situations in which the transmitted radar signal is reflected

and a receiving satellite. The closer the satellites are, the more they will behave as a monostatic SAR system. When the relative velocity between the satellites is non-zero and large, for example when the spacecraft are in different orbits or very far away from each other, the geometry of the resulting image will change drastically [18], thereby increasing processing time and costs. Therefore, a very close formation between the receiving spacecraft and transmitting spacecraft is preferred.

4.2 Ship Detection Using SAR Images

This section looks into the methods of using SAR image to detect and track maritime activity. A monostatic setup is assumed to simplify the problem, as the bistatic FMCW SAR is designed to perform similarly as a monostatic SAR.

Every ship detection method that uses SAR images has the same purpose: to find the shape of a ship through the speckle. This speckle is visible as noise on an image. If the surface of the sea is calm, the speckle level is low. When the sea is rough, the speckle level is much higher. This is due to the fact that a signal emitted by the satellite is reflected away from the satellite due to a flat sea. A larger part of the signal is reflected back to the satellite when the sea surface is rough [19]. The first case is explained in Figure 4.2a, the second case is shown in Figure 4.2b.

If a (near-)flat sea is assumed, then ships can be easily detected in a radar intensity image. The intensity image can be created from a Single-Look Complex (SLC) image. An SLC image provides the phase and amplitude of each pixel in an image, which is stored as a complex number. The magnitude of the complex number is the intensity [16]. An image can be formed of the intensities in each pixel. An example of an intensity image can be found in Figure 4.3, which is a

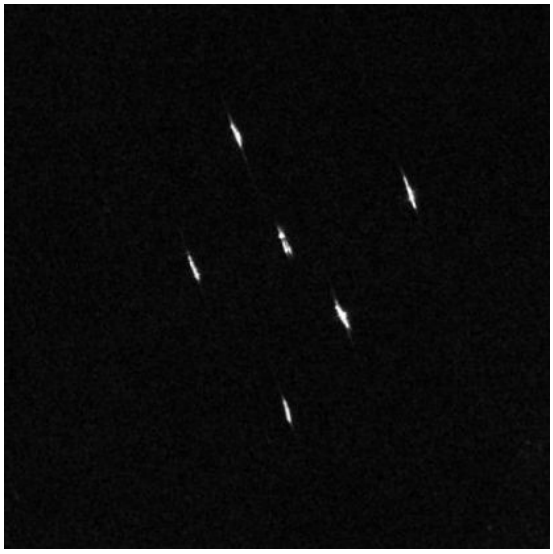

Figure 4.3: A cropped part of the Sentinel 1 capture of the western part of the Netherlands (Source: [20])

cropped image taken from a larger SAR image of the western part of the Netherlands including a piece of the North Sea. It was taken by the Sentinel 1a on the 15th of April 2014. This day was sunny with calm winds, hence there is virtually no speckling visible in the sea.

The location of the ships can be found using the Constant False Alarm Rate (CFAR) method. With this technique, a pixel cell is compared to a set of reference cells which are assumed to contain no target. Hence, the reference cells are an indication of the noise level of the sea. If the intensity of the i^{th} cell is larger than the noise level, then it is a target. This method is generally applied together with an extra margin in the noise level to account for variations in the noise levels [21]. One must be certain that the assumption that the reference cells do not contain a target is true.

CFAR is a well-performing algorithm when the sea is smooth. Nevertheless, when the sea is rough the CFAR method becomes more unreliable. Although methods have been developed that bring this unreliability down [22], there are several methods involving interferometry that are more suited for these situations.

Interferometry involves measuring the phase of one or more signals to find information about the subject being measured. The phase is always measured in modulo 2π. Hence if a signal travels a distance R, then the measured phase ϕ of the signal at R is (assuming the phase of the signal at the origin is 0) [23]

$$\phi = \frac{2\pi}{\lambda} \cdot R \mod 2\pi \tag{4.3}$$

where λ is the wavelength of the radar signal.

The phase information of one single image is not enough to get any useful information, since the phase appears randomly distributed across the image. The phase becomes useful once it is combined with a second image. For each image cell, the phase of the first image is cross-multiplied with the cell at the same location in the second image. This results in an image with so-called fringes. Figure 4.4 shows an example of such fringes. Each fringe band is a 2π cycle of the phase. The phase can change due to a lot of external influences on the surface, hence this type of image is used by remote sensing scientists for information on the Earth surface. There are three ways in which interferometry can be used to detect ships. The first two methods use two separate images. Since ships move, it is necessary to make the two images at nearly the same time. This means two separate receivers are required, looking at the same scene at the same time. When the receivers are placed on two individual satellites, two different relative positioning methods are available, namely the satellites may be separated along-track or cross-track. The former means the satellites travel behind each other in the same orbit, the latter requires two different phasing orbits to maintain a cross-track (horizontal) separation. In along-track interferometry (ATI), the cross-multiplied phase is a function of the target's velocity [25]. The phase in cross-track interferometry (XTI) is a function of the target's height and elevation. Although XTI can theoretically be used to detect ships, its engineering complexity and high error rate [26] results in a high noise level and high false alarm rate. ATI is more suited for ship detection. Firstly, because the satellites follow each other in the same track, the amount of engineering challenges is much lower. Namely, to create a cross-track configuration the satellites must have different ascending nodes, which means the satellites cross their orbits twice every orbit. Secondly, since the velocity of a ship is usually larger than the sea around it, ships will stand out as peaks in the image [27]. A drawback of the method is that stationary ships will be very hard to detect, so one may have to fall back to the intensity image to supplement the ship detection process.

The third method for ship detection, proposed by [28], is a simple method that only requires one phase image. The SAR measurement is split into two sub images through a process called multilooking. It essentially splits an azimuth beam into multiple parts. This results in two images with phase information of the same locations, though each at a lower resolution

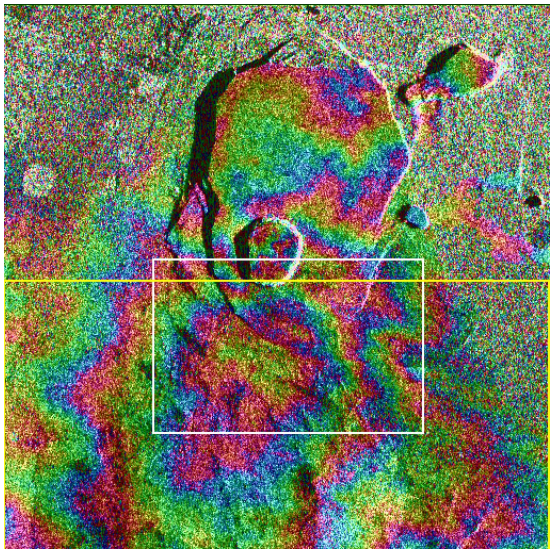

Figure 4.4: An image from the Space-borne Imaging Radar C (SIR-C) mission on-board of space shuttle Endeavor showing the interferometric fringes (Source: [24])

than can be achieved with one full image [29]. The drop in resolution is why this splitting of images is not usable for ATI. However, this new method is not influenced greatly by the drop in resolution. The next step in the technique is to create one coherence image out of the two sub images.

The coherence of two radar image cells γ is defined as [30]:

$$\gamma = \frac{E[v_1 \overline{v_2}]}{\sqrt{E[|v_1|^2]E[|v_2|^2]}} \tag{4.4}$$

where v_1 and v_2 are the complex values in the cells of image 1 and 2 respectively. $\overline{v_2}$ is the complex conjugate of v_2. Each E function is the statistical expected value of the argument. Conventionally, the mean value of a set of reference pixels is taken. The resulting coherence is a measure on the variation of the phase information between two image cells, where the value ranges from 0.0 to 1.0. A coherence of 0.0 is fully incoherent: this means the phase information is completely different between the two images. With $\gamma = 1.0$, the phase information in the two images is exactly the same. Both extremes virtually never occur in real datasets, though are found to be somewhere in between. A coherence image is a mapping in which the coherence for each cell is plotted.

Ships can be detected by analysing the coherence image. Because the sea is constantly changing, the coherence of the ship's surroundings is very low. Hence, it will show up as dark on the image. Because the shape of a ship remains constant, the coherence of the cell or cells that contain a ship is much higher. Figure 4.5 shows an example of a coherence image with ships. One is able to see the ships clearly visible within the sea. Geography is visible as well, since it is also coherent. However, this can easily be filtered out using a digital elevation model (DEM).

This coherence imaging method works best when the level of coherence of the sea is lowest. This is the case with a rough sea. Hence, the intensity image detection method could be used to supplement this technique when the sea is calm. It must be noted that the coherence imaging technique still works when the sea is calm.

To summarize, there are three practical ways for detecting ships. The first is using CFAR on an intensity image, which requires only one SAR image and hence one satellite pass. The second method is along-track interferometry, where the velocity of a ship can be measured using the phase differences. This method requires at least two receivers to be able to perform it on ship detection. The final method is using coherence imaging and experimentally yields the best results [29].

4.3 Automatic Identification System

The Automatic Identification System, or AIS, is a transponder system broadcasting the position of a ship, its direction and velocity. The system is mandatory for all new ships travelling internationally since 2002 [3]. Typically, the horizontal range of such a system is slightly over 20 [nm] (1 [nm] (nautical mile) $\approx$ 1.85 [km]) [31]. This means that monitoring of ship traffic is difficult to do from land-based receivers due to the range restriction. Furthermore, many developing countries do not have official receivers, causing large holes for monitoring networks. For this reason, space-based AIS monitoring is an attractive solution.

One or more SAR satellites in the constellation may be equipped with an AIS receiver. The AIS data can be used to filter the results from the SAR ship detection process, because both measurements are done at the same time. Data from

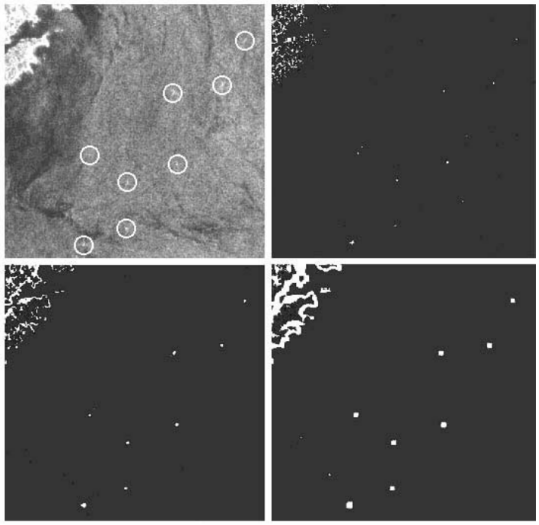

Figure 4.5: The topleft image of the Kumano Sea has eight ships circled. The three other images are coherence images of the first image, each with a different moving window size. The moving window is used to determine the mean value to calculate the coherence image. The vessels are clearly visible against the dark background (Source: [29]).

both measurements may be put on top of each other, which makes it possible for the system to find ships without an AIS signal. Moreover, streaks caused by oils spills can be easily traced back to the ship that caused them.

AIS devices broadcast over two different channels, each containing 2250 timeslots for messages to be sent. This means that a total of 4500 messages can be sent per minute. If more than 4500 messages are sent within the swath of the satellite, information will be lost. According to Eriksen [4], the optimal swath width to detect ships in and around the North Sea is 800 [nm]. A 99% detection chance for all ships is then guaranteed. If a wider swath width is chosen, the chance of saturation of the two channels becomes too large. To get a useful data the received signal should be at least -107 [dBm] for the 25 [kHz] and -98 [dBm] for the 12.5 [kHz] bandwidth. To calculate the received signal power Equation 4.5 is used. In this equation P_t is the transmitter power which is 12.5 [W], G_t is the transmitter gain equal to 3 dB, and finally λ is the wavelength which is 1.85 [m]. These values have been derived from the AIS system aboard the ships [4]. For the receiver gain (G_r) it is assumed that a straight omnidirectional antenna is used: such an antenna has a gain of 3 [dB]. The distance d is the length that the signal needs to travel and therefore is dependent on the altitude of the satellite and the ground range to be measured, which are 516 [km] and 800 [nm] respectively. From these values it can be determined that the received signal power is -93.58 [dBm], this proves that the AIS signal can be received by the satellites.

$$P_r = P_t G_t G_r \left[\frac{\lambda}{4\pi d}\right]^2 \tag{4.5}$$

The antenna that will be used is a simple whip antenna, the length needs to be an quarter of the wavelength to receive the signal [32]. The antenna will therefore be 0.6425 [m]. Furthermore, the pointing accuracy must be 1 [deg] or better. This is easily attainable, because the SAR instrument's pointing accuracy is more than that. The AIS system will gather 2 [MB] per 10000 ships, this would mean that for total coverage of the world where there are about 501442 ships with AIS [33] (found on 18-06-14) a total of 100.29 [MB] is needed. This is just a fraction of the data gathered by the SAR instrument.

The resulting numbers lead to the conclusion that it is quite possible to add an AIS receiver to one or even all spacecraft in the constellation. It is not an intensive system, since it is passively receiving the signals from the Earth and not transmitting. Therefore, it only requires a couple of Watts of electrical power to operate. The data obtained from the AIS broadcasts may be sent down to the ground stations via the same downlink as the SAR data.

Chapter 5

Launcher and Orbital Insertion Module

To comply with the mission requirements, five pairs of satellites need to be transferred to five different inclinations, as resulted from the Astrodynamic Design Chapter. This chapter therefore discusses several currently available launch vehicles to achieve the orbit altitude of the satellite pairs. To reach the designed inclination a separate module is needed. Hence, in the second part of the chapter the Orbital Insertion Module (OIM) is designed, based on the fairing of the selected launcher. Finally, a technical risk management is done for both the launch vehicle and the OIM.

5.1 Launch Vehicle

The selection procedure of the launch vehicle consists of several phases: the requirements generation, trade-off and selection.

5.1.1 Requirements

In the list below, the requirements are stated which are the results from the Astrodynamic Design Chapter 2 and the mass iteration of the spacecraft and the OIM done in this report.

- **Launch Vehicle Requirement [LVa]**: The launch vehicle shall be able to reach an altitude of 516 [km].
- **Launch Vehicle Requirement [LVb]**: The launch vehicle shall be able to reach an inclination of 64.3 [deg].
- **Launch Vehicle Requirement [LVc]**: The launch vehicle shall reach its target orbit with a payload mass consisting of 5 pairs of satellites and a module.
- **Launch Vehicle Requirement [LVd]**: The launch vehicle shall provide a volume for at least 5 pairs of satellites and a module.
- **Launch Vehicle Requirement [LVe]**: The launch vehicle shall provide protection of the spacecraft against external environment during the launch phase.

5.1.2 Trade-off

There are several aspects which have to be considered in the trade-off process, in which the following have been selected: cost, maximum payload mass, diameter/height (D/H), successes/tries (S/T) and fuel types. Resulting from the requirements stated previously, several launch vehicles can be excluded. The launch vehicle should be capable of reaching the target orbit with a mass of 6000 [kg] for the satellite pairs and an added mass of 1500 [kg] for the OIM. It should provide a volume of at least 48 [m^3] for the satellites and an estimated amount of 30 [m^3] for the OIM, which is based on the Automated Transfer Vehicle developed by the European Space Agency [34]. In table 5.1 the trade-off matrix is shown with the launch vehicles fulfilling the minimal requirements. The information on these parameters are based on the Launch Vehicle Catalog provided by ESA [35]. The star indicates that the maximum payload mass of Falcon 9 v1.1 has been estimated by comparing the fuel consumption for the inclination change of the Falcon 9 v1.0 model [36]. The dagger indicates an estimation of the total lift of mass, based on the Soyuz Fregat at the inclination of 60 [deg] and an altitude of 500 [km] [37].

5.1.3 Selection

From the list it can be deducted that the Soyuz is the most suited for the mission, as it provides an OIM for the mission and sufficient space for the five pairs of satellites needed. Besides this, the driving parameter is the cost of the launcher, as four launches are needed to send 40 satellites into space as computed from chapter 2. Although the price per kg for the Falcon 9 v1.1 or Ariane V-ECA is lower, sending another set of ten satellites is not feasible as it requires an inclination change of arround 60 [deg]. Another method to compensate this is to sell the remaining space and mass to a third party, this however

Table 5.1: Launch Vehicle Trade-off Matrix

LV	Cost [$]	Mass [kg]	D/H [mm]	S/T [38]	Fuel Type
Delta 4	150M	22700	4752/17000	2/2	LOX,LH_2
Proton K/DM-2	85M	20900	4100/15882	101/109	N_2O_4, UMDH
Ariane V-ECA	120M	18000	5400/17000	43/44	LOX,LH_2
Atlas 5	110M	8000	4570/23400	45/46	HTPB, Kerosine RP-1, LO_2
H 2A	80M	10000	4600/9124	23/24	HTPB, LH_2, LO_2
Falcon 9 v1.1	61.2M [39]	12755*	4600/11400	4/4	LOX,Kerosine RP-1
Soyuz 2-1b/Freg	40M	7000 †	3800/9518	11/12	Kerosine, UMDH, LO_2, N_2O_4

should be done four times due to the four launches and is therefore not mission efficient. Another downside is the usage of kerosene which reacts with oxygen to carbon dioxide, monoxide, hydrocarbon and with contact with air, nitrogen oxides which have an environmental impact on the ozone layer [40] [41]. However, this is of secondary importance compared to the cost of the launcher.

Note that the Soyuz 2-1B uses Unsymmetrical DiMethyl Hydrazine (UMDH). This substance is carcinogenic and is listed as a hazardous air pollutant in "the National Emissions Standards for Hazardous Air pollutants" by the Environmental Protection Agency [42]. However, this is used only for the fregat and not during the three stages where it might damage the environment.

Besides the cost of the launcher, the number of launches of the Soyuz 2-1B/Freg is relatively low. Nevertheless, this Soyuz rocket series have been launched more than 800 times and have a successes to tries ratio of 97.4%. Another advantage of the Soyuz is the provided fregat which can act as the OIM needed for the mission.

5.2 Orbital Injection Module

The fregat provided with the Soyuz 2 launcher can act as the propulsion system of the Orbital Injection Module of the mission. There are however functions and requirements for the fregat to be considered. This section discusses the usability of the chosen fregat and provides the design and arrangement of the OIM and its propulsion and structural subsystem. It is assumed that the other subsystems are provided with the fregat.

5.2.1 Functional Breakdown Structure

The following Functional Breakdown Structure Figure 5.1 shows what functions are involved in inserting the satellites into the required orbits in order to achieve formation flying and desired constellation of satellites:

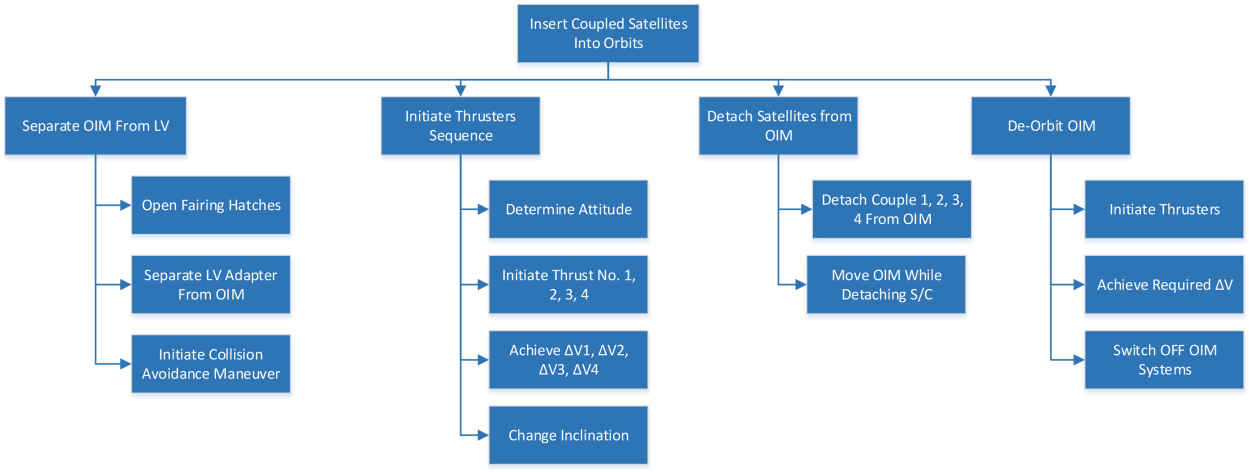

Figure 5.1: OIM Functional Breakdown Structure

As it can be seen, OIM FBS is split into 4 main sections. It consists of the Separate OIM From Launch Vehicle phase, followed by the Initiate Thrusters Sequence phase, in which the satellite pairs are inserted in their required inclinations. It is decided to use a separate propulsion system for OIM to achieve this phase. The next important part is detaching the satellite pairs from the OIM. Finally, a de-orbiting phase is achieved. It includes removing OIM safely from the space to the Earth's atmosphere.

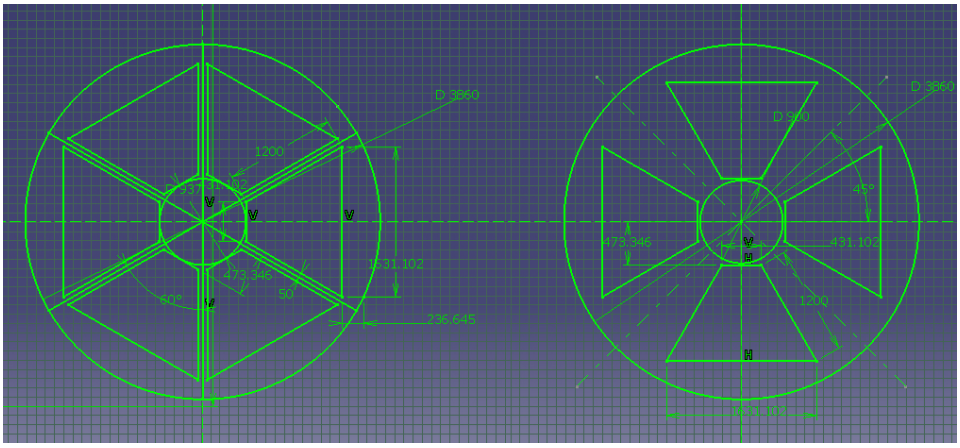

Figure 5.3: Arrangement of the Satellite Pairs in the Fregat

5.2.2 Functional Flow Block Diagram

The FFBD of the OIM can be found in figure 5.2.

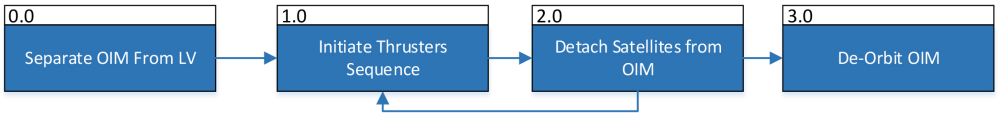

Figure 5.2: Top Level of the Functional Flow Block Diagram of the OIM

5.2.3 Requirements

The requirements concerning the OIM are listed in this subsection. These are derived from the orbit [BSAR-1c] in chapter 2.

- **Orbital Injection Module Requirement [OIMa]**: The OIM shall provide multistage orbital injection of the satellite pairs.
- **Orbital Injection Module Requirement [OIMb]**: The OIM shall provide an end-of-life manoeuvre.
- **Orbital Injection Module Requirement [OIMc]**: The OIM shall fit in the fairing of the Soyuz 2-1A/Fregat launcher.
- **Orbital Injection Module Requirement [OIMd]**: The OIM shall provide a structural support for the satellites.

5.2.4 Arrangement

To accommodate requirement [OIMc] and the set of five pairs of satellites in the fairing of the launcher, several constraints and parameters have to be considered. The fairing's dimensions and location of the fregat's propulsion system may be found in the Soyuz User's Manual [43]. These dimensions determine the outer boundaries of the design of the OIM.

Another constraint is the size and form of the satellite. The length of the satellite is determined to be 2.1 [m] to accommodate for efficient space usage in the launcher. This allows for a maximum of two levels of satellites. Due to the minimal width of 1.6 [m] to fit the SAR panels and other communication instruments, a maximum of 6 satellites in a round configuration is possible. Other configurations such as a square or a triangular formation are not efficient in space usage. The round configuration provides a central structural pillar and simple mechanisms to eject the spacecrafts from the module.

For the arrangement, six satellites at the lower level and four at the upper level is chosen. This is done as this results in lower mass for the structural system of the OIM as the bending loads reduces. The arrangement of the satellites can be seen in Figure 5.3, where the left figure shows the configuration of the lower level and right the upper level of the OIM.

5.2.5 Propulsion Subsystem

Although a propulsion system is delivered with the fregat, it should comply with the subsystem requirements of the OIM. These requirements are based on the results from chapter 2 and requirements [OIMa] and [OIMb].

- **OIM Propulsion Subsystem Requirement[OIMPROPa]**: The OIM's propulsion subsystem shall provide at least 5 pulses.

- **OIM Propulsion Subsystem Requirement[OIMPROPb]**: The OIM's propulsion subsystem shall provide a maximal burn time of 60 [s].
- **OIM Propulsion Subsystem Requirement[OIMPROPc]**: The OIM's propulsion subsystem shall provide a delta V of 166 [m/s] for each stage.
- **OIM Propulsion Subsystem Requirement[OIMPROPd]**: The OIM's propulsion subsystem shall provide a delta V of 10 [m/s] for the de-orbit phase.
- **OIM Propulsion Subsystem Requirement[OIMPROPe]**: The OIM's propulsion subsystem shall provide a fuel storage system.

The manual of Soyuz User's Manual by Arianespace shows that the fregat is able to provide 20 pulses which is sufficient for the orbital injection. Requirement [OIMPROPb] can be checked by applying equation 5.1 [44]. This results in a thrust of 16.3 [kN] for UMDH with a specific impulse of 327 [s] and a burn time of 60 [s] which results in a propellant mass usage of 305 [kg]. The fregat is able to deliver 19.6 [kN], so this is sufficient.

$$T_{min} = g_0 I_{sp} \frac{m_{burn,max}}{t_{burn}} \tag{5.1}$$

The propellant mass and volume required are listed in table 5.2 per stage.

$$m_p = m_i(e^{\frac{\triangle V}{I_{sp} g_0}} - 1) \tag{5.2}$$

The propellant mass is calculated using Equation 5.2 [44]. A nominal and a residual margin of 15 % and 1.5 % respectively have been applied to the propellant mass. To calculate the volume, equations 5.3, 5.4 and 5.5 is applied. An average value of 2.025 has been taken for the mixture ratio [43]. This results in 0.411 [m^3] for UMDH with a density of 789 [kg/m^3] and 0.575 [m^3] for oxygen with a density of 1142 [kg/m^3] [45]. The propellant tanks are present in the fregat and are assumed to be sufficient.

$$m_{fuel} = \frac{m_{prop}}{1 + O/F} \tag{5.3}$$

$$V_{fuel} = \frac{m_{fuel}}{\rho_{fuel}} \tag{5.4}$$

$$V_{fuel} = \frac{m_{ox}}{\rho_{ox}} \tag{5.5}$$

Table 5.2: Required delta V per stage

Stage	Mass [kg]	Oxidizer/Fuel Volume [kg/m^3]
I	355	0.149/0.209
II	278	0.117/0.163
III	206	0.086/0.121
IV	136	0.057/0.080
de-orbit	4	0.002/0.002
Total	**979**	0.411/0.575

5.2.6 Structural Subsystem

A support structure inside the launcher is required in order to launch 10 satellites with one rocket. The satellites will be attached to this structure so it can support the mass of all 10 satellites.

- **OIM Structural Subsystem Requirement [OIMSTRUCTa]**: The OIM's structural subsystem shall be able to withstand the loads during the launch phase.
- **OIM Structural Subsystem Requirement [OIMSTRUCTb]**: The OIM's structural subsystem shall have a diameter smaller than 930 [mm].
- **OIM Structural Subsystem Requirement [OIMSTRUCTc]**: The OIM's structural subsystem shall be lighter than 200 [kg].

The structure will be a cylinder with a diameter of 937 [mm]. This diameter is small enough to allow enough space in the fairing for the satellites. This way the structure will fit perfectly onto the adapter that has the same diameter. A thickness of 4 [mm] has been chosen. This results in a weight of 79.7 [kg]. Calculations have shown that this structure can easily withstand the forces applied to it. In order to take into account the extra structure and mass that is needed at the mounting points another 20 [kg] is assumed to be needed. So the total mass of the support structure is 100 [kg].

5.3 Risk Management

Resulting form the Baseline Report, it had been concluded that the launcher risks were high to moderate. These are observed more carefully and analysed in this section. Besides these risks, the risks concerning the Orbital Injection Module have been added.

5.3.1 Identification and Assessment

The identification and assessment process of the risk management is divided into two parts. The first part elaborates the risks related to the launch vehicle and the second part related to the OIM.

Launch Vehicle

The launch vehicle risks can be split up into its different stages. The failure of each stage is catastrophic and is therefore critical. This failure can have a significant impact on the environment as well and should be handled carefully.

Other risks of the launch vehicle includes minor problems, such as initial ignition failure and launch vehicle software problem which delays the mission. Though this will not have high impact on the mission performance.

OIM

There are several risks involved in the Orbital Injection Module. One of these is the failure of the main thruster. As the fregat is provided, tested and proven, the likelihood is very low and the impact of the failure however will result in the loss of ten satellites which is a fourth of the total. This will result in a lower temporal resolution, though will not result in mission failure.

Next to it, is the failure to eject a satellite. Ejection failure can result in losing one satellite, this as a consequence will inevitably lose in losing two satellites as the satellites work in pairs. This will result in a reduced performance of the mission, though will not deteriorate the mission as the main thruster failure.

Other risk can involve in the structural and propulsion subsystem failure. Failure in the structural system will result in damaged payload or other instruments. Failure of the propulsion subsystem's restarting ability results in the failure of the OIM's main task to bring the satellite to its correct orbit.

The assessment of the risks is shown in table 5.3. The impact and likelihood are categorized: very low, low, medium, high, very high.

Table 5.3: Technical Risk Assessment Table

RN	Risk Title	Impact	Likelihood
F-LV1	Launch Vehicle Stage Failure	VH	VL
F-LV2	Initial Ignition Failure	L	M
F-LV3	Launch Vehicle Software Problem	L	H
F-OIM.PROP1	Main Thruster Failure	H	VL
F-OIM.PROP2	OIM Thruster Restart Failure	M	VL
F-OIM.MECH1	Satellite Ejection Failure	M	M
F-OIM.STRUCT1	OIM Structural Subsystem Failure	H	L

5.3.2 Risk Analysis and Mitigation

The risk map concerning the launch vehicle and the OIM is located in Appendix B.

5.3.3 Mitigation

There are several mitigation of risks which should be done. Note that most of the risks in the risk map are not able to mitigate as failure would lead to mission failure. As the structural subsystem and its mechanism is yet to be proven it might induce problems and should be tested extensively to reduce its occurrence.

Chapter 6

Guidance, Navigation and Control

The Guidance, Navigation and Control (GNC) has, as its name implies, three main tasks. Guidance is the orbital control part of the system. This means that information on the current orbit of the spacecraft and its targets is used to calculate the future path and control inputs. This orbital information is retrieved from the navigation part of the subsystem. Thus, navigation is determining the current position and motion of the spacecraft and hence its orbital parameters. The spacecraft is then controlled by the control part of the subsystem [46]. Within this mission, the third task, the control, is performed by a combination of the propulsion system and the ADCS. The entire subsystem is vital for the formation flying being performed during this mission. It is required for separation control and simply knowing where the other spacecraft within the bistatic radar pair is.

This chapter will focus on the guidance and navigation tasks of the subsystem. First, the components on board the spacecraft will be described for it to be able to perform orbit determination. Secondly, the procedures and safety margins of the formation control and the orbital control are defined. This describes the guidance part of the GNC. Thirdly, the risks of the subsystem are presented with finally the verification and validation of the methods that have been used.

6.1 Navigation

The basis of the mission is to use a Synthetic Aperture Radar for ship detection. To perform this, the orbit must be determined highly accurately. It has been shown by Rigling and Moses [47] that the accuracy of determining the spacecraft's velocity is the most critical. In the Mid-Term Report, the method was used to determine that the accuracy must be less than 1 [cm/s] [5]. Furthermore, the subsystem shall be available for the entire lifetime of the spacecraft system, namely five years. These values are set as requirements for the navigation. These are as follows:

- **Subsystem Requirement [GNC1a]**: The GNC system shall be able to provide guidance and navigation during formation flying
- **Subsystem Requirement [GNC2b]**: The GNC system shall have a minimum lifetime of 5 years.
- **Subsystem Requirement [GNC2e]**: The GNC shall determine the velocity of the spacecraft with an accuracy of 1 [cm/s]

It must be noted that the numbering of these requirements shows some missing requirements. This is because several requirements on the weight and sizing of the system were found to be unnecessary.

One of the only options able to obtain the stated accuracy are the Global Navigation Satellite Systems or GNSS. This only requires a relatively small receiver on board to be able to find the position and velocity vector of the spacecraft. It is furthermore capable of synchronising time between spacecraft [48] within an accuracy of 5 [ns] [49]. This is useful for the data processing of the bistatic SAR data which would otherwise require a dedicated direct data link for time synchronisation between the two spacecraft in each pair.

The NASA JPL's BlackJack receiver has been shown to be able to perform at the required accuracy [50], though it is not available as a commercial-of-the-shelf product. A device that is able to perform similarly is the Septentrio PolaRx2, which is available for roughly €10,000 per device [51]. The accuracy of the PolaRx2 is between 1.5 [mm/s] and 1.9 [mm/s] in the velocity vector and between 1 [cm] and 2 [cm] for the position determination [52].

At least one antenna is required for the operation of the device. It is assumed that the antenna is to be designed for the primary civilian L1 GPS channel, which has a wavelength of approximately 0.19 [m]. A simple monopole antenna is the most efficient when the length is a multiple of the quarter wavelength [32], hence the minimum antenna length is 0.19 [m]$/4 = 0.0475$ [m] or 4.75 [cm]. This means that a second antenna can easily be added due to its small size. These antennas are directly connected to the PolaRx2 so no additional processors are necessary.

For on-orbit validation of the GNSS data, Satellite Laser Ranging (SLR) capabilities are used. The SLR is a network of ground stations that are able to precisely determine the locations, velocity and orbits of the target spacecraft within a

couple of millimetres using lasers [53]. This is within the same accuracy range provided by the PolaRx2 and can hence be used to provide orbit references to complement the GNSS data. It must be noted that the post-processing time of the SLR data is quite high, so it can't be used as a real-time positioning method in the same way as a GNSS receiver.

6.2 Guidance

The guidance part of the GNC consists of the formation control and orbital control and does not consist of any new hardware for the spacecraft. This is because the navigation and guidance processing is assumed to be done by the main on board computer defined within the TT&C subsystem where the navigational equipment feeding information has been defined in the previous section. This section will look into the protocols and logic to perform the formation and orbital maintenance.

The formation management is done with the *chief-deputy* method, where the chief is assumed to be in a stable, near circular orbit. The deputy is then responsible for maintaining the separation between the two spacecraft. This separation is defined in requirement GNC2f:

- **Subsystem Requirement [GNC2f]**: The GNC shall maintain a separation of 200 [m] to 2 [km] between spacecraft within a formation

This requirement was defined in the Midterm Report for optimum operation of the SAR instrument.

During orbital management operations, the formation can be kept the same by performing impulsive burns at the same time, assuming the changes are small. When large orbital transfers are required, the ground control must increase the separation between the spacecraft in the formation and then perform the burn. This is necessary to reduce the risk of collision during the transfer.

For analysis of the formation, a relatively new method is used that was developed mainly for the TerraSAR-X/TanDEM-X formation [54, 55]. It is based on the classic Hill or Clohessy-Wiltshire equations. These equations model the relative motion between a stable orbiting reference, in this case the chief satellite, and a second chasing satellite: the deputy. The reference frame is an inertial Cartesian reference frame with the chief satellite at the origin. The model is based on the fact that this reference frame rotates around a centre located at a large distance from the chief satellite. The equations were initially developed for rendezvous operations though eventually they were found to be useful for modelling formations of satellites [56]. A problem with these equations is that it is difficult to model perturbations. The TSX/TDX model works around this problem by rewriting the equations into terms of the standard Keplerian orbital elements [57].

First, it is assumed, as stated earlier, that the chief satellite is in a stable, near circular orbit (i.e. $e \ll 1$). Besides, the deputy is assumed to be very close to the chief (e.g. between 200 [m] and 2 [km] as stated in the requirements). Because the Hill equations are a linearisation, they are only allowed to be used with these conditions. The Hill reference frame is defined with the following right-hand coordinate axes [58]: the $\boldsymbol{e_R}$ axis points in the radial direction ('up'), the $\boldsymbol{e_T}$ axis is parallel to and in the same direction as the motion vector. The third axis, the $\boldsymbol{e_N}$ axis is in the cross-track direction. The axes are always oriented as the LVLH (Local Vertical, Local Horizontal).

The extended model works by analysing the relative inclination vectors $\boldsymbol{\Delta i}$ and the relative eccentricity vector $\boldsymbol{\Delta e}$ [57]. Assuming a very small difference in inclination between the two spacecraft in the formation, the inclination vector is then defined as

$$\boldsymbol{\Delta i} = \begin{Bmatrix} \Delta i_X \\ \Delta i_Y \end{Bmatrix} = \sin \delta i \begin{Bmatrix} \cos\theta \\ \sin\theta \end{Bmatrix} \tag{6.1}$$

with the angle θ as the argument of latitude where the orbits of both spacecraft cross each other. The magnitude of the difference in inclination is described by δi. Note that the argument of latitude is defined as the sum between the true anomaly and the argument of periapsis: $u = \nu + \omega$ [59]. The absolute eccentricity vector of a spacecraft $\boldsymbol{e}$ is defined with respect to the argument of periapsis ω as:

$$\boldsymbol{e} = \begin{Bmatrix} e_X \\ e_Y \end{Bmatrix} = e \cdot \begin{Bmatrix} \cos\omega \\ \sin\omega \end{Bmatrix} \tag{6.2}$$

Hence, the vector is pointing towards the periapsis of the orbit and has a magnitude equal to the scalar eccentricity of the orbit. Taking the difference between the eccentricity vectors of both spacecraft results in

$$\boldsymbol{\Delta e} = \boldsymbol{e_2} - \boldsymbol{e_1} = \begin{Bmatrix} \Delta e_X \\ \Delta e_Y \end{Bmatrix} = \delta e \begin{Bmatrix} \cos\varphi \\ \sin\varphi \end{Bmatrix} \tag{6.3}$$

Equation 6.3 shows two new values: the difference in scalar eccentricity δe and the $\boldsymbol{e}$-vector phase angle φ.

D'Amico and Montenbruck [55] have shown that the Hill equations can be written in matrix form as:

$$\begin{Bmatrix} r_R/a \\ r_T/a \\ r_N/a \end{Bmatrix} = \begin{bmatrix} \Delta a/a & 0 & -\Delta e_X & -\Delta e_Y \\ \Delta u & -3\Delta a/a & -2\Delta e_Y & +2\Delta e_X \\ 0 & 0 & -\Delta i_Y & +\Delta i_X \end{bmatrix} \cdot \begin{Bmatrix} 1 \\ u - u_0 \\ \cos u \\ \sin u \end{Bmatrix} \tag{6.4}$$

Here, every r value is a coordinate in the Hill frame ($\boldsymbol{e_R}$, $\boldsymbol{e_T}$, $\boldsymbol{e_N}$). These coordinates, together with the difference in semi-major axis Δa, have been made non-dimensional using the value for the semi-major axis.

Eq. 6.4 may be used to solve the relative motion of the spacecraft for u. Figure 6.1 shows the motion history of 1000 orbits with two arbitrary though parallel relative $\boldsymbol{e}/\boldsymbol{i}$-vectors. In this simulation the difference in semi-major axis $\Delta a/a$ is set to 0. It is clear that the motion shows a repeating elliptical pattern with the chief at the centre. A nearly identical pattern

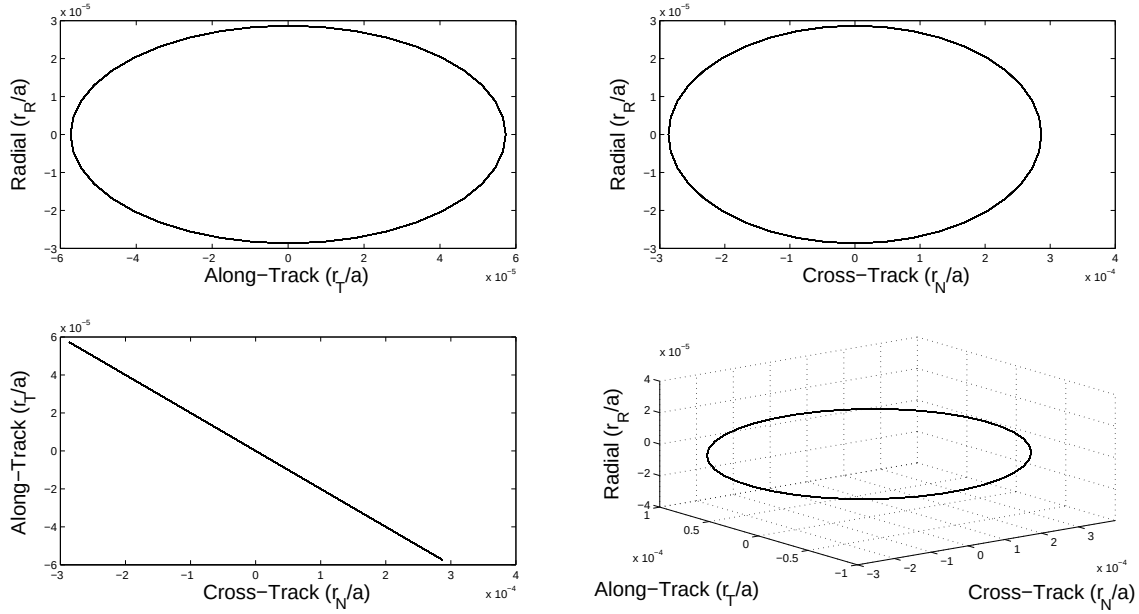

Figure 6.1: The relative motion of the deputy with respect to the chief over 1000 orbits in a non-perturbing environment with parallel $\boldsymbol{e}/\boldsymbol{i}$-vectors

is visible when the same initial conditions are used, though with orthogonal $\boldsymbol{e}/\boldsymbol{i}$-vectors in Figure 6.2.

The geometry defining the ellipsoid shown in the Figure is presented in Figure 6.3. The axes are either linearly dependent on $a\delta i$ or $a\delta e$ [55]. Requirement *GNC2f* states that the separation between the two spacecraft must lie between 200 [m] and 2 [km]. Hence, with a semi-major axis of the orbit equal to 6894 [km], the values of δi and δe may be found:

$$\delta i = \frac{a\delta i}{a} = \frac{2000 \text{ [m]}}{6.894{\times}10^6 \text{ [m]}} = 2.901 \times 10^{-4} \text{ [rad]} = 1.662 \times 10^{-2} \text{ [deg]}, \tag{6.5}$$

$$\delta e = \frac{a\delta e}{a} = \frac{200 \text{ [m]}}{6.894 \times 10^6 \text{ [m]}} = 2.901 \times 10^{-5}, \tag{6.6}$$

Thus, two small manoeuvres are required to create a stable formation. If it is assumed the two spacecraft are following each other in exactly the same plane, then the ΔV required for starting up the formation can be calculated. Using simple trigonometry, it can be shown that the amount of ΔV required for the inclination change is equal to [46]

$$\Delta v_i = 2v \cdot \sin\left(\frac{\delta i}{2}\right) = 2 \cdot \sqrt{\frac{\mu}{a}} \cdot \sin\left(\frac{\delta i}{2}\right) = 2.206 \text{ [m/s]} \tag{6.7}$$

with $\mu = GM_{Earth}$. For the ΔV due to the change in eccentricity, standard Keplerian equations [46] can be used:

$$e = \delta e = 2.901 \times 10^{-5} \tag{6.8}$$

$$r_a = a(1+e) = 6.894 \times 10^6 \cdot (1+e) = 6.8942 \times 10^6 \text{ [m]} \tag{6.9}$$

$$\frac{v_{new}^2}{2} = \frac{\mu}{r_a} - \frac{\mu}{2a} \rightarrow v_{new} = 7.603 \times 10^3 \text{ [m/s]} \tag{6.10}$$

$$\Delta v = |v_{new} - v| = |v_{new} - \sqrt{\frac{\mu}{a}}| = 0.2206 \text{ [m/s]} \tag{6.11}$$

Hence, the total ΔV required for the two initial manoeuvres is 2.206 [m/s] $+ 0.2206$ [m/s] $= 2.4266$ [m/s]. One must note that if the assumption of the equal orbit is not fulfilled, the total ΔV shall decrease, as it is expected that the differences in eccentricity and inclination shall lie in the safe range between zero and twice the target value.

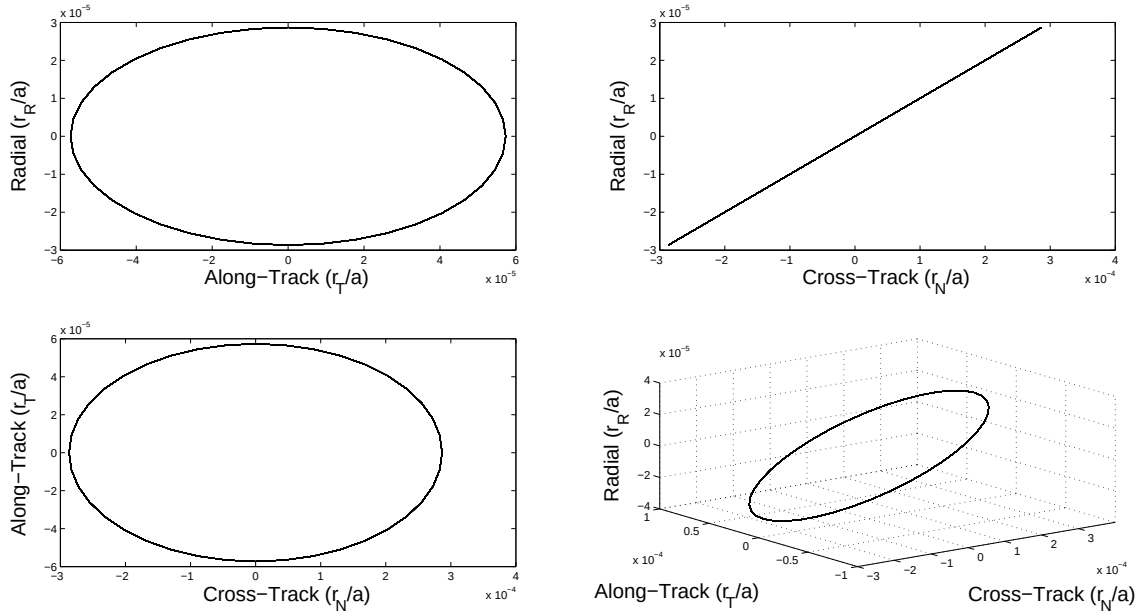

Figure 6.2: The relative motion of the deputy with respect to the chief over 1000 orbits in a non-perturbing environment with orthogonal $\boldsymbol{e}/\boldsymbol{i}$-vectors

The magnitude of the $\boldsymbol{e}/\boldsymbol{i}$-vectors has been found, though not their phasing angles φ and ω. The following method to find these angles presented in this section is based on the separation of $\boldsymbol{e}/\boldsymbol{i}$-vectors already used for GEO satellite systems [60]. Although a different $\boldsymbol{i}$-vector is used in the GEO methods, the $\boldsymbol{i}$-vector in the new method is defined in such a way such that the method for GEO satellites can still be used [55].

As can be seen in Figures 6.1 and 6.2 the ellipsoid does not change shape at a different angle, only its orientation with respect to the local vertical. When the $\boldsymbol{e}/\boldsymbol{i}$-vectors are parallel (Figure 6.1), the ellipsoid is orthogonal to the r_N/r_T plane. This means the deputy crosses the origin in this plane. This does not necessarily mean they collide: because at the point at where they cross, the separation in the other two planes is at a maximum. When the $\boldsymbol{e}/\boldsymbol{i}$-vectors are orthogonal to each other (Figure 6.2), the deputy crosses the origin in the r_R/r_N plane. According to D'Amico *et al.* [55], the radial (r_R) and cross-track (r_N) separation and relative velocity between the spacecraft are generally determined more accurately than the separation in along-track direction (r_T). Due to these higher uncertainties in the along-track direction, the chief spacecraft appears to move away from the origin in along-track direction. If the $\boldsymbol{e}/\boldsymbol{i}$-vectors are set to be orthogonal, a collision might occur because of the chief passing through the path of the deputy. There is no risk of this happening when the $\boldsymbol{e}/\boldsymbol{i}$-vectors are parallel, because the paths cross in a different plane. Hence, for the safest formation, the $\boldsymbol{e}/\boldsymbol{i}$-vectors are set to be parallel to each other.

Now the formation has been defined, it becomes necessary to look at the perturbations influencing the relative orbits of the two spacecraft. The model defined in Equation 6.4 always results in a stable configuration, which in reality is impossible due to many external perturbations. It is assumed that the spacecraft are close enough to each other so that most perturbations have the (nearly) same effect on both spacecraft at each point in time. The only two significant effects left are effects of differential drag and the perturbation due to the Earth's oblateness. This perturbation consists out of many different 'J' factors, though the J2 term normally has the largest effect and hence will be used to model the perturbation it

The J2 effect causes a change in the value of the argument of periapsis [61]. This, in turn, causes a change of the phase angle φ of the $\boldsymbol{e}$-vector [57]:

$$\boldsymbol{\Delta e} = \delta e \cdot \begin{Bmatrix} \cos(\varphi_0 + \varphi' u) \\ \sin(\varphi_0 + \varphi' u) \end{Bmatrix} \tag{6.12}$$

with

$$\varphi' = \frac{d\varphi}{du} = \frac{3}{2}\gamma\left(5\cos^2 i - 1\right) \tag{6.13}$$

$$\gamma = \frac{J_2}{2}\left(\frac{R}{a}\right)^2 \frac{1}{(1-e^2)^2} \tag{6.14}$$

where J_2 is the constant of the largest factor describing the Earth's oblateness. The value R is the radius of the Earth at the equator. Equation 6.12 may replace Equation 6.2 and can then be used to model the relative motion of the spacecraft with J2 perturbation. Figure 6.4 shows the effect of the perturbations on the relative motion of the formation. The initial

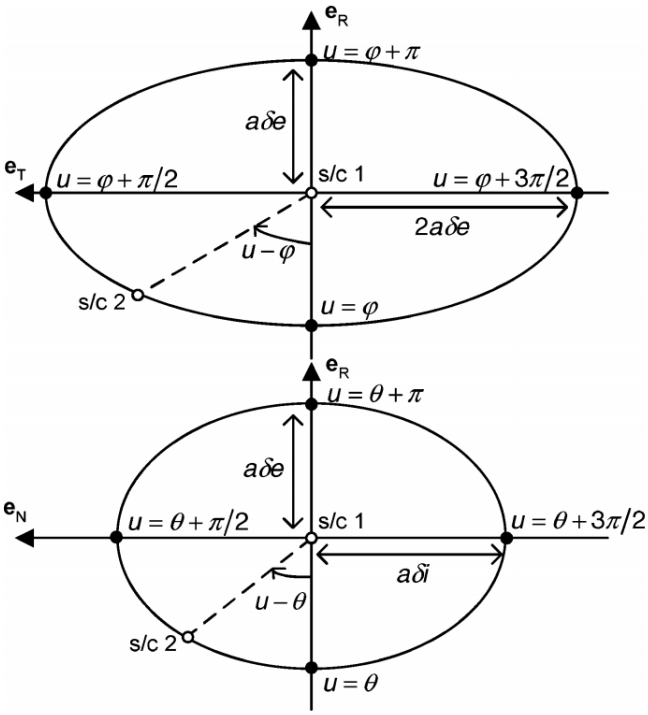

Figure 6.3: The geometry of the ellipsoid which is described by the deputy spacecraft. (Source: [55])

conditions are exactly the same as in Figure 6.1. It is clear that the effect of the J2 perturbations is very small over each individual orbit. The relative geometry starts exactly the same as in Figure 6.1, though the plane of the ellipsoid slowly rotates around the r_N and r_T axes, creating a rectangular box in which the deputy is moving and which it does not leave.

Because φ is increasing linearly, the e/i-vectors will constantly change to being parallel and back to orthogonal with respect to each other. Since it was determined for safety reasons that the eccentricity and inclination vectors must not be orthogonal to each other, the induced motion must be countered. This can be done by keeping the eccentricity phase angle φ equal to zero. From [55], the required daily ΔV to compensate the J2 effect can be approximated by

$$|\Delta v| \approx (3 \times 10^{-5})(a\delta e)/s \tag{6.15}$$

Hence the daily required ΔV for this mission is $(3 \times 10^{-5})(300\ \text{[m]})/\text{[s]} = 0.0060$ [m/s]. Multiplying this with 5 years results in a total ΔV of 10.95 [m/s]. This Equation is the reason why $a\delta e$ was chosen to be 200 [m], and not 2000 [m] as it results in a lower amount of ΔV.

A different problem is the one due to differential drag between the two spacecraft. Because of a difference in drag, a relative acceleration is present. This difference is nearly always there, even if the spacecraft would have been built completely identical. This is because there are always differences in fuel that has been consumed and differences in attitude. These both influence the ballistic coefficient $C_D \frac{A}{m}$ as defined in chapter 7. The amount of ΔV budgeted for counteracting the effect has been found in the same chapter, and is equal to 9.57 [m/s].

It has been determined in this section that an amount of ΔV must be added to the deputy spacecraft for formation maintenance. This is to be added on top of the already available ΔV budget for orbital maintenance. Because the 'receiving' spacecraft (which receives the SAR signal) has a lighter power system, it is decided that the fuel is added to this satellite. This means the receiver is designated deputy and the other spacecraft is automatically the chief.

Communication between the two spacecraft will be performed via the ground using the standard command and data link, since position updates are not required at a very high frequency. This is because the motion of the spacecraft can be easily modelled and predicted at each point.

6.3 Sensitivity Analysis

A sensitivity analysis of the GNC design is required to make sure that the current design does not change too much when certain design parameters change. The choice for the PolaRx2 is fully fixed, because the required velocity accuracy stated by requirement *GNC2e* will not change. Therefore, the focus of the sensitivity analysis will lie on the guidance part of the GNC.

The semi-major axis in Equations 6.5 and 6.6 is varied slightly to see the effect of the changes further in the calculations. For the analysis, the semi-major axis is varied 100 [km] up and 100 [km] down from the nominal value. Going through the calculations, the total ΔV for $a_{+100} = 6.994 \times 10^6$ is equal to 2.375 [m/s]. This is a 2.2% decrease in ΔV for the formation

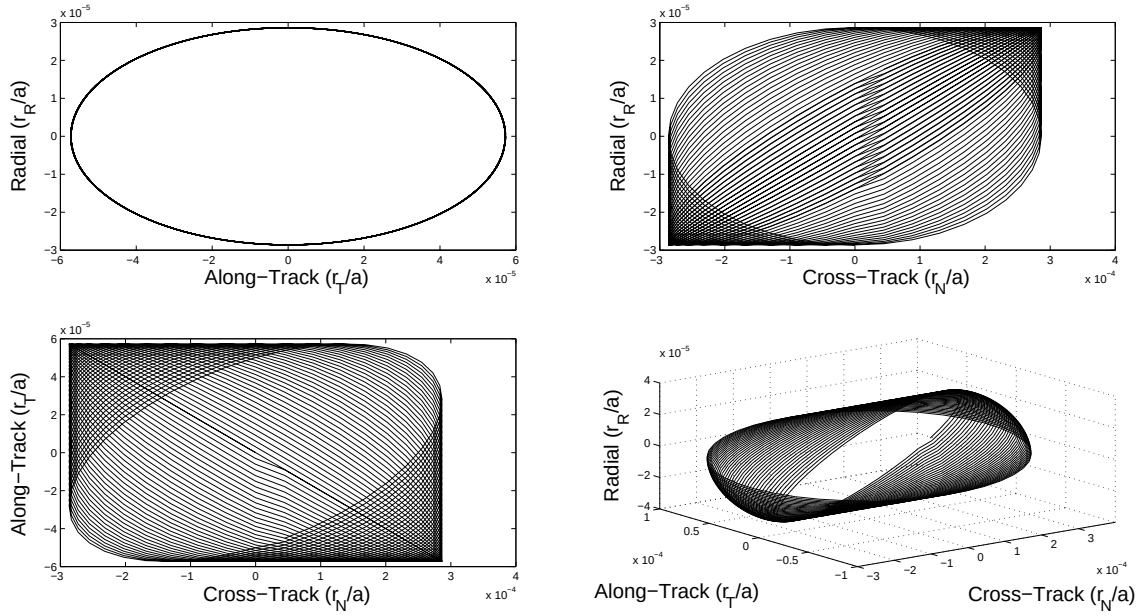

Figure 6.4: The relative motion of the deputy with respect to the chief where the J2 effect affects the motion over 2000 orbits. The e/i-vectors are in this case parallel. Only one in fifty orbits has been plotted for clarity.

initialisation, which is not found significant. Doing the same for $a_{-100} = 6.794 \times 10^6$ yields a ΔV equal to 2.480 [m/s], which is a 2.2% increase. Thus, the amount of ΔV required for stabilising the initial formation is linearly dependent on the semi-major axis. The same may be said about Equation 6.15, as it is a simple approximation in linear form.

To conclude, the ΔV required for the formation control of the mission changes linearly when either the semi-major axis is changed or when the separation due to difference in eccentricity δ_e is changed.

6.4 Risk Management

The GNC subsystem only consists of the GNSS receiver and its antennas, therefore the amount of total risks is low. The main risk is total failure of the GNSS receiver. This would mean that the spacecraft would not be able to autonomously determine its orbit and relative position within the formation. A collision between spacecraft in a formation may be the result. This can be mitigated by adding multiple GNSS receivers at the expense of increased costs. An extra backup is using the data link to track the spacecraft from the ground. When this is done, the tracking information has to be uploaded back to the spacecraft using the same data link.

It is possible that the GNSS antenna itself is very hard or impossible to point in the right direction towards the GNSS satellites as well. This might mean the loss of the GNSS signals. A simple mitigation strategy is adding a second antenna which, as has been shown in section 6.1, is very easy and inexpensive.

A third risk is the fact that the PolaRx2 has not been flight-tested for longer than 5 years. It has been flight-tested for just under two years [62]. Although it did not show any signs of failure, there is some uncertainty. This risk can be mitigated by adding cold redundant receivers.

The final risk that has been identified is the loss of the ability of communicating the locations and orbits between spacecraft in a formation. This is especially a problem if it results in the deputy spacecraft not knowing where the master is, because then formation flying becomes impossible. There is no direct mitigation available, though the likelihood of this risk is low.

All the risks are shown together in Table 6.1 without taking mitigations into account. When the mitigations are included as described in this section, the impact or likelihood of the failures will decrease. As a result, the total risks will go down.

Table 6.1: The risks related to the GNC subsystem

RN	Risk Title	Impact	Likelihood
GNC-GNSS1	Failure of GNSS/GPS module	VH	M
GNC-GNSS2	GNSS Antenna pointing failure	M	H
GNC-GNSS3	Uncertainty in GNSS Receiver lifetime	M	M
GNC-FORM1	Failure in communicating orbit information within formation	H	L

This is shown in Table 6.2.

The two tables shown in this section are visualised as risk maps in appendix B, Figures B.1e and B.1f.

6.5 Architecture

The navigation subsystem is the only part of the GNC that contains dedicated hardware to be added to the spacecraft. Furthermore, it only consists of three main components: two antennas and three GNSS receivers/processors. Hence, the architecture is fairly simple, which is shown in Figure 6.5. The subsystem consists of three main GNSS processor/receivers,

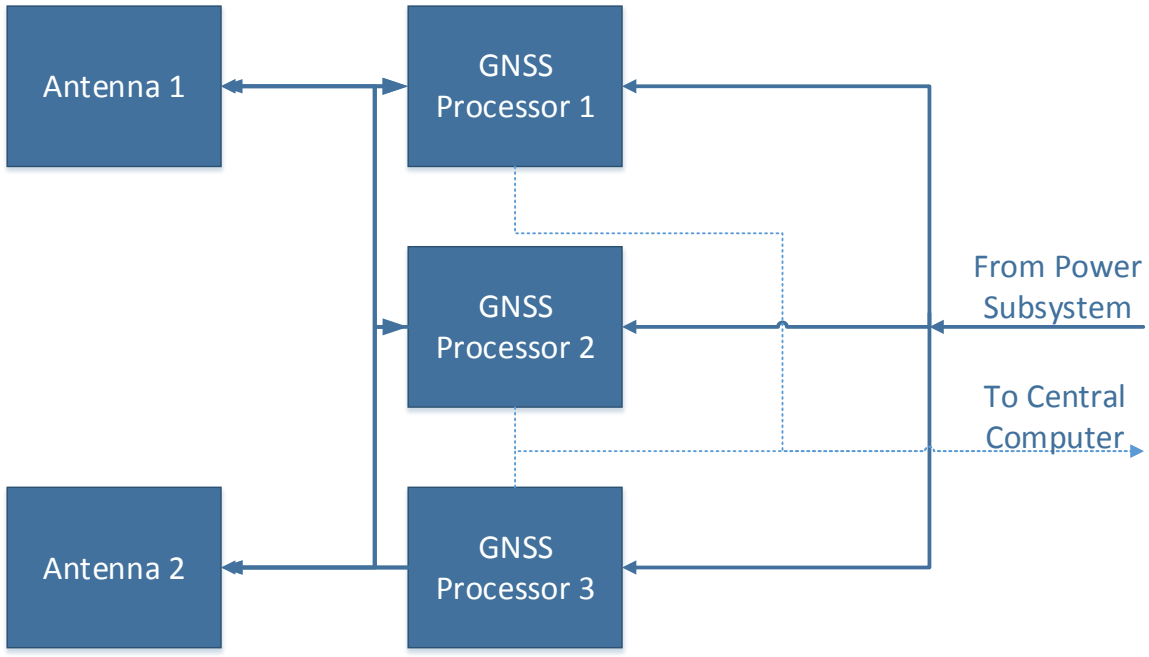

Figure 6.5: The architecture of the guidance, navigation and control subsystem. The normal lines indicate power and the dotted lines indicate data going from the processors to the main computer

all connected to the two antennas. The PolaRx2 device chosen as GNSS processor can be connected up to a maximum of three antennas, so two antennas can easily be connected to the modules. Each processor feeds part of its power through to the antennas. Hence, no additional power lines need to be connected directly to the antennas. The processors calculate the position of the satellite using the signals received from the antenna, then pass the results to the main computer (the dotted line in Figure 6.5).

The main characteristics of the system are summarized in Table 6.3. The size of the antenna has been approximated by assuming that its diameter is a third of its length. Furthermore, a material thickness of 1 [mm] is assumed. Using these values and the density of aluminium [63], the weight of the antenna can be approximated. By adding a safety factor of two, any parts for mounting the antenna are accounted for.

6.6 Verification and Validation

The method can be verified using traditional Keplerian mechanics. The values calculated in Equations 6.5 and 6.6 can be used to verify the separations between the spacecraft throughout the orbit.

Table 6.2: The risks related to the GNC subsystem with the effect of mitigations

RN	Risk Title	Impact	Likelihood
GNC-GNSS1	Failure of GNSS/GPS module	M	M
GNC-GNSS2	GNSS Antenna pointing failure	M	L
GNC-GNSS3	Uncertainty in GNSS Receiver lifetime	M	M
GNC-FORM1	Failure in communicating orbit information within formation	H	L

Table 6.3: The physical characteristics of the GNC hardware

	Amount of units	Mass per unit [kg]	Dimensions per unit [mm]	Price per unit	Remarks
PolaRx2	3	0.72	230 x 140 x 37	€10,000	Assuming the board is in its own housing
Antenna	2	0.025	Diameter: 16, Length: 47.5	€1000 (Rough Order of Magnitude)	Assuming aluminium, including mass safety margin of 2
Total	5	2.21			

In Figure 6.6a, the geometry of the inclination is shown. The pair of spacecraft at the top right hand are approximately at inclination i, with a difference δi in between. Since the separation d_i is much smaller than the distance d_{chief}, the length of the hypotenuses of both apparent triangles can be assumed equal. Therefore, both values are equal to the semi-major axis a. The length of d_i can therefore be found via

$$a \sin \delta i = a \sin \left(1.662 \times 10^{-2}\right) = 2000 \text{ [m]} \tag{6.16}$$

which is equal to the required maximum separation $a\delta i$. Furthermore, it is equal to the values generated by the model described by Equation 6.4.

Figure 6.6b shows two different orbits around a planet, where one orbit is circular and one orbit is elliptical. The apoapsis is the point where the separation between the two orbits is largest. It can be shown that the radius of the apoapsis r_a is equal to [46]

$$r_a = a(1 + e) \tag{6.17}$$

and so the maximum separation is equal to

$$d_e = a(1 + e) - a = (6.894 \times 10^6 \text{ [m]})(1 + 2.901 \times 10^{-5}) - 6.894 \times 10^6 \text{ [m]} = 200 \text{ [m]} \tag{6.18}$$

which is equal to the specified separation $a\delta e$ as well.

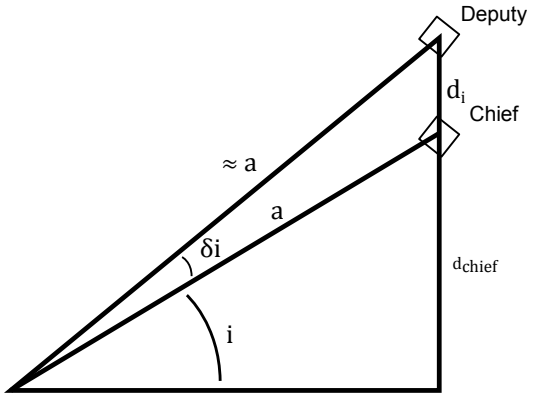

(a) The geometry of the inclination and difference in inclination (not to scale)

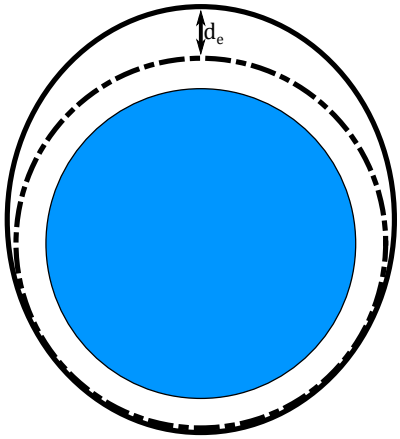

(b) Two orbits with different eccentricity. The dashed line has $e = 0$, the solid line has $0 < e < 1$.

Equation 6.15 can be validated using data from the TerraSAR-X/TanDEM-X formation [57]. The daily ΔV budget for along-track formation manoeuvres was found to be equal to 0.0133 [m/s] per day. Since for the TSX/TDX mission $a\delta e = 500$ [m], substituting this value into Equation 6.15 results in a daily ΔV budget $\Delta v = 0.015$ [m/s]. The resulting error is approximately 11%. In some cases this is a lot, though since the values being discussed here are all very small, it is found to be valid.

Chapter 7

Propulsion

The final design of the propulsion system for the satellite is presented in this section. First, the de-orbiting phase of the spacecraft constellation at the end of life phase of the mission is explained. Following that, the changes in the propellant type and the configuration of the propulsion system for the orbit control and attitude control are described. The next part lists the final subsystem requirements. Afterwards, the in-depth design of the components for the propulsion system is shown. Then what risks are involved and how they are mitigated concerning different parts of the propulsion system are described. Finally, the configuration, the flow of the design in MATLAB, and verification and validation are explained.

7.1 De-Orbiting of the Constellation

The Aegir satellite constellation is going to operate in LEO orbit range, which requires it to meet a 25 year de-orbiting regulation. After a few iterations of calculating the operational altitude of the satellites, it was decided to use 507.3 to 517.6 [km] (different altitudes per pair of satellites). In order to see if the 25 year requirement is met, it is checked using MATLAB, how long it would take for the satellites orbit to decay at the end of the mission and burn in the Earth's atmosphere. To achieve that, the following Equation 7.1 [46] is used:

$$\Delta a = -2\pi(C_D A/m)\rho a^2 \tag{7.1}$$

It describes the semi-major axis decrement per orbit at a given altitude. This value varies per two pairs of spacecraft, because each two pairs are stationed at different altitudes, which give five different lifetime altitudes. The drag coefficient is taken to be the same as for the altitude maintenance calculations which is 2.2, though it is different for each satellite. It is assumed that the leader satellite has a drag coefficient of 2.2 and the follower satellite has a 10% increase in that value, based on the iterations from the Astrodynamics section (chapter 2). The area over mass ratio A/m is the effective cross-sectional area of the satellite in the direction of the velocity path. The mass m is the end of life mass, which is again taken to be 10% higher for the follower satellite. ρ is the atmosphere density at a given altitude and is defined using the Harris-Priester atmospheric density model [64, 65]. Atmospheric density values at a maximum solar radiance together with the corresponding altitude are implemented in EXCEL software and a plot is generated and is finally shown in Figure 7.1.

An exponential interpolation is used to generate a trendline equation which is used in the MATLAB code. a is the semi-major axis at a given altitude. The goal is to bring the satellite at the end of the mission to an altitude of 130 [km] which was defined in the Mid-Term Report [5]. It follows from the model that the time which it would take to bring the satellite down to the required altitude is ranging from 10.05 years to 10.3 years, depending on the initial satellite altitude ranging from 507.3 [km] to 517.6 [km] Therefore, the 25 year requirement is met.

During the de-orbiting phase of the satellites it is important to take into account the collision avoidance of the coupled satellites. It is known that the coupled satellites are separated by approximately 1 [km] distance, which is provided by the GNC in chapter 6. Two situations are considered. In case when the leader satellite is being de-orbited first, a good solution to initiate the de-orbiting is to turn the satellite up to increase the atmospheric drag by rotating around y axis. Figure 7.2 shows the effective cross-sectional area change due to the satellite maneuver.

The red lines in Figure 7.2 indicate the effective cross-sectional area. It has an effect on the A/m ratio which affects the drag value and the decrement of the semi-major axis. Before the maneuver, the cross-sectional area is calculated to be 1.62 [m^2]. After the maneuver it is equal to 9.17 [m^2]. The drag coefficient is assumed to increase from 2.2 to 3.2. Using Equation 7.1 the decrement of the semi-major axis can be found. However, there are two pairs of satellites that are at five different altitudes, so their values of Δa will be slightly different from other pairs of satellites. For simplicity it is assumed that the leader satellite's drag coefficient changes insignificantly at higher orbits and is kept at a 2.2 value for all pairs. After implementing the given values in MATLAB code, Table 7.1 shows for all ten pairs the decrement of the semi-major axis when the leader satellite is being de-orbited first:

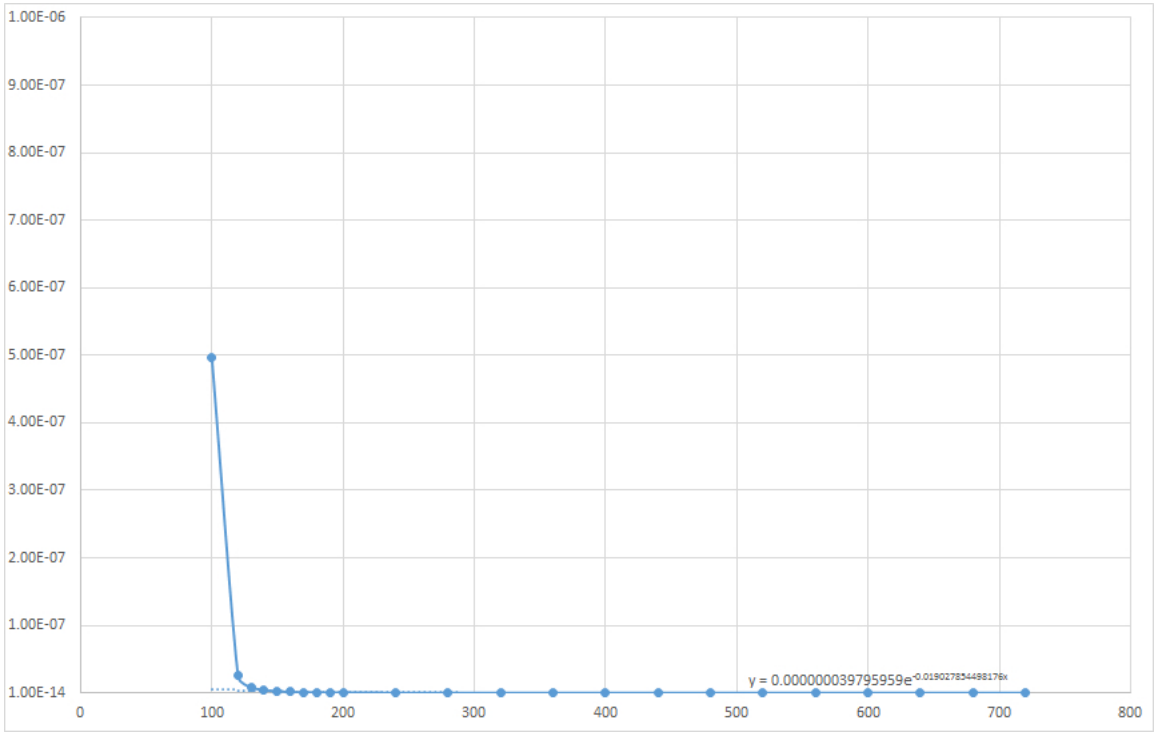

Figure 7.1: Harris-Priester Atmospheric Density Graph

Table 7.1: Change in the Semi-Major Axis of the Leader Satellite

Pair No. [-]	Initial Altitude [km]	Δa_1 [m]	Δa_2 [m]
1	507.3	-9.02	-74.29
2	507.3	-9.02	-74.29
3	509.82	-8.61	-70.86
4	509.82	-8.61	-70.86
5	512.38	-8.20	-67.53
6	512.38	-8.20	-67.53
7	514.98	-7.81	-64.30
8	514.98	-7.81	-64.30
9	517.62	-7.43	-61.19
10	517.62	-7.43	-61.19

As can be seen, for each pair the maneuver increases significantly dependent on the change in semi-major axis value. Δa_1 represents the decrement per orbit when the satellite's effective cross-sectional area is initially left unchanged (Figure 7.2 left side) and Δa_2 shows the decrement per orbit when the satellite is turned up with a new cross sectional area (Figure 7.2 right side). This implies that the leader satellite will reach a lower orbit and the coupled satellites will start drifting apart, increasing the separation distance, which would lead to a situation without any collisions. The de-orbiting would be sustainable and no extra propellant is needed.

The other case is that considered is when the follower satellite is being de-orbited first. The same assumptions are made for this model, where the follower spacecraft has 2.2 C_D value and its area is increased to 9.17 [m^2]. The simulation of this scenario is done using MATLAB and Figure 7.3 was plotted:

The figure shows red an blue lines which represent the decaying orbits of both satellites. After reaching the target orbit of 130 [km] height, both satellites will not collide in space and there would be no catastrophic consequences, meaning new space debris is not created. The zoomed in view of the above graph is shown in Figure 7.4.

7.2 Single Propulsion System for Orbit and Attitude Control

In the Mid-Term Report it was stated that two separate propulsion systems might be used, in order to increase the robustness of the coupled satellites formation flying. After an initial trade off it can be seen that both the orbit control and the attitude control are going to use the same type of propellant. It can be stated that two separate same propellant systems would increase the complexity, occupied volume and costs of the system, which is not preferable. Moreover, to provide enough thrust for different parts of the mission, such as performing a plane change, phasing or de-orbiting, it was estimated that a

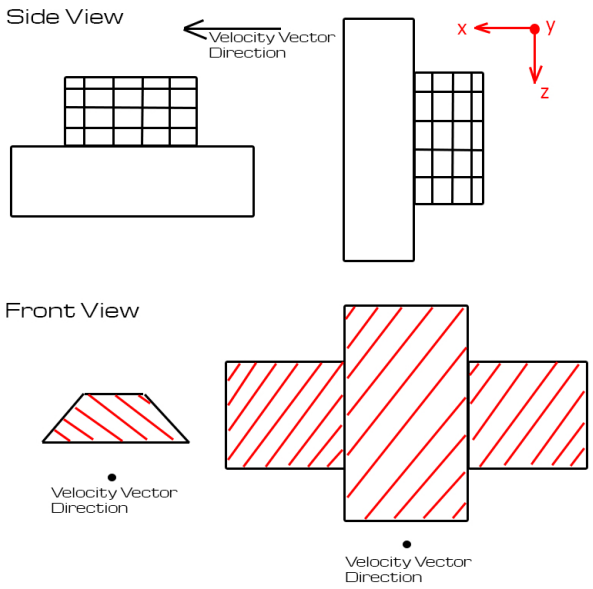

Figure 7.2: Change in Effective Cross-Sectional Area Due to the Maneuver

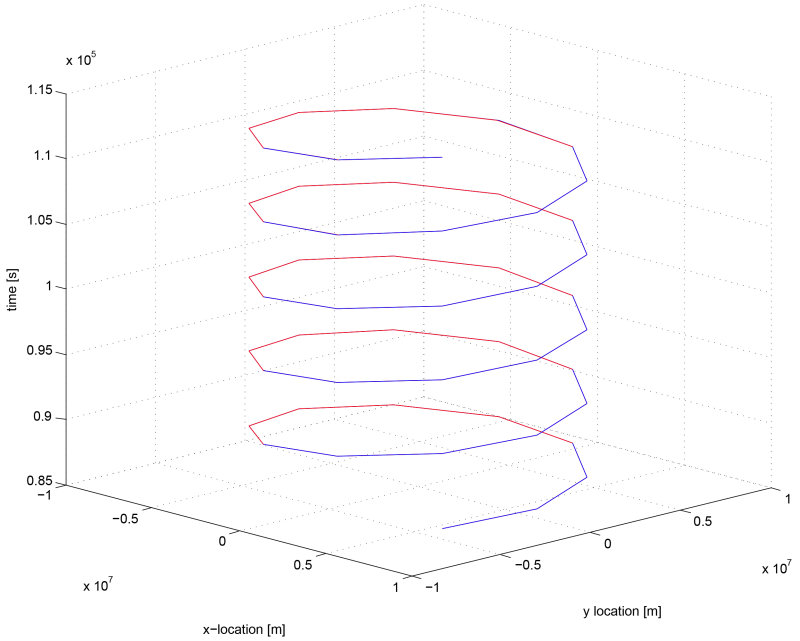

Figure 7.3: Collision Model for Two End-of-Life Satellites

quite large ΔV would be needed. During the further stages of the mission design, the mass, ΔVs and orbit requirements changed. They affected the required total ΔV budget for orbit control, basically, reducing the amount of the propellant required and consequently the thrust needed to achieve it. Additionally, the chosen launcher will be used to phase the satellites and insert into correct inclination, which implies that no plane changes and no extra propellant are required by the satellites anymore. Moreover, the de-orbiting phase is within 25 years and the collision model shows that only a relatively small ΔV is needed. In conclusion, it can be said that a single propulsion system is the optimal choice to be used for the satellites.

7.3 Requirements

In this section the requirements for the propulsion system, its functions and performance are presented.

- **Subsystem Requirement [PROP1A]** 3.15 [m/s] of ΔV over the lifetime of the mission shall be provided for the formation keeping due to the disturbances
- **Subsystem Requirement [PROP1B]** 9.97 [m/s] of ΔV over the lifetime of the mission shall be provided for the

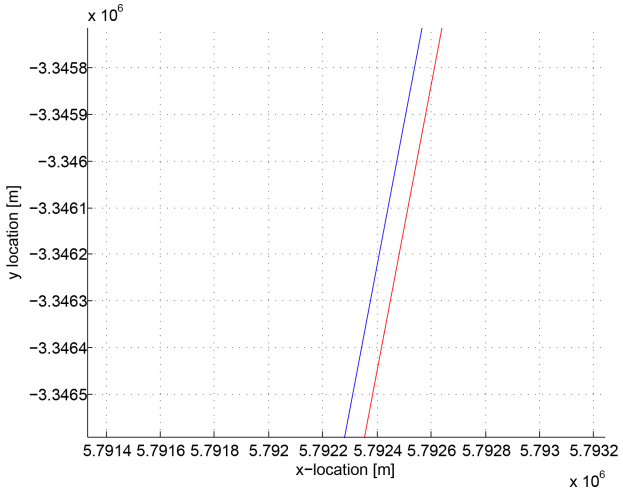

Figure 7.4: Collision Model for Two End-of-Life Satellites (Close Up View)

differential drag maintenance

- **Subsystem Requirement [PROP1C]** 99.72 [m/s] of ΔV over the lifetime of the mission shall be provided for the altitude maintenance
- **Subsystem Requirement [PROP1D]** 20 [m/s] of ΔV over the lifetime of the mission shall be provided for the attitude maintenance
- **Subsystem Requirement [PROP1F]** 2.42 [m/s] of ΔV shall be provided for the insertion of the spacecraft into orbit
- **Subsystem Requirement [PROP2A]** 3-axis control shall have a 2 [s] pulse expulsion of the propellant during ΔV
- **Subsystem Requirement [PROP2B]** Attitude control shall have a 1 [s] pulse expulsion of the propellant during ΔV
- **Subsystem Requirement [PROP3A]** The propulsion system shall have a minimum lifetime of 5 years
- **Subsystem Requirement [PROP4A]** The orbit control thrusters' reaction force shall act through the center of gravity of the satellite
- **Subsystem Requirement [PROP5A]** The attitude thrusters shall provide 3 DOFs to a satellite's attitude control
- **Subsystem Requirement [PROP6A]** The propulsion system's attitude and orbit control thrusters shall have a maximum impulse of 213 [s]
- **Subsystem Requirement [PROP7A]** The propulsion system shall use off the shelf components and have minimum modifications
- **Subsystem Requirement [PROP8A]** The de-orbiting phase shall not take longer than 25 years

At this point all the necessary requirements are covered for the final design of the propulsion system.

7.4 Components Selection

All the necessary components for the propulsion system are presented in the following section.

7.4.1 Propellant

During the further design of the satellite quite a few design details have changed. It affected the choice of the propellant type and amount of it needed. The selection procedure of a new type of the propellant is presented in this section. The mentioned changes are the initial mass, the cross sectional area of the satellite's bus, and ADCS and orbital requirements. Consequently it affected the ΔV budget. Using a MATLAB generated script, a new ΔV budget is produced, which is listed in Table 7.2 (these values are for the total mission lifetime averaged over all ten satellites for different altitudes).

Table 7.2: Total ΔV budget

Function	ΔV [m/s]
Insertion Into Orbit	2.42
Formation Keeping Due to Disturbances	3.15
Differential Drag Maintenance	9.97
Altitude Maintenance	99.72
Attitude Maintenance	20
Total	**143.07**

Table 7.3: Required Thrust per Operation

Function	F [N]
Insertion Into Orbit	1.1
Formation Keeping	0.23
Altitude Maintenance	0.86
Attitude Maintenance	0.82

The formation keeping due to the disturbances ΔV and insertion into orbit ΔV is provided by GNC. Differential drag maintenance is calculated using Equation 7.2:

$$\Delta V = \Delta V_1 - \Delta V_2 \tag{7.2}$$

Where ΔV_1 and ΔV_2 are calculated using Equation 7.3:

$$\Delta V = \pi \left(C_D \frac{A}{m} \right) \rho a V \tag{7.3}$$

The same assumption as from the MTR report is used. The second satellite has 90% of the first satellite drag coefficient, but a new value of C_D is taken which is 2.2. The new cross-sectional area is calculated to be equal to 1.62 [m^2], the mass equal to 480 [kg], the atmosphere density is $2.12 \cdot 10^{-12}$ [kg/m^3] and the orbital velocity is 7.6 [km/s]. Similarly the altitude maintenance ΔV is calculated using Equation 7.3. Attitude maintenance ΔV is taken from MTR report which was already averaged before and did not change.

To define the type of the propellant, the necessary thrust for each of the propulsion system functions must be defined. At this point this overlaps with the selection of the thrusters, but more explicit information on that will follow in section 7.4.5. Using Equation 7.4 [45] the thrust amount for each phase is calculated:

$$\sum F_x = \frac{d}{dt}(m v_x) \tag{7.4}$$

This thrust represents the amount of force needed to correct the satellite per orbit, not the whole lifetime of the mission. Satellite insertion into orbit is a one time operation, so the required ΔV stays the same as defined previously. The mass is assumed to be the initial mass. The thrusting time is taken to be 260 [s], where the thrust is divided by four, since it is assumed that four thrusters are going to be used to perform this function. 260 [s] thrusting time is chosen in order to fit in the other thrust ranges for different maintenance functions. Moreover, it is a one time function, so it is not feasible to attach extra thrusters to perform this operation and then keep the unused weight. At this point the formation keeping due to the disturbances and differential drag maintenance ΔV are added together, because they are part of the same maintenance functions group that is now called Formation Keeping. This gives a value of $4.74 \cdot 10^{-4}$ [m/s]. Moreover, the satellites mass is assumed to stay the same during the thrusting. The thrust time is taken to be 1 [s] for this type of operation. The altitude maintenance requires $3.6 \cdot 10^{-3}$ [m/s] ΔV, where the thrusting time is assumed to be 2 [s]. The mass is kept the same as for the formation keeping operation. The thrust required for attitude control is simply calculated from the given momentum, which is 0.82 [Nm] and is taken from ADCS subsystem section. The arm to compensate that momentum is assumed to be 1 [m] due to the bus configuration. Thus the thrust is 0.82 [N]. After plugging in the values in the given equation, a summary of the required thrusts is presented in Table 7.3.

Due to the reliability, development, cost, and time constraints the new thrusters are not designed and it is decided to take off the shelf ones. After some research the most suitable thruster was found in order to provide the required thrust. Trade-off is not possible, since there are no other similar matches to this thruster. MR-103G hydrazine thruster is chosen for this mission (more information about this thruster will follow in the Thrusters section)[66]. This type of thruster has a range of 1.13-0.19 [N] thrust, which meets the mission's required thrusts. It provides a specific impulse of 224-202 [s]. The average value of specific impulse is taken to be 213 [s]. This is used in calculating the total required propellant mass. The

Table 7.4: Total Propellant Mass Budget

Function	Mass [kg]
Insertion Into Orbit	0.56
Formation Keeping Due to Disturbances	2.51
Differential Drag Maintenance	2.29
Altitude Maintenance	22.37
Attitude Maintenance	4.57
Margin	3.23
Residual	0.71
Total	**36.23**

Table 7.5: Properties of Hydrazine Fuel [45]

Propellant	T_{FP} [K]	T_{BP} [K]	P_{vap} [Pa]	ρ [kg/m^3]	Stability	Handling	Storage	Mat. Compatibility
Hydrazine (N_2H_4)	274	386	19300	1010	Toxic, Flammable	Toxic, Flammable	good	Al, SS, Teflon, Kel-F, Polyethelene

same equation from the MTR report is used to calculate the propellant mass budget. Equation 7.5 [46] is given below:

$$m_p = m_f \left[e^{(\Delta V / I_{sp} g)} - 1 \right] = m_0 \left[1 - e^{-(\Delta V / I_{sp} g)} \right] \tag{7.5}$$

Table 7.4 shows the propellant mass budget for the different propulsion system functions, including a margin of 10 % for contingencies and residual propellant of 2 % [46]. The total mass for the lifetime of the mission is given below:

Since in this case the thruster already pre-defines the type of the propellant, which is mono-propellant: hydrazine, the properties of the fuel are presented in Table 7.5:

The current retail price of hydrazine is 38 $ per 1 [mL][67]. For the required amount of hydrazine for this mission, it adds up to 1 330 000 $.

7.4.2 Pressure-Fed vs. Pump-Fed System

A completely new type of the propellant, mono-propellant, is going to be used for the propulsion system. This is different from the choices as previously stated in the MTR. The option to use a pump-fed system drops off, since it is mainly used in the liquid bi-propellant systems, which require high mass-flow rates and propellant flow pressure [45] as well as high levels of thrust and specific impulse [46]. The only issue that must be covered is what kind of pressure-fed system is going to be used. Two options are possible: pressure regulated or blowdown system. The most common configuration used is the blowdown pressure system, which does not require extra pressurised tanks and its components. It is proven to be reliable, simple, and less weight is required [46, 68, 69, 70]. A simple representation of a blowdown configuration is given in Figure 7.5:

A blowdown system is chosen for the reasons stated above. In the next section the exact propellant tank volume and the method of expulsion are explained.

7.4.3 Propellant Storage

A total tank volume is defined using Equation 7.6 [45]:

$$V_{tot} = V_{pu} + V_{ull} + V_{bo} + V_{trap} \tag{7.6}$$

V_{pu} is a volume of a usable propellant. It can be defined using the value of the propellant mass without residual propellant and the density of the hydrazine, which gives a value of 0.035 [m^3]. V_{ull} is a volume of the tank left for expansion or contraction of the structure. Typical values are 1-3 % of the total volume. In this case the average percentage is taken, which is 2 and is assumed to be a percentage of the total propellant volume, which gives a value of $7.034 \cdot 10^{-4}$ [m^3]. V_{bo} is a volume of cryogenic propellant boil off. Since hydrazine is not a cryogenic fuel, this volume component is omitted. V_{trap} is a volume of the propellant trapped in the feed lines, valves and tank. It can be related to the residual propellant mass which is taken to be 2 % and gives a value of $7.034 \cdot 10^{-4}$ [m^3]. Additionally, pressurant gas volume must be added to the whole tank volume, since it is decided a blowdown configuration will be used, where the pressurant gas is stored together with the propellant in the same tank. Moreover, using reference data, it can be seen that the two most common pressurant gases that are used are helium and nitrogen [45]. A small trade off is done in choosing the pressurant gas. Two criteria are considered: price and mass. The density of helium is 0.1664 [kg/m^3] and nitrogen's is 1.165 [kg/m^3], which makes it almost 10 heavier, but the price of helium per liter is on average 12.5 $ and nitrogen's is 0.75 $ [71], which is 16 times less expensive. Since there is no killer requirement for the mass of the propulsion system, nitrogen is chosen to be

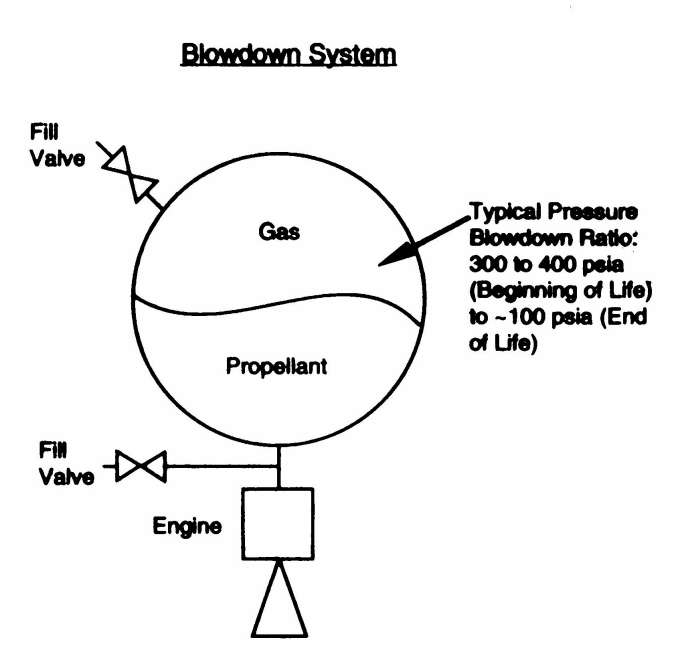

Figure 7.5: Blowdown Configuration of Mono-Propellant System [46]

Table 7.6: Total Tank Volume

Component	V [m^3]
Usable Propellant Volume	0.035
Ullage Volume	$7.034 \cdot 10^{-4}$
Boil-Off Volume	-
Trapped Volume	$7.034 \cdot 10^{-4}$
Pressurant Gas Volume	$9.14 \cdot 10^{-}3$
Total Tank Volume	**0.046**

the pressurant gas. Furthermore, from reference data, the ratio of pressurant gas and propellant is four to one [72]. This gives an amount of $9.14 \cdot 10^{-}3$ [m^3] volume. The summary of the total tank volume is given in Table 7.6:

Knowing the total tank volume, its shape can be defined. The most common shapes used for the tanks are spherical and cylindrical. Spherical tanks are lighter than cylindrical due to their offered volume for a given surface area. Cylindrical tanks provide structural rigidity to longer vehicles. A small trade-off is going to be made in order to choose the most feasible shape of the tank. To begin with, one of the most important factors having a big effect on the tanks is the pressure. The following burst pressure of the tank is defined [45]:

$$p_b = f_s MEOP \tag{7.7}$$

f_s is a factor of safety, which is typically equal to two for pressure vessels [45]. MEOP is a Maximum Expected Operating Pressure of the tank. This value is defined from reference data, which is in the range of 22-26 [bar] [72], which gives 2.2-2.6 [MPa]. An average value of 2.4 [MPa] is defined. The burst pressure is calculated to be 4.8 [MPa]. The following step is to define what kind of material is going to be used for the tank. The most common used materials are Al-2219, Titanium, SS-4130, and Graphite [45]. However, only two of the materials listed above are compatible with the hydrazine from the listed ones, which are aluminium and stainless steel. Only these two materials are considered in the sizing of the tanks. First, the spherical tank sizing is considered. The following equations are used for sizing [45]:

$$V_s = \frac{4}{3}\pi r_s^3 \tag{7.8}$$

$$A_s = 4\pi r_s^2 \tag{7.9}$$

$$t_s = \frac{p_b r_s}{2F_{all}} \tag{7.10}$$

$$m_s = A_s t_s \rho_{mat} \tag{7.11}$$

The given equations elements are:

Table 7.7: Tank Shape Parameters

Parameter	Spherical	Cylindrical
Radius [m]	0.176	0.123
Length [m]	-	0.479
Surface Area [m^2]	2.212	0.371
Thickness (Al) [m]	0.01	0.014
Thickness (SS) [m]	0.005	0.007
Mass (Al) [kg]	63.362	14.872
Mass (SS) [kg]	84.893	19.926

- r_s is the radius of sphere, [m]
- A_s is the surface area of the sphere, [m^2]
- V_s is the volume of the sphere, [m^3], assumed to be the same as from the Table 7.6, which is 0.046 [m^3]
- t_s is the wall thickness of the sphere, [m]
- p_b is the burst pressure [Pa], is calculate using Equation 7.7 which gives 4800000 [Pa]
- F_{all} is the material strength, [Pa], which is taken for aluminium and stainless steel from reference data [45], F_{all}(Al) = 413000000 [Pa] and F_{all}(SS) = 862000000 [Pa]
- m_s is the spherical tank mass, [kg]
- ρ_{mat} is the density of the tank material, [kg/m^3],which is taken for aluminium and stainless steel from reference data [45], ρ_{all}(Al) = 2800 [kg/m^3] and ρ_{all}(SS) = 7830 [kg/m^3]

Similarly the cylindrical tank shape is calculated. The following equations are used for calculations:

$$V_c = \pi r_c^2 l_c \tag{7.12}$$

$$A_c = 2\pi r_c l_c \tag{7.13}$$

$$t_c = \frac{p_b r_c}{F_{all}} \tag{7.14}$$

$$m_c = A_c t_c \rho_{mat} \tag{7.15}$$

The given equations elements are explained:

- r_c is the radius of cylindrical section, [m]. It is assumed to be 70 % of the spherical tank radius.
- l_c is the length of the cylindrical section, [m]
- A_c is the surface area of the cylindrical section, [m^2]
- V_c is the volume of the cylindrical section [m^3], assumed to be the same as from the Table 7.6, which is 0.046 [m^3]
- t_c is the wall thickness of the cylinder wall, [m]
- p_b is the burst pressure [Pa], is calculate using Equation 7.7 which gives 4800000 [Pa]
- F_{all} is the material strength, [Pa],which is taken for aluminium and stainless steel from reference data [45], F_{all}(Al) = 413000000 [Pa] and F_{all}(SS) = 862000000 [Pa]
- m_c is the cylindrical section tank mass, [kg]
- ρ_{mat} is the density of the tank material, [kg/m^3], which is taken for aluminium and stainless steel from reference data [45], ρ_{all}(Al) = 2800 [kg/m^3] and ρ_{all}(SS) = 7830 [kg/m^3]

Table 7.8: Advantages and Disadvantages of Positive Expulsion Devices [45]

	Metal Diaphragm Tank	Rubber Diaphragm Tank	Metal Bellow Tank
Advantages	High Volume Eff. Good c.g. Control No Ullage Volume No Sliding Seals Proven Design	Ext. Database Low Δp Not Cycle Limited Proven Design High Expulsion Eff.	No Sliding Seals Good c.g. Control Proven Design Compatibility Sealing
Disadvantages	High Mass High Cost High Expulsion Δp For Special Envelope	Compatibility Limits	High Mass High Cost Limited Cycles Low Vol. Eff.

Table 7.9: Trade Off of Fill/Drain Valves

Name	Reliability (4)	Cost (3)	Performance (3)	Mass (1)	Total
Airbus [73]	3	3	2	2	29
Moog [74]	2	2	4	1	27

The summarized values of the above equations (after implementing them in MATLAB) are provided in the following Table 7.8:

Important note: due to the constraints of the structural components and available space inside the satellite, the given values in the table were divided by a factor of two. This means that two separate tanks are used to accommodate the required propellant volume. The only issue that must be covered is the method of expulsion to manage the propellant feed to the thrusters. There are two methods used: Active and Passive propellant expulsion devices. Since the simplicity, which increases the reliability, is the driving factor for the propulsion system, it can be seen that the most commonly used method is active expulsion devices [45]. Active expulsion devices are split into different types. Those are: Metal Diaphragm Tank, Rolling Diaphragm Tank, Piston Tank, Rubber Diaphragm Tank, Metal Bellows Tank. Rolling Diaphragm Tank and Piston Tank types are disregarded, because they are more applicable to high acceleration and maneuvering missiles. In order to choose from the other three types, a table with their advantages and disadvantages is provided, which can be used as a trade off for the best choice:

As it can be seen, the Rubber Diaphragm Tank type has the least disadvantages. It has proven design, high expulsion efficiency, extensive database and low Δp.

This concludes the sizing of the propulsion tank system. The shape of the tank is going to be cylindrical and it is made out of aluminium, since it has the lowest mass. As it was previously mentioned, the pressurant gas is going to be nitrogen. The rubber diaphragm will be used as an expulsion method.

7.4.4 Propellant Flow Control

Propellant Flow Control includes such components as on/off valves, directional flow valves, transducers, and the computers to control this hardware. Two reference spacecraft,which use mono-propellant system, are used to derive the necessary propellant flow control components. One spacecraft is called New Horizons [69] which uses fill/vent valve for the pressurant gas, fill/drain valve for the propellant, two pressure transducers, system filter, flow control orifice and six latch valves for thrusters. The other mission is called ROCSAT-1 [68], which uses fill/vent valve for the pressurant gas, fill/drain valve for the propellant, heater and temperature transducer for the tank, filter, orifice, ISO valve, pressure transducer, and latch valves for the thrusters. It can be deducted that Aegir satellite's propulsion system is going to consists of latch valves for thrusters, temperature indicators and heaters, at least one pressure transducer, filter, flow control orifice, fill/drain valve for the propellant, and fill/drain valve for the pressurant gas.

A trade off between the two most common fill/drain valves used in spacecraft applications (using their technical specifications) is presented below:

As it can be seen the Airbus fill/drain valves are going to be used in the satellite's propulsion system. At least four of them will be integrated in the system. Two valves for the first of the two propellant and pressurant gas tanks and two for the second propellant and pressurant gas tank.

Since the information on latch valves for 1 [N] thrusters is limited, the trade off is excluded and the Airbus [75] company latch valve is chosen which is compatible to the chosen 1 [N] thruster. There are going to be nine latch valves. Eight of them are assigned to eight thruster clusters and ninth one is for cross connection between two propellant tanks according to the reference data [76].

Similarly the decision to have a pressure transducer is simply made on the information found on the internet. The only

company which provides any data is Bradford Engineering [77]. Looking at reference data from other missions [76], it can be seen that at least two pressure transducers should be used, one for each tank.

The choice of filters is based on the available information on the internet. The only company which provides reasonable data is VACCO [78]. Using Aerojet provided information on reference data [76], at least two filters are needed, one per each tank.

Fuel control orifice exact choice is excluded, since there is no sufficient information on the possible component. Looking at reference data [76] it is only known that two orifices might be used for each filter.

7.4.5 Thrusters

As it was mentioned previously in the calculations of the mass and ΔV budgets, the thrusters which are going to be used to propel the satellite are the MR-103G hydrazine thrusters [66]. They provide thrust levels between 0.19 to 1.13 [N] which complies with the required thrust for the different functions of the mission. The thruster consumes from 6.32 to 8.25 [W] for valves and catalyst bed heating. One thruster weighs 0.33 [kg]. It can deliver 205136 pulses at LEO orbit and has a maximum of 300 [s] steady state thrusting at LEO orbit. In order to have a full control of the satellite during the orbit and attitude control phases, the number of thrusters is defined. It follows from the requirements that the satellite should have 3 axis control. This is achieved by mounting 12 thrusters at the back of the satellite and eight thrusters at the front of the satellite. The following Figure 7.6 shows how all 3 axes are covered with the thrusters:

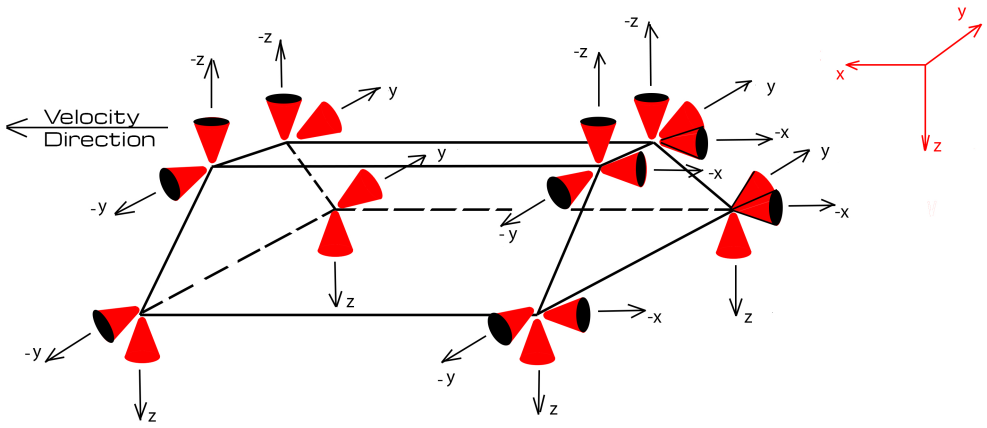

Figure 7.6: Thrust Directions of Each of the Thrusters

Figure 7.6 shows which thrusters cover which axes. The actual representation and placement of the thrusters can be found in the engineering drawings.

7.4.6 Structural Mounts

Structural mounting components for the propulsion system are bolts for attaching the thrusters, CPU, propellant tank, plumbing, filters and valves. Moreover, the cylindrical tank has two rings attached at the both ends of the tank and are attached to the bottom of the satellite with bolts. Special brackets or frames are used to attach the components such as valves, filters, pipes, and wires. The actual structural mounts can be seen in the engineering drawings.

7.4.7 Interconnect Plumbing and Components

The plumbing is designed in such a way that it would comply with the material compatibility of the propellant, formability and simplicity of layout. The pipes through which the propellant flows are made of aluminium just like the propellant tank. The plumbing should have the most efficient length to provide the optimal pressure to the thrusters and small pressure losses can be neglected.

7.4.8 Summary of Propulsion System Components

In this part the total mass, power and cost summary is given.

As it can be seen not all the parameters can be found for each of the components, which gives only a basic idea of what the propulsion system might weigh, cost or how much power it consumes.

Table 7.10: Summary of Propulsion System Components

Component	Mass [kg]	Power [W]	Cost [€]
Propellant	36.23	-	978034.69
Pressurant	0.011	-	5.04
Tank (2x)	29.74	-	56.5
Thruster (20x)	6.6	56 (1x use)	-
Latch Valve (9x)	15.3	50	-
F/D Valve (4x)	0.36	-	-
F.C. Orifice (2x)	-	-	-
Press. Tansducer (2x)	-	-	-
Filter (2x)	0.6	-	-
Total	88.84	106	978096.33

7.5 Sensitivity Analysis

The sensitivity analysis for the propulsion system is performed in order to check how significantly the parameters related to the sizing of the system change, when requirements or, for example, the orbital parameters vary. During the design of the propulsion system, it is seen that its calculations really rely on the satellite's semi-major axis, or more exactly the altitude. To begin with, the de-orbiting model is checked, whether it meets the 25 year requirement if the altitude is varied 100 [km] up and down. Using the same MATLAB file for the de-orbiting model, it shows that for the initial given orbit of 507.6 [km] it takes 10.1 years to de-orbit, where increasing or reducing the orbit by 100 [km] gives a change of around 25 % in the de-orbiting time which varies from 7.52 to 12.5 years. Nevertheless, the 25 year requirement is still met. The collision model is not affected by this altitude change since both satellites would have the same 100 [km] change. Similarly the calculations for propellant mass and volume is done. The change of 100 [km] in altitude, only gives a change of 1 % in propellant mass and volume needed for the propulsion system, which is insignificant for the tank sizing. Moreover, this does not influence the other elements of the propulsion system, such as valves, filters, transducers. They were taken off-the-shelf with already high safety margins.

7.6 Risk Management

A technical risk management is applied to the propulsion system. It consists of a risk identification and an assessment, a risk analysis and a risk handling.

7.6.1 Identification and Assessment

In this part of the propulsion system design the possible risks involved with a type of propulsion, and hardware equipment are discussed. In Table 7.11 the risk statements are listed.

7.6.2 Thrusters

Thrusters are the most commonly used components of the propulsion system, which provide the required thrust in order to move the spacecraft. The risks involved with thrusters are misalignment of the thruster's fitting, the throat does not provide the required pressure (over-expanded or under-expanded), propellant freezing at the throat or combustion chamber, the heating elements do not provide enough energy to warm up the thrusters.

7.6.3 Piping and Wiring

The possible risks are freezing of the propellant, cracks and leaks, corrosion. The freezing of the propellant would not provide the fuel to thrusters and then it would be impossible to perform a needed function. Cracks of the pipes would initiate leakage of the propellant, which would reduce the amount of stored propellant needed for the whole mission. Moreover, it could leak on the other subsystem components and cause their failure or fire.

Similar conditions apply to a wiring. Risks includes overheating of the wires, melt down of the insulation material and faulty connectors. Possible impacts would be loss of propulsion control and telemetry, fire and inaccurate data.

7.6.4 Valves

The risks involved are the open/close mechanism malfunction and malfunctions due to the manufacturing errors. The impact would be that the produced pressure is not sufficient to provide enough propellant to the thrusters.

7.6.5 Tanks

The risks involved are depressurisation and leakage of the tank, defitting of the tank from the bus due to launch forces and vibrations, corrosion of the tank's walls. The impact of these risks might be catastrophic. For example, if there is a leakage, then the lifetime of the propulsion system would reduce. A loose tank could damage other spacecraft components and reduce the performance of the propulsion system.

7.6.6 Regulating and Control Equipment

The regulating and control element of the propulsion subsystem gives the status. It is crucial to have it function reliably, since the data and information is used to perform the functions. Risks involved are malfunctioning of the pressure gauges and indicators (propellant, valves, tank, thrusters) or board computer. Wrong numbers could confuse the mission operators and wrong actions could be performed at a wrong time and location. Malfunctioning board computer would result in inability to process the commands and data.

7.6.7 Type of Propulsion

The risks related to the type of the propulsion are interdependent on the components of the propulsion system, such as thrusters, tanks and etc. To generalise the risks in this case the stability, safety and storability are considered. The propellants such as liquid should be stable, in which no possible explosions or fires should occur. Its pressurisation should reach the required safety limits. The propulsion system risk statement Table 7.11 is given:

Table 7.11: Propulsion System Risk Statement Table

RN	Risk Title	Condition	Consequence
PRP-THR1	Misalignment of Thrusters	While fitting the thruster, it was not attached accurately	The attitude control and orbit control accuracy reduces
PRP-THR2	Over/Underexpansion of Thruster's Throat	Thruster is not able to provide a required Thrust	The required accuracy or condition might not be reached
PRP-THR3	Freezing of the Propellant Inside the Thruster	The heating element is not able to warm up the throat or combustion chamber	The thrusters are not able to perform
PRP-PIPWIR1	Freezing of the Propellant	The propellant is frozen inside the pipes	The feed of the propellant is disrupted
PRP-PIPWIR2	Cracks and Leaks	There are cracks and leaks at the mounting spots	Loss of the propellant, possible fire and termination of mission
PRP-PIPWIR3	Corrosion	Over the lifetime of the mission it might corrode	Cracks and leaks might appear, pollution of the thruster's throat or combustion chamber
PRP-PIPWIR4	Overheating and Melting of the Wires	Overlaoding with power or placed next to Hot components	Loss of propulsion control and telemetry, fire, inaccurate data
PRP-VLV1	Open/Close Mechanism Malfunction	Due to manufacturing errors does not close or not enough power provided to close it	Leakage of propellant or inability to mix the two propellants
PRP-TNK1	Depressurisation and Leakage	Due to built up pressure or misfit mountings	Loss of propellant over lifetime, possible fire
PRP-TNK2	Defitting of the Tank	Due to launch forces or vibrations	Detachment from the bus, damage to other components
PRP-TNK3	Corrosion of the Tank's Walls	Corrosion of the inside material over lifetime	Polluting pipes,valves and combustion chamber
PRP-RCEQP1	Malfunction of Pressure Gauges and Indicators	Broken parts of gauges	Wrong data provided to board computer
PRP-RCEQP2	Malfunction of Board Computer	Broken parts of computer	Wrong data provided to ground control and inability to perform
PRP-TPRP1	Stability	Unstable propellant products are used	Internal explosion might occur
PRP-TPRP2	Safety	propellant might pollute spacecraft instruments or damage them	Functions of mission can not be performed fully
PRP-TPRP3	Storability	Tanks are not able to provide the required storable space	Breakage of tanks or storing space might affect other subsystems

Table 7.12: Technical Risk Assessment Table for Propulsion System

RN	Risk Title	Impact	Likelihood
PRP-THR1	Misalignment of Thrusters	H	L
PRP-THR2	Over/Underexpansion of Thruster's Throat	H	L
PRP-THR3	Freezing of the Propellant Inside the Thruster	VH	M
PRP-PIPWIR1	Freezing of the Propellant	VH	M
PRP-PIPWIR2	Cracks and Leaks	H	M
PRP-PIPWIR3	Corrosion	M	L
PRP-PIPWIR4	Overheating and Melting of the Wires	H	H
PRP-VLV1	Open/Close Mechanism Malfunction	M	VL
PRP-TNK1	Depressurisation and Leakage	H	L
PRP-TNK2	Defitting of the Tank	M	VL
PRP-TNK3	Corrosion of the Tank's Walls	M	L
PRP-RCEQP1	Malfunction of Pressure Gauges and Indicators	M	M
PRP-RCEQP2	Malfunction of Board Computer	VH	M
PRP-TPRP1	Stability	M	VL
PRP-TPRP2	Safety	H	L
PRP-TPRP3	Storability	M	VL

7.6.8 Risk Assessment Scaling

To compare the risks with each other, an order of the risks is arranged in very high (VH), high (H), moderate (M), low (L) and very low (VL) for both the impact and likelihood attributes. In Table 7.12 the impact and the likelihood of each risk is shown:

7.6.9 Risk Analysis

The risks listed in Table 7.12 can be mapped. This is shown in Figure B.1c.

7.6.10 Mitigation

As it can be seen in the risk map, there are a few components that are in the orange colored area. These risks will have the highest priority for the mitigation. Blue colored risks should be mitigated if there are enough resources available. Green colored risks are of the lowest importance for mitigation and will be considered after the other categories have been treated.

7.6.11 Highest Priority Risks

As it can be seen from the risk map there are five risks in the orange area. Those are freezing of the propellant inside the thruster, freezing of the propellant in the pipes, cracks and leaks in the pipes, overheating and melting of the wires, and malfunction of the board computer.

7.6.12 Risk Handling

As the risks identified above are the most likely to happen from all of them, they need to be mitigated. To prevent the freezing of the propellant inside the thruster, extra heating elements should be added for a redundancy purpose or they should be attached in a way that the highest heating efficiency is achieved. Freezing of the propellant in the pipes can be prevented by adding heating elements on the pipes or have special indicators showing the status of the propellant condition. The piping system should be already designed for a range of operational temperatures. Cracks and leaks in the pipes can be mitigated using self healing materials. Overheating and melting of the wires can not really be prevented. They should be placed during the building of the spacecraft in a way that they have the least exposure of heat and made of highly thermal resistant insulation, but as always extra lining of wires can be added for the redundancy to prevent from shutting off the propulsion system completely. The board computer can have a redundant one if it is malfunctioning, this would add extra cost and mass to the whole spacecraft, but relatively it is small compared to the whole propulsion system. The board computer can have redundant components itself if any fail. Applying the mitigation above will result in the following modified risk map as seen in Figure B.1d.

7.7 Architecture of the Propulsion System

The following Figure 7.7 shows the schematic representation of Aegir's satellite propulsion system:

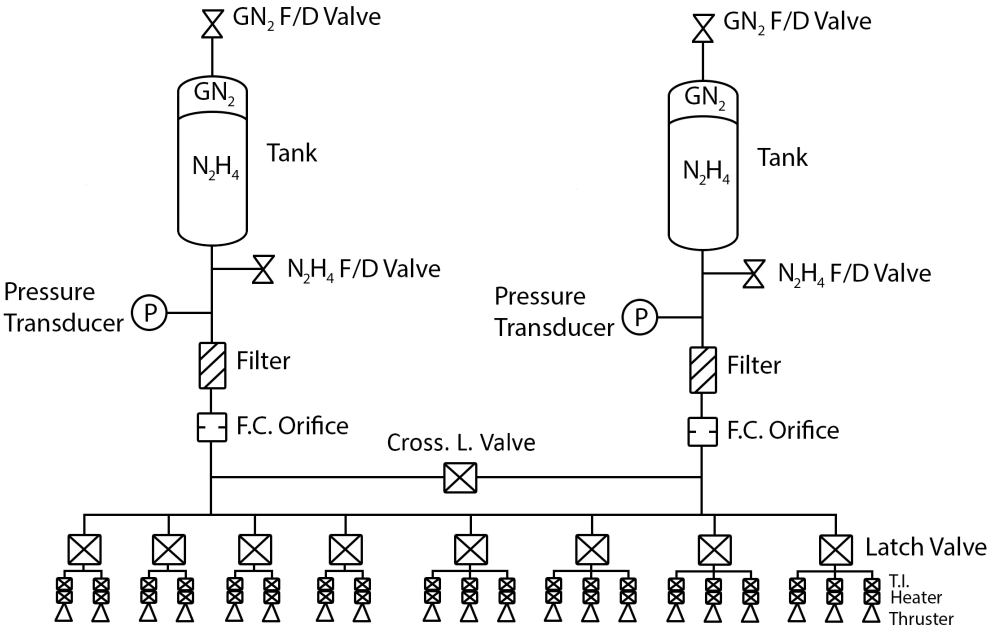

Figure 7.7: Shematic representation of the Propulsion System

It can be seen that the propulsion system as previously mentioned contains of nitrogen gas fill/drain valves, cylindrical shape tanks with nitrogen gas and hydrazine separated by the rubber diaphragms for expulsion, hydrazine fill/drain valves, pressure transducers, filters, flow control orifices, then on the left side the front thrusters contain temperature indicators, heaters and for each pair a latch valve is assigned, similarly rear thrusters contain of heaters and temperature indicators as well as latch valves per three thrusters. Additionally, there is a cross latch valve connecting two tanks. In order for the propulsion system to work as an integrated system of the whole spacecraft, it must interact with other subsystems. It means that information comes from ADCS, TT & C, and GNC subsystems. This can be found in the architectures sections of each subsystems.

7.8 Subsystem Sizing

In this part the explanation of propulsion system sizing in MATLAB is explained. Before the actual sizing of the propulsion system could be done, the two mentioned previously issues are addressed, which is the de-orbiting function and the collision avoidance during the de-orbiting phase. A function file for de-orbiting is created, containing a differential semi-major axis equation which was explained in the first section of this chapter, where its value is used in another script file. The function file calculates the time required to reach 130 [km] altitude and see if the 25 year requirement is met and if an additional propellant is needed. It uses the same equations defined from astrodynamics part and the values from atmospheric density file, which was created using Harris-Priester model as it was mentioned before. Similarly the collision model is created, which is more explained in the sustainability part. After that, another two function files are used. First one is for the propellant sizing, containing all the necessary outputs for the mass and volume sizing. The second one is for the tank sizing, which is interrelated with the mass sizing file. Both of these function files have script files with all inputs needed. The propellant mass data script file contains the orbital parameters predefined by astrodynamics part, and propellant data, which is area over mass ratio, average specific impulse, thrusting times, propellant density, then propellant tank data, which is safety factor and max. operating pressure. These values together with the equations mentioned before are implemented in propellant mass function file, which gives the outputs such as all the ΔVs, thrusts, propellant masses for different mission parts, and propellant volumes. Similarly the tank size data script file contains the necessary values of propellant tank data calculated from propellant mass file and additionally has the material properties, such as densities and ultimate stresses. Then these values are implemented in tank sizing function file. It calculates the geometrical parameters as well as masses of spherical and cylindrical tanks. The same equations are used which are mentioned in the previous sections.

7.9 Verification and Validation

In this part the verification and validation procedure for the propulsion system design is shown. To begin with, the components such as fill/drain valves, latch valves, filters, orifices, pressure transducers are taken off-the-shelf, their verification and validation is not needed, since they are proven as operational parts in other space missions. Similarly, the choice of the propellant is predefined by the choice of thrusters. The amount of the propellant can be verified or validated comparing

to reference missions. However, due to the reasons that this mission is unique and a completely new propulsion system is created for the purpose of this mission requirements, the results would not match exactly. This affects the tank sizing. It is influenced by the amount of the propellant needed and the structural constraints of the satellite bus. Only by comparing to the similar missions and their averaged values for the propulsion system, it can be checked whether it is within the limits of reasonable size. However, a possible high error might influence the results, since this mission is unique. Only the ΔV budgets can be checked together with ADCS, GNC and astrodynamics parts. The above mentioned calculations must meet the requirements from other subsystems, which are checked with the compliance matrix that can be found in Table **??**.

Chapter 8

Attitude Determination and Control

To achieve the required performance for the payload, communication, de-tumbling or orbital maintance, an Attitude Determination and Control Subsystem (ADCS) is needed to orientate the spacecraft accurately. For the design of the ADCS, there are three main components which have to be considered. This includes the attitude determination with the use of sensors, control hardware and the control process. The last part comprises of the software part of the attitude control subsystem. Furthermore this chapter discusses the external disturbances and the verification and validation of the model used.

8.1 Control Modes

Besides the operative modes mentioned in chapter 3, there are several control modes which need further discussion for the attitude determination and control subsystem.

8.1.1 De-tumbling Mode

Misalignment of the center of gravity with the thruster force will results in a rotating motion of the satellite during the ejection phase from the launch vehicle. This requires a specific control mode, called the de-tumbling mode. It is a critical mode of the mission, as there is limited power available and the initial attitude has to be determined in a short period of time. To de-tumble, and to start the acquisition mode, the satellite is going to use the B-dot method controller. It works using the differential change in the Earth's magnetic field as the satellite orbits over it.

The torque due to this tumbling must therefore be countered with the torques produced on the spacecraft. Due to the limited availability of power, since it is not yet possible to aim the solar cells, batteries are the main power source, and low power attitude determination and control components are chosen for this control mode. For this phase a worst case tumbling rate of 10 [deg/s] which is equal to 0.174 [rad/s] is assumed. When the satellite de-tumbles to a rate of 1 [deg/s], the satellite solar panels can be deployed, so that more accurate determination and control techniques can be used. If the orbital period of a median satellite is 95 minutes at an altitude of 516 [km], it will produce a satellite's angular velocity of 0.126 [deg/s].

8.1.2 Acquisition mode

The acquisition mode consists of the initial determination and control of the spacecraft's orientation. Different requirements are specified for the initial determination and control as no payload operations are in effect. These requirements are going to be coarse and less accurate than the ones used for scanning operation.

8.1.3 Scanning mode

Scanning mode dictates the most accurate attitude determination and control requirements. To achieve them the satellite will need to consume a large amount of power and make use of at least two different scanning techniques. This larger power consumption comes from the more accurate components which require more power to operate.

8.2 Requirements

To perform each stage of the mission successfully and produce valid results, specific ADCS requirements must be computed. Each of these requirements is bound to a specific control mode. It should be noted that the payload requirements are assumed to be dominant over the others, as the highest accuracy requirements are made for the payload, the SAR instrument.

8.2.1 De-tumbling Mode

- **Subsystem Requirement [ADCS]**: The ADCS shall de-tumble in half a day (12 hours).

8.2.2 Acquisition Mode

- **Subsystem Requirement [ADCSAa]**: The ADCS shall provide an initial determination time of one orbital period.
- **Subsystem Requirement [ADCSAb]**: The ADCS shall be able to provide the initialization during an eclipse.
- **Subsystem Requirement [ADCSAc]**: The ADCS shall provide an initial determination range within the minimal normal attitude determination sensor range.
- **Subsystem Requirement [ADCSAd]**: The ADCS shall provide an initial control accuracy of 1 [deg].
- **Subsystem Requirement [ADCSAe]**: The ADCS shall provide an initial attitude control range of 180 [deg].
- **Subsystem Requirement [ADCSAf]**: The ADCS shall provide an initial attitude minimum settling time of 10 [s].

8.2.3 Slew Mode

- **Subsystem Requirement [ADCSSa]**: The ADCS shall provide a slewing rate of at least 72 [deg] in half an orbital period during payload inoperative time periods.
- **Subsystem Requirement [ADCSSb]**: The ADCS shall provide a slewing rate of at least 10 [deg] in 10 [s] during payload operative time periods.

8.2.4 Scanning Mode

- **Subsystem Requirement [ADCS1a1]**: The ADCS shall provide a pointing accuracy of at least 13.5 [arcsec] in x-axis.
- **Subsystem Requirement [ADCS1a2]**: The ADCS shall provide a pointing accuracy of at least 5 [arcsec] in y-axis.
- **Subsystem Requirement [ADCS1b]**: The ADCS shall provide an attitude determination range of $\pm$ 40 [deg] of nadir.
- **Subsystem Requirement [ADCS1c1]**: The ADCS shall provide an attitude control accuracy of at least 27 [arcsec] in x-axis.
- **Subsystem Requirement [ADCS1c2]**: The ADCS shall provide an attitude control accuracy of at least 10 [arcsec] in y-axis.
- **Subsystem Requirement [ADCS1d]**: The ADCS shall provide an attitude control range of $\pm$40 [deg] of nadir.
- **Subsystem Requirement [ADCS1e1]**: The ADCS shall maintain a maximum jitter of 0.0087" over $1.64 \cdot 10^{-4}$ [s] in x-direction.
- **Subsystem Requirement [ADCS1e2]**: The ADCS shall maintain a maximum jitter of 0.0033" over $6.25 \cdot 10^{-5}$ [s] in y-direction.
- **Subsystem Requirement [ADCS1f]**: The ADCS shall provide a minimum settling time of 2 [s].

8.2.5 Eclipse Mode

- **Subsystem Requirement [ADCSEa]**: The ADCS shall provide the same attitude requirements during an eclipse.

8.2.6 Contingency/Safe Mode

- **Subsystem Requirement [ADCSCSa]**: The ADCS shall have a safe mode.

8.2.7 Constraints

- **Subsystem Requirement [ADCS4b]**: The ADCS shall have a minimum lifetime of 5 [yr].
- **Subsystem Requirement [ADCS4d]**: The ADCS shall have a maximum mass of 35 [kg].
- **Subsystem Requirement [ADCS4e]**: The ADCS shall have a maximum power consumption of 97.8 [W].

8.2.8 Pointing Accuracy

To compute the pointing accuracy, Equation 8.1 is used with a θ of 31 [deg], h, the altitude of the spacecraft of 516 [km] and w_s the swath width of 100 [km]. Note that a 0.1 $\%$ of the swath width is taken as the shift. This results in a pointing accuracy of 26.9 [arcsec].

$$\beta = \arctan\left(h\tan\theta + \frac{w_s}{2} + 0.001w_s\right) - \arctan\left(h\tan\theta + \frac{w_s}{2}\right) \tag{8.1}$$

8.2.9 Jitter

For the jitter requirement an image stability of 20^{th} of the image resolution is taken. As the resolution is present in two directions, this results in two different jitter requirements in x and y-direction. Equations 8.2 and 8.3 [79] are applied to determine the pointing stability and the stability time. This gives a jitter requirement of 0.0087" over $1.64 \cdot 10^{-4}$ [s] and 0.0033" over $6.25 \cdot 10^{-5}$ [s].

$$\delta_s = \frac{\frac{x_{res}}{20}}{h} \tag{8.2}$$

$$t = \frac{\frac{x_{res}}{20}}{V} = \frac{\frac{x_{res}}{20}}{\sqrt{(\frac{\mu_E}{R+r})}} \tag{8.3}$$

8.3 Disturbances

To design control methods for the ADCS, one must first compute all the disturbances that the satellite is going to encounter at a certain orbit. In this section the focus will be on the external disturbances as they are much higher than the internal ones. The disturbances that are going to be discussed in detail are: the gravity gradient, solar radiation, aerodynamic and solar pressure; and finally the magnetic field disturbances. In table 8.1 these disturbances are listed.

Disturbance Torque	M_x [Nm]	M_y [Nm]	M_z [Nm]
Gravity Gradient	$3.09 \cdot 10^{-5}$	$2.73 \cdot 10^{-4}$	$1.42 \cdot 10^{-4}$
Solar Radiation	$6.13 \cdot 10^{-6}$	$3.98 \cdot 10^{-6}$	$2.95 \cdot 10^{-6}$
Aerodynamic	0	$4.35 \cdot 10^{-5}$	$4.35 \cdot 10^{-5}$
Magnetic Field	$7.1 \cdot 10^{-5}$	$7.6 \cdot 10^{-5}$	$4.11 \cdot 10^{-6}$
Total	$\mathbf{1.08 \cdot 10^{-4}}$	$\mathbf{3.96 \cdot 10^{-4}}$	$\mathbf{1.93 \cdot 10^{-4}}$

Table 8.1: Maximum Disturbances on the Principal Body Axes of the Spacecraft

8.3.1 Gravity Gradient

Due to variations in the Earth's gravitational force, all the spacecraft orbiting the Earth are subjected to the gravitational torque disturbance. As the gravity gradient would not exist in a uniform gravitational field it must be a product of an inverse squared gravitational force field. The gravity gradient potential is primarily influenced by the satellites inertias and the orbital altitude. The equations for the gravity gradient torque in Euler angles are shown below. Note that it has been assumed that J_2 is the leading orbital perturbation on the satellite and that the effect of the other terms is negligible. The satellite has been assumed to be rigid. The mass moments of inertia of the spacecraft have been computed using CATIA to be 99.6 [kg m^2], 270.6 [kg m^2] and 296.6 [kg m^2] for the x, y and z principal axes respectively.

$$T_g = 3\left(\frac{\mu}{R_c^3 s}\right)(I_3 - I_2)\sin\theta_1\cos\theta_1\cos^2\theta_2 \tag{8.4}$$

$$T_g = 3\left(\frac{\mu}{R_c^3 s}\right)(I_3 - I_1)\cos\theta_1\sin\theta_2\cos\theta_2 \tag{8.5}$$

$$T_g = 3\left(\frac{\mu}{R_c^3 s}\right)(I_1 - I_2)\sin\theta_1\sin\theta_2\cos\theta_2 \tag{8.6}$$

Whereby R_c is the radius of the orbit, μ the gravitational constant of Earth, θ_1 the roll angle and θ_2 the pitch angle. Computing these equations using maximum allowable roll and pitch angles of 31 [deg], will result in the maximum torque induced by the gravity gradient of the Earth.

8.3.2 Solar Radiation

Solar radiation comes from the Sun in the form of electromagnetic waves. It produces a constant torque and is altitude independent for all Earth orbiting spacecraft. Solar radiation pressure is primarily influenced by three factors. First is the intensity and spectral distribution, second the geometry of a spacecraft surface and its reflectivity, and the last is the orientation of the Sun vector. Solar radiation pressure largely depends on the type of surface used for the spacecraft exterior. It can be either transparent, an absorber or a reflector. For most spacecraft operations, the exterior surface is a combination of all three. The worst case solar radiation torque can be computed using Equation 8.7 [46].

$$T_{sp} = \frac{F_s}{c} A_s (1+q) \cos i (l_{ps} - l_{cg}) \tag{8.7}$$

Where T_{sp} is the solar radiation pressure, F_s is the solar constant ($F_s = 1367 W/m^2$), c is the speed of light ($c = 3 \cdot 10^8 m/s$), A_s is the surface area, i is the incidence angle of the Solar rays, q is the reflectance factor (ranging from 0 to 1), l_ps is the location of the centre of solar pressure and l_cg is the location of the centre of pressure.

The maximum solar radiation on each principal axis of the spacecraft can be determined by applying an incidence angle of zero [rad], a worst-case reflectance factor of 1, an off-set of the pressure centre of 0.2 [m] and taking the corresponding surface area of each axis. The resulting torques are shown in table 8.1.

8.3.3 Aerodynamic

The third in the list is the aerodynamic disturbance. To determine the impact of this disturbance, Equation 8.8 is used [46]. For the use of this equation several parameters of the spacecraft are assumed to estimate the value of the torque.

$$T_a = 0.5 \rho C_d A V^2 (c_{pa} - cg) \tag{8.8}$$

Atmospheric Density

Following from COSPAR International Reference Atmosphere - 2012, it can be concluded that the mass density of the air at an altitude of 500 [km] is equal to $2.1 \cdot 10^{-12} [kg/m^3]$ [80]. This value corresponds to high long term solar and geomagnetic activity which is taken as the worst case scenario for the spacecraft's mission. The model used to derive the atmospheric drag is the JB2008 model. The uncertainty of this model is as high as $\pm 100\%$ at extreme cases which is hard to predict due to the complex behaviour of the atmosphere.

For the determination of the aerodynamic disturbance vector, it is assumed that the disturbance only affects the satellite in the y and z axes of the satellite's reference frame, as the velocity in y and z components is negligible compared to the flight component. Besides, it is assumed that the velocity vector acts on the x-axis of this reference frame. Several other parameters include the drag coefficient of 2.2 [-], a surface area of 1.62 [m^2], the satellite's velocity of 7.61 [km/s] and a centre of mass offset of 0.2 [m] in both y and z direction. This results in a torque of $4.35 \cdot 10^{-5}$ [Nm] around both the y and z axes.

8.3.4 Magnetic Field

One of the difficulties to determine the magnetic field is due to the irregularities in the ambient magnetic field around the Earth. This can be caused by influences outside the magnetosphere of the Earth such as the solar effects of the Sun. There are several different analytical models to consider. These consist of the Spin-axis, centred dipole, Tilted, centred dipole, Quadrupole, and the Spherical harmonic expansion model. To determine the magnetic field strength of the Earth, the Tilted, centred dipole model is used. This model consists of two irregularities; one due to time varying effects on the magnetic field and the other the magnetic field changes due to field distortions. The field distortions can be accurately described within five Earth radii and this model is therefore applicable. The temporal variations however are not modelled which include the effect of geomagnetic storms and sudden impulse disturbances. The other models are more complex and are therefore not used [81].

To calculate the magnetic field strength of the Earth at an altitude R, equations 8.9 to 8.11 are used. These equations represent the Tilted, centred dipole model and are an analytical representation with three terms in a harmonic expansion [81].

$$B_X = \frac{R_e}{R} (g_1^0 \sin\theta + g_1^1 \cos\theta \cos\lambda + h_1^1 \cos\theta \sin\lambda) \tag{8.9}$$

$$B_Y = -\left(\frac{R_e}{R}\right)^3 (g_1^1 \sin\lambda - h_1^1 \cos\theta) \tag{8.10}$$

$$B_Z = 2\left(\frac{R_e}{R}\right)^3 (g_1^0 \cos\theta + g_1^1 \sin\theta \cos\lambda + h_1^1 \sin\theta \sin\lambda) \tag{8.11}$$

To compute the values for the magnetic field strength the angles θ and λ have been computed, these represent the latitude and longitude respectively. The poles of the magnetic field can be found using equations 8.12 and 8.13 [82].

$$\theta = \arccos \frac{m_z}{m} \tag{8.12}$$

$$\lambda = \arccos \frac{m_x}{\sqrt{m_x^2 + m_y^2}} \tag{8.13}$$

Where the values for m, m_x, m_y, m_z can be calculated using formulas 8.14 to 8.17, respectively [82]. Note that for a, the mean radius of the Earth is taken. The values for g_1^1, h_1^1 and g_1^0 corresponding to the epoch 2010 which are the harmonic coefficients known as Gauss coefficients, are taken from the International Geomagnetic Reference Field (IGRF) model 11 released by the International Association of Geomagnetism and Aeronomy (IAGA) [83]. These correspond to -1585.9, 4945.1 and -29496.5 $[nT]$, respectively.

$$m = \sqrt{m_x^2 + m_y^2 + m_z^2} \tag{8.14}$$

$$m_x = \frac{4\pi}{\mu_0} a^3 g_1^1 \tag{8.15}$$

$$m_y = \frac{4\pi}{\mu_0} a^3 h_1^1 \tag{8.16}$$

$$m_z = \frac{4\pi}{\mu_0} a^3 g_1^0 \tag{8.17}$$

Computing equations 8.12 and 8.13 give angles of $(170.0°, 107.8°)$ and $(10.0°, 287.8°)$ with a permeability of vacuum of $12.566 \cdot 10^{-7} [N/A^2]$ [44], for the north and south geomagnetic poles respectively. Applying equations 8.9 to 8.11, the magnetic field strength in the three axes can be determined. Where the Z axis is pointing in the negative nadir direction, the X axis directed to the local meridian and the Y axis completing the right-hand coordinate system.

Table 8.2: Magnetic Field Induction

	x	y	z
Magnetic Field Strength [nT]	-9,485	-2,679	47,764

8.3.5 Effective Dipole Moment

The dipole moment of the spacecraft is categorised by NASA into three different classes which are divided by the relative impact of the magnetic torque compared to other torques. This is represented in Table 8.3 for a non-spinning spacecraft [81].

Table 8.3: Spacecraft Dipole Moment Estimation

	Class I	Class II	Class III
Dipole moment/SCmass $[Am^2/kg]$	$1 \cdot 10^{-3}$	$3.5 \cdot 10^{-3}$	$10 \cdot 10^{-3}$

Comparing the magnetic torque to other torques, it can be concluded that the spacecraft corresponds to class II, as it is comparable to other torques. With a spacecraft mass of 480 [kg], the effective dipole moment is equal to 1.68 $[Am^2]$.

8.3.6 Magnetic Disturbance Torque

The maximum value for this torque can be determined by assuming that the dipole moment of the satellite is the same for all its three axes and assuming that the magnetic flux density vector **B** is normal to one of the axes. The maximum torque can be calculated using Equation 8.18 [81]. The result is plotted in figure 8.1 on the Earth.

$$|\boldsymbol{T}|_{max} = \sqrt{2}\,|\boldsymbol{B}|_{max}\, M \tag{8.18}$$

The magnetic torque can be divided on the spacecraft's principal axes using the Equation 8.19 [81]. Note that similar equations can be found for y and z axes. The maximum value of each axis can be found in table 8.1.

$$T_{x,max} = B_{z,max} M - B_{y,max} M \tag{8.19}$$

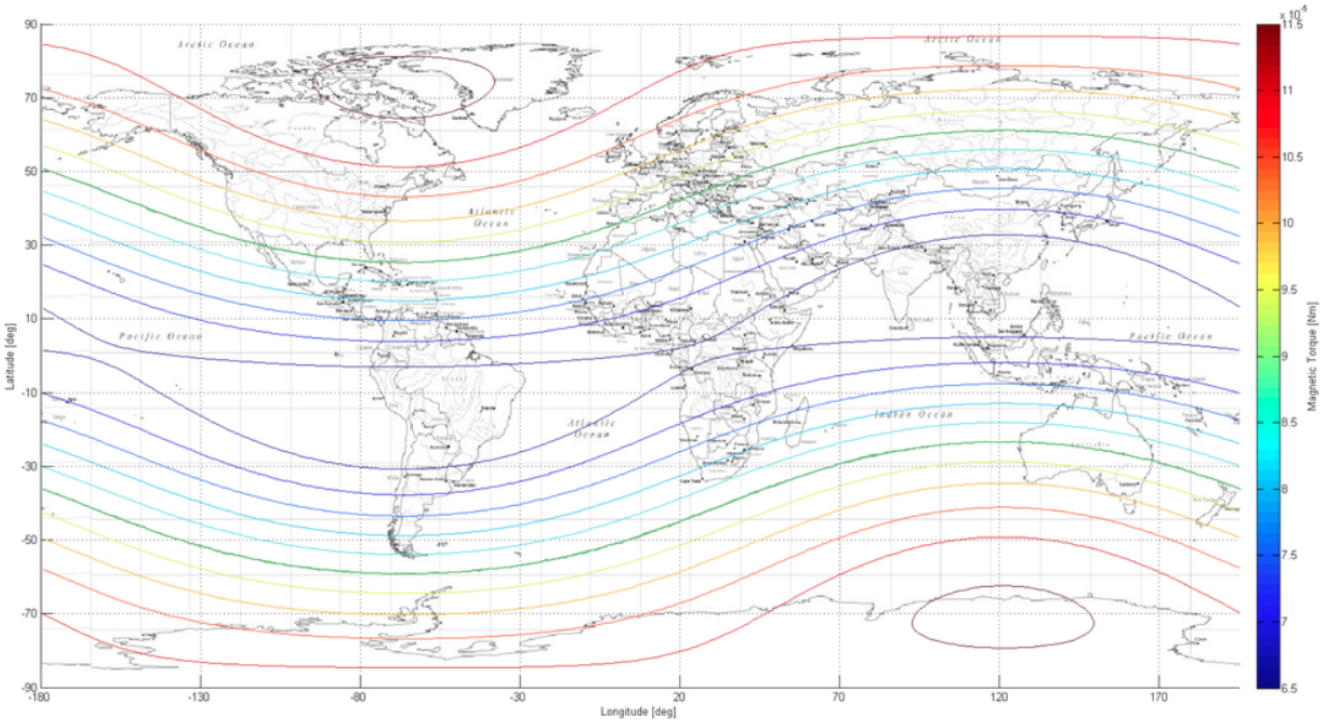

Figure 8.1: Magnetic Disturbance Torque Contour Plot at an altitude of 500 [km]

8.3.7 Internal Disturbances

Besides the external disturbances which are caused by environmental effects, there are internal disturbances. All these internal disturbances can be neglected as their value is small comparable to the external ones. These consist of the following [46]:

- Uncertainty in centre of gravity
- Thruster misalignment
- Mismatch of thruster outputs
- Rotating machinery
- Liquid Sloshing
- Dynamics of flexible bodies
- Thermal shocks on flexible appendages

8.4 Components and Architecture

Table 8.4 shows all components that will be used on both the transmitrer and the receiver satellites. The total amount of components will be shown in the architecture of this system in figure 8.2

Table 8.4: ADCS Components

Component	Manufacturer	Model	Performance	Power	Mass	Cost
Star tracker	SSTL	Procyon [84]	$X/Y < 5[arcsec], Z < 50[arcsec]$	$7W(DC)$	$2.2kg$	$\$354,300$
Fine Sun Sensor	SSBV	Fine Sun Sensor [85]	$360[arcsec]$	$7.2[mA](avg.), 26[mA](peak)$	$0.035[kg]$	N/A
Inertial Sensor	SSTL	Miras-01 [84]	$\pm 8[deg/s]$	$5[W]$	$2.8[kg]$	N/A
Magnetometer	SSTL	Magnetometer [84]	N/A	$< 300[mW]$	$0.14kg$	$\$125,800(2unit)$
Reaction Wheel	Honeywell	HR-12 [86]	$12, 25, 50Nms$	$105, 195[W](peak), < 22[W](ss)$	$6, 7, 9.5[kg]$	N/A
Reaction Wheel	Honeywell	HR 0610 [86]	$4 - 12[Nms]$	$< 80[W](peak), < 15[W](atV_{max})$	$3.6 - 5[kg]$	N/A
Magnetorquer	SSTL	MRT-30 Dual Coil [84]	$\pm 42[Am^2]$	$1.7[W]$	$1.8kg$	$\$125,100$

Figure 8.2 presents the ADCS architecture. It can be seen from the figure that the system consists out of three parts. The first part is concerned with the attitude determination, second concern with processing of obtained data and the last, the attitude control components. At initial stage, the de-tumbling stage satellite is going to use two fine sensors, two

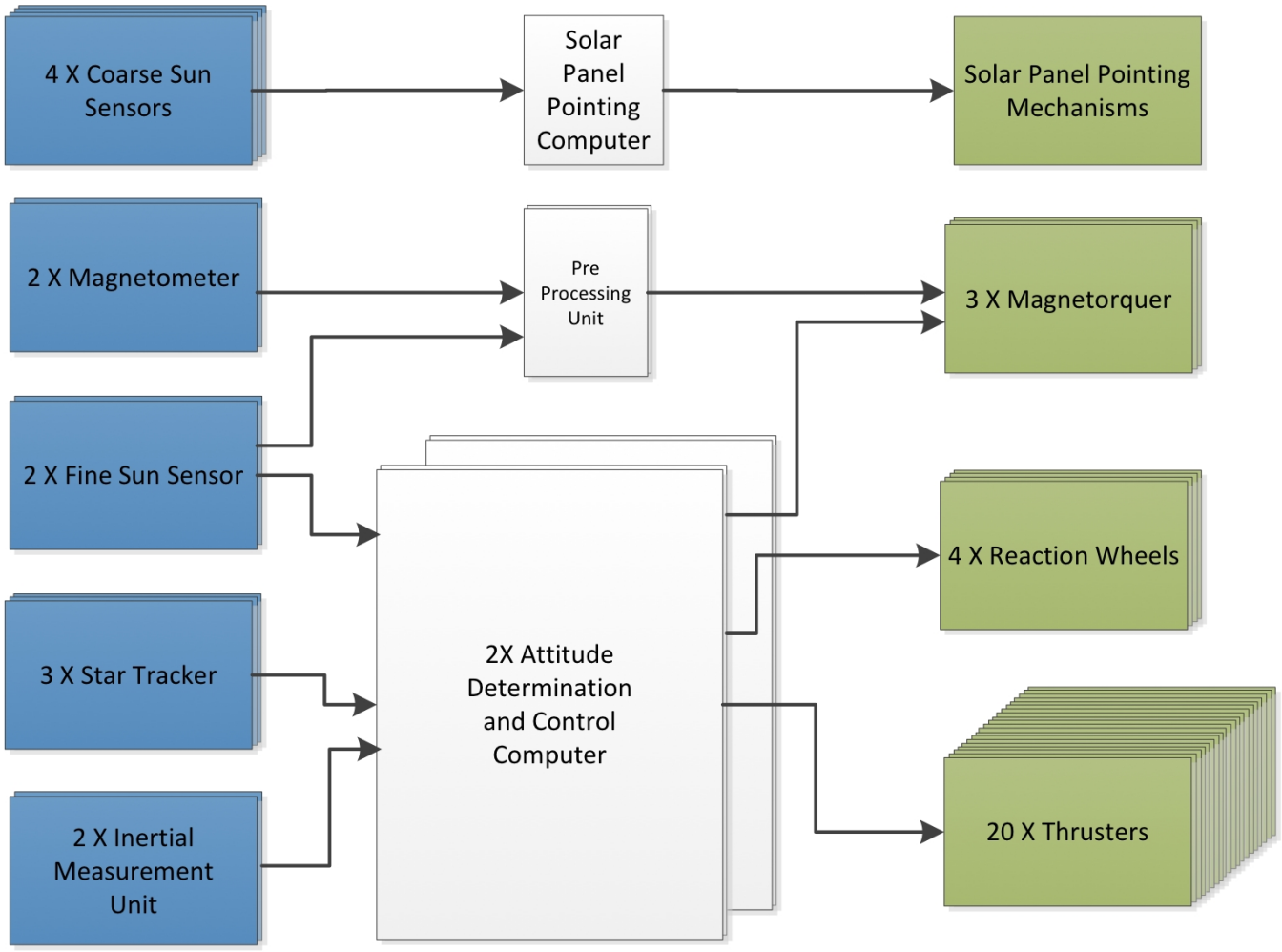

Figure 8.2: ADCS Architecture

magnetometers and pre-processing unit which will send signal and control two magnetorquers. This pre-processing unit is used for low power consumption requirements. For scanning and normal operation mode satellite is going to use two star trackers and two inertial measurement units (IMUs). These IMUs are going to be used only for scanning operation. As the error of IMUs increase with longer period of usage, each time the scanning mode starts, the IMU is switched on. IMUs are used in order to obtain high accuracy when SAR panels configuration are obtaining data. This information from sensors goes to the ADCS computer processor and then to the attitude control techniques. Attitude control is going to be done using three reaction wheels. Momentum obtained with these reaction wheels is going to be dumped with twenty thrusters position as showed in Figure 7.6. The redundancy of systems is taken into account as well. For attitude determination one more star tracker and one IMU are added. For the processing unit, one more computer is added for pre processing and one for processing of determination data. One more reaction wheel and magnetorquer are added to make the control part of the system more redundant.

8.4.1 Reaction Wheels Selection and Placement

Resulting from the Midterm Report, it had been concluded that the slewing requirement [ADCSSb] was the main driver for the size of the reaction wheels. The slewing operation, $theta_{slew}$, of 10 [deg] with t, the slewing time of 10 [s], demands torques of 2.16 [N], 5.86 [N] and 6.42 [N] in the roll, pitch and yaw axes of the spacecraft which is computed using Equation 8.20 [46].

$$T_{RW_i} = \frac{4\theta_{slew} I_i}{t^2} \tag{8.20}$$

Reaction Wheel Configuration

There are six different configurations which are of main importance as concluded by the work of H. B. Hablani [87]; Two wheel per axis, Six wheel hexagon, Four-wheel pyramid where the base edges are parallel to spacecraft axes, Four-wheel

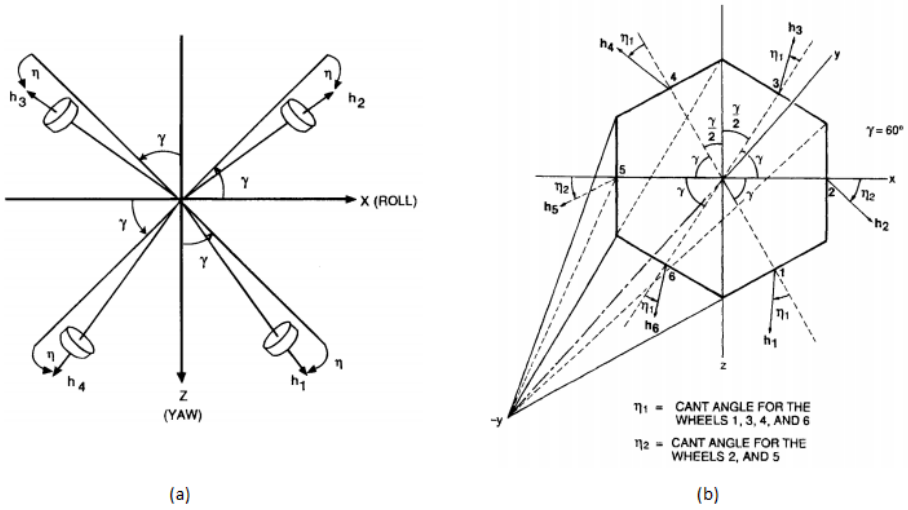

Figure 8.3: Reaction Wheel Configuration Options

pyramid where the base edges are at 45 [deg] to roll and yaw axes, Three wheel pyramid and Three orthogonal configurations. Due to the high accuracy requirements of the mission, the configuration has to be designed such that one wheel failure does not cascade into mission failure. Therefore a minimum amount of four wheels is required. The required control torque resulting from the slewing requirement has been assumed to be the same for all axes, as more axes control might be needed for secondary missions. The remaining four configurations, excluding the two wheel per axis configuration, are shown in figure 8.3 [87]. The three wheel configuration consists of two wheels opposing at each axis. In the figure 8.3 η is the cant angle which is the angle between the XZ-plane and the negative Y axis in the figure. For the four wheel parallel configuration the angle γ is equal to one and 45 [deg] for the 45 [deg] configuration. Note that for the spacecraft, the Z-axis and Y-axis are switched. In Hablani's work it was concluded that a cant angle of 35.26 [deg] was the most optimal solution for the Six wheel hexagon and the Four-wheel pyramid configurations.

There are three main parameters to be considered in the selection of the configuration, these are the torque capacity, power consumption and cost. In table 8.5 the torque capacity is given by $H_w, \dot{mx}/T_{mx}$ and the total power intercept due to nonzero initial wheel speed by $\sum_{i=1}^{n_{wheel}} |H_{w,mx}|/T_{mx}$. For this mission, the cost and the power are the two driving parameters of the system. Using six wheel configuration will increase reliability of the ADCS, this however will increase the mass and cost of the spacecraft which is not preferred. The remaining two options consist if the pyramid configurations. Note that the 45 [deg] setup will result in a reduction of the torque capacity by 17.2 %, though this will require 24.2 % increase in power compared to the parallel setup in the one wheel failure scenario. As the power consumption is more constraining for the mission, the four wheel pyramid (parallel) configuration is selected.

Table 8.5: Reaction Wheel Trade-off Matrix

	Torque Capacity No Failure	Torque Capacity One Wheel Failure	Total Power No Failure	Total Power One Wheel Failure
Two wheel per axis	0.5	1.0	3.0	3.0
Six wheel, hexagon	0.846	1.311	2.509	3.073
Four wheel pyramid (parallel)	1.045	2.091	2.449	4.182
Four wheel pyramid (45 [deg])	1.3	1.732	2.598	5.196

Selection

There are several reaction wheels in the market and a selection has to be chosen based on the torque and momentum storage capability. The configuration selected requires that 2.091 times the control torque is needed. The minimal momentum storage depends on the worst-case disturbance scenario, which is equal to adding all the external disturbances. Using Equation 8.21 the momentum storage required can be computed [46]. In this formula n is the number of disturbances, $T_{D,i}$ the disturbance, P_{orbit} the orbital period and k_i a factor of the orbit in which a disturbance maximizes. In Table 8.6 the momentum required for each axis is listed.

$$h = \sum_{i=1}^{n} T_{D,i} \frac{P_{orbit}}{k_i} \frac{\sqrt{2}}{2} \tag{8.21}$$

Table 8.6: The momentum stored in each axis

	h_x	h_y	h_z
Momentum Storage [Nm·s]	0.186	0.610	0.332

Placement

The placement of the reaction wheels has to be chosen such that the torque required does not increase. This can be done by placing the centre of gravity of both the reaction wheels and the satellite as close as possible. As an offset of these two centre's will result in increased torque requirement due to increased moment of inertia of the satellite due to effect of the parallel axis theorem [88].

8.4.2 Thruster

To unload momentum after saturation of the reaction wheels, thrusters are needed. The placement of the thruster has been specified in section 7.4.5. Using the centre of gravity computed using CATIA, the moment arm of different thrusters can be determined for the momentum unloading. Using Equation 8.22 with a burn time of 2 sec, as the momentum unload time, results in different force requirement for the thrusters. In table 8.7 the force of each thruster required is shown using the numbering in Figure 7.6. For the selection of the thrusters the see Chapter 7. Note that the values for some thruster is slightly lower than the minimum thrust level of 0.19 [N], this can be solved by applying a moment with the ADCS or with counteracting thrusters.

$$F = \frac{h}{L_{thruster} t_{burn}} \tag{8.22}$$

Table 8.7: Thrust Required for Each Thruster

Thruster	Force [N]	Thruster	Force [N]
1-y	0.418	5-z	0.144
1-z	0.159	6-x	0.127
2-y	0.418	6-y	0.418
2-z	0.159	6-z	0.144
3-y	0.953	7-x	0.290
3-z	0.159	7-y	0.953
4-y	0.953	7-z	0.144
4-z	0.159	8-x	0.290
5-x	0.127	8-y	0.953
5-y	0.418	8-z	0.144

8.5 Control Process

The last part of the attitude control system is the control process which is known as control law. There are two systems available; an open-loop and a closed-loop system. The open-loop system has its advantage in its simplicity, though can not compensate for any disturbances. Usually this system needs human input from the ground and is therefore slow and not suited for the mission compared to the closed-loop system [89] [90]. The closed-loop system has the advantage that the disturbances can be taken into account in real time which results in a faster response time of the spacecraft. To design the control process of the satellite the block diagram of the system, attitude dynamics and the controller of the subsystem is discussed in this section.

8.5.1 Block Diagram

The attitude determination and control subsystem consists mainly of three components; the plant which describes the attitude dynamics of the satellite, the controller and the sensors. The block diagram of the satellite can be seen in Figure 8.4.

Note that the sensor dynamics is included in the remainder of the section for simplicity. It is therefore assumed that the sensors are capable of providing perfect measurement and a unity feedback is used instead in the report.

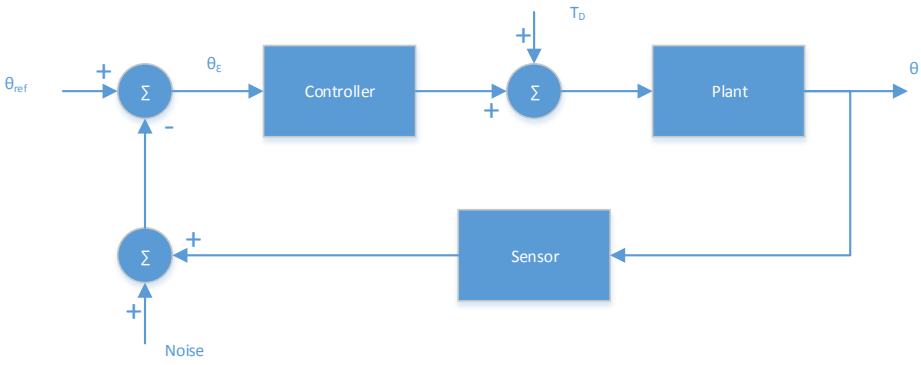

Figure 8.4: Control Process Block Diagram

8.5.2 Attitude Dynamics

For the plant the dynamics is needed of the spacecraft and of the requirement. In this report the disturbances effects except the gravity gradient have been taken to be constant as listed in table 8.1. The gravity gradient however has been implemented into the design. For this report the satellite has been assumed to be rigid.

The attitude dynamics is derived from the rotational Newtonian equation of motion which is shown in Equation 8.23 [91]. To apply this the Earth reference system has been taken as the inertial reference system. In this equation $\omega^{Body/IJK}$ is the angular velocity vector of the rigid body in an ECI frame IJK, $\boldsymbol{H}$ the angular momentum and M the external moment.

$$\dot{\boldsymbol{H}} = \left(\frac{d\boldsymbol{H}}{dt}\right)_{Body} + \boldsymbol{\omega^{Body/IJK}} \times \boldsymbol{H} = \boldsymbol{M} \tag{8.23}$$

This can be further derived to an Euler's rotational equation of motion as shown in Equation 8.24 [91] where $\boldsymbol{\omega} \equiv \boldsymbol{\omega^{Body/IJK}}$ and $\boldsymbol{I}$ is the mass moment of inertia matrix.

$$\boldsymbol{I} \cdot \boldsymbol{\omega} + \boldsymbol{\omega} \times \boldsymbol{I\omega} = \boldsymbol{M} \tag{8.24}$$

where,

$$\boldsymbol{I} = \begin{bmatrix} I_{11} & I_{12} & I_{13} \\ I_{21} & I_{22} & I_{23} \\ I_{31} & I_{32} & I_{33} \end{bmatrix} \tag{8.25}$$

$$\boldsymbol{\omega} = \begin{bmatrix} \omega_1 \\ \omega_2 \\ \omega_3 \end{bmatrix} \tag{8.26}$$

$$\boldsymbol{M} = \begin{bmatrix} M_1 \\ M_2 \\ M_3 \end{bmatrix} \tag{8.27}$$

Applying this to a principal axis reference frame to the equation of motion results in Equations 8.28 to 8.30. This is done as the product mass moment of inertias is negligible compared to the principal mass moment of inertias.

$$I_1\dot{\omega}_1 - (I_1 - J_3)\omega_2\omega_3 = M_1 \tag{8.28}$$

$$I_2\dot{\omega}_2 - (I_3 - I_1)\omega_3\omega_1 = M_2 \tag{8.29}$$

$$I_3\dot{\omega}_3 - (I_1 - I_2)\omega_1\omega_2 = M_3 \tag{8.30}$$

The gravity gradient torque in vector form is expressed in Equation 8.31 [91].

$$\boldsymbol{M_{gg}} = 3n^2 \cdot -\frac{\boldsymbol{R}_c}{R_c} \times \hat{I} \cdot -\frac{\boldsymbol{R}_c}{R_c} \tag{8.31}$$

To transform the orientation to the satellites body reference system with respect to the ECI reference system, Equation 8.32 has to be used which includes the rotational transformation due the circular motion of the satellite [91].

$$\boldsymbol{\omega} = \begin{bmatrix} 1 & 0 & -\sin\theta_2 \\ 0 & \cos\theta_1 & \sin\theta_1\cos\theta_2 \\ 0 & -\sin\theta_1 & \cos\theta_1\cos\theta_2 \end{bmatrix} - n \begin{bmatrix} \cos\theta_2\sin\theta_3 \\ \sin\theta_1\sin\theta_2\sin\theta_3 + \cos\theta_1\cos\theta_3 \\ \cos\theta_1\sin\theta_2\sin\theta_3 - \sin\theta_1\cos\theta_3 \end{bmatrix} \tag{8.32}$$

where,

$$n = \sqrt{\frac{\mu_E}{R_c^3}} \tag{8.33}$$

For small θ_i and $\dot{\theta}_i$ the system can be linearized which simplifies Equation 8.32 into Equation 8.34 to 8.36.

$$\omega_1 = \dot{\theta}_1 - n\theta_3 \tag{8.34}$$ $$\omega_2 = \dot{\theta}_2 - n \tag{8.35}$$ $$\omega_3 = \dot{\theta}_3 - n\theta_1 \tag{8.36}$$

Substituting Equations 8.34 to 8.36 and Equation 8.31 into Equations 8.28 to 8.30 results in the dynamic Equations 8.37 to 8.39.

$$I_1\ddot{\theta}_1 - n(I_1 - I_2 + I_3)\dot{\theta}_3 + 4n^2(I_2 - I_3)\theta_1 = M_{x,disturb} \tag{8.37}$$

$$I_2\ddot{\theta}_2 + 3n^2(I_1 - I_3)\theta_2 = M_{y,disturb} \tag{8.38}$$

$$I_3\ddot{\theta}_3 + n(I_1 - I_2 + I_3)\dot{\theta}_1 + n^2(I_2 - I_1)\theta_3 = M_{z,disturb} \tag{8.39}$$

In the above mentioned equations the angles θ_1, θ_2 and θ_3 represents the roll, pitch and yaw angles respectively. The torques $M_{i,disturb}$ represents the remaining disturbances which acts on the satellite. Theretofore the maximum value has been used for each axis which is listed in table 8.1.

8.5.3 Controller

Using MATLAB and its built in function SIMULINK the control process is designed as the control block diagram mentioned earlier. Note again that the sensor dynamics has been excluded and instead a unity feedback is applied. Removing the controller, thus by removing the reaction wheels one can deduce that applying the disturbance torque will result in an unstable configuration. This is clearly visible in figures 8.5a to 8.5c where a step function is applied to the control system, from left to right, the roll, pitch and yaw angles.

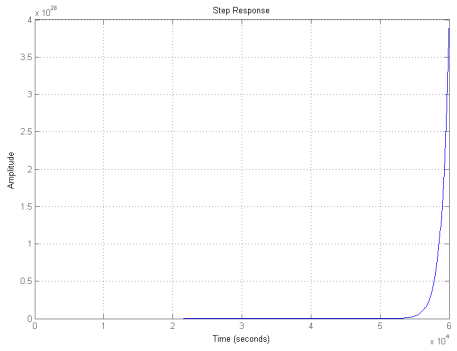

(a) Step Response Plot of Roll Angle without Controller and Feedback

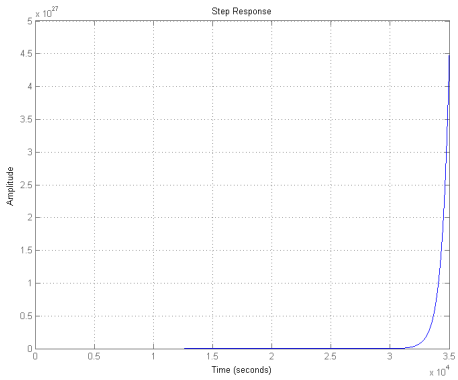

(b) Step Response Plot of Pitch Angle without Controller and Feedback

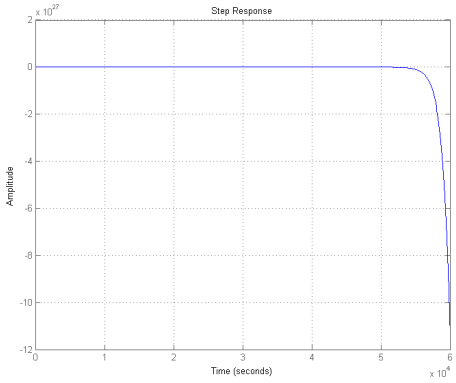

(c) Step Response Plot of Yaw Angle without Controller and Feedback

As seen in Figures 8.5a to 8.5c, the model is unstable as the function goes to infinity. Stabilizing the model with just a feedback loop can be seen in Figures 8.5d to 8.5f. Note that the model is still unstable as the function oscillates.

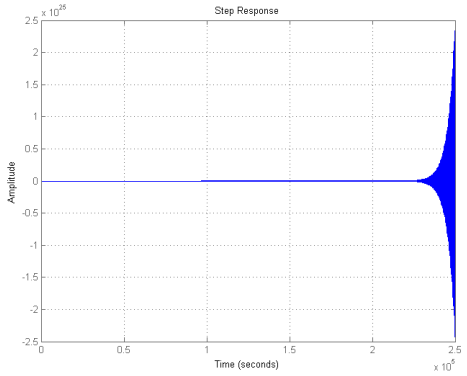

(a) Step Response Plot of the Roll Angle with Feedback and without Controller

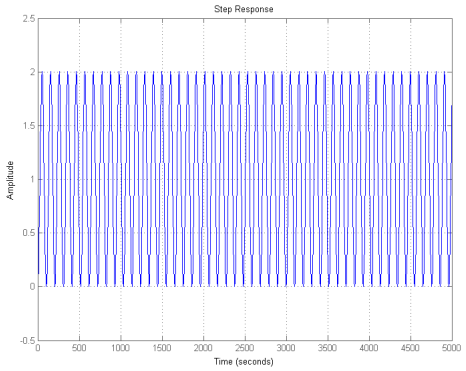

(b) Step Response Plot of the Pitch Angle with feedback and without Controller

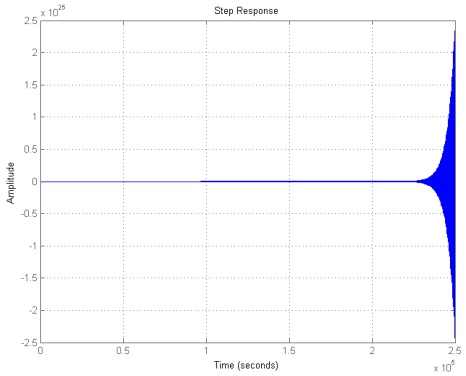

(c) Step Response Plot of the Yaw Angle with Feedback and without Controller

Table 8.8: Gains for each axis

	Roll	Pitch	Yaw
K_p	$5.50 \cdot 10^{10}$	$8.03 \cdot 10^{9}$	$1.88 \cdot 10^{9}$
K_r	$1.17 \cdot 10^{7}$	$1.58 \cdot 10^{7}$	$3.73 \cdot 10^{6}$
N	$3.74 \cdot 10^{5}$	$6.65 \cdot 10^{6}$	$40.0 \cdot 10^{5}$

To stabilize the system a controller has to be added. This controller consists of a proportional part and a differential part as noted in Equation 8.40 which results from the wheel dynamics [91].

$$T_{RW} = -K_p\theta - K_r\dot{\theta} \tag{8.40}$$

The variables K_p and K_r represent the proportional and the differential gains of the controller. This can be translated into the Laplace domain as shown in Equation 8.41 [89]. A slight modification has been added to the equation as MATLAB uses this convention in which K_d is the modified differential gain and N the filter coefficient.

$$TF_{controller}(s) = -K_p - K_d\frac{N}{1 + N\frac{1}{s}} \tag{8.41}$$

Adding the controller to the model and tuning the model in SIMULINK results in the numbers for the proportional and differential gains and filter coefficient shown in Table 8.8. The controller is tuned regarding the settling times of $1.64 \cdot 10^{-4}$ for both roll and yaw, and $6.25 \cdot 10^{-5}$ [s] for pitch due to subsystem requirements [ADCS1e1] and [ADCS1e2]. In Figures 8.5g to 8.5i, the results are shown for with the PD controller.

Note that the difference is noticeable as the oscillations does not occur. In Figure 8.5h the rise time is shown with 1, which is the time duration of the signal to increase from 10% to 90% of the reference level. With 2, the settling time is shown.

The model including the controller for the yaw performance however shows an unstable reaction after 45000 [s]. This can be explained due to the fact that a pole as seen in the root locus diagram in Figure 8.5 is located at 0.000000202287900 + 0.000000000000000i which is at the positive side of the real axis. Note that the cancellation of these poles is not possible

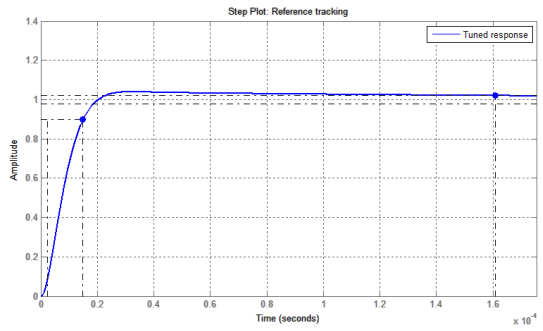

(a) Step Response of the Roll Angle with Feedback and Controller

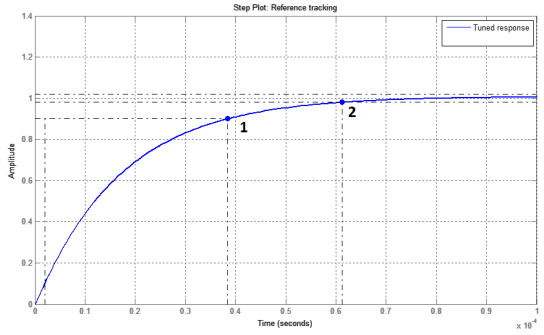

(b) Step Response of the Pitch Angle with Feedback and Controller

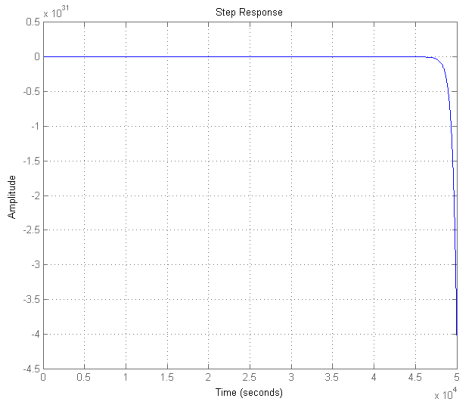

(c) Step Response of the Yaw Angle with Feedback and Controller

due to the numerical round-off and it is practically not able to make this stable. This however will not affect the system much as the time to reach instability is larger than one orbital period.

8.6 Sensitivity Analysis

Sensitivity analysis is a very important part of design. It shows if and how the design varies if some requirement is changed. If the altitude of a satellite is changed it will primarily influence the disturbances in orbit. Figure 8.6 shows all the disturbances as a function of an altitude. In this graph the aerodynamic drag is represented by the green continuous line, gravity gradient with a blue dashed line, magnetic field torque is presented as the continuous red line and the solar radiation pressure is presented by the continuous black line which is very close to the altitude axis line. At an altitude of about 415 [km] the aerodynamic drag is not a dominant disturbance any more. At this point gravity gradient takes it's place and stays reasonably constant. This means that if the altitude requirement is increased, there will be not many changes to disturbance torques and the design of ADCS.
If altitude is decreased the aerodynamic drag and gravity will increase while the magnetic torque will decrease. This change requires larger reaction wheels and thruster re-design for the momentum dumping. For an example if the altitude is decreased by 10 [%] the required momentum will increase for 17 [%]. This means that for an altitude of 465 [km] the required accumulated momentum is equal to 0.513 [Nms]. This change will not influence our design as the reaction wheels are able to cope with this change in design. This shows that our design is not sensitive in this aspect.
If the accuracy requirement of the satellite is changed, than there will be no changes, as the present ADCS subsystem is using the highest accuracy sensors and actuators types. One could only chose different model of a sensor, not the type. The present combination of star sensor and IMU used for attitude determination provide enough redundancy that if even an accuracy was increased for 20 % our subsystem will be able to cope with it.
If the mass, power or cost requirements were changed the new design should be made as the current ADCS just fits in the budgets.

8.7 Verification and Validation

In this chapter mainly two models have been made, the magnetic field model and the control model. These therefore should be verified and validated to evaluate its usability.

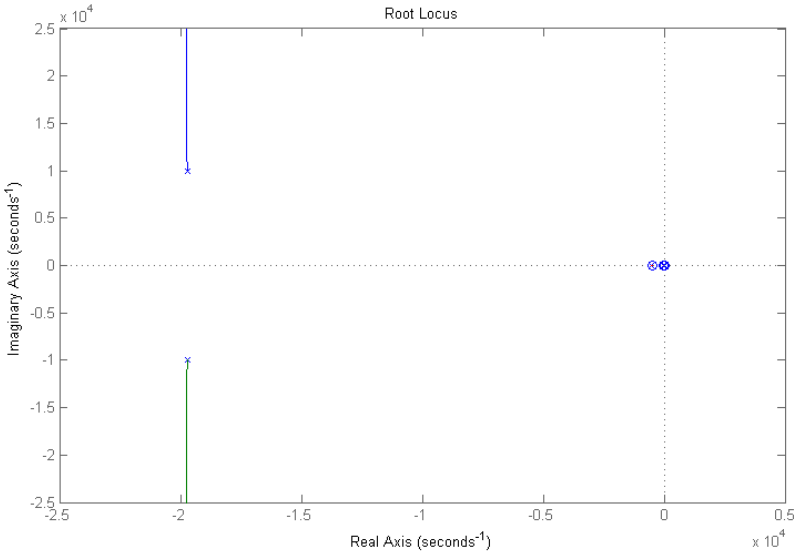

Figure 8.8: Root Locus of the Yaw Model Including Feedback and Controller

8.7.1 Magnetic Field Model

Verification of the magnetic field model should be done by comparing the analytical values to that of the computed values.

The validation part of the model can be done in several methods. The geomagnetic poles of the model can be computed and compared to the values of data centres. The poles are located at (170.0 [deg], 107.8 [deg]) for the south pole and (10.0 [deg], 287.8 [deg]) for the north pole determined by the model used in this report as calculated in section 8.3. This yields the following locations for the geomagnetic north and south pole respectively (80.0 [deg] N, 72.2 [deg] W) and (80.0[deg] S, 107.8 [deg] E) on the World Geodetic System [92]. Comparing this value to the data provided of (80.08 [deg] N, 72.21 [deg] W) for the north pole and (80.08 [deg] S, 107.79 [deg] E) by the National Geophysical Data Center using the World Magnetic Models [93] [94] results that the model is validated.

8.7.2 Control Process Model

The verification of the control process model developed with MATLAB can be done by comparing it to the analytical model. This model can be determined by finding the transfer function of the steady state matrix and compare it that to MATLAB's model. This Laplace transformation can be done using basic differential analysis. Besides verifying the transfer functions, the model can be checked on certain values of the disturbance torques.

Validating the control process model can be more difficult, as multiple parameters of the satellite have to be tested and measured to be accurate. Besides the geometric parameters of the satellites such as the mass moments of inertia, the disturbances model which is used in the control model need to be validated.

Gravity Gradient

Note that the gravity gradient is complex. The model used in this report only considers the J2 effect of the Earth which is not complete. Several other effects need to be taken into account to design for a better model such as J2,2 and the effects of other celestial bodies. Note that the several

Solar Radiation

The verification of the solar radiation can be done by comparing the analytical calculation of that of the model.

The validation part can be done by comparing the solar constant. This constant actually varies and comparing this to observations done by the SOlar Radiation & Climate Experiment (SORCE) mission [95] as shown in Figure 8.7.

Note that to improve this model the surface area and the reflectance factor should be tested and measured. Besides the incidence of the solar rays should be modeled to increase the accuracy.

Aerodynamic

Verification for the aerodynamic disturbances should be done as same as the other models.

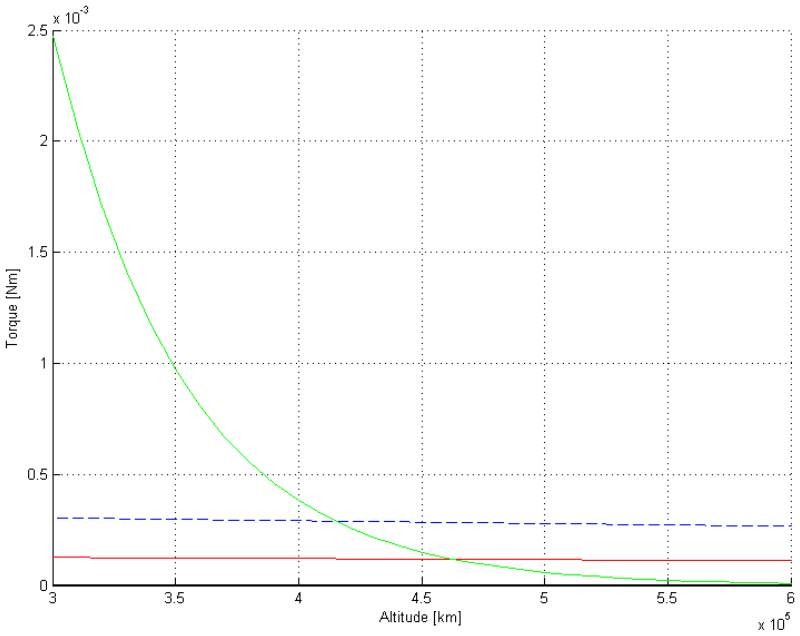

Figure 8.9: Disturbances as a function of altitude

The aerodynamic model should be validated using observations data from satellites. Errors might be induced due that the atmospheric density is hard to predict due to varying solar activity and the magnetic field. As the model used can have 100% deviation which is quite inaccurate. Besides the surface area, offset and the drag coefficient should be measured.

8.8 Risk Management

Consistent with the other subsystem, a risk management should be done as well for the attitude determination and control subsystem. The baseline report's risk management concluded, that the attitude maintenance failure is of highest priority for mitigation which therefore is the main focus on this section. The risk assessment of the ADCS can be found in Table 8.10.

Identification and Assessment

This section identifies and assess several risks regarding the attitude determination and control subsystem. In Table 8.9 the risk statement can be found of the Attitude Determination and Control Subsystem.

De-tumbling Mode There are several risks that can occur while the satellite is in this mode. First one is the failure of either magnetometer or magnetorquer. To reduce this risk, a redundant of each is used. Second risk that can occur is the failure of pre-processing unit or the computer for the de-tumbling. This is taken care of by use of redundant computer unit as well. If both fail, the batteries allow use of main computer. Likelihood of this is very low. Due to the reason that the de-tumbling is one of the most critical part of the mission, its impact is very high.

Acquisition Mode There are several risks that can be identified in this mode. The initial determination and control demands as the normal mode subsystem can not provide an adequate range. Failure of the acquisition determination and control system is not critical for the mission, though it is going to delay it, thus will delay generation of a revenue.

Slewing Mode The risks involved in the slewing operation is of high importance. If the satellite is not able to provide a slewing maneuverer, the spacecraft's mission will deteriorate as the slewing is needed to achieve the temporal resolution requirement. Failure in the slewing will result in a lower resolution.

Normal Mode Failure of the determination or the control system of the spacecraft will lead to mission failure as the acquisition ADCS system cannot provide the required accuracy. A redundant system can provide however a reduction in the likelihood of failure, though this will increase the mass, power and cost of the system. Another risk in the normal mode is the thruster failure for momentum dumping. This results in an disability to release the momentum which is accumulated by the external environment disallowing accurate payload operations. The last risk to be assessed of the normal mode is the

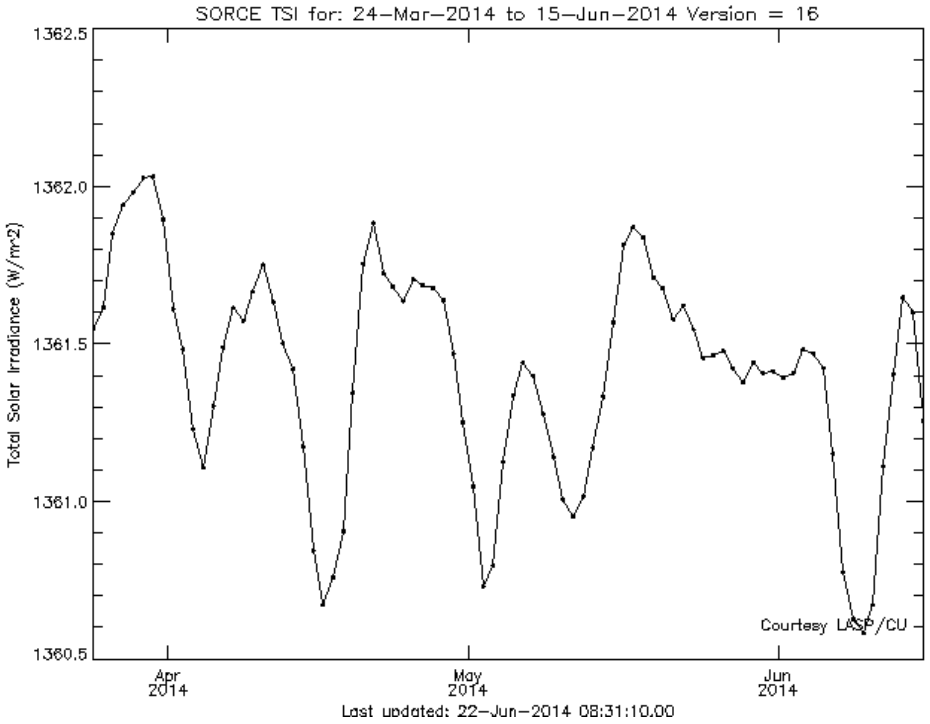

Figure 8.10: Solar Irradiance Data

risk concerning the gyros. As gyros will be used when the star sensors are blinded, failure of the inertial measurement unit results in an-inoperative state during this period.

Eclipse Mode Failure to provide the attitude determination during the eclipse mode will reduce its performance. A star eclipse will result in non-operation of the star sensors, failure of the gyroscopes will then result in .

End of Life At the end of the mission life, it is important that collisions with other spacecraft can be prevented. The likelihood of this is very low during this stage, though the impact of this risk is very high.

Table 8.9: Risk statement table

RN	Risk Title	Condition	Consequence
B-TO1	Attitude Determination Failure	The spacecraft is not capable to determine the attitude correctly.	The spacecraft will not achieve its target orbit.
B-TO2	Attitude Control Failure	The spacecraft is not able to adjust and control its attitude.	The spacecraft will not able to align its thrust to achieve the correct transfer orbit.
B-TO3	Thruster Failure	The spacecraft is not able to utilize its thrusters.	The spacecraft will fail to achieve its target orbit.
B-PM1	Initialization Failure of Payload	The payload is not able to initialize.	The payload is not able to operate.
B-PM2	Target Location Failure	The payload is not able to perform target locative functions.	The spacecraft may lead to not continuously monitoring.
B-PM3	Data Processing/Storing Failure	The data processing/storing unit malfunctions.	It will not be able to process or store the collected data.
B-PM4	Inability to Send Data	The communication system of the spacecraft malfunctions.	It may result in disability of transmission of the data.
B-MO1	Orbit Maintenance Failure	The spacecraft cannot maintain its orbit.	The orbit of the spacecraft will be decreased during its operational life time.
B-MO2	Attitude Maintenance Failure	The spacecraft cannot maintain its attitude correctly.	The spacecraft is not able to point its payload to the target location.

Risk Analysis

The assessed risks listed in Table 8.10 are mapped in a risk map as shown in Figure B.1g.

Table 8.10: Technical Risk Assessment Table

RN	Risk Title	Impact	Likelihood
F-ADCS.AM1	Acquisition Determination Failure	L	L
F-ADCS.AM2	Acquisition Control Failure	M	L
F-ADCS.SM1	Slewing Failure	H	L
F-ADCS.NM1	Inertial Attitude Measurement Failure	H	L
F-ADCS.NM2	Absolute Attitude Measurement Failure	VH	L
F-ADCS.NM3	Payload Attitude Control Failure	VH	L
F-ADCS.NM4	Incapability of Momentum Dumping	H	M
F-ADCS F-ADCS.EL1	End of life ADCS failure	L	VL

Mitigation

There are several high priority risks which should be mitigated to lower most of the risks to lesser priorities a redundancy system can be applied to lower the likelihood. This can be used by risks M-ADCS.AM1, M-ADCS.AM2, M-ADCS.NM1, M-ADCS.NM2, M-ADCS.NM3 and M-ADCS.NM4. However applying a redundant system to the Slewing Failure should be traded off between costs and performance. This will make system more complex and heavier. The mitigated risk map can be found in Figure B.1h.

Risk Handling

The tracking of these risks is of high importance during the Final Report. High risks should be monitored constantly to follow the sensitivity of applying the mitigation as it affects the performance, cost and time of the component. The changes to the ADCS should be documented and justified.

Chapter 9

Telemetry, Tracking and Command

The Telemetry, Tracking and Command subsystem is responsible for two different functions on board of the satellite, the on-board date handling as well as the communication between the satellite and external sources.

The on-board data handling is responsible for the regulation of the data streams on-board of the satellite, such as the housekeeping data generated by the different subsystems or the distribution of the commands received from the ground station to the different subsystems. Furthermore, it is responsible for the storage of the data generated by the housekeeping or payload data when it is not possible to transmit it to Earth in real time. The communication is responsible for the data transfer between the satellite and external sources, such as the ground station. It must ensure that the satellite is able to send all data generated on board down to Earth, within the time that the satellite is in contact with the ground station.

First, the requirements that the TT&C subsystem must fulfil are provided. Following this, the errors that can occur during operations as well as their mitigation is discussed in the risk management. Next, the architecture that is able to perform all tasks dictated by the requirements is chosen. The different components of this architecture are then sized, and the chapter is ended with an explanation of the model used to simulate the behaviour of the TT&C subsystem.

9.1 Requirements

The requirements for the TT&C subsystem are displayed below. The requirements mostly deal with the amount of data that needs to be handled by the system, as well as the speed with which this must be sent to Earth.

- **Subsystem Requirement [TT&C1a]**: The TT&C system shall be able to process 2.4 [Gb/s] during observations.
- **Subsystem Requirement [TT&C1b]**: The TT&C system shall be able to communicate the data to ground stations with a maximum delay of 10 minutes.
- **Subsystem Requirement [TT&C1c]**: The TT&C system shall be able to transmit data to Earth with a maximum bit error rate of 1e-8.
- **Subsystem Requirement [TT&C1d]**: The TT&C system shall be able to receive uplink commands from the ground station.
- **Subsystem Requirement [TT&C2a]**: The TT&C system shall record 5 [mb/orbit] housekeeping and position data.
- **Subsystem Requirement [TT&C3a]**: The TT&C system shall be able to store 50 [GB] of data.
- **Subsystem Requirement [TT&C4b]**: The TT&C system shall have a minimum lifetime of 5 years.
- **Subsystem Requirement [TT&C4d]**: The TT&C system shall have a maximum mass of 20.2 $[kg]$.
- **Subsystem Requirement [TT&C4e]**: The TT&C system shall have a maximum power consumption of 117.4 $[W]$.
- **Subsystem Requirement [TT&C4f]**: The TT&C system shall use existing ground stations during operational lifetime.

9.2 Risk Management

In order to assess the sensitivity of the subsystem, as well as to give an idea of which components are critical, the risks that are involved with the subsystem must be quantified.

Table 9.1: Technical Risk Assessment Table

RN	Risk Title	Impact	Likelihood
M-TT&C.C1	Payload Communication Failure	VH	VL
M-TT&C.C2	Telemetry Communication Failure	L	VL
M-TT&C.DH1	On Board Computer Malfunction	L	L
M-TT&C.DH2	Memory Storage Failure	L	M
M-TT&C.GS1	Ground Station Failure	M	VL

9.3 Architecture

In order to size the different components of the TT&C subsystem, first an estimation on the required components for the subsystem needs to be made. In order to assist in this estimation, an idea needs to be formed on the data moving through the satellite as well as the communication between the different subsystems. Therefore a data handling block diagram as well as a communications flow diagram are created. These can be found in Figure 9.1.

The communication flow diagram in Figure 9.1 shows the flow of information between the different subsystems, and it indicates the structure that is required to support the functions of the TT&C subsystem.

In order to be able to link all the different subsystems of the satellite, and to perform commands generated on board, or sent by the ground station, a computer needs to be incorporated into the satellite design. Furthermore, data storage is required on-board of the satellite, to gather and store sensor data generated by the satellite, or to store payload data, if it is not possible to transmit it down to Earth directly.

There are two different communication links between the satellite and the ground station, one link for the payload transmission of the data, and a second link for the actual communication between the satellite and the Earth.

- Housekeeping data
- Position data

The payload transmission is handled by a dedicated antenna due to the large amount of data generated by the payload. While this antenna could be used for the communication between the satellite and the ground station, this would require too much power and make inefficient use of resources. Therefore a smaller secondary antenna is added to the satellite, to provide communication at a lower data rate than that is required for the payload.

In order to determine the data that needs to be transferred by this secondary antenna, an estimation on the housekeeping data gathered on-board of the satellite needs to be made.

9.4 Subsystem Sizing

In order to reduce the risk and cost involved with designing a new system, off-the-shelf products are used. For the TT&C subsystem, two different types of antennas are required in order to communicate between the satellite and the ground. An X-band antenna, provided by SSBV, for the payload data, and an S-band antenna for the housekeeping data. The dimensions are shown in table 9.2.

Table 9.2: Antenna Size Satellite

Characteristics	X-band	S-band
Required Power [W]	125	20
Antenna Type	Horn Antenna	Helix Antenna
Antenna Size [mm]	0.274 (diameter)	100x100
Length [mm]	300	500

In order to check whether the link closes for these satellites, the different link budgets are calculated.

9.4.1 Link Budget

In this section the communication link budget is discussed. A link budget is a quantitative model that allows for analysing and predicting the performance of a connection between a transmitter and a receiver. In this budget the Signal to Noise Ratio (SNR) is determined which eventually, when compared to the required SNR, will define whether the link closes or not.

The following equation is applied to set up the overall link budget:

$$\frac{E_b}{N_0} = \frac{P \cdot L_l \cdot G_t \cdot L_a \cdot G_r \cdot L_s \cdot L_{pr} \cdot L_r}{R \cdot k \cdot T_s} \tag{9.1}$$

If this equation is expressed in [dB], it can be written as a summation or subtraction of successive terms. This eases the way of processing the data. The equation then can be written as:

$$\frac{E_b}{N_0}[dB] = P + L_l + G_t + L_a + G_r + L_s + L_{pr} - 10log_{10}R - 10log_{10}k - 10log_{10}T_s \tag{9.2}$$

The various terms included in this equation are explained in more detail below:

- *P, Transmitter power*
  The transmitter power is the power of the signal which is generated by the transmitter. This is an important aspect of the link budget. More power means more mass. Moreover, a higher transmitter power results in a higher channel capacity, which means a higher data rate is achieved, and consequently a higher SNR.
- L_l & L_r, *Transmission and reception feeder loss factors*
  Some losses occur over the connection feeders between the transmitter/receiver and the antenna. These losses are accounted for using these factors.
- G_t, *Transmitter Gain*
  Transmitter gain is a measure of how concentrated the signal power can be transmitted. Literally, G_t is the ratio between the power flux density send out to earth and the power flux transmitted by an ideal isotropic antenna (an antenna which emits signals with equal power in all directions). Transmitting with a higher gain means the signal is transmitted over a smaller region. The gain is related to the antenna size and the frequency which is used. A trade-off needs to be made between power and gain. This is dependent on the desired area that needs to be covered, and with what kind of quality.
- L_a, *Transmission Path losses*
  These are losses caused by the mediums the signal encounters when travelling to or from earth. The main factors are atmospheric and rain attenuation. These effects depend on the frequency at which the signal is transmitted. Measurement data is available for the amount of these effects and is allocated as a function of the different frequencies in several graphs [46].
- G_r, *Receiver Gain*
  The receiver gain is a measure of the ability of the receiving antenna to convert the received signal into power. Literally, G_r is defined as the ratio of its effective aperture area to the effective area of an isotropic antenna. Obviously, this value is linearly related to the size of the antenna. In addition, a higher frequency increases the gain of the receiving antenna.
- L_s, *Space Loss*
  The power of the signal diminishes when travelling a certain distance. Hence, how bigger the distance how bigger the loss. This loss is called the space loss. This loss is determined by considering the worst case scenario. Hence, this is the situation in which the biggest distance is to be travelled by the signal (S). Moreover, the space loss factor is dependent on its frequency and thus its wavelength.

$$L_s = \left(\frac{\lambda}{4\pi S}\right)^2 \tag{9.3}$$

- L_{pr}, *Antenna pointing loss*
  The antenna pointing loss accounts for the amount of signal loss due to inaccurate pointing of the antennae. The loss is determined by equating the pointing offset angle (e_t) and the antenna half-power beam width ($\alpha_{1/2}$) as follows:

$$L_{pr}[dB] = -12 \cdot \left(\frac{e_t}{\alpha_{1/2}}\right)^2 \tag{9.4}$$

- *R, Data rate*
  The data rate is the rate at which data is sent to earth. A bigger data rate is inversely proportional to the bit energy. Hence, the signal to noise ratio (SNR) is decreasing with an increase in demanded data rate. The amount of data rate follows from, the data rate which is generated during data acquisition (R_G), the percentage of orbit time the satellite is spending in this phase (Duty cycle, D_c) and the time per day needed or required to get this data to a ground station (T_{DL}). Because in this specific case the generated data rate cannot be altered the latter two parameters are influenced by the requirements stated. The following equation is applied:

$$R = R_G \cdot \left(\frac{D_c}{T_{DL}}\right) \tag{9.5}$$

- *k & T_s, Boltzmann Constant and System Noise Temperature*
  The constant "k" defines the relation between temperature and energy. Combined with the system noise temperature T_s it gives the Noise Power Spectral density (N_0). This specifies the power level of noise present over a certain bandwidth. The noise temperature or the system noise of a satellite is mostly dependent on the frequency it operates in.

- *$\frac{E_b}{N_0}$, Signal to Noise Ratio*
  This is the theoretically determined SNR which follows from the application of equation 9.1. This SNR is compared to the required SNR. The required SNR originates from the BER requirement. Different relations exist between BER and the required Signal to noise ratio dependent on the modulation type applied. Mostly, a safety factor of 3 [dB] needs to be added to the required SNR to account for filtering, timing and frequency errors [46]. Thus, this means that if a difference of 3 [dB] exists between the required and the theoretically determined SNR the link closes.

Different configurations can be analysed by adjusting the parameters accordingly. Different design choices can be made for antenna size, data rate or frequency. Alterations may be applied in such a way that the link closes eventually.

9.4.2 Communication Links

There are three important links to consider in order for the satellite to be able to perform its mission. The downlink of the payload data, the downlink of the telemetry data, and the uplink of commands from the ground station. The two most critical links, both downlinks, are shown in Table 9.3 and Table 9.4.

Table 9.3: Payload Downlink Link Budget

Item	Symbol	Value	Unit
Frequency	f	8	GHz
Transmitter Power	P	12	W
Transmitter Power	P	10.8	dBW
Transmitter and reception feeder loss	L_l&L_r	0.8	dB
Transmit Antenna Gain	G_t	24.4	dBi
Spacecraft Antenna Diameter	D_r	0.2740	m
Receiver Antenna Gain	G_r	55.9	dBi
Total Antenna Pointing loss	L_{pr}	-0.1	dB
Transmission path loss	L_a	0.40	dB
Space Loss	L_s	-178.7	dB
System Noise	T_s	135	K
Required Data rate	R	0.5	Gb/s
Calculated SNR	E_b/N_0	19.7	dB
Bit Error Rate	BER	10^{-8}	-
Required SNR	Req E_b/N_0	12	dB
Margin	-	7.7	dB

Table 9.4: Telemetry Downlink Link Budget

Item	Symbol	Value	Unit
Frequency	f	2.2	GHz
Transmitter Power	P	0.125	W
Transmitter Power	P	-9	dBW
Transmitter and reception feeder loss	L_l&L_r	0.8	dB
Transmit Antenna Gain	G_t	24.4	dBi
Spacecraft Antenna Diameter	D_r	0.100	m
Receiver Antenna Gain	G_r	55.9	dBi
Total Antenna Pointing loss	L_{pr}	-0.27	dB
Transmission path loss	L_a	0.40	dB
Space Loss	L_s	-178.7	dB
System Noise	T_s	135	K
Required Data rate	R	1	Mb/s
Calculated SNR	E_b/N_0	78.7	dB
Bit Error Rate	BER	10^{-8}	-
Required SNR	Req E_b/N_0	12	dB
Margin	-	66.7	dB

It is shown that for this specific configuration both links close because the margins are bigger than 3 [dB]. It must be notified that the required data rate is much lower than the generated data rate. The PanelSAR measures with a data rate of about 2.4 [Gb/s]. As a result the downlink time (T_{DL}) needs to be increased in order to get all the data to Earth. This means contact with the ground station needs to be withheld for a longer time. A simulation presented in the following section is designed to determine the amount of ground stations necessary for this connection. Consequently, based on equations regarding horn and helical antennas [46] the gain (G_r) and the half power beam angle ($\alpha_{1/2}$) of the spacecraft antennas are calculated.

9.4.3 Redundancy

In order for the satellite to not fail when one of the components fails, redundancy needs to be applied to the system. For the TT&C subsystem this leads to following the path of Noah, and including two of every component. This means that if one antenna fails, the second one can be activated so that communication is still possible with the ground. By combining two different transmitters, the data rate currently chosen of 0.5 [Gb/s] can be double in order to send all data down to Earth in a timely manner.

9.4.4 Memory Budget

Since it is not feasible to have 100% contact time with the ground, there needs to be room on-board of the satellite to store data. The amount of data storage required depends mainly on the difference between the generation of SAR data and the transmission of this data down to Earth. In order to estimate this difference, a simulation of the contact time between the ground and the satellite is created.

9.5 Simulation

As mentioned in the memory budget calculation, a model was made in order to calculate the communication time between the satellite and the ground station. The satellite is in contact with the ground station for a certain time before it starts measuring. During this time period, there is no data to be sent to Earth, so the total downlink time is only a fraction of the time that the satellite is contact with the ground station.

Furthermore, at the start of the mission, five different satellite pairs will cross the North Sea almost simultaneously, and all of these satellites must be able to transmit the data generated by the SAR instrument down to Earth.

In order to assess whether there is enough time to downlink all the generated payload data down to Earth a simulation of the five pairs of satellite flying over the North Sea is created. From this simulation, the measurement time, as well as the ground contact time for each individual satellite can be calculated, and from this the memory storage and the contact time can be found.

The link budgets are not included in this simulation, since they are calculated to close in the worst case scenario, so they will close at all other points in the orbit as well.

9.5.1 Model

The link duration model consists of several steps. These steps are graphically displayed in the following flow diagram.

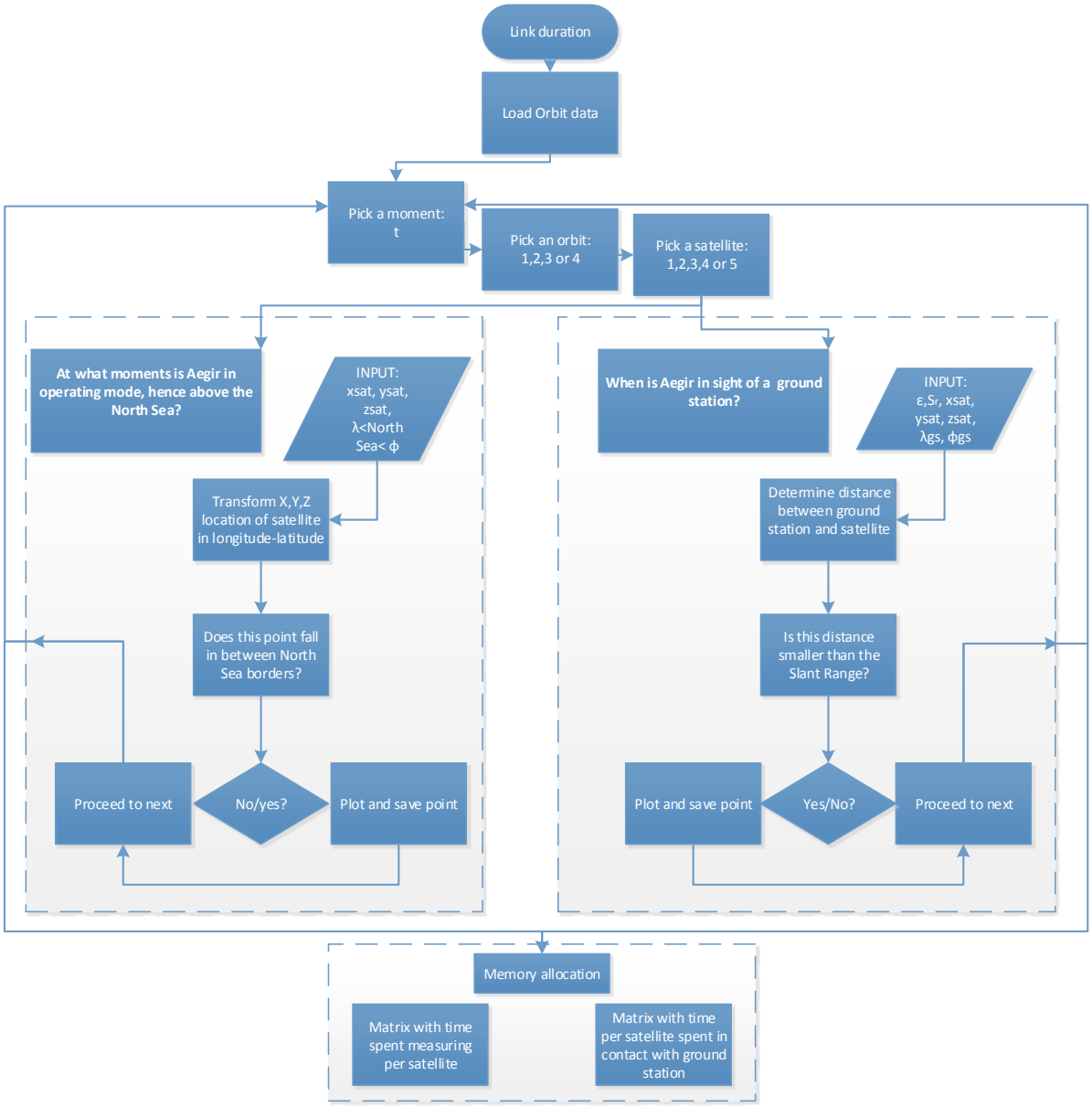

Figure 9.2: Simulation flow diagram

The model utilizes the orbit data obtained in the astrodynamics section. With these points, defining the orbits of the satellites, the link duration is determined. Two main loops can be distinguished:

- Loop 1: At what moments is Aegir in operating mode, hence at what moments is an Aegir satellite located above the North Sea?
- Loop 2: When is Aegir in sight of a ground station?

Thus, in loop 1, it is checked whether the satellite is in operating mode. This corresponds to the situation in which the satellite is flying over the North Sea and is close enough to obtain images. The North Sea is simplified to a quadrilateral area. The borders are defined by -5 to 10 degrees in longitude, and 50 to 60 degrees in latitude as is shown in Figure 9.3.

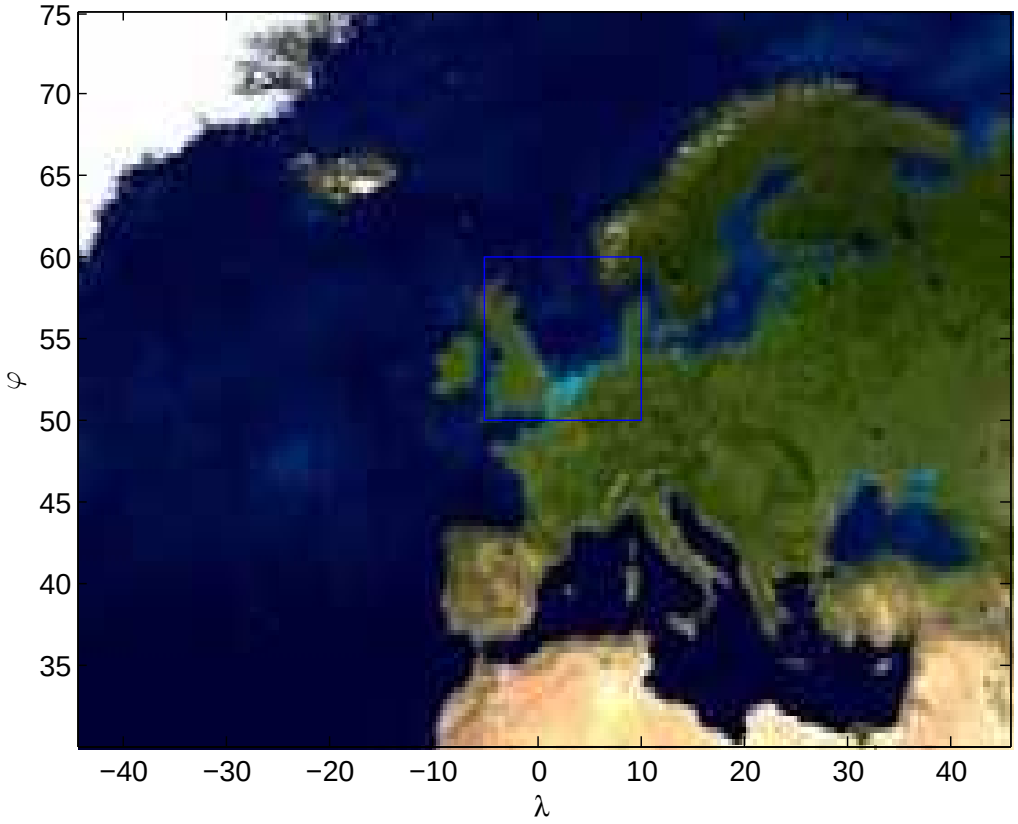

Figure 9.3: North Sea Area

If the satellite in a specific orbit is located above the North Sea as shown in Figure 9.3, the corresponding moment of time is saved and the ground track of the scanning beams are plotted on a world map (See Fig. 9.7a). The ability to "look sideways" with a certain side-look angle is taken into account. This procedure is repeated for every specific moment of time, orbit, and satellite. By marking the initial and final moment of measuring the total time can be derived.

In loop 2, a check is performed whether the satellite is in range of a ground station. This situation is encountered when the distance from satellite to ground station is smaller than the Slant Range. The Slant Range is the maximum distance the ground station's view is limited to.

The Slant Range is dependent on the elevation ϵ and geocentric semi-angle φ. These are calculated using the following formulas.

$$S_r = \frac{(R_e + h) \cdot sin(\varphi)}{cos(\epsilon)} = 2941[km] \tag{9.6}$$

$$\varphi = -\epsilon + cos^{-1}(\frac{R_E cos\epsilon}{R_E + h} = 0.3236[rad] \tag{9.7}$$

In which 'R_E' stands for the radius of the earth and 'h' for the altitude of the spacecraft. The altitude varies with inclination. Nevertheless, it is assumed the altitude is constant for the satellites at different inclinations. This difference in altitude is small and does not have a big influence on the result. The procedure of loop 2 thus consists of checking whether the distance of satellite to ground station is smaller than the calculated Slant Range. This is done for all satellites in all orbits at all moments. By applying the same method as has been done for loop 1, the time frame in which a link is possible can be derived. By allocating all of these data points followed by the corresponding satellites and orbits in matrices a clear overview is given. This can be seen in the following section.

9.5.2 Results of the model

In this section the results of the simulation are exemplified. The simulation was executed for a period of approximately 2 hours, applying time intervals of 10 seconds. Three X-band receiving ground stations were chosen as conveniently located as possible, to aid in the downlink of data. The results would eventually show that 3 ground stations are enough for the downlink. These are the following:

- Kiruna, Sweden
- Matera, Italy
- Neustrelitz, Germany

It was assumed that all ground stations consisted of more than one receiving antenna in order to handle fly-overs that follow each other closely. The coverage of the three ground stations and their locations are plotted in Figure 9.4.

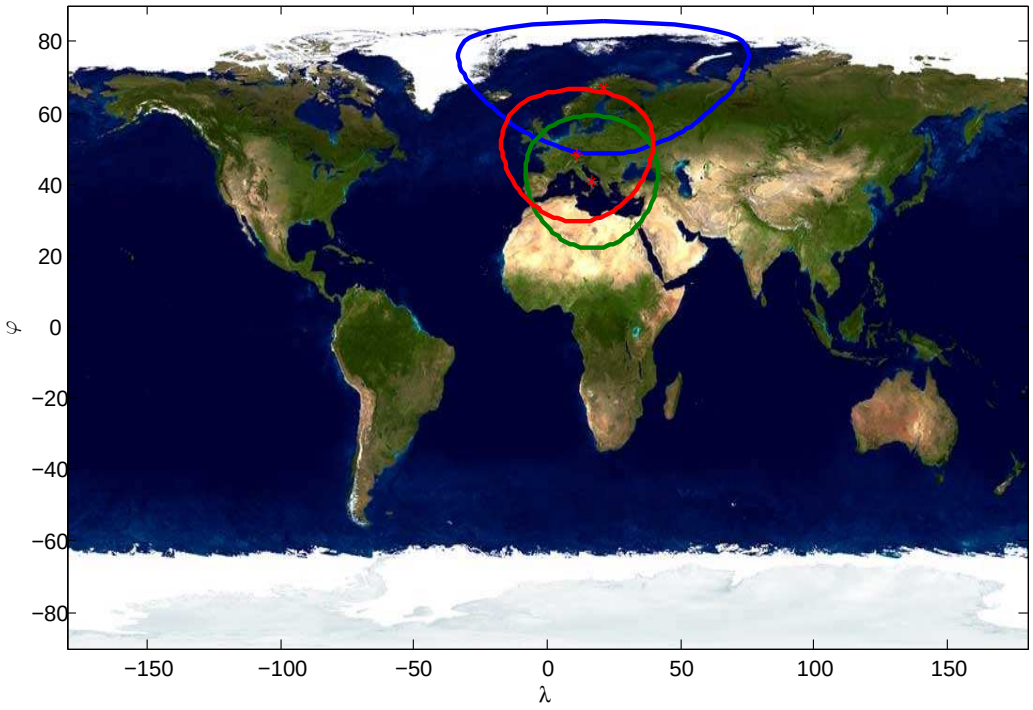

Figure 9.4: Selected Ground stations for the downlink of payload data

The results of loop 1 and 2 are presented in Table 9.5 and 9.6 respectively. Table 1 shows, for each orbit, and for each satellite in that orbit, the moments it starts and stops measuring. Furthermore, it shows the total time measured. This total time is combined with the earlier defined data rate for the SAR-panel of 2.4 [Gbits/s] to calculate the total amount of data produced. For example, satellite number 1 of orbit 2 started its operation on the 541st time interval and ended it on the 547th. Note that the time intervals are equal to 10 seconds. Hence, the satellite begins at the 5410th second and ends at the 5470th. This corresponds to a total operating time of 60 seconds, and a data amount of 144 [Gbits].

Table 9.5: Measuring time and data

Satellite #	Orbit #	Start	End	Total time [s]	Amount of data[Gbits]
1	2	541	547	60	144
1	3	471	489	180	432
2	2	554	564	100	240
2	3	487	503	160	384
3	2	567	580	130	312
3	3	502	518	160	384
4	2	1	9	80	192
4	2	580	597	170	408
4	3	518	533	150	360
5	2	7	23	160	384
5	2	594	613	190	456
5	3	534	548	140	336

In Table 9.6 the same parameterse are presented, however, these are regarding loop 2. Hence, instead of starting its operational mode, it initializes the transmission of data down to Earth. Moreover, the downlink of the measured data is performed using a data rate of 0.5 [Gbits/s]. For example, satellite 1 of orbit 2 commences its downlink in time interval 541

and stops at 600. The satellite is able to downlink data for 590 seconds with a data rate of 0.5 [Gbits/s]. This results in an amount of 295 [Gbits] which can be transmitted to the ground stations.

Table 9.6: Link Duration with ground station

Satellite #	Orbit #	Start	End	Total time [s]	Amount of data[Gbits]
1	2	541	600	590	295
1	3	471	526	550	275
2	2	554	615	610	305
2	3	487	541	540	270
3	2	567	630	630	315
3	3	502	557	550	275
4	2	1	53	520	260
4	2	580	645	650	325
4	3	518	572	540	270
5	2	7	67	600	300
5	2	594	660	660	330
5	3	534	588	540	270

For an estimation on the memory budget of the satellite, the "worst case" is taken, where the satellite is measuring for the longest time. This generates 456 [Gb] of data. The estimated amount of memory required on-board of the satellite is taken to be equal to 1.5 this amount, 85 [GB].

9.5.3 Discussion of results

In this section the results presented in Tables 9.5 and 9.6 are discussed. The question that needs to be answered is whether the satellites have enough time to complete their downlink, or in other words are capable of transmitting the data in one fly-over. Several things can be noticed when reviewing the tables of the former section:

- The starting points of loop 2 coincide with the starting moments of loop 1. This is as stated earlier a consequence of the fact that data cannot be sent down to earth when the satellite has not performed any measurements yet.
- Not all satellites make an appearance in the tables. This is caused by the fact that the analysis is conducted only for a period of 2 hours. In these 2 hours, orbit 1 and 4 just do not happen to fly over the area of interest.
- A distinct number of satellites do not achieve enough contact time with the ground station in order to transmit all data. To illustrate this: the maximum amount of data that is obtained during one fly-over is 456 [Gbits]. The total amount of seconds this particular satellite is in contact with the three ground stations is 660, corresponding to an amount of data of 330 [Gbits]. So there is not enough time to send all the data down to Earth. A solution needs to be found. This can be solved in a variety of approaches. One can add either ground stations to increase contact times, or transmitters to increase downlink datarate.

9.6 TT&C Ground track

As it was mentioned in the discussion about the simulation model, ground stations for the downlink of payload data are chosen as conveniently as possible dependent on the data rates and locations. However, these ground stations are specifically used for the downlink of the payload data and are operative in X-band to achieve a higher data rate. The communication for the TT&C does not depend on such high data rates. Consequently, the S-band is used for these purposes. Secondly, a TT&C communication link needs to be acquired as much as possible during an operating life. This is in contrast to the case in which payload downlink is performed for the shortest instance of time possible. Thus, in order to maintain contact with the satellites encircling the Earth a smart global distribution of ground stations needs to be chosen. These ground stations are located in convenient places along the track of the satellites.

Building a dedicated system increases the costs of the entire project. This is the main reason existing ground stations are used for the tracking of the satellites. Examples of existing ground systems are EStrack [96], AFSCN [97] and TDRSS . Besides these well-known ground systems many commercial ground stations offer their services for housekeeping and payload data down- and uplink. Because the mission at hand concerns a Dutch mission a logical choice is the EStrack. The EStrack is a collection of ground stations operated by ESA, and ground stations which are operated by commercial faculties in collaboration with ESA. The ground stations of the Estrack are shown in Figure 9.5.

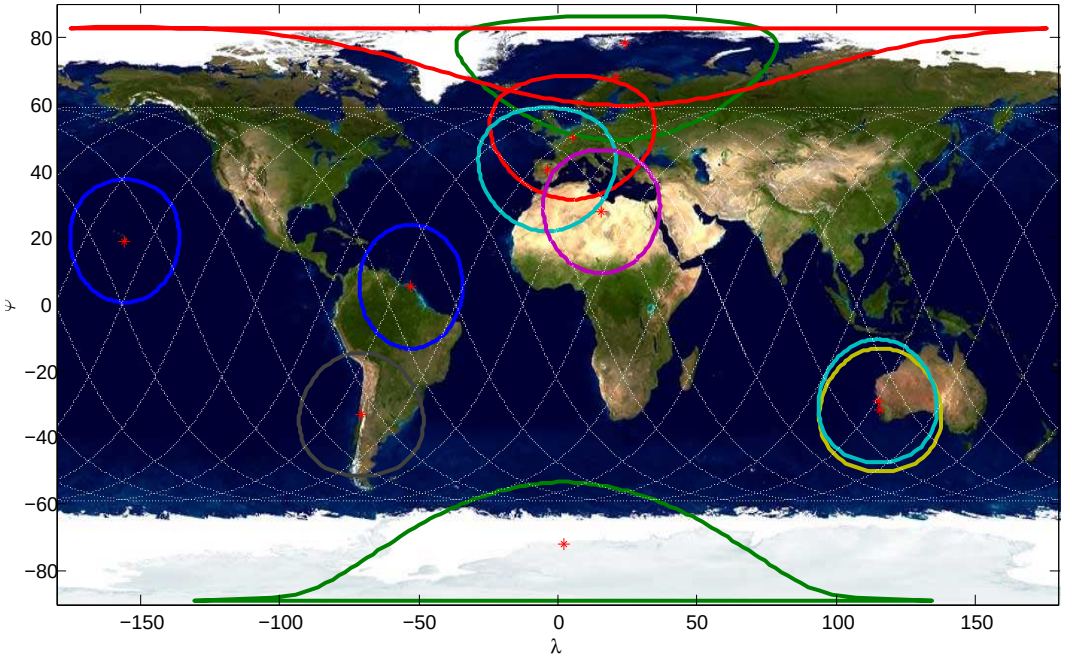

Figure 9.5: EStrack ground station including the corresponding coverage

As can be seen, eleven ground stations are included:

- Kiruna, Sweden
- Kourou, French Guyana
- Redu, Belgium
- Villafranca, Spain
- Maspalomas, Gran Canaria
- Perth, Australia
- Santiago, Chile
- South Point, Hawaii
- Trollstation, Antarctica
- Svallbard, Norway
- Dongara, Australia

The ground stations are either operated by ESA or by companies offering their ground station for commercial use in cooperation with ESA. All of these ground stations make use of antennas with sizes ranging from 13 to 15 [m], and which are capable of sending and receiving S-band signals.

Besides the ground stations and their coverage areas, the ground track is plotted for one satellite pair for one entire day. It can be noted from Figure 9.5 that several fly-overs take place with the EStrack ground stations. The total amount of desired contact time depends on the amount of housekeeping, telecommand and telemetry data that needs to be transmitted. The housekeeping data mainly consists of information about the satellite. Furthermore, a rapid response is needed in case of an emergency. These kinds of data exchange do not need a lot of contact time and can be easily transmitted in one fly over. However, when the satellites are in operation above the North Sea adequate positioning data needs to be supplied by ground systems in order to focus both satellites of one pair on the same area. In the worst case, when 5 satellites follow each other closely when scanning the North Sea more than one antenna is needed to track the 5 satellites. Because of this, several ground stations are distributed over Europe.

9.7 Sensitivity Analysis

In order to test the sensitivity of the TT&C, a small analysis is made to see how changing the input values of the system affects the sizing. The most important aspects that influence the sizing of the TT&C subsystem, are the altitude that the satellite is flying at, and the amount of data that needs to be transferred down to Earth.

Increasing the altitude that the satellite is flying at will affect the strength of the link budget. An increase in the altitude of 100 [km] will lead to a decrease in the link budget of 1 [dB], which can still easily be covered by the current budget. On the positive side, the increase in altitude will lead to a longer contact time with the ground station. This increase in contact time decreases the amount of data that needs to be transferred to the Earth per second.

The amount of data transferred down to Earth is directly related to the amount of data generated by the payload. Increasing the measurement time during a single orbit means that either the amount of data transferred per second will increase, or the amount of contact time with the ground station. Increasing the measurement time by 30 [s] in an orbit, will increase the amount of data generated by 9 [GB]. Since the antennas are already working at maximum capacity, this would lead to an increase in the number of transmitters on-board of the satellite.

Another solution is to add multiple ground stations, which means that more data needs to be stored on-board of the satellite. Due to the safety factor in the memory budget, no changes to the satellite need to be made.

9.8 Verification and Validation

In this section the verification and validation of the model are outlined. At first the verification is discussed in more detail.

Verification needs to be performed in order to assure the quality of work. Hence, a closer look can be taken at the results of the simulation. A convenient way of reviewing the data is by plotting the data. In Figure 9.6 the ground tracks are plotted for the period of the simulation, including the areas of interest. The areas of interest can be distinguished as being the North Sea area and the ground station visibility regions.

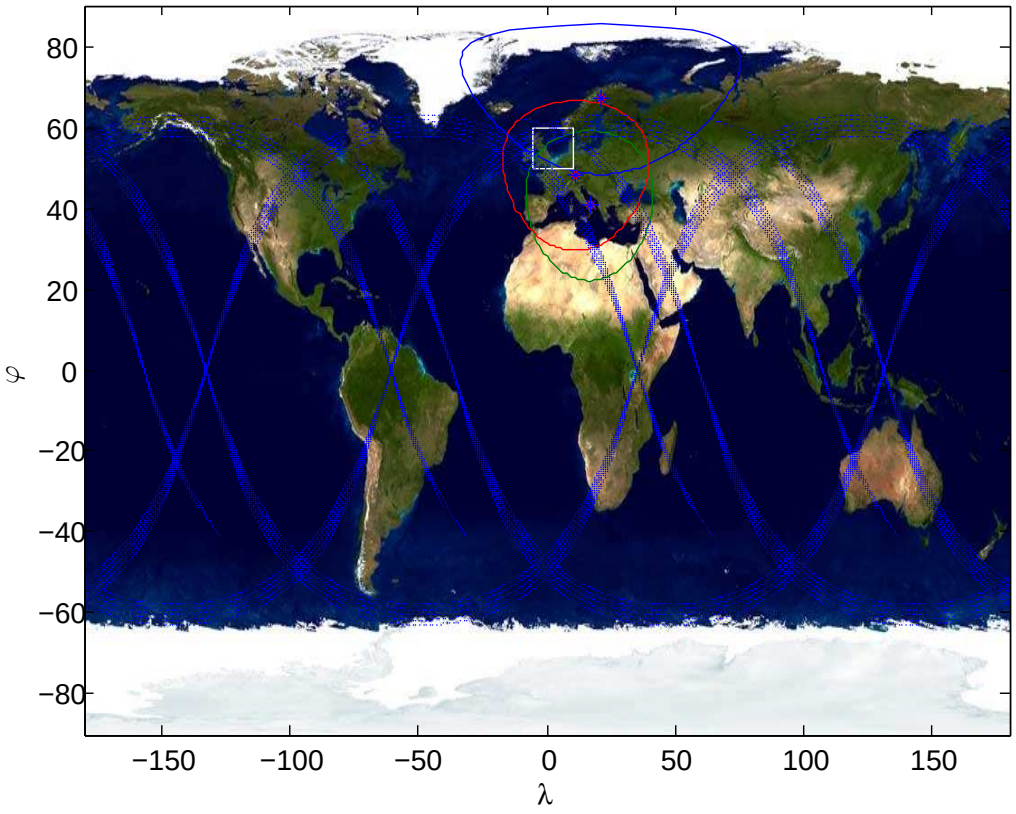

Figure 9.6: The 2 hour orbits for which the analysis is performed

The only relevant data points of these ground tracks are the ones which are inside of the areas of interest. Hence, the corresponding locations to the listed values in the aforementioned tables are plotted on the Earth map. These plots are shown in Figure 9.7a and 9.7b.

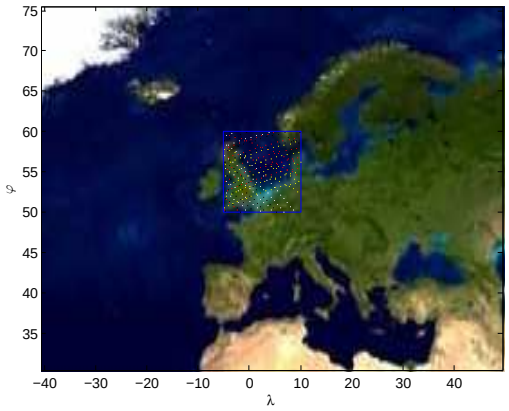

(a) Points at which Aegir is scanning the North Sea

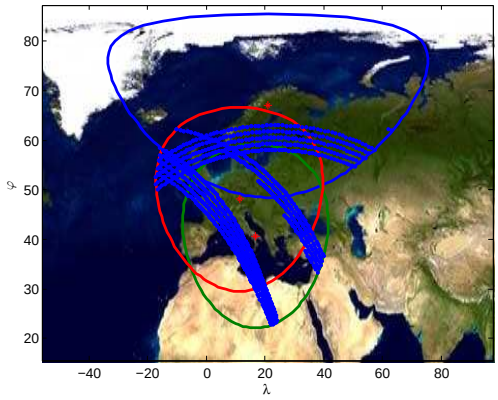

(b) Points at which Aegir is in contact with one of the three ground stations

As can be seen, only the points of interest are considered. Thus, the points used to determine the amounts of data correspond to the right corresponding locations. Further verification needs to be performed for the orbit data. This is discussed in the astrodynamics section.

Validation needs to be conducted to justify the simulation and to determine how accurate the model approaches reality. This is done by comparing the obtained results with other SAR using satellite missions. For example, the NovaSAR-S [98] has a duty cycle of 2 to 3 minutes per orbit. This is a similar amount compared to the obtained results, of which the maximum amount of time spent measuring is equal to 190 seconds.

For the validation of the downlink time the coverage areas of the ground stations are compared. This is presented in the following Figures:

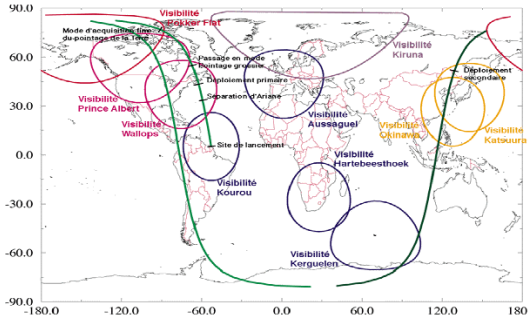

(a) Reference coverage area mapping [99]

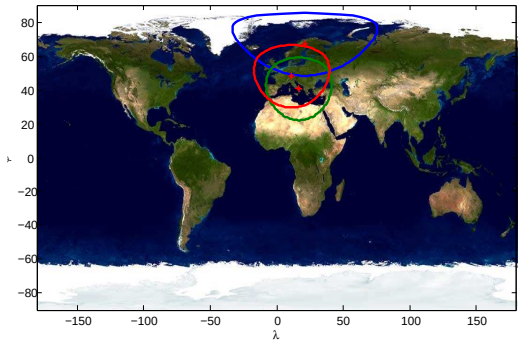

(b) Coverage area which is obtained using the model

Figure 9.7c shows the ground station network of the Spot-4. This satellite flies at an altitude of 830 [km]. Coverage areas are dependent on the operating altitude of the satellite. So, in order to be able to compare these two figures correctly, the ground station coverage should be determined for this specific altitude. This is shown in Figure 9.7d. If a close look is taken at the ground coverage of the Kiruna station, it is noted that both ground coverages are similar in shape. The resulted link durations are mainly based on these coverage areas. Hence, it is concluded that the results are valid.

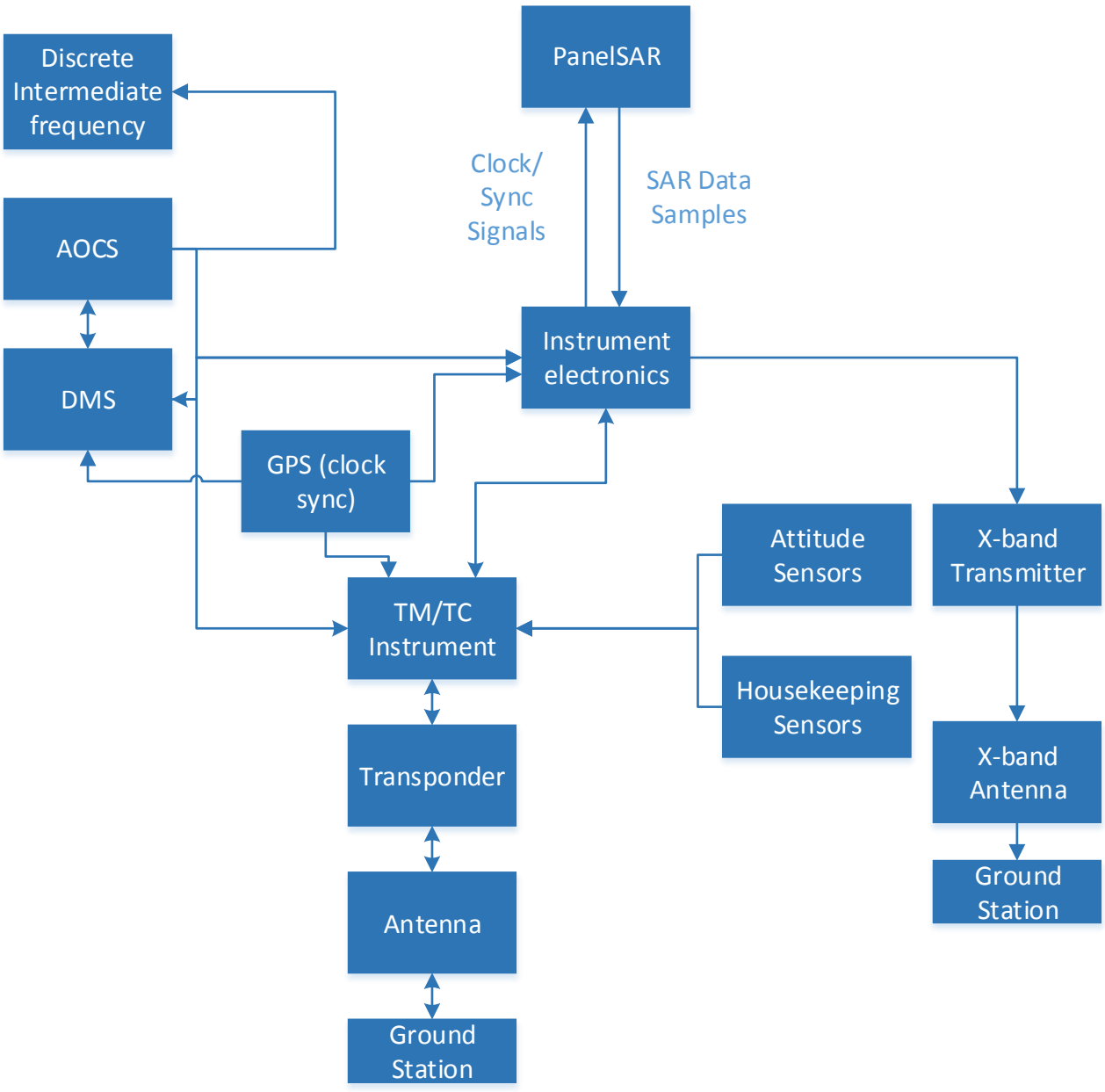

Figure 9.1: The communication between the different subsystems of the satellite

Chapter 10

Structures and Mechanisms

This section will cover the design of the structural system and some necessary mechanisms. Structures includes providing a skeleton to attach everything on and protection from the environment, both in the launcher and in space. The structure must be able to withstand the launch forces, shocks, and vibrations. Besides, it is important to take into account the building process of the satellite. The design and sizing of the support structure in the launcher has been discussed in chapter 5.

10.1 Requirements

This subsection will show all the requirements for the structure. The toughest structural requirements come from the launch. The launch conditions can be found in the Soyuz User Manual [100].

- **Subsystem Requirement [STR1a]**: The structure shall provide attachment points for all components.
- **Subsystem Requirement [STR2a]**: The structure shall withstand a compressive load factor of 5 during launch.
- **Subsystem Requirement [STR2b]**: The structure shall withstand a load tensile factor of 3 during launch.
- **Subsystem Requirement [STR2c]**: The structure shall withstand a side load factor of 0.5 during launch.
- **Subsystem Requirement [STR3a]**: The structure shall comply with the vibrations of the launcher.
- **Subsystem Requirement [STR3b]**: The structure shall comply with the acoustic vibrations of the launcher.
- **Subsystem Requirement [STR4a]**: The structure shall have a minimum lifetime of 5 years.
- **Subsystem Requirement [STR5]**: The structure shall have dimensions 2.10x1.60x1.05 [m].
- **Subsystem Requirement [STR6]**: The structure shall have a maximum mass of 112.5 [kg].
- **Subsystem Requirement [STR7]**: The mechanisms shall have a maximum power consumption of 9.8 [W].
- **Subsystem Requirement [STR8]**: The solar panels shall be able to rotate 150 degrees.

Sine Vibration Figure 10.1 shows the sine vibrations for the Soyuz

Table 10.1: Soyuz Vibrations [100]

Direction	Frequency Band [Hz]	Sine Amplitude [G]
Longitudonal	2-50	0.8
	50-100	0.5
Lateral	2-25	0.6
	25-100	0.4

Acoustic Noise Table10.2 shows the acoustic noise for the Soyuz rocket

Shock Loads Shock loads can produce very high G's for an extremely short period. This can be dangerous to very stiff structures and will most likely not form a problem. Tests should be performed to confirm that the structure can handle the shock loads.

Table 10.2: Acoustic Noise Soyuz [100]

Octave Center Frequence [Hz]	Flight Limit Level
31.5	126
63	133
125	136
250	138
500	134
1000	125
2000	121
OSPL (20-2828)	141.9

10.2 Risk Management

The identified risks and their likelihood and impact are listed in table 10.3.

Table 10.3: Structure Risk Assessment Table

RN	Risk Title	Likelyhood	Impact
M-STR1	Structural Failure	VL	VH
M-STR2	SAR Deployment Mechanism Failure	L	VH
M-STR4	Solar Panel Directioning Mechanism Failure	VL	H

As can be seen, the impact of the indicated risks are all high. Therefore it is important to keep the likelihood low. Applying redundancy to these components is not an option. So the design shall have to be reliable and a proper verification and validation shall be performed. The risk map for structure can be found in Figure B.1m.

10.3 Architecture

The bottom of the satellite is an aluminium honeycomb plate. The SAR panels are mounted underneath it. All electronic boxes such as IMU's, computers ,and batteries will be placed on this aluminium honeycomb plate on the inside of the satellite. Part of the aluminium plate will function as a radiator to radiate all the heat produced by these electronic boxes into space.
A truss structure is designed that transfers the loads from the bottom plate to the support structure in the launcher. This is not truly a truss structure because the beams are welded and not pinned, though for the stress calculations it will be simplified as a truss structure. Besides the beams, some cables will be used. They only have to carry small tensile forces.
The solar panels on the sides of the satellite are placed under a 60 [deg] angle relative to the bottom plate. They can be rotated over an angle of 150 [deg] with the use two small electro motors. There are three SAR panels underneath the satellite. One of the panels must be deployed after launch. This is done by releasing a pre-wound torsional spring. Figure 10.1 show the layout of the satellite structure.

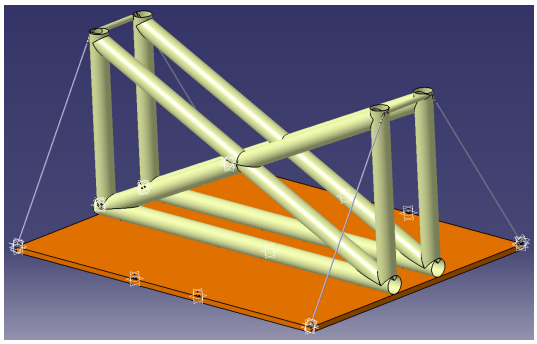

Figure 10.1: Structure Layout

10.4 Subsystem Sizing

This subsection will discuss the sizing of the truss structure, the aluminum honeycomb panel, and the solar panels. Lastly, the position of the centre of gravity is discussed.

10.4.1 Truss Structure Sizing

Figure 10.2 shows a schematic drawing of the main part of the truss structure. On the right side, the honeycomb panel will be attached. Points A and D are attached to the support structure in the launcher. Two of these planes will be placed parallel so they will both take half of the load applied by the honeycomb panel. For this calculation all the mass of the satellite, without structural weight, is assumed to be on the honeycomb plate. This is a reasonable assumption because almost all the satellite components will actually be mounted on this plate.

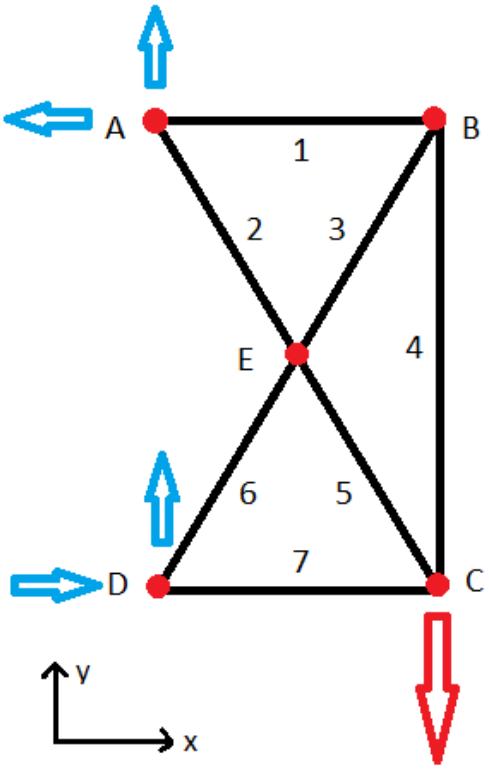

Figure 10.2: Truss Structure Schematic

Two load cases are considered. The first case is a gravitational load of 5. The second case is a gravitational load of -3. In order to find the force in each member, equilibrium equations must be set up for points B, C and E in both x and y direction. The result is the following matrix equation. [A] shows the directions of the trusses, [f] shows the forces in the trusses and equation 10.1 shows the applied loads. Equations 10.1 to 10.6 are taken from [101].

$$[A][f] = [X] \tag{10.1}$$

This system has more unknowns than equations. This means that the truss structure is statically indeterminate and more information is required to solve the system. This extra information is the stiffness of the beams. With the following equation, the system stiffness matrix [K] can be calculated.

$$[K] = [A] \cdot [k] \cdot [A]^T \tag{10.2}$$

[k] is the stiffness matrix and it contains the stiffness of all elements. The stiffness of each element can be calculated with equation 10.3.

$$k = (\frac{E \cdot O}{L}) \tag{10.3}$$

In this equation O is the cross sectional area of a beam. A circular cross section is chosen because this can cope well with compression loads.
With the equation 10.4, matrix [u] can be calculated. This contains the change in position of points B, C, and E.

$$[K][u] = [X] \tag{10.4}$$

Now the change in length of the beams is easily calculated.

$$[d] = [A]^T \cdot [u] \tag{10.5}$$

And with this, the forces in all the members can be determined.

$$[f] = [k] \cdot [d] \tag{10.6}$$

For both cases, the beams must be strong enough to deal with the maximum stress and must not buckle. Buckling turns out to be critical for most beams. Therefore a large diameter of 10 [cm] is chosen. This will allow for a smaller cross sectional area and therefore a lighter design. Coming to a final thickness of each beam requires an iterative process because the [k] matrix changes when the thickness's are adjusted. In the end, the following results were obtained.

Table 10.4: Truss Thickness

Truss Number	1	2	3	4	5	6	7
Thickness [mm]	1.5	3	3	4	3	3	2

This results in a mass of 40.34 [kg] (for both planes). Two more small beams and some cables are used to strengthen the structure. This leads to a total mass of the truss structure of approximately 43 [kg].

10.4.2 Bottom Panel Sizing

In order to have a panel that is both stiff and light, a honeycomb panel is chosen. This panel will be made out of aluminium because this can easily conduct the heat that is produced by the components that are mounted onto it. Part of this panel panel will function as a radiator. The panel will have a total thickness of is 2.5 [cm]. The honeycomb is 2.3 [cm] thick and the skins are 1 [mm] thick. The density of the honeycomb can be approximated with equation 10.7 [102].

$$\rho_{core} = \frac{8}{3\sqrt{3}} \frac{t}{d} \rho \tag{10.7}$$

Figure 10.3 shows what t and d are in the equation. The mass of the panel can now be calculated and turns out to be 34.2 [kg].

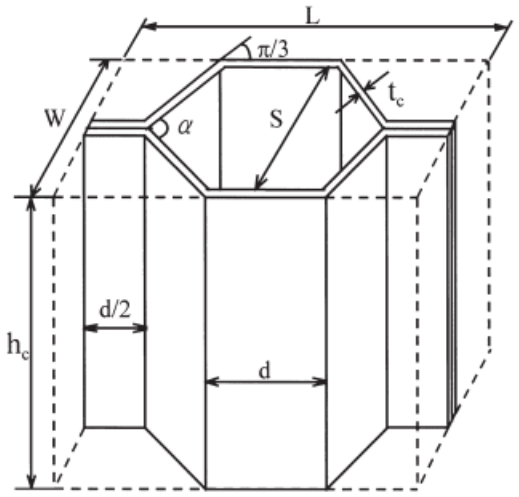

Figure 10.3: Honeycomb Material [102]

10.4.3 Solar Panel Sizing

Three solar panel configurations were considered: the body mounted configuration, two degrees of freedom configuration and the one degree of freedom configuration. The body mounted configuration is discarded because it can not be pointed towards the sun and therefore a large area is required. There is not enough surface area available for this configuration. The two degrees of freedom configuration is omitted as well, as it requires more mass and complexity for the pointing mechanism. Besides, the freedom in pointing the solar panels would be limited because the thruster fumes could damage them. Therefore the one dimensional configuration has been chosen.
For this configuration, the power system requires a solar panel area of 4 [m^2]. The weight of the solar cells is included in the power system though the mass of the panels that support the solar cells is included in the structural mass. A thin honeycomb panel will be used with a mass of 4 [kg] per square meter. This results in a mass of 16 [kg].

10.4.4 Centre of Mass

Adding up the mass contributions of the truss structure, the bottom panel, and the solar panels, a mass of 93.3 [kg] is obtained. Adding the weight of the 4 small electromotors that turn the solar panels and the torsional springs that deploy the SAR panel, a total mass of 95 [kg] is obtained. An extra 5% of mass is added to account for other small contributions like fittings ,screws and harnesses. This adds up to a total weight of roughly 100 $[kg]$ for the structures and mechanisms subsystem.

It is important to know the centre of mass of the satellite for both propulsion and for attitude control. The x, y, and z coordinates of the centre of mass can be calculated with the following simple formulas.

$$x_{cm} = \frac{\sum m_i x_i}{\sum m_i}, y_{cm} = \frac{\sum m_i y_i}{\sum m_i}, z_{cm} = \frac{\sum m_i z_i}{\sum m_i} \tag{10.8}$$

In these equations, x , y, and z are taken with respect to the body reference frame.

10.5 Sensitivity Analysis

If the satellite mass increases, a heavier structure will be required in order to still be able to withstand the launch forces. The easiest way to strengthen the struss structure would be to increase the thickness's of the beams. This way the dimensions of the beams can stay the same and no other complications will arise. The bottom panel might have to adjusted as well. This can be done by making it thicker, using a thicker skin, or changing the values of d and t in equation 10.7.

10.6 Verification and Validation

Verification: Manual checks have been performed in order to verify that the script that is made to calculated the forces in the truss structure works as intended. Tests must be performed to verify that both the satellite structure and the support structure in the launcher can handle the applied loads and vibrations.
Validation: Honeycomb panels are often used in space. This validates the use of them.

Chapter 11

Power

In this chapter the power subsystem is discussed starting with the requirements. The risk management is discussed in the second section. Thereafter the architecture is discussed with the help of an electrical block diagram. In the fourth section the sizing of the subsystem is explained and a final design is given. Then a sensitivity analysis is done in the fifth section. The last section of the chapter contains the verification and validation of this subsystem.

11.1 Requirements

The requirements that were found in the Baseline Report are listed below. The maximum mass of a satellite changed to 498 [kg] due to new launcher requirements, therefore the mass budget decreased for the power system to 121.02 [kg]. This is 24.3 % of the total satellite mass. The maximum dimensions of the solar array are determined by the structure of the satellite which is 6.84 [m^2].

- **Subsystem Requirement [POWER1a]**:The power system shall provide a minimum power to the payload of 150 [W] per panel.
- **Subsystem Requirement [POWER2b]**:The power system shall have a minimum lifetime of 5 years.
- **Subsystem Requirement [POWER2c]**:The solar array shall have a maximum dimension of 6.84 [m^2]
- **Subsystem Requirement [POWER2d]**:The power system shall have a maximum mass of 121.02 [kg].
- **Subsystem Requirement [POWER2e]**:The power system shall have a maximum power consumption of 88.0 [W].
- **Subsystem Requirement [POWERpc]**:The power system shall be able to shut down power for each component that needs power.

11.2 Risk Management

The risks listed in Table 11.1 can be mapped. This is shown in Figure B.1i. The colour shown in the table shows the criticality of the risk, which can be red, yellow, blue, or green in descending order.

Table 11.1: Technical Risk Assessment Table for Power System

RN	Risk Title	Impact	Likelihood
PWR-SC1	Solar array damage due to radiation	L	H
PWR-SC2	Solar array damage due to small objects	M	M
PWR-BTR1	Damage to Battery	M	L
PWR-BTR2	Battery overload	M	L
PWR-PCN1	Power conversion failure	H	L
PWR-CB1	Short circuit	M	L

All risks mentioned are on the same level of criticality which is in the blue area. As the risks identified in Table 11.1 are the most highly to happen from all of them, therefore they need to be mitigated. The damage due to the solar radiation (PWR-SC1) will be accounted for in the design of the solar cells, such that there will be enough power at the End Of Life (EOL). Small objects that float in space (PWR-SC2) cannot be accounted for and collisions will happen, this can be mitigated by dividing the solar array area between several places on the satellite. The risk of battery failure (PWR-BTR1, PWR-BTR2) will be mitigated by adding a redundant battery cell and an existing battery will be chosen that is already

been proven to be space worthy. To counter the impact of the power conversion failure (PWR-PCN1) and short circuit (PWR-CB1) a fuse box will be added. The mitigations can be found in Figure B.1j.

11.3 Architecture

The power subsystem will exist out of 3 parts, these are the solar arrays which are composed of Photo voltaic cells, the batteries, and the power management. While designing the structure of the satellite it was decided that the solar array will have one degree of freedom. For the solar cells it was decided to use Spectrolabs Ultra Triple Junction (UTJ) Solar Cells [103] which should deliver 350 [W/m^2].

To make the system work while in eclipse, secondary batteries (rechargeable) are required. The VES 16 Li-ion battery cells of Saft [104] are lightweight and have a small size and are therefore selected. It is recommended to spread the load on the batteries, in this case there is chosen for 4 batteries of which one is for redundancy.

The power system will be managed by a Power Conditioning and Distribution Unit (PCDU). Most of the PCDU systems are modular and will differ for each mission. For the design of the PCDU an electronic block diagram is made, which can be found in Figure 11.1. The figure shows the relations between each system that uses power and the bus voltages. From the figure it can be seen that the PCDU needs at least thirty-one exits for a 28 [V] unregulated current, twelve exits for a 5 [V] regulated current and 20 connections for the thrusters so that each component that uses power can be shut down. Besides, each exit will have it's own fuse. The Modular Medium Power Unit from Terma will be used, it is completely modular and

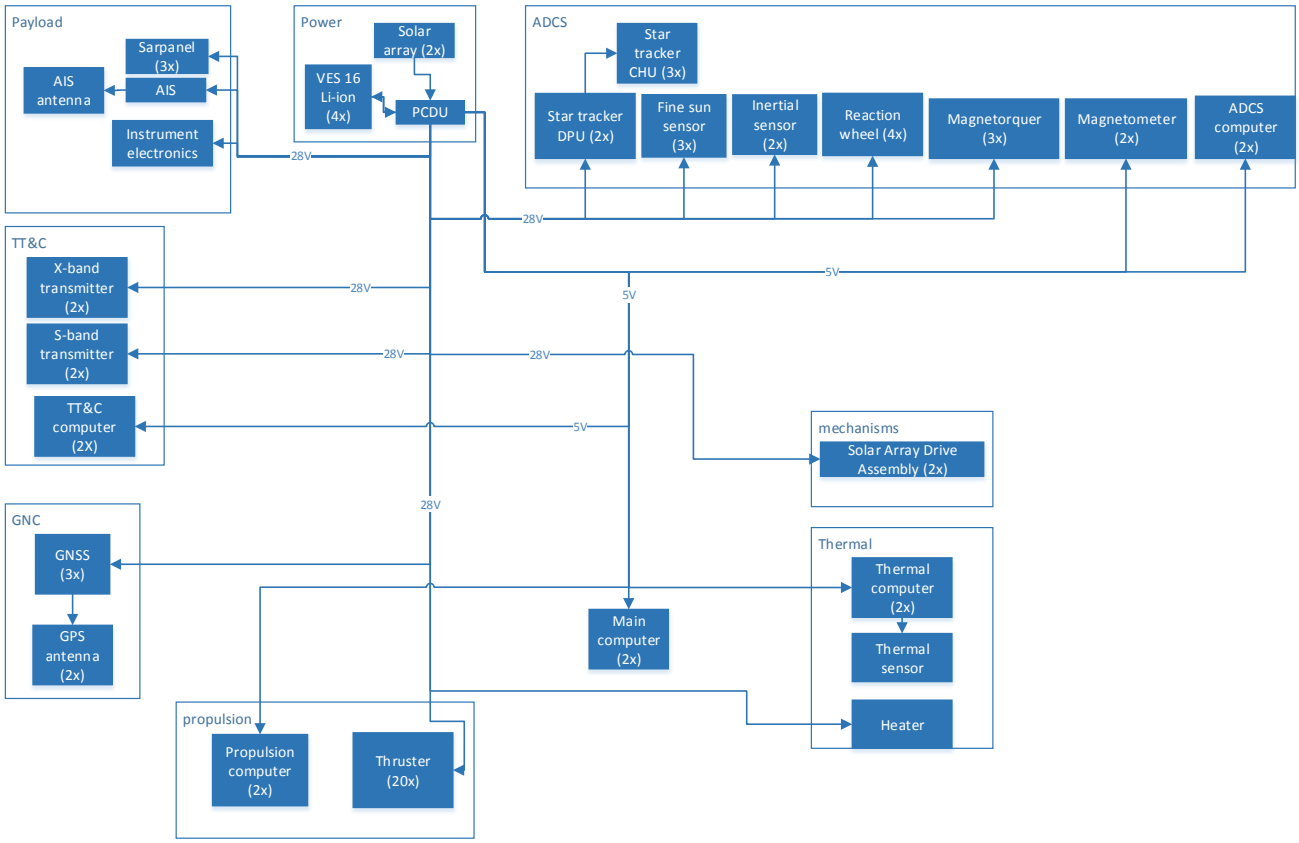

Figure 11.1: The electronic block diagram

will exist of the following elements [105]. There will be four Equipment Power Distribution Modules, for the 28 [V] systems there will be three modules and for the 5 [V] system there will be one module (this one is not off the self though it can be ordered). Two Battery C/D Regulation Modules are necessary to regulate power to and from the batteries. To control the power from the solar array two Array Power Regulation Modules are needed. A TM/TC Interface Module is added to provide the ground segment information about the power management and commands can be send to regulate te power. Finally a Pyro Firing Drive Module is necessary for the thrusters. This leads to a PCDU with a weight of 8.75 kg.

11.4 Subsystem Sizing

The satellite, as the Earth, will change its position w.r.t. the Sun, this results in a varying length of the eclipse. The power system must be able to provide the other components with power at any moment in time, therefore the power system will be designed for the worst case scenario. This happens when the duration of the eclipse is longest, to calculate this Equation 11.1 is used [106]. In this equation f is the fraction spent in sunlight, R is the radius of the Earth, h is the altitude of the orbit, and θ is the angle between the normal of the orbit and the direction off the Sun. Figure 11.3 shows the relation between the sun angle on the equator and the sun light time for an inclination of 62 [deg] and 58 [deg], this is done only for winter to spring period because the graph will be mirrored. The shortest period spent in daylight will be 67.48 % of the orbit. As can be seen there will be days that there is no eclipse for the satellite with a higher inclination.

$$f = \frac{1}{2} + \frac{1}{\pi} \sin \sqrt{\frac{1 - (\frac{R}{h+R})^2}{\sin \theta}} \tag{11.1}$$

The size of the solar arrays and the batteries are calculated using the method described in section 11.4 of SMAD [46]. The power needs for the payload can be found in Table 11.2. The payload, as can be seen in the table, has different operating modes which use power. The power usage of the other systems and the losses due to the electronics can be found in Table 11.3,. Most power values mentioned are the maximum each system uses, for example the power system does not constantly use 80 [W]. It is assumed that only four thrusters work at the time and for the ADCS the average power that the reaction wheels use is taken into account. The reaction wheels have a high peak value when operating at their highest speed, this happens in a short amount of time and the battery will be able to compensate. The solar cells can not constantly produce peak power, because the power that is not used will be converted in heat. Therefore an average power is calculated, this is done by making an estimation of the time that each mode is operating. The battery will compensate for the peak power. The average power is calculated for each orbit and the satellite should be able to scan each orbit. The time each subsystem is working is used for the calculation of average power, the scanning is done in three minutes and the communication system takes two and a half times as long the scanning. The propulsion system works only a fraction of time and is assumed to work 0.1 [min]. It is assumed that the power, the ACDS, the GNC, the Thermal, and AIS systems are constantly working. The peak power is calculated for the moment that all systems need power at the same moment, the battery is designed for using peak power.

Equation 11.2 is used to calculate the power that needs to be generated by the solar cells. In this equation the indices e and d stands for the values of the variables during eclipse and sunlight respectively, P stands for the average power that is needed for the given period. In this case it is the same while in sunlight and eclipse because the satellite must be able to preform in both situations. T stands for the time it spends in the stated situation and X depends on the power regulation technique used.

$$P_{sa} = \frac{\left(\frac{P_e T_e}{X_E} + \frac{P_d T_d}{X_d}\right)}{T_d} \tag{11.2}$$

Table 11.2: The power consumption of the payload

SAR Panel Operating Modes	Panel (W)	Instrument Electronics (W)	X Band transmitter (W)	Total (W)
Data Acquisition	150/panel	120	1	121 + 150/panel
Configuration	40	20	1	61
Ground Contacts	10	50	125	185
Data Elaboration	10	100	1	111
Stand by	10	20	1	31
Peak	450	120	125	

Equations 11.3 and 11.4 are used to calculate the power one square meter of solar panel must be able to generate. Here P_{BOL} is the power generated per square meter at the Begin Of Life (BOL), P_0 is the power per square meter the selected solar cell should generate. There are losses due to the angle between the solar cell and the direction of the sun. These losses are called the cosine loss (θ). I_d is the inherent degradation which is a combination of design and assembly flaws, temperature variations and, shadowing. SMAD [46] gives a nominal value of 0.77. Finally the P_{EOL}, power per square meter at EOL, can be calculated by taking into account the degradation due to radiation which is defined as L_d. The power generated at EOL is important because the satellite still needs to function after al its time in space.

$$P_{BOL} = P_0 I_d \cos \theta \tag{11.3}$$

$$P_{EOL} = P_{BOL} L_d \tag{11.4}$$

Table 11.3: Power Budget

Part	Transmitter Power [W]	Active Time [m]	Receiver Power [W]	Active Time [m]
SAR Scanning	501	3	151	3
SAR During Communication	80	7.5	80	7.5
SAR Idle	51	84.45	51	84.45
AIS	-	-	10	94.95
GNC	21	94.95	21	94.95
Propulsion	33	0.1	33	0.1
ADCS	62	94.95	62	94.95
TT&C	15.5	7.5	265.5	7.5
Power*	82	94.95	82	94.95
Thermal*	50	94.95	50	94.95
Mechanisms*	9.8	94.95	9.8	94.95
Data Handling	131	0	131	3
Losses*	50	94.95	50	94.95
Total Average Power	343.6	94.95	354.8	94.95

Part	Transmitter Power [W]	Receiver Power [W]
SAR	501	100
AIS	-	10
GNC	21	21
Propulsion	33	33
ADCS	62	62
TT&C	15.5	265.5
Power	82	82
Thermal	50	50
Mechanisms	9.8	9.8
Data Handling	-	120
Losses	50	50
Total Peak Power	824.3	803.3

*This is the maximum power of the system, these values will change during the lifetime of the mission.

The life time of the solar cells comes directly from the stakeholder requirement BSAR-1e which states that the life time needs to be 5 years. The orbit altitude is determined to be 516 [km]. Maximum Power Point Tracking (MPPT) shall be used as a regulation technique because it has a better normalized power output.

To get the required EOL power, the degradation per year of the solar cells differs per orbit. The different sources of radiation are described in Spacecraft Power Technologies [106]. For a LEO the worst value of radiation is 9.56E12 [MeV/year] for a 6 millimetre protection screen [107].

To calculate the effective solar cell area it is assumed that the arrays are pointed in the same direction and do not change. This is done so that the necessary power can be generated when the motors can not turn fast enough to get peak power. The optimum situation is when one sollar array in position against the satellite's body and the other is parallel to the first, the satellite is a trapezoid where the bottom corners are both at an angle of 60 [deg]. In Figure 11.2a the power generation per orbit for the summer can be found, Figure 11.2b shows the power generated in autumn. As can be seen the summer is the worst case scenario and is therefore used for the design. An average is taken from the power generated to get the necessary solar panel area. The solar array area is calculated this way so that there is no constant motion of the arrays and there is a possibility to extend mission parameters. The mission will exist of multiple orbits though the solar array size will be almost the same when the altitude changes as long as the orbital period is the same. The solar array size will be slightly different if there is a change in inclination due to eclipse time, as can be seen in Figure 11.3 the worst case is an inclination of 58 [deg]. Some orbits will have a different node of right ascension which means that the longest eclipse will happen at another moment in time.

The battery capacity can be calculated using Equation 11.5, here the peak power is defined as P_e and T_e is the eclipse time. The number of batteries is given by N and n is the transmission efficiency between the battery and the load. Besides, the Depth Of Discharge (DOD) is needed.

$$C_r = \frac{P_e T_e}{(DOD) N n} \tag{11.5}$$

The DOD is the percentage of power removed each cycle. The number of charge cycles that a battery needs to endure is the biggest factor in choosing a DOD. To keep it simple it is assumed that the battery has one charge cycle each orbit. The number of cycles can then easily determined by multiplying the number of orbits a day and the life time in days. For this mission the required lifetime, as mentioned before, is 5 years and there will be around 15 orbits a day. A low DOD will

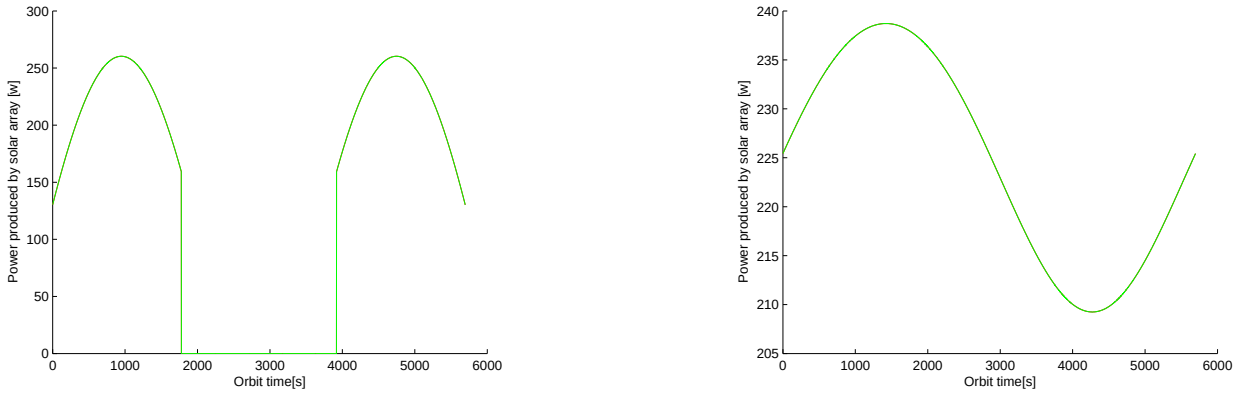

(a) Summer

(b) Autumn

Figure 11.2: The power generated in one orbit

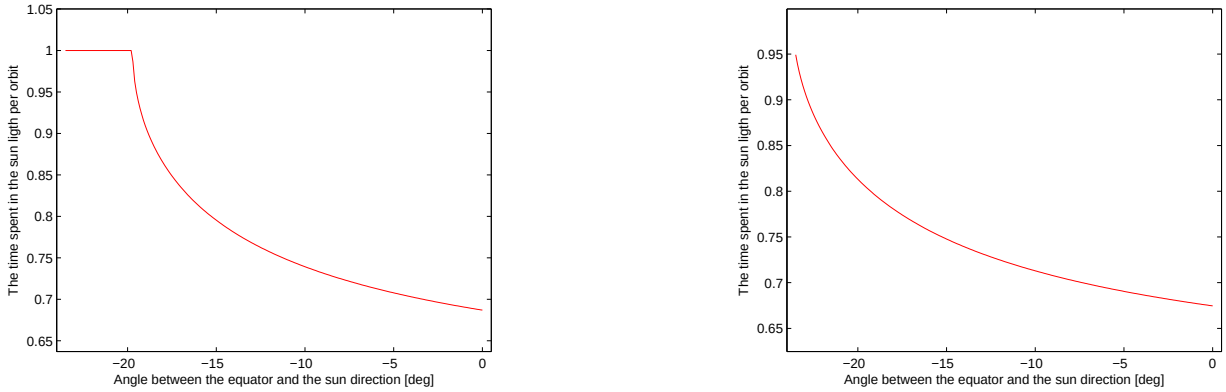

(a) An inclination of 63 [deg]

(b) An inclination of 58 [deg]

Figure 11.3: The daylight time of the satellite

result in a longer cycle life and is dependent on the kind of battery, for a Li-ion it is 25 %. As stated before there will be four batteries, of which three will be used for normal operations and one for redundancy. The transmission efficiency is 0.9. All values used for all calculations can be found in Table 11.4.

The sizes and mass of each part of the system can be found in table 11.5.

11.5 Sensitivity Analyses

For the sensitivity analyses some of the input values are changed to find if there is a change in the results. As stated before if the inclination changes the shadow time increases or decreases. The power needs of the system will be the same so to get the same total power the solar array area needs to change, if the battery capacity changes by 23.7 [kWh] if the inclination changes from 58 [deg] to 62 [deg]. As said before if the orbit altitude changes and the orbital period stays the same, the system size will not change. If another subsystem will need 10 [W] more power then the solar array size will increase by 0.1 [m^2] and the battery capacity changes by 23.7 [kWh]. There will not always be a change in battery size because the number of battery cells need to be rounded up to the nearest integer.

11.6 Verification and Validation

The calculations for the shadow cone was verified using geometric drawings and a MATLAB model of the Earth with satellite rotating around the sun to get the angels between the satellite and the sun. The calculations of the size of the solar array and the batteries were verified with the examples in [46] and calculations done by hand. The solar Array size will be recalculated by Spectrolabs when the panels are ordered and they will be tested before delivery. The total system needs to be tested in a controlled condition if the whole system works.

Table 11.4: Inputs used

	Value	Unit
Altitude	516	km
Inclination	58	degrees
Design life time	5	yr
MPPT eclipse	0.60	-
MPPT daylight	0.80	-
Inherent degradation	0.77	-
Solar cell power delivery	350	W/m2
Degradation/year	0.006914	-
Voltage	28	V
DOD	25	%
Number of batteries	3	-
Transmission efficiency	0.9	-

Table 11.5: Results for the power system

	Weigth [kg]	Size
PCDU	8.75	279 x 235 x 156 [mm]
Solar Cell Transmitter	7.14	3.47 [m^2]
Solar Cell Receiver	7.58	3.68 [m^2]
Battery Transmitter	18.4	264 x 165 x 60 [mm]
Battery Receiver	18.4	264 x 165 x 60 [mm]

Chapter 12

Thermal Control

Many systems require a certain operational temperature range to work properly. The thermal control system has to make sure that this is achieved for all components. The driving requirements are for the payload and the batteries. During operations, the payload temperature must stay between -15 [$^{\circ}C$] and 45 [$^{\circ}C$] and the temperature of the batteries must stay between 10 [$^{\circ}C$] and 40 [$^{\circ}C$].

12.1 Requirements

The requirements for the thermal control system are as follows;

- **Subsystem Requirement [TC1a]**: The thermal control system shall keep all components within operating temperature range during operations.
- **Subsystem Requirement [TC1b]**: The thermal control system shall keep all components within survival temperature range at all times.
- **Subsystem Requirement [TC2a]**: The thermal control system shall have a minimum lifetime of 5 years.
- **Subsystem Requirement [TC2b]**: The thermal control system shall have a maximum mass of 12.5 [kg].
- **Subsystem Requirement [TC2c]**: The thermal control system shall have a maximum power consumption of 97.8 [W].

Table 12.1 shows the allowable minimum operating temperature (Min. Op.), maximum operating temperature (Max. Op.), and the minimum and maximum survival temperature (Min. Sur. and Max. Sur.) for the satellite components.

12.2 Passive Thermal Control

In order to design the passive thermal control for the satellite, its thermal equilibrium temperature has to be determined. In space it is only possible to exchange heat with other objects through radiation since there is no convection or conduction possible. There are four contributions that heat up the satellite;

- Direct solar radiation
- Albedo radiation
- Planetary radiation
- Internally dissipated power

Direct solar radiation is caused by the sun. Albedo radiation is the reflection of sunlight from the earth surface. Planetary radiation is in this case the heat radiated by earth. The radiation from the moon is neglected. The internally dissipated heat is the heat generated by all the components on board. The satellite can only lose heat by radiating it into space.

The solar radiation at earth is about 1371 [W/m^2]. Equations 12.1 to 12.10 are taken from [108].

$$J_s = 1371 \tag{12.1}$$

The planetary radiation can be calculated by using the Equation 12.2.

$$J_a = J_s \cdot a \cdot F \tag{12.2}$$

Table 12.1: Thermal Ranges

Component	Min. Op.[$^\circ C$]	Max. Op.[$^\circ C$]	Min. Sur.[$^\circ C$]	Max. Sur.[$^\circ C$]
ADCS				
Star Trackers	-20	50	-30	60
Fine Sun Sensors	-25	50		
Inertial Sensors	-20	50	-40	80
Magnetometers	-20	50	-40	80
Reaction Wheels	-30	50	-40	80
Magnetotorquers	-30	50	-40	80
Power				
Solar Panels	-120	110	-200	130
Batteries	10	40	0	50
Communication				
X-Band Transmitter	-15	45	-30	60
X-Band Antenna Base	-15	45	-40	60
GNC				
GPS Antenna Base	-20	45		
GNC Receiver	-30	70	-40	85
Propulsion				
Hydrazine Tanks	7	55		
Thrusters	7	65		
Structure				
Structure	-80	100		
Electro Motors	-45	80		
Data Processing and Storage				
Main Computer	-10	40		
Data Storage	-10	45		
Instruments				
SAR Panels	-15	45	-40	60
SAR Electronics	-15	45		
AIS Receiver	-50	70		

In this equation, a is the albedo of earth. The albedo differs slightly depending on where the satellite is above the earth. A value of 0.33 can be used as an average value. F is the visibility factor. Its value can be taken from figure 11.2 from [108]. A value for F of 0.7 is used.
The planetary radiation is determined by equation 12.3.

$$J_p = 237 \cdot (\frac{R_{rad}}{R_{orbit}})^2 \tag{12.3}$$

Now the actual heats absorbed and radiated can be determined. Here, α is the absorptance of the surface, ε is the emittance and σ is the Stefan-Boltzmann constant.

$$Solar = J_s \cdot \alpha \cdot A_{sol} \tag{12.4}$$

$$Albedo = J_a \cdot \alpha \cdot A_a \tag{12.5}$$

$$Planetary = J_p \cdot \varepsilon \cdot A_p \tag{12.6}$$

$$Dissipated = Q \tag{12.7}$$

$$Radiated = \sigma \cdot T^4 \cdot \varepsilon \cdot A_{sur} \tag{12.8}$$

Now the thermal equilibrium equation for the satellite can be set up as shown in equation 12.9.

$$(A_{sol}J_p + A_aJ_a)\alpha + A_pJ_p\varepsilon + Q = A_{sur}\sigma T^4\varepsilon \tag{12.9}$$

This equation can be rearranged to solve for T.

$$T^4 = \frac{A_p J_p}{A_{sur}\sigma} + \frac{Q}{A_{sur}\sigma\varepsilon} + \frac{A_{sol}J_s + A_a J_a}{A_{sur}\sigma}(\frac{\alpha}{\varepsilon}) \tag{12.10}$$

With Equation 12.10 the equilibrium temperature can be determined for any case. Two extreme cases are looked into to ensure that the thermal control system can handle all situations. Because many different orbits are used in the constellation, the satellites experience different sun conditions. One of the orbits will be almost constantly in sunlight. This orbit will be called case one. The internally dissipated power changes constantly as well. Extreme values for the internally dissipated power are taken to be zero and 20% of the peak power. For the transmitter satellite this would be 170 [W] and for the receiver 138 [W].
Table 12.2 shows the thermal equilibrium temperatures calculated for case one.

Table 12.2: Equilibrium Temperatures for Case One

Dissipated Power [W]	Temperature [$^\circ C$]
0	22.9
138	25.9
170	26.6

These temperatures comply with all the temperature range requirements in Table 12.1.

Case two is for the orbit with the longest eclipse time. The satellite will be in eclipse for 35% of the orbit. Table 12.3 shows the obtained equilibrium temperatures for case two.

Table 12.3: Equilibrium Temperatures for Case Two

Dissipated Power [W]	Eclipse Temperature [$^\circ C$]	Sunside Temperature [$^\circ C$]	Average Temperature [$^\circ C$]
0	-40.2	49.0	17.8
138	-34.0	51.5	21.5
170	-32.66	52.0	22.4

For this case, the equilibrium temperatures are calculated both in sunlight and in eclipse. The temperatures in sunlight are higher than the temperatures in case one because of the angle of the solar rays. In case one only the side of the satellite is in sunlight. In case two the sun shines on a bigger part of the surface area of the satellite and therefore more heat is absorbed. The average temperature is calculated by multiplying the maximum temperature by 0.65 and the minimum temperature by 0.35. (This is done in degrees Kelvin and then converted back to degrees Celsius).
Because the satellite never stays in the sunlight or in the eclipse for long these temperatures will never be reached. The actual temperature of the satellite will swing around the average temperature though it should not go below zero degrees Celsius.

These are the results when goldized kapton is used on the top and the sides of the satellite and white paint is used at the bottom. In total 8.06 [m^2] of goldized kapton is needed. Assuming a mass of 0.3 [kg/m^2] [109] the insulation mass will be 2.4 [kg]. The mass of the white paint and the coating that protects it are assumed to be no more than 0.3 [kg]. This brings the total mass estimation for the passive control to 2.7 [kg].

12.3 Active Thermal Control

Active thermal control will be necessary to ensure that the batteries, the hydrazine tank, and the thrusters stay within their operating temperature ranges. Thermistors [110] are used to monitor the temperature of these components and polymide strip heaters [111] are used to maintain operating temperatures when needed. Table 12.4 shows the amount of thermistors and heaters used.

Table 12.4: Active Thermal Control

Components	Polymide Strip Heater	Thermistor
Batteries	2	2
Thrusters	8	8
Hydrazine Tank	4	2

The total cost of the active thermal control is 963[€] and the mass is estimated to be 1 [kg]. The heaters require 20 [W] power, though they are not always turned on. The average power consumption plus a safety margin is 50 [W].

12.4 Architecture

For the thermal control of this satellite, mostly passive control is applied. The top and the sides of the satellites are covered with goldized kapton MLI blankets. The bottom aluminium honeycomb plate functions as a radiator with an area of 1.26 $[m^2]$ and is painted white to increase its emittance. Thermal fillers will be used when mounting heat producing components onto the honeycomb panel to ensure good heat conduction. The temperature of various components is regularly measured with the use of thermistors. The electrical resistance of a thermistor changes with temperature and it can therefore be used to measure temperature. Several polymide film heaters will be used to make sure that the batteries and propulsion system will not experience temperatures that are too low. No dedicated thermal control measurement unit is needed. The measurements and the control of the heaters shall be done by the main computer.

12.5 Sensitivity Analysis

The sensivity of the thermal control system can be checked by looking at the difference in temperature when the internally dissipated power or the orbit altitude are changed. The effect of changing the internally dissipated power can be seen in table 12.2 and table 12.3. The change in temperature is significant though not to much.
A decrease in altitude of 100 [km] will change the temperatures by no more than half a degree. It can be concluded that a small change in these parameters will require no change in the thermal control design.

12.6 Risk Management

The technical risk assessment for the thermal control system is split up into three risks: failure of passive control, thermistor failure, and heater failure. The likelihood and impact of these risks are given in table 12.5.

Table 12.5: Thermal Control Risk Assessment Table

RN	Risk Title	Likelyhood	Impact
F-TC1	Passive Thermal Control Failure	VL	H
F-TC2	Thermistor Failure	L	M
F-TC3	Polymide Heater Failure	L	H

Passive thermal control should be chosen more predominantly due to its reliability. When active control is necessary, the reliability should be the driving design factor. Redundant thermistors and heaters could be used to decrease the risk. The risk map for thermal control can be found in Figure B.1k.

12.7 Verification and Validation

Verification: In order to verify that the script that was written to perform the calculations for the passive thermal control works as intended, an example was worked out using the same calculations as in the script. Tests should be performed to determine if the values for the estimated maximum power dissipation are correct. The thermistors and heaters must be tested to ensure they work correctly.
Validation: Thermistors and polymide heaters strips are often used in space. This validates that they can indeed be used.

Chapter 13

System Characteristics

This chapter contains all the systems characteristics, including the power budget, the mass budget, the cost budget, the astrodynamic characteristics, the ΔV budget and the data characteristics.

13.1 Power, Mass, and Cost Budget

In Table 13.1 the required power for all the subsystems can be seen.

Table 13.1: Power Budget

Part	Transmitter Power [W]	Active Time [m]	Receiver Power [W]	Active Time [m]
SAR Scanning	501	3	151	3
SAR During Communication	80	7.5	80	7.5
SAR Idle	51	84.45	51	84.45
AIS	-	-	10	94.95
GNC	21	94.95	21	94.95
Propulsion	33	0.1	33	0.1
ADCS	62	94.95	62	94.95
TT&C	15.5	7.5	265.5	7.5
Power*	82	94.95	82	94.95
Thermal*	50	94.95	50	94.95
Mechanisms*	9.8	94.95	9.8	94.95
Data Handling	131	0	131	3
Losses*	50	94.95	50	94.95
Total Average Power	343.6	94.95	354.8	94.95

Part	Transmitter Power [W]	Receiver Power [W]
SAR	501	100
AIS	-	10
GNC	21	21
Propulsion	33	33
ADCS	62	62
TT&C	15.5	265.5
Power	82	82
Thermal	50	50
Mechanisms	9.8	9.8
Data Handeling	-	120
Losses	50	50
Total Peak Power	824.3	803.3

*This is the maximum power of the system, these values will change during the lifetime of the mission.

In Table 13.2, the mass budget breakdown for the system can be seen in Figure 13.2.

Table 13.2: Mass Budget

Part	Transmitter Mass [kg]	Receiver Mas [kg]
AIS	0	1
GNC	2.21	2.21
Propulsion	88.84	88.84
ADCS	37.95	37.95
TT&C	6.3	17.3
Power	30.65	30.73
Thermal	3.7	3.7
Structure	100	100
SAR	206.2	206.2
Total mass	475.85	487.93

The cost budget per subsystem can be seen in Table 13.3. As can be seen the cost budget is only includes the bus, the operational cost must be analysed in a later stadium when more is known about the clients.

Table 13.3: Cost Budget

Part	Transmitter Cost [1000 [€]]	Receiver Cost [1000 [€]]	Pair Cost [1000 [€]]
Panels	-	-	-
AIS	0	10	10
GNC	32	32	64
Propulsion	2000	2000	4000
ADCS	4000	4000	8000
TT&C	733.8	2240.8	2974.6
Power	461.4	461.4	922.8
Thermal	35	35	70
Structure	750	750	1500
Data Handeling	243.6	673.4	917
Production	7000	7000	14000
Total	15255.8	17202.6	32458.4

13.2 Astrodynamic Characteristics

The astrodynamic characteristics are found in Chapter 2. The characteristics are summarized in Table 13.4. Note the satellite pairs are flying at five different inclinations and altitudes, and the four groups of satellites have different starting Ω_0. The values shown are the initial values used in simulations.

Table 13.4: Astrodynamic Characteristics

Element	Values
a (per pair)	6881.2, 6883.0, 6884.9, 6886.7, 6888.6 [km]
i	58, 59.25, 60.50, 61.75, 63 [deg]
e	0
Ω_0 (per orbit)	30, 126, 222, 294 [deg]
ω	0 [deg]
θ_0	0 [deg]

The ΔV budget can be seen in Table 13.5. The ΔV budget has been derived in Chapter 7.

Table 13.5: Total ΔV budget

Function	ΔV [m/s]
Insertion Into Orbit	2.42
Formation Keeping Due to Disturbances	3.15
Differential Drag Maintenance	9.97
Altitude Maintenance	99.72
Attitude Maintenance	20
Total	**143.07**

Table 13.7: Collection of reference satellite data

Satellite	Project Costs (million €)	Year launched [-]	Payload mass [kg]	S/C mass [kg]	Payload peak power [W]	S/C nominal power [W]
ERS-1 [112, 113]	778.68	1992	1000	2384	1000	2300
ERS-2 [112, 113]	468.65	1995	1000	2516	1000	2300
Sentinel 1A [114]	280	2014	880	2300	4400	4800
TanDEM-X [115, 116]	165	2007	500	1330	2260	730
TerraSAR-X [117]	130	2007	394	1346	2260	605
Radarsat-1 [118, 119]	405.48	1995	1540	3200	5000	3400
Chandrayaan-1 [120, 121]	57.68	2008	55	550	164.2	750
JERS-1 [122]	Unknown	1992	174	1400	1750	2000
ALOS [123]	Unknown	2006	600	4000	2000	7000
CosmoSkyMed [121, 124, 125]	216.3	2007	650	1700	14000	4000

13.3 Data characteristics

The data rates between the satellite and the ground station are shown in table 13.6.

Table 13.6: Data rates

Type	Amount
Housekeeping Data	5 mb/orbit
Payload Data	2.4 Gb/s when measuring

13.4 Reflection on the design

In order to reflect on the design, the AEGIR satellites are compared to reference SAR satellites. These satellites have already been presented in the Baseline Report and are shown in Table 13.7 .

The payload has a mass fraction of 43.8 % for the transmitter satellite and 42.9 % for the receiver satellite. This mass fraction is in the same order as other SAR missions, such as ERS-1 (41.9%), ERS-2(39.7%) and RadarSat-1(48.1%) [126]. The design of the AEGIR satellites have a lower mass than the design of reference satellites. This is due to the fact that the payload for this mission is lower and as well as the payload peak power consumption is lower than the reference satellites. Furthermore, the reference satellites are designed as mono-static SAR, while the AEGIR system is designed as a bi-static SAR, spreading the mass over two satellites instead of one satellite. The current cost estimation excludes the costs during operations and the payload costs. This explains a part of the high difference. Still, the AEGIR satellites are less expansive than the other reference satellites since most components are build from commercial off-the-shelf products.

Chapter 14

Market Analysis

To determine the feasibility of this project in terms of economical aspects a market analysis is conducted for potential SAR-specific missions. Synthetic Aperture Radar can be used in all weather conditions and at any time of day. If the SAR instrument is placed on a satellite it can cover large areas around the Earth on a daily basis. Placing an AIS receiver on board of the satellite will significantly improve the performance, since actual images can be linked to ships. In this chapter the potential customers and typical costs of security are identified. The environmental benefits to the North Sea are researched as well. Finally some experimental applications are mentioned. The European Maritime Safety Agency (EMSA) is the organization in Europe that gathers all shipping data from each country and makes it accessible to them.

14.1 Security

The North Sea is a busy maritime traffic area with a relatively small size. Most of the ships are destined for the big ports like Antwerpen, Rotterdam and Hamburg. As a consequence accidents are not a rare phenomenon. Navigation and traffic control still remain a challenge in these crowded waters [2]. Several accidents can be distinguished. Potential hazards are sinking, grounding, collisions/contacts and or explosions/fires on board of the ship. Research shows that in 2009 still 437 accidents occurred in contrast to an amount of 485 in 2008(Fig. 14.1).

Table 14.1: Ship collisions

	Sinking	Grounding	Collisions/Contacts	Explosions/Fires	Other	Total
2008	47	128	197	59	54	485
2009	22	124	197	46	48	437

As can be imagined a lot of money is lost due to these accidents. Most can be solved by applying adequate navigation and control. These kind of systems do already exist. One example is the SafeSeaNet [127]. This is a system based on the Automatic Identification System(AIS), which does not include a space-based element so only AIS data from around the coasts is known. Aircraft are used to monitor the open sea using SAR and AIS to cover this area, such an aircraft costs 14.74 million [€] [128]. To cover the whole North Sea multiple aircraft are needed. A pilot costs on average 112500 [€] a year, and each plane requires at least two pilots to be operational. Furthermore, these planes require maintenance, as well funds are needed for landing fees and fuel, this leads to a high maintenance cost. The SAR-satellite can aid in navigation and control by combining the SAR-data with the AIS-data so that all ships can be identified even in open sea.

An exact number on what budget stakeholders are willing to invest in such a project is still hard to define. A related spacecraft for the monitoring of vessels is the nano satellite AISSat-1 [129]. It makes use of the AIS for its target detection. The satellite was financed by the Norwegian Ministry of Trade and Industry with an amount of 3.9 million Euro and was designed for a lifetime of 3 years. However, most illegal ships do turn off the AIS system to keep themselves from being detected. Thus, combining an AIS system with radar imagery drastically increases the possibility of detecting illegal ships. In turn, this increases the rough value of the satellite system.

14.2 Illegal fishing

A major market in which this can be applied is the detection and identification of Illegal, Unreported and Unregulated fishing (IUU). Illegal fishing and smuggling still occurs in the North Sea. The North Sea is a popular fishing spot for several surrounding European countries. A wide variety of species inhabit these waters from which only a few are of interest for the active fisheries. A research of recent years has shown that these fish stocks suffer depletion due to overfishing [130]. Fish stocks are diminishing every year resulting in less income, reduced employment, and most importantly, damage to the environment.

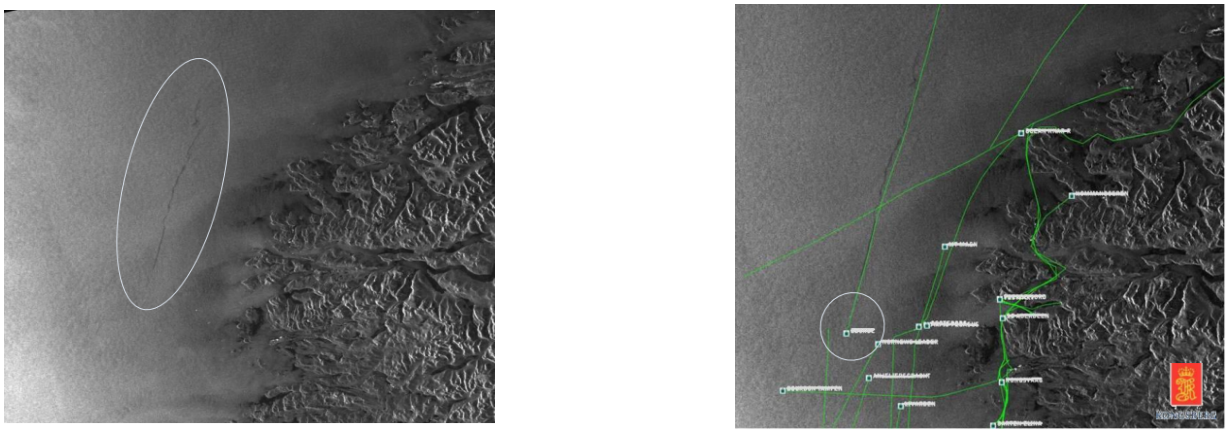

(a) only SAR data

(b) SAR adn AIS data

Figure 14.1: A SAR image of a detected oil spill off the coast of Norway

Several policies have been applied in order to counteract these effects. For example, Total Allowable Catch (TAC) limits are set up by different authorities. Nonetheless, due to inconsistent abidance of the different countries with regard to these regulations the problem still exists.

The main cause of overfishing is the incomplete overview that the authorities have due to IUU fishing still present these days. These activities are facilitated by the fact that the sea is regarded as a global common. Most of the activities happen out of reach of the land based scanning equipment and monitoring is problematic. Surveillance is currently being performed by naval and aerial vehicles, however these vehicles have a low coverage and a high cost. A space based SAR monitoring system can increase the coverage of the security systems and will result in earlier detection of illegal activities and unidentified ships. In 2008 it was estimated that 66% of all catches were unreported. It is hard to express this percentage in actual costs. However, simulations show that over the period 2008 till 2020 ending the IUU fishing would result in extra fish stocks of more than 4 billion [€] worth. In contrast, when the current actions would be continued without any change in approach, fish stocks in the North Sea will suffer a decrease of 6 billions [€] worth in the period from 2008 till 2020, without mentioning the corresponding losses in jobs.

A satellite system monitoring shipping can increase prosecution numbers immensely and help the fish stocks and fish market recover. Customers for such a system would be coast guards and navies [131]. The amount of money involved is based on estimations and may be far-off from the actual value. However, the problem is present and a big interest exists in solving it.

New Zeeland can be a possible client in this area because they have a lot fishing that need to be monitored, most of these spots are in open sea which are hard to monitor. In 1990 they spend 2.68 million [€] for aerial surveillance which resulted in 2400 flight hours in a year [132]. The amount of money spent should at least be the same and possibly higher becase of inflation, that there are more fishing ships and that New Zeeland want to preserve nature as much as possible.

14.3 Oil Pollution Monitoring

The technique of SAR images have proven to be of excellent use for detecting oil spills because the presence of oil changes the characteristics of the sea surface, and consequently the way radiation from satellite radar is scattered. It dampens down the wind-generated waves on the sea surface, reducing the reflected power measured by the radar: for this reason, oil slicks, some of which are just micrometres thick, appear as dark areas on an otherwise brighter sea. This can be seen in figure 14.1a [133].

Oil pollution can occur in different ways: ships dump oil in order to clean their fuel tanks, accidents cause oil rigs to sink or leaks on the oil rigs occur due to malfunctioning equipment. Polluting the North Sea with oil is an illegal activity, however often detection of oil pollution is too late to prosecute the polluters. SAR monitoring of the North Sea can shorten the detection time of oil pollution, which limits the possible environmental damage and increases the chances of prosecution [131]. Furthermore, the system may be used to find locations where dumping often occurs, making the prevention of the dumping more feasible.

One of the project of ESMA is the CleanSeaNet [134] which makes use of SAR data from current satellites such as RadarSat-2 to find oil spills. To operate this system they spend 2.9 million [€] per year and save 30 million [€] by not using aircraft. The satellites that provide the used images are designed for other missions therefore the temporal resolution is at best once a day for any location. To find the person responsible for the oil spills planes are still sent to find them because most of the AIS data is from the coastal regions. The system designed in this report would be able to provide both the SAR and AIS data at the same time with 100 minutes interval, this would lead to a lower cost for the used aircraft. In Figure 14.1b an example is shown how AIS and SAR data can be used to find oil spills and their culprit.

These are some of the main reasons an oil spill detection system, designed specifically for a high temporal resolution monitoring of the North Sea, has a great potential.

14.4 Remaining experimental options

The SAR instrument is a versatile piece of equipment. Besides the options stated above, more potential markets may be of interest to investigate. Even though the options are experimental, the possibilities are worth mentioning.

14.4.1 Bathymetric Mapping

Bathymetric mapping or sea depth mapping is usually done by ships which can cover only a fraction of the sea floor. Due to the low speed of ships, the required crew, and the required fuel and supplies, mapping of the sea floor is a time consuming and expensive process. Generally speaking, new depth maps are required every two years, but some areas such as the Wadden Sea require new depth maps every four to six months. The required accuracy of the depth maps should at least be two meters for admiralty maps with a position accuracy better than 40 meters. Shallow waters require a depth accuracy of about 30 centimetres. It is possible to perform this mapping using SAR instruments. The data could then in turn be sold to sea floor mapping agencies [131].

14.4.2 Wind and Wave Forecasting

The wind and wave conditions are currently being monitored by a network of buoys and monitoring stations. SAR measurements can measure the roughness of the sea based on the intensity of the backscatter signal. When there are stronger winds and higher waves the sea will get rougher. The SAR instrument can measure this, and the data can be sold to weather monitoring institutions.[131]

14.4.3 Ice Monitoring

Icebergs and the development of ice require extensive monitoring, especially in the Northern countries. Uncertainty in the development of ice and the location of ice bergs can result in dangerous situations for ship traffic or unnecessary detours, with or without the use of ice breakers. Having access to up-to-date ice maps can significantly boost the efficiency of northern shipping lines. A typical resolution required to detect icebergs and ice development is 100 meters. The customers would include: Coast guard, Shipping corporations, and non-government environmental organizations. [131]

14.4.4 Subsea Hydrocarbon-deposit Location

There are still oil deposits located underneath the ocean, and these reserves leak a small amount of oil from time to time. When the weather conditions are mild and do not disrupt the sea, the oil slick can be spotted from space using SAR. New locations of oil deposits are valuable to energy companies [131].

14.5 Return On Investment

The specific cost of monitoring any sea or the value of an equivalent service are hard to find. In Table 14.2 there is a summary of the estimated cost of the current project, to make a good comparison the costs are calculated for a duration of 5 years. EMSA has a budget of 58.8 million [€] a year, a lot of this money goes to personnel and maintenance, the satellites can provide a lot of the necessary data they need within a small time interval. Their budget increases each year since they started so it should be possible to get 15 million [€] a year. New Zealand pays 2.68 million [€] a year for surveillance, there will always be a couple of planes needed. Because of inflation it will be a bit higher so it is assumed that the amount that can be earned is 3 million [€] a year. Norway paid 3.9 million [€] for a 3 year AIS mission, this was more cost efficient for them then pay for AIS data from existing missions. For the designed mission it is only possible to provide the AIS data. Because of the regular interval it is possible to get about 10 % more money. There are existing AIS satellites services that provide data for different prices. Usually if you want satellite data with a 12 hour delay it will cost 300 [€] a month and if you want data with a 6 hour delay prices need to be discussed [33]. There are easily 1000 shipping agencies that can be interested in the services which can be provided, and SAR data can be provided in the same package. A relatively new concept is the hosted payload principle where a government or space agency places a self contained payload on a spacecraft that only need power and a transponder or access to it. The agencies get a more affordable mission in a smaller amount of time, thirty million [€] can easily be earned from it. The seas around China and Japan are very busy seas they will at least pay the same for monitoring as Europe or even more. All the money mentioned are prices customers are willing to pay for existing systems, because the designed mission has a better temporal resolution it is possible that more can be earned.

In Figure 14.2 there is shown the relationship between the cost and the temporal resolution. The number of launches are stated in the top axis to have a better understanding of what the values mean, each launcher will have 5 pairs of satellites.

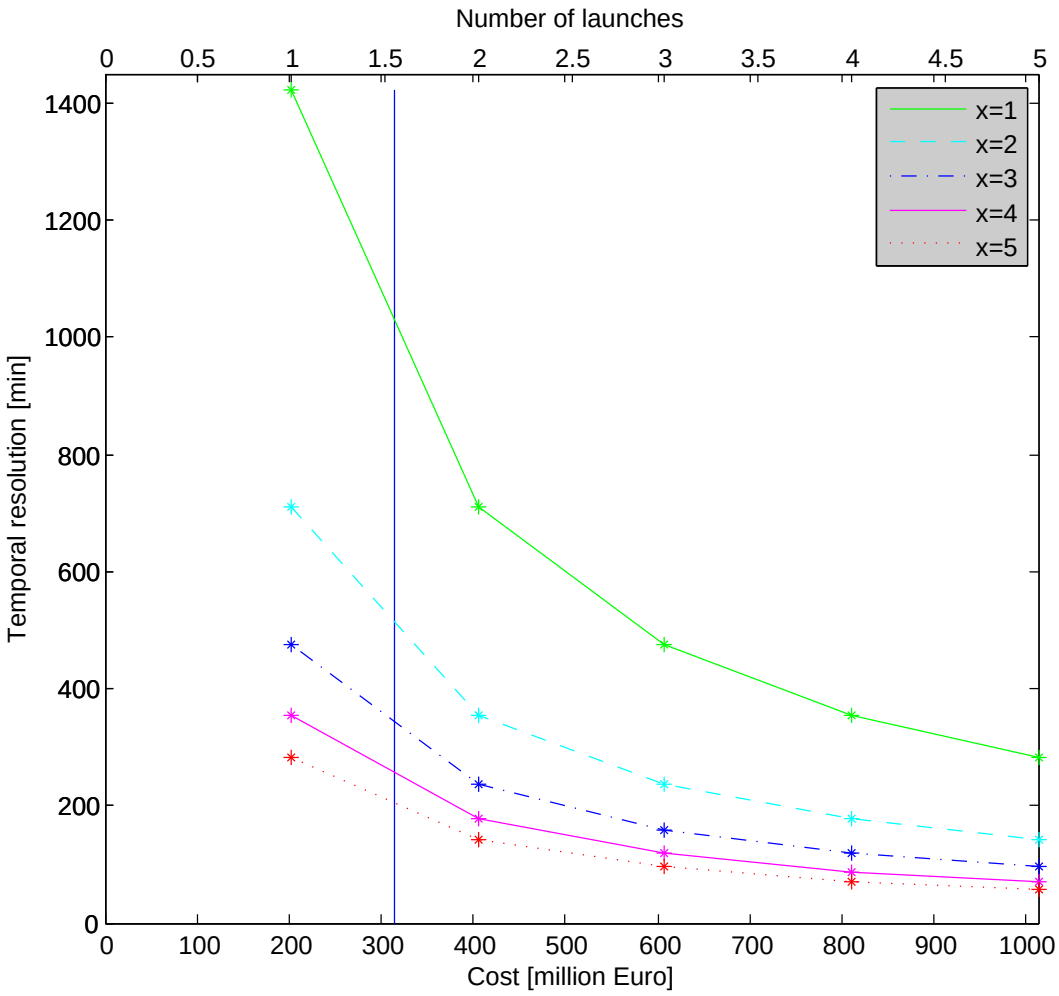

Figure 14.2: Temporal resolution vs cost

The straight vertical line gives the estimated income, as can be seen one launcher full with satellites can be justified and there is 85 million [€] more needed to have a second launcher full of satellites.

Table 14.2: Estimated Costs

Source	Possible income [million €]
EMSA	75
New Zealand	15
Norway	7.15
Shipping agencies	18
Hosted payload	30
China	90
Japan	80
total	315.15

Chapter 15

Sustainable Development Strategy

Launching a satellite in to orbit requires a lot of fuel and is often not considered sustainable. However, aircraft and ships require fuel as well. In this chapter, the carbon footprint of the entire constellation is estimated and it is compared with respect to an aircraft mission. The North Sea is a busy area. Beside ships, there is a lot of maritime wildlife. In this chapter the benefits for the environment of this specific SAR mission are identified.

15.1 Sustainability in Operations

The development and operation of the system will have to go through different life phases. Efficiency of each of these phases will be relevant to the design of a sustainable mission.

1. **Design** - The design phase is relatively short, with only ten weeks to design the system. This means an intensive process where the cooperation is the central theme. It is necessary to keep the communication as efficient as possible. Hence, the project team works concurrently at the same location to minimise the amount of waiting on different team members and to make efficient use of the available resources. Any written communication is done as much as possible in electronic form.

2. **Production** - The mass of the satellite(s) must be kept at minimum. This results in a minimum of required resources, as well as less fuel needed for the launch of the system. Production of components must, if possible, be centralised and as efficient as possible. Off-the-shelf products are used when possible, this means that less testing and designing needs to be done for this product. Some products harm the environment when being produced, a choice will be made for products that will have as low as possible impact on the environment.

3. **Deployment** - The launch of the satellites shall be done with an already existing launcher. This results in less development and production costs, while still providing the same result. Existing launchers usually have already gone through a long trial where many problems have been solved, ensuring a higher chance of a successful deployment. Furthermore, ground based systems, such as ground stations, must be accounted for. Already existing stations shall be used, thus reducing the need for construction of new stations.

4. **Operating Life** - To reduce the amount of fuel needed during the orbital phase of the mission, the orbit must be defined accurately. This orbit must have the amount of required ΔV as a minimum. This can be done by reducing the amount of orbital transfers required to get to the operational orbit. By determining a stable orbit with relatively low disturbances, the total ΔV budget shall be reduced.

5. **End-Of-Life** - It is important for any space system that satellites do not form an obstacle for future mission. The satellites will be in a low earth orbit therefore the satellite shall to be de-orbited at the end of the satellite's life.

The results that have been produced during this project will be made available to other people. This prevents people from doing work twice, which saves the use of human resources.

15.2 Carbon footprint

Satellites are sustainable vehicles. Satellites do not require fuel or other types of propulsion during operations. The carbon footprint of a satellite launch is estimated in this section. The carbon footprint for the satellite will be compared to other systems.

The satellite will be launched using the Soyuz-2 rocket. In total four launches are required to put all 40 satellites in space. The Soyuz-2 burns kerosene together with liquid oxygen. The fuel and oxidizer used per stage by the Soyuz-2 can be found in Table 15.1.

Table 15.1: Fuel per Soyuz-2 stage [35]

Stage	Fuel (Kerosene)	Oxidizer (LO2)
1	11260 x 4 [kg]	27900 x 4 [kg]
2	26300 [kg]	63800 [kg]
3	6480 [kg]	14900 [kg]
Total	**77820 [kg]**	**190300 [kg]**

A total of 77820 kg of kerosene is required as well as 190300 kg liquid oxygen. The energy density of kerosene is found to be equal to $\frac{43.28MJ}{kg}$ [135]. The carbon footprint of kerosene is found to be equal to $\frac{0.26kg_{CO2}}{kWh_{kerosene}}$. This carbon footprint is mainly released during the launch itself. The production of liquid oxygen requires a lot of electricity. Therefore, the CO_2 footprint is dependent on the overall footprint of the electricity network at the location. The footprint of producing liquid oxygen in the United Kingdom is found to be equal to $\frac{0.800kg_{CO2}}{Nm^3}$ [136]. One kWh of electricity in the UK has a footprint of 457 grams while in Russia this footprint is equal to 639 grams [137], the creation of liquid oxygen is thus assumed to be done in the UK. $1Nm^3$ is the mass of one cubic meter of gas at standard pressure. For liquid oxygen: $\frac{1.4291kg_{LO2}}{Nm^3}$ [138]. Based on these numbers the total carbon footprint for the system is estimated. This is done using Equations 15.1, 15.2 and 15.3.

$$m_{CO2,kerosene} = 77820kg_{kerosene} \cdot \frac{43.28MJ_{kerosene}}{kg_{kerosene}} \frac{kWh_{kerosene}}{3.6MJ_{kerosene}} \frac{0.26kg_{CO2}}{kWh_{kerosene}} = 243248kg_{CO2} \tag{15.1}$$

$$m_{CO2,LO2} = 190300kg_{LO2} \cdot \frac{Nm^3}{1.4291kg_{LO2}} \frac{0.800kg_{CO2}}{Nm^3} \frac{0.457kg_{CO2,UK}}{0.639kg_{CO2,Russia}} = 76187kg_{CO2} \tag{15.2}$$

$$m_{CO2} = m_{CO2,LO2} + m_{CO2,kerosene} = 319435kg_{CO2} \tag{15.3}$$

A total of 319 ton of CO_2 will be produced during launch. Currently the North Sea area in the Netherlands is being monitored using two Dornier 228 aircraft [139]. These aircrafts have a fuel consumption during cruise of $\frac{213kg}{hr}$. The carbon footprint after a specific time can be calculated using Equation 15.4.

$$m_{CO2,aircraft} = \frac{213kg_{kerosene}}{hr} \frac{43.28MJ}{kg_{kerosene}} \frac{kWh}{3.6MJ} \frac{0.26kg_{CO2}}{kWh} \cdot t = \frac{665.8kg_{CO2}}{hr} t \tag{15.4}$$

If Equation 15.3 and 15.4 are equated, it can be calculated that 480 flying hours, or 20 flying days, are required to produce the same amount of CO_2 as a single Soyuz launch. In total four launches are required to put all satellites in orbit. This produces the same amount of CO_2 as 1920 flying hours. On average, the Dutch Dornier 228 has 1290 flying hours per year [140]. The satellites are therefore considered more sustainable than aircraft based monitoring. It should be noted that only one aircraft is considered, while for the space based system 40 satellites are considered. The space based system can cover the entire North Sea with an temporal resolution of at least 100 minutes, while the aircraft based system can only monitor small areas along the Dutch coast for 1290 hours per year.

15.3 Benefits for the environment

The benefits of a SAR monitoring mission for the environment are discussed in this section.

15.3.1 Illegal Unreported and Unregulated Fishing

The North Sea is subjected to Illegal, Unreported and Unregulated (IUU) fishing. The AEGIR system is able to detect fishing ships and reduce the amount of illegal fishing activities in the North Sea. IUU fishing will deplete current fish populations [130]. Also, the use of harmful fishing methods in protected areas cause longterm damage to the North Sea environment [141].

15.3.2 Oil pollution monitoring

Ships regularly perform tank cleaning operations. During cleaning operations, residual oil is removed from the fuel tanks and is dumped into the sea. These operations are illegal in the North Sea area since it causes a lot damage to the environment. Prosecution of these activities is hard since the ships have to be caught in the act. Using space based SAR data it is possible to detect ships and oil spills. Combined with AIS data, it is possible to determine which ships are dumping oil in the North Sea. Detecting these and identifying ships from space will result in reduction of polluters in the North Sea. A more efficient prosecution will result in less oil dumping and in the long-term in a cleaner sea.

15.3.3 Efficient Shipping Routes and Security

The continuously availability of AIS data and SAR images of the environment will result in safer and more efficient shipping routes. If ships have a better knowledge of their position and ships closeby, the navigation can be improved and less unexpected manoeuvres will be required. This will result in a higher fuel efficiency for ships in the North Sea. Unidentified ships can be detected with the SAR panel, which can be used to increase safety on the North Sea. In 2008, 485 accidents occurred in the North Sea [134]. Accidents may lead to oil spills and environmental damage. Besides, due to construction of new ships to replace the sunken ships will result in increased CO_2 emissions.

15.3.4 Ice Monitoring

Ice monitoring will result in more efficient and safe shipping routes. Ice maps are currently constructed based on data provided by other ships and aircraft based SAR [112]. The temporal resolution of ice maps remains low and it is uncertain whether all ice infested areas are covered. Since the ice bergs drift through the sea, a high temporal resolution is important to obtain accurate ice maps. The space based SAR can provided ice maps with a temporal resolution of 100 minutes. This will result in a more accurate map of the environment which benefits the ships as no detours are required. These improved ice maps will increase the knowledge about the distribution of ice around the planet which can be used to create more accurate climate models.

Chapter 16

Project Design and Development Logic

Although a fairly complete design has been created during this project, a lot must still be done in order to achieve a succesfull mission. The amount of time ranging from the end of the DSE project until the end of the mission can be split up into seven main phases, as shown in figure 16.1.

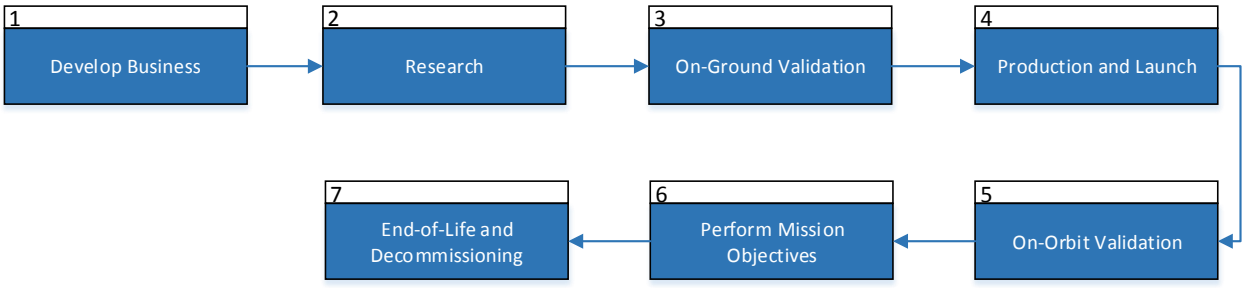

Figure 16.1: The main phases within the further development and execution of the mission

The phases may be described as follows:

1. **Develop Business**: The business and business plan supporting the mission must be developed in full. This includes relatively small actions such as requesting tax numbers, and larger actions such as acquiring employees and contacting investors and customers. The phase ends with finding a manufacturer for assembling all the different components: first for a prototype (phase 3) and later for line production.
2. **Research**: In this phase, part of the work done during the DSE is redone for verification purposes. Furthermore, the design being created during this phase is even more in depth than the current detailed design. Namely everything ranging from the electrical wiring to the bolts used to attach the structures must be modelled and drawn for production.
3. **On-Ground Validation**: During the on-ground validation phase, prototypes of both the SAR transmitter and receiver satellites are created. These are tested in ground facilities, for example the ESA Testing Centre at the ESTEC in the Netherlands. This phase is used to optimise and validate the design.
4. **Production and Launch**: Once the design and validation phases have been finished, the rest of the satellites are to be produced. The number of spacecraft depends on the amount of money invested into the project in phase 1. The production is finalised with short tests to rule out manufacturing errors. When finished, the spacecraft are transported and mated with the launch vehicles. Afterwards, the spacecraft are launched and the orbit initialisation commences.
5. **In-Orbit Validation**: During the first orbital phase, all the on-board systems as well as the ground segment are checked and validated. This includes first tests using actual data. The target detection capabilities can for example be validated by detecting ships with a known location.
6. **Perform Mission Objectives**: After the end of the in-orbit validation phase, the actual mission is performed.
7. **End-of-Life and Decommissioning**: When the spacecraft reach the end of their lifetime, the decision must be made to decommission the system. All relevant manoeuvres and operations are performed to make sure the spacecraft will eventually de-orbit, thereby leaving no orbiting debris behind.

The amount of time that is expected to be spent in all the above-mentioned phases and sub-phases is shown in the Gantt chart in appendix E.

Chapter 17

Conclusions and Recommendations

17.1 Conclusions

The aim of this project was to design a constellation for the monitoring of the North Sea using a bistatic SAR satellite configuration. This configuration should be able to monitor the sea with a revisit time of 100 minutes. In this report, the final design for the constellation, as well as the design of the satellite pairs was given.

In order to achieve a 100 minute average temporal resolution it was found in Chapter 2, that 20 satellite pairs are required. The satellites will have an Earth repeat orbit which repeats every 15 revolutions. To cover the North Sea efficiently, the satellites have to be spread out over inclinations between 58 [deg] and 63 [deg]. The satellites will be launched to orbit using four Soyuz-2 launchers. The Soyuz-2 launcher, combined with a fregat upper stage is used to launch all the satellites into a single orbital plane, so that the fuel on-board of the satellites is minimized. This will result in different starting values for right ascending node per group launched. A rough scanning pattern was derived resulting in a good coverage of the busiest areas in the North Sea.

The payload of the satellites, the PanelSAR provided by SSBV, is used to scan the North Sea in order to detect ships. By employing side-looking SAR, combined with single-pass interferometry, the required resolution to detect the ships is reached. The addition of AIS to the satellite allows for the combination of the two systems to have a higher chance to detect ships.

The total mass for the transmitter satellite is found to be equal to 470.85 [kg] while the receiver has an mass of 482.93 [kg]. The transmitter satellite has an average power consumption of 347 [W] and a peak power consumption of 823.3 [W]. The receiver satellite has an average power consumption of 354.8 [W] and a peak power consumption of 793.3 [W]. The final cost for the transmitter satellite is equal 15.2 million [€], while the receiver satellite has a costs of 17.2 million [€]. The launch costs of the Soyuz-2 is equal to 40 million [€].

The costs of the entire constellation would be equal to 808 million [€]. It has been estimated that 315.15 million [€] can be earned directly by saving costs of current monitoring systems. Current solutions have a lower coverage with respect to a space based SAR mission and can only cover areas efficiently near the coastline. The AEGIR project can provide a temporal resolution of 71 [min], 88 [min], 118 [min], 178 [min] or 355 [min] depending on the area of the North Sea. Since space based SAR has a better temporal resolution compared to ground based systems, it can be estimated that more money would be available to this project than current solutions.

The North Sea can be monitored efficiently with a space based SAR system, however the size of the constellation is remains dependent on the amount of available resources of North Sea monitoring organizations.

17.2 Recommendations

In order to further improve the design, several different steps can be taken. First of all, in Chapter 2, the orbits that are decided upon have different altitudes and inclinations. These orbits have different orbital periods, which will result in the fact that the satellites in the different orbits drift apart during the mission life. More investigation can be done into this phenomenon, since it will lead to a variable temporal resolution.

A more in depth market analysis can be performed linking the return on investment with respect to temporal resolution. The current market analysis does not take the temporal resolution into account while the temporal resolution is a major performance parameter.

Furthermore, the design for the different subsystems that have been presented in this report have not yet been fully optimized with respect to mass and cost. These subsystems can be further improved upon in order to improve the final design of the satellite.

Bibliography

[1] (2014, April) Trade routes. [Online]. Available: http://www.worldshipping.org/about-the-industry/global-trade/trade-routes

[2] Maritime accident review 2010. European Maritime Safety Agency. [Online]. Available: http://www.emsa.europa.eu/news-a-press-centre/external-news/item/1219-maritime-accident-review-2010.html

[3] Solas 1974: Brief history - list of amendments to date and where to find them. [Online]. Available: http://www.imo.org/KnowledgeCentre/ReferencesAndArchives/HistoryofSOLAS/Documents/SOLAS%201974%20-%20Brief%20History%20-%20List%20of%20amendments%20to%20date%20and%20how%20to%20find%20them.html#43

[4] T. Eriksen, G. Høye, B. Narheim, and B. J. Meland, "Maritime traffic monitoring using a space-based ais receiver," *Acta Astronautica*, vol. 58, no. 10, pp. 537–549, 2006.

[5] T. Buijs, D. Ju, N. de Kogel, S. van der Linden, A. Melaika, T. van de Oever, D. Petkovic, B. van Putten, and C. Verhoeven, "DSE - bi-SAR satellite network: Designing a satellite network for maritime monitoring of the north sea - midterm report," Delft University of Technology, Tech. Rep., 2014, internal Publication.

[6] M. Pastena, "first correspondence e-mail," private communication, first correspondence e-mail with Max Pastena.

[7] V. A. Chobotov, *Orbital Mechanics*, 3rd ed. American Institute of Aeronautics and Astronautics, Inc., 2002.

[8] D. D. M. Roger R. Bate and J. E. White, *Fundamentals of Astrodynamics*, 1st ed. Dover Publications, Inc., 1971.

[9] (2014, Februari) Black and white map of the world. Afranko Blog. [Online]. Available: www.afranko.net/2014/02/black-and-white-map-of-the-world/

[10] AGI. (2014) Stk. agi. [Online]. Available: www.agi.com/products/stk/

[11] (2014, June). [Online]. Available: http://www.n2yo.com/satellites/?c=15

[12] (2014, June). [Online]. Available: http://www.gmat.unsw.edu.au/snap/gps/gps_survey/chap2/222sats.htm

[13] (2014, June). [Online]. Available: http://www.esa.int/Our_Activities/Navigation/The_future_-_Galileo/Galileo_a_constellation_of_30_navigation_satellites

[14] W. A. Holm, "Continuous wave radar," in *Principles of Modern Radar*. Springer, 1987, pp. 397–421.

[15] Y. Chan and V. Koo, "An introduction to synthetic aperture radar (SAR)," *Progress In Electromagnetics Research B*, vol. 2, pp. 27–60, 2008.

[16] H. Maître, *Processing of Synthetic Aperture Radar Images*. John Wiley & Sons Ltd, 2008.

[17] C. Allen. Synthetic-aperture radar (sar) basics. [Online]. Available: http://people.eecs.ku.edu/~callen/826/826_SAR_basics-S09.ppt

[18] M. Cherniakov, *Bistatic Radars: Emerging Technology*. John Wiley & Sons, 2008.

[19] A. Freeman and S. L. Durden, "A three-component scattering model for polarimetric sar data," *Geoscience and Remote Sensing, IEEE Transactions on*, vol. 36, no. 3, pp. 963–973, 1998.

[20] Radar image of the Netherlands. European Space Agency. [Online]. Available: http://www.esa.int/spaceinimages/Images/2014/04/Radar_image_of_the_Netherlands

[21] M. Kolawole, *Radar systems, peak detection and tracking*. Newnes, 2003.

[22] Z. Zhao, K. Ji, X. Xing, and H. Zou, "Adaptive cfar detection of ship targets in high resolution SAR imagery," in *Eighth International Symposium on Multispectral Image Processing and Pattern Recognition*. International Society for Optics and Photonics, 2013, pp. 89 170L–89 170L.

[23] F. Gatelli, A. M. Guamieri, F. Parizzi, P. Pasquali, C. Prati, and F. Rocca, "The wavenumber shift in sar interferometry," *Geoscience and Remote Sensing, IEEE Transactions on*, vol. 32, no. 4, pp. 855–865, 1994.

[24] [Online]. Available: http://photojournal.jpl.nasa.gov/catalog/PIA01762

[25] R. Siegmund, M. Bao, S. Lehner, and R. Mayerle, "First demonstration of surface currents imaged by hybrid along-and cross-track interferometric SAR," *Geoscience and Remote Sensing, IEEE Transactions on*, vol. 42, no. 3, pp. 511–519, 2004.

[26] S. N. Madsen, H. A. Zebker, and J. Martin, "Topographic mapping using radar interferometry: Processing techniques," *Geoscience and Remote Sensing, IEEE Transactions on*, vol. 31, no. 1, pp. 246–256, 1993.

[27] Stiefvater Consultants, "Along track interferometry synthetic aperture radar (ATI-SAR) techniques for ground moving target detection," Air Force Research Laboratory, Tech. Rep., 2005.

[28] A. Arnaud, "Ship detection by SAR interferometry," in *Geoscience and Remote Sensing Symposium, 1999. IGARSS'99 Proceedings. IEEE 1999 International*, vol. 5. IEEE, 1999, pp. 2616–2618.

[29] K. Ouchi, S. Tamaki, H. Yaguchi, and M. Iehara, "Ship detection based on coherence images derived from cross correlation of multilook sar images," *Geoscience and Remote Sensing Letters, IEEE*, vol. 1, no. 3, pp. 184–187, 2004.

[30] F. Rocca, C. Prati, and A. Ferretti, "An overview of ERS-SAR interferometry," in *ERS Symposium on Space at the Service of Our Environment, 3 rd, Florence, Italy*, 1997.

[31] G. K. Høye, T. Eriksen, B. J. Meland, and B. T. Narheim, "Space-based ais for global maritime traffic monitoring," *Acta Astronautica*, vol. 62, no. 2, pp. 240–245, 2008.

[32] M. M. Weiner, *Monopole antennas*. CRC Press, 2003, vol. 1.

[33] (2014, April) Live Ships Map - AIS - Vessel Tracks and Positions - AIS Marine Traffic. [Online]. Available: https://www.marinetraffic.com/en/

[34] E. Astrium. (2014) Automated transfer vehicle - propulsion. [Online]. Available: http://cs.astrium.eads.net/sp/spacecraft-propulsion/showcase/atv.html

[35] ESA, "Launch vehicle catalog," December 2004.

[36] SpaceX, *Falcon 9 Launch Vehicle Payload User's Guide*, Space Exploration Technologies Corpartion, October 2008.

[37] SLR. (2014, May) R-7/soyuz data sheet. [Online]. Available: http://www.spacelaunchreport.com/soyuz.html#config

[38] S. L. Report. (2014, May) Launch vehicle/site statistics. [Online]. Available: http://www.spacelaunchreport.com/log2014.html

[39] SpaceX. (2014) Capabilities and services. [Online]. Available: www.spacex.com

[40] C. I. Heghes, "C1-c4 hydrocarbon oxidation mechanism," Master's thesis, the Rupertus Carola University of Heidelberg, 2006.

[41] G. Boyle, *Renewable Energy : Power for a Sustainable Future*. OUP Oxford, 2004.

[42] NTP, "Report on carcinogens," National Toxicology Program, Department of Health and Human Services, Tech. Rep., 2011. [Online]. Available: http://ntp.niehs.nih.gov/ntp/roc/twelfth/profiles/dimethylhydrazine.pdf

[43] Arianespace, "Soyuz user's manual," June 2006.

[44] J. R. Wertz and W. J. Larson, *Space Mission Analysis and Design*, 2nd ed. Microcosm Press, 1993.

[45] W. J. Larson, G. N. Henry, and R. W. Humble, *Space propulsion analysis and design*. McGraw-Hill, 1995.

[46] J. R. Wertz and W. J. Larson, *Space Mission Analysis and Design*, 3rd ed. Microcosm Press, 1999.

[47] B. D. Rigling and R. L. Moses, "Motion measurement errors and autofocus in bistatic sar," *Image Processing, IEEE Transactions on*, vol. 15, no. 4, pp. 1008–1016, 2006.

[48] G. Blewitt, "Basics of the gps technique: observation equations," *Geodetic applications of GPS*, pp. 10–54, 1997.

[49] M. Weiss, "Synchronisation of bistatic radar systems," in *Geoscience and Remote Sensing Symposium, 2004. IGARSS'04. Proceedings. 2004 IEEE International*, vol. 3. IEEE, 2004, pp. 1750–1753.

[50] O. Montenbruck and R. Kroes, "In-flight performance analysis of the CHAMP BlackJack GPS receiver," *GPS Solutions*, vol. 7, no. 2, pp. 74–86, 2003.

[51] O. Montenbruck. (2001) GNSS receivers for space applications. [Online]. Available: http://www.iapg.bv.tum.de/mediadb/14973/14974/04_ACES_WS_08_SGNSS.pdf

[52] Polarx2. Septentrio. [Online]. Available: http://www.iapg.bv.tum.de/mediadb/14973/14974/04_ACES_WS_08_SGNSS.pdf

[53] D. Coulot, F. Deleflie, P. Bonnefond, P. Exertier, O. Laurain, and B. de Saint-Jean, "Satellite laser ranging," in *Encyclopedia of Solid Earth Geophysics*. Springer, 2011, pp. 1049–1055.

[54] O. Montenbruck, R. Kahle, S. DAmico, and J.-S. Ardaens, "Navigation and control of the tandem-x formation," *The Journal of the Astronautical Sciences*, vol. 56, no. 3, pp. 341–357, 2008.

[55] S. D'Amico and O. Montenbruck, "Proximity operations of formation-flying spacecraft using an eccentricity/inclination vector separation," *Journal of Guidance, Control, and Dynamics*, vol. 29, no. 3, pp. 554–563, 2006.

[56] K. Alfriend, S. R. Vadali, P. Gurfil, J. How, and L. Breger, *Spacecraft formation flying: dynamics, control, and navigation*. Butterworth-Heinemann, 2009, vol. 2.

[57] E. Gill, O. Montenbruck, and S. D'Amico, "Autonomous formation flying for the prisma mission," *Journal of Spacecraft and Rockets*, vol. 44, no. 3, pp. 671–681, 2007.

[58] G. W. Hill, "Researches in the lunar theory," *American journal of Mathematics*, vol. 1, no. 2, pp. 129–147, 1878.

[59] Y. Kozai, "The motion of a close earth satellite," *The Astronomical Journal*, vol. 64, p. 367, 1959.

[60] M. Eckstein, C. Rajasingh, and P. Blumer, "Colocation strategy and collision avoidance for the geostationary satellites at 19 degrees west," in *CNES Symposium on Space Dynamics*, 1989, pp. 6–10.

[61] H. Schaub and K. T. Alfriend, "J2 invariant relative orbits for spacecraft formations," *Celestial Mechanics and Dynamical Astronomy*, vol. 79, no. 2, pp. 77–95, 2001.

[62] Tet-1 (technology experiment carrier-1). [Online]. Available: https://directory.eoportal.org/web/eoportal/satellite-missions/t/tet-1

[63] Aluminum 6061-t6; 6061-t651. [Online]. Available: http://asm.matweb.com/search/SpecificMaterial.asp?bassnum=MA6061t6

[64] I. Harris and W. Priester, "Time-dependent structure of the upper atmosphere," *Journal of the Atmospheric Sciences*, vol. 19, no. 4, pp. 286–301, 1962.

[65] ——, "Theoretical models for the solar-cycle variation of the upper atmosphere," *Journal of Geophysical Research*, vol. 67, no. 12, pp. 4585–4591, 1962.

[66] (2014). [Online]. Available: http://www.rocket.com/propulsion-systems/monopropellant-rockets

[67] (2014). [Online]. Available: http://spexcertiprep.com/products/product_organic.aspx?part=S-2231

[68] A.-S. Yang and T.-C. Kuo, "Design analysis of a satellite hydrazine propulsion system," *Journal of propulsion and power*, vol. 18, no. 2, pp. 270–279, 2002.

[69] J. Stratton, "The use of the aerojet mr-103h thruster on the new hhorizon mission to pluto," in *55th International Astronautical Congress 2004*, 2004.

[70] W. Hsieh, C. Lin, and A. Yang, "Blowdown and waterhammer behavior of monopropellant feed systems for satellite attitude and reaction control," in *33* AIAA/ASME/SEA/ASEE Joint Propulsion Conference*, 1997.

[71] [Online]. Available: http://answers.ask.com/science/chemistry/how_much_does_nitrogen_cost

[72] "Propellant tanks for spacecraft."

[73] Fill, drain & vent valves for spacecraft propulsion systems. [Online]. Available: http://cs.astrium.eads.net/sp/spacecraft-propulsion/valves/fill-drain-vent-valves.html

[74] Moog. Fill drain valves. [Online]. Available: http://www.moog.com/products/propulsion-controls/spacecraft/components/fill-drain-valves/low-pressure-fill-drain-valve/

[75] Propellant control valves for thrusters. [Online]. Available: http://cs.astrium.eads.net/sp/spacecraft-propulsion/valves/propellant-valves.html

[76] Aerojet, "Themis (time history of events and macroscale interactions during substorms)," 08 2005.

[77] Bradford Engineering. [Online]. Available: http://bradford-space.com/news/2011/the_galileo_iov_was_launched_at_october_21st

[78] V. S. Products, "Low pressure gas filters," 07 2004.

[79] E. K. A. Gill, "Aerospace design and system engineering elements II: Attitude control systems," November 2012.

[80] COSPAR International Reference Atmosphere, "Models of the earth's upper atmosphere."

[81] E. Blackburn, D. DeBra, B.Dobrotin, J.Scull, R. Fischell, D. Fosth, J.Kelly, A. Fleig, H. Perkel, R. Roberson, J. Rodden, B. Tinling, S. O'Neil, F. Caroll, and R. Bohling, "Spacecraft magnetic torques," March 1969.

[82] R. J. Blakely, *Potential Theory in Gravity and Magnetic Applications*, 1st ed. Cambridge University Press, 1996.

[83] the International Association of Geomagnetism and Aeronomy. (2009, December) the international geomagnetic reference field (igrf) model 11. [Online]. Available: http://www.ngdc.noaa.gov/IAGA/vmod/igrf11coeffs.txt

[84] S. S. T. US. [Online]. Available: www.sst-us.com

[85] SSBV Aerospace & Technology Group. [Online]. Available: http://www.ssbv.com

[86] Honeywell, "Hr 0610 reaction wheel," December 2003.

[87] H. B. Hablani, "Sun-tracking commands and reaction wheel sizing with configuration optimization," *Journal of guidance, control, and dynamics*, vol. 17, no. 4, pp. 805–814, 1994.

[88] T. Megson, *Aircraft Structres for Engineering Sudents*, 4th ed. Butterworth-Heinemann, 2007.

[89] N. S. Nise, *Control Systems Engineering*, 6th ed. John Wiley & Sons, Inc, 2011.

[90] J. R. Wertz, *Spacecraft Attitude Determination and Control*. Kluwer Academic Publishers, 1978.

[91] B. Wie, *Space Vehicle Dynamics and Control*, 2nd ed. AIAA Education Series, 2008.

[92] World geodetic system 1984. National Geospatial-Intelligence Agency. [Online]. Available: http://web.archive.org/web/20120402143802/https://www1.nga.mil/ProductsServices/GeodesyandGeophysics/WorldGeodeticSystem/Pages/default.aspx

[93] Geomagnetism. National Geophysical Data Center. [Online]. Available: http://www.ngdc.noaa.gov/geomag/geomag.shtml

[94] S. Maus, S. Macmillan, S. McLean, B. Hamilton, A. Thomson, M. Nair, and C. Rollins, "The US/UK world magnetic model for 2010-2015," NOAA Technical Report NESDIS/NGDC, Tech. Rep., 2010.

[95] (2014) Total solar irradiance data. University of Colorado. [Online]. Available: http://lasp.colorado.edu/home/sorce/data/tsi-data/

[96] Estrack network. [Online]. Available: http://www.esa.int/Our_Activities/Operations/Estrack_tracking_stations

[97] J. R. Wertz, D. F. Everett, and J. J. Puschell, *Space Mission Engineering: The New SMAD*, 1st ed. Microcosm Press, 2011.

[98] Novasar-s. eoportal. [Online]. Available: https://directory.eoportal.org/web/eoportal/satellite-missions/n/novasar-s

[99] Spot 4 ground network. [Online]. Available: http://spot4.cnes.fr/spot4_gb/stat2ghz.htm

[100] *Soyuz User's Manual (Issue 2 Revision 0)*, Ariane Space, May 2012.

[101] MIT, *Engineering Mechanics of Solids*. MIT, 1989.

[102] P. et al., "The strength characterichara of aluminum honeycomb sandwich panels," *Elsevier*, 1991.

[103] (2014, may) Spectrolab. Spectrolab inc. [Online]. Available: http://www.spectrolab.com/

[104] (2014, 06) Ves & vl batteries for satellites. Saft. [Online]. Available: http://www.saftbatteries.com/battery-search/ves-vl-batteries-satellites

[105] (2014, 06) Power systems & electronics. Terma. [Online]. Available: http://www.terma.com/space/space-segment/power-systems-electronics/

[106] A. Hyder, R. Wiley, G. Halpert, D. Flood, and S. Sabripour, *Spacecraft Power Technologies*. Imperial College Press, 2000.

[107] T. J. Woike, "EOL performance comparison of GaAs/Ge and Si BSF/R solar arrays," Applied Solar Energy Corporation, Tech. Rep., 1993.

[108] P. Fortescue, J. Stark, and G. Swinerd, *Spacecraft Systems Engineering*. John Wiley & Sons Ltd, 2003.

[109] Thermal insulation products. [Online]. Available: http://www.ruag.com/de/Space/Products/Satellite_Structures2C_Mechanisms_Mechanical_Equipment/140110_Broschuere_Thermal_May2014_singleside.pdf

[110] Vibration tested thermistor probes. [Online]. Available: http://www.omega.com/pptst/TH-21.html

[111] Kapton polymide film heater. [Online]. Available: http://www.omega.com/pptst/KHR_KHLV_KH.html

[112] (2014, April) ERS overview. European Space Agency. [Online]. Available: http://www.esa.int/Our_Activities/Observing_the_Earth/ERS_overview

[113] C. Francis, G. Graf, P. Edwards, M. McCaig, C. McCarthy, A. Lefebvre, B. Pieper, P.-Y. Pouvreau, R. Wall, F. Weschler, J.Louet, W. Schumann, and R. Zobl, "The ERS-2 spacecraft and its payload," *ESA Bulletin*, vol. 1, pp. 13–31, 1995.

[114] E. Attema, P. Bargellini, P. Edwards, G. Levrini, S. Lokas, L. Moeller, B. Rosich-Tell, P. Secchi, R. Torres, M. Davidson *et al.*, "Sentinel-1-the radar mission for gmes operational land and sea services," *ESA bulletin*, vol. 131, pp. 10–17, 2007.

[115] German Aerospace Center (DLR). (2014, April) TanDEM-X - the earth in three dimensions. [Online]. Available: http://www.dlr.de/eo/en/desktopdefault.aspx/tabid-5727/10086_read-21046/

[116] TDX (TanDEM-X: TerraSAR-X add-on for digital elevation measurement). [Online]. Available: https://directory.eoportal.org/web/eoportal/satellite-missions/t/tandem-x

[117] Encyclopedia astronautica: TerraSAR-X. [Online]. Available: http://www.astronautix.com/craft/terasarx.htm

[118] RADARSAT-1. [Online]. Available: https://directory.eoportal.org/web/eoportal/satellite-missions/r/radarsat-1

[119] MacDonald Dettwiler, "The growing costs of RADARSAT-1 and -2," *Press for Conversion*, vol. 58, pp. 28–29, 2006.

[120] A. Ragunathan. Chandrayaan-1 mission completed in cost-effective manner, says top official. [Online]. Available: http://www.thehindu.com/news/national/tamil-nadu/chandrayaan1-mission-completed-in-costeffective-manner-says-top-official/article1495884.ece

[121] COSMO-SkyMed. [Online]. Available: https://directory.eoportal.org/web/eoportal/satellite-missions/c-missions/cosmo-skymed

[122] JERS-1 (japan earth resources satellite) / Fuyo-1. [Online]. Available: https://directory.eoportal.org/web/eoportal/satellite-missions/j/jers-1/

[123] ALOS (advanced land observing satellite) / Daichi. [Online]. Available: https://directory.eoportal.org/web/eoportal/satellite-missions/a/alos

[124] World Meteorological Organization. Instrument: SAR-2000. [Online]. Available: http://www.wmo-sat.info/oscar/instruments/view/447

[125] COSMO-SkyMed. Deagel. [Online]. Available: http://www.deagel.com/C3ISTAR-Satellites/COSMO-SkyMed_a000256001.aspx

[126] T. Buijs, D. Ju, N. de Kogel, S. van der Linden, A. Melaika, T. van de Oever, D. Petkovic, B. van Putten, and C. Verhoeven, "DSE - bi-SAR satellite network: Designing a satellite network for maritime monitoring of the north sea - baseline report," Delft University of Technology, Tech. Rep., May 2014.

[127] How safeseanet works. [Online]. Available: http://emsa.europa.eu/ssn-how-it-works.html

[128] K. Tringham. (2014, 06) Saab launches affordable maritime surveillance aircraft. IHS. [Online]. Available: http://www.ihs.com/events/exhibitions/farnborough-2012/news/july-10/Saab-launches-affordable-maritime-surveillance-aircraft.aspx

[129] Aissat-1. [Online]. Available: https://directory.eoportal.org/web/eoportal/satellite-missions/a/aissat-1

[130] R. Tinch, "Costs of illegal, unreported and unregulated (IUU) fishing in EU fisheries," Economics for the Environment Consultancy Ltd, Tech. Rep., 2008.

[131] (2014, April) Oil pollution monitoring. European Space Agency. [Online]. Available: http://www.esa.int/esapub/br/br128/br128_1.pdf

[132] (2014, 06) Review of maritime patrol requirements. Ministry of Fisheries New Zealand. [Online]. Available: http://www.dpmc.govt.nz/sites/all/files/publications/annex_iiia_fisheries-aerial_surveillance.pdf

[133] T. Bauna. Satellite based services for maritime envirment monitoring and maritime situational awareness. Kongsberg satellite service. [Online]. Available: http://www.forskningsradet.no/servlet/Satellite?blobcol=urldata&blobheader=application%2Fpdf&blobheadername1=Content-Disposition%3A&blobheadervalue1=+attachment%3B+filename%3D%226-KSATNowaySingaporeworkshopNRC03june2013.pdf%22&blobkey=id&blobtable=MungoBlobs&blobwhere=1274502907175&ssbinary=true

[134] EMSA, "Pollution preparedness and response activities," European Maritime Safety Agency, Tech. Rep., 2014.

[135] (2003, Januari) Energy density of aviation fuel. The Physics Factbook. [Online]. Available: http://hypertextbook.com/facts/2003/EvelynGofman.shtml

[136] (2012, January) Towards a smaller environmental impact. The Linde Group, AGA. [Online]. Available: http://www.aga.com/international/web/lg/aga/like35agacom.nsf/0/784E94956806250EC12579020045F5CF

[137] (2014, June) Co2 emissions. Sun Earth Tools. [Online]. Available: www.sunearthtools.com/tools/CO2-emissions-calculator.php#txtCO2_16

[138] (2007, January) Unit conversion data for oxygen. Universal Industrial Gases, Inc. [Online]. Available: http://www.uigi.com/o2_conv.html

[139] (2013, Januari) Royal netherlands air force-coastguard dornier 228. AIR TATTOO. [Online]. Available: www.airtattoo.com/airshow/visiting/aircraft/aircraft-in-the-spotlight/royal-netherlands-air-force-coastguard-dornier-228

[140] M. Meeuwisse, T. C. Rien Eykelenboom, Martin Bobeldijk, and the Audio Visuele Dienst Defensie, "De nederlandse kustwacht in 2012," Dutch Coastguard, Tech. Rep., 2012, dutch Publication.

[141] J. D. H. Polet, "Impact assessment of the effects of a selected range of fishing gears in the north sea," Stichting Noordzee and WWF, Tech. Rep., 2012, international Publication.

Appendix A

Satellite Layout

In this appendix the technical drawings for the two different satellites are given.

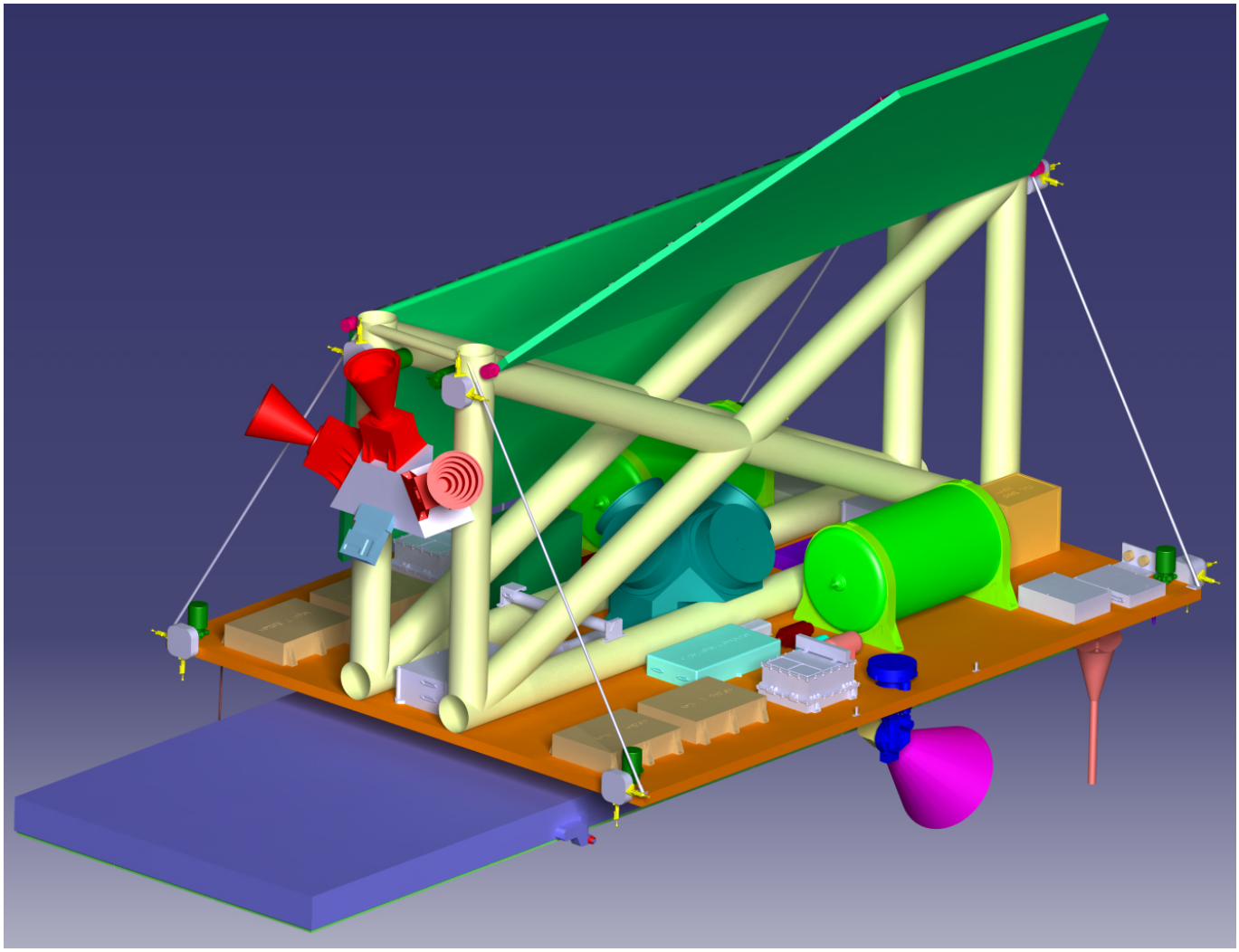

Figure A.1

Front view
Scale: 1:8

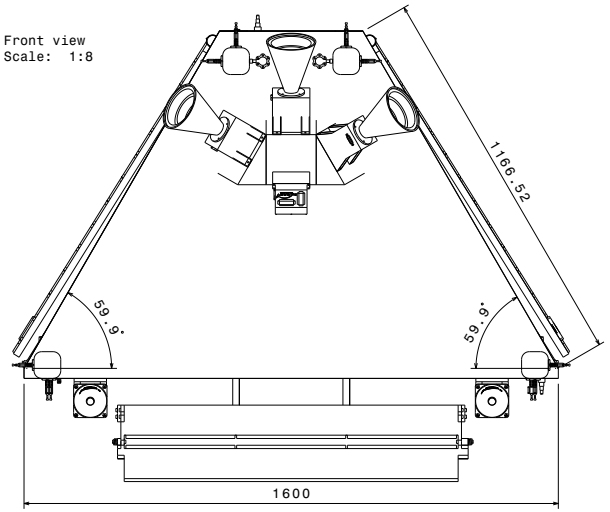

Left view
Scale: 1:8

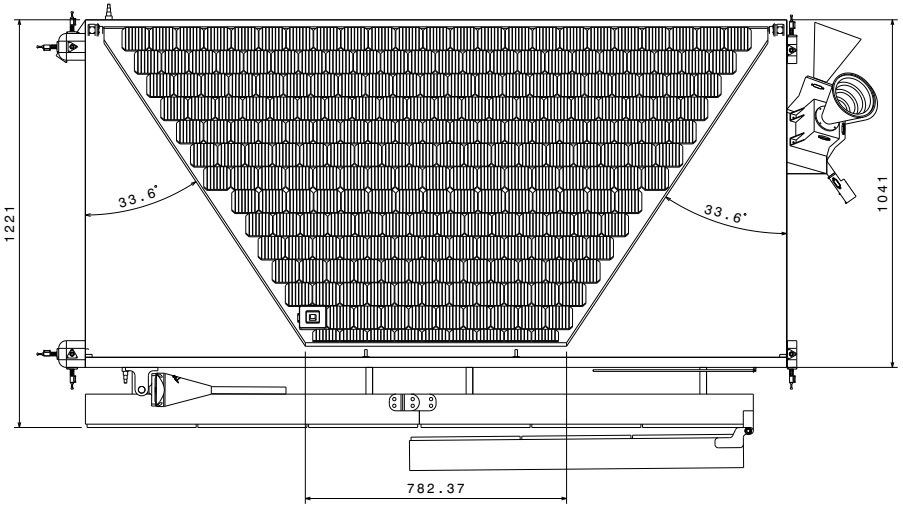

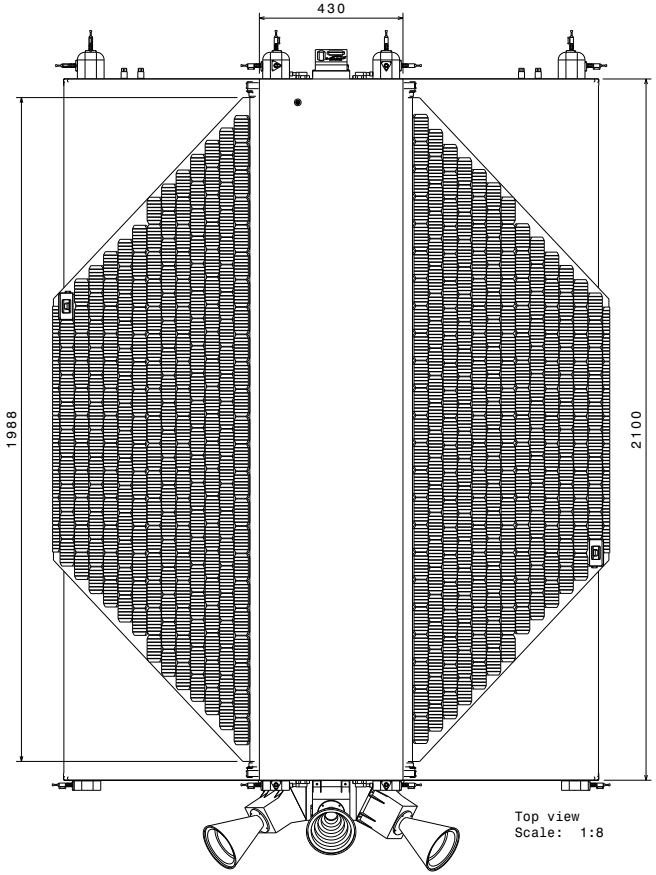

Top view
Scale: 1:8

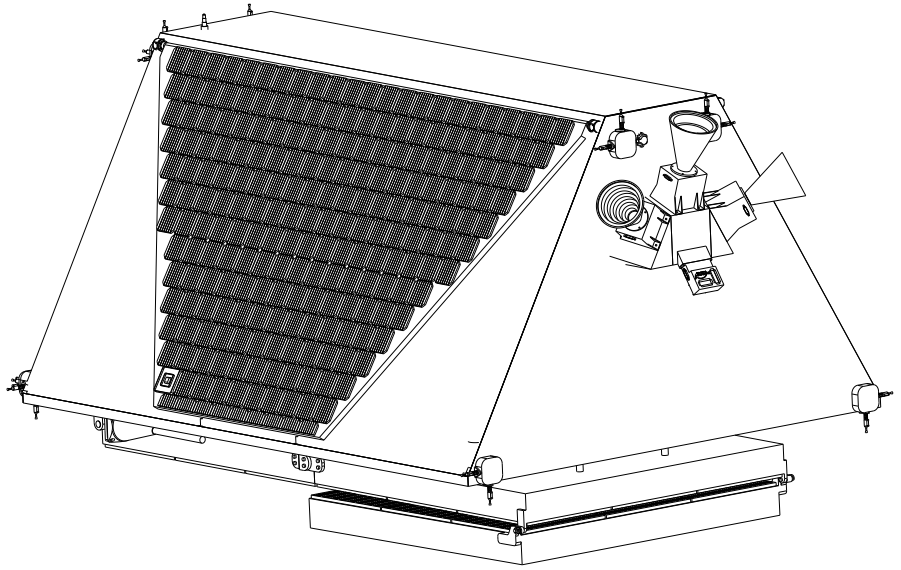

Isometric view
Scale: 1:8

DRAWN BY: Antanas Melaika	DATE: 2014-06-23	
CHECKED BY	DATE	
DESIGNED BY: Antanas Melaika	DATE: 2014-06-23	

TU Delft: Aeropspace Engineering Faculty

DRAWING TITLE: Transmitter Satellite

SIZE	DRAWING NUMBER	REV
A1	1	

SCALE 1:8 | WEIGHT(kg) | SHEET 1/1

Front view
Scale: 1:8

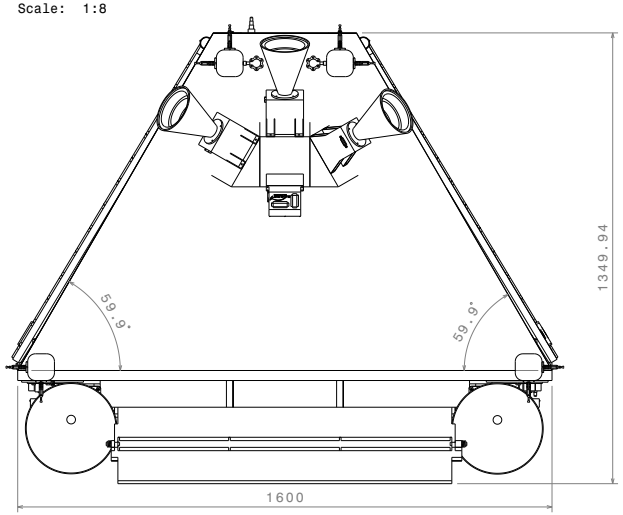

Left view
Scale: 1:8

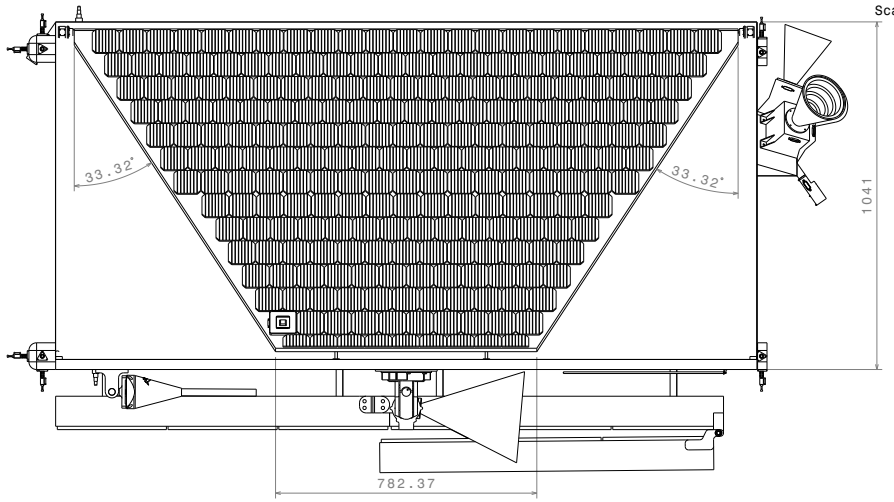

Top view
Scale: 1:8

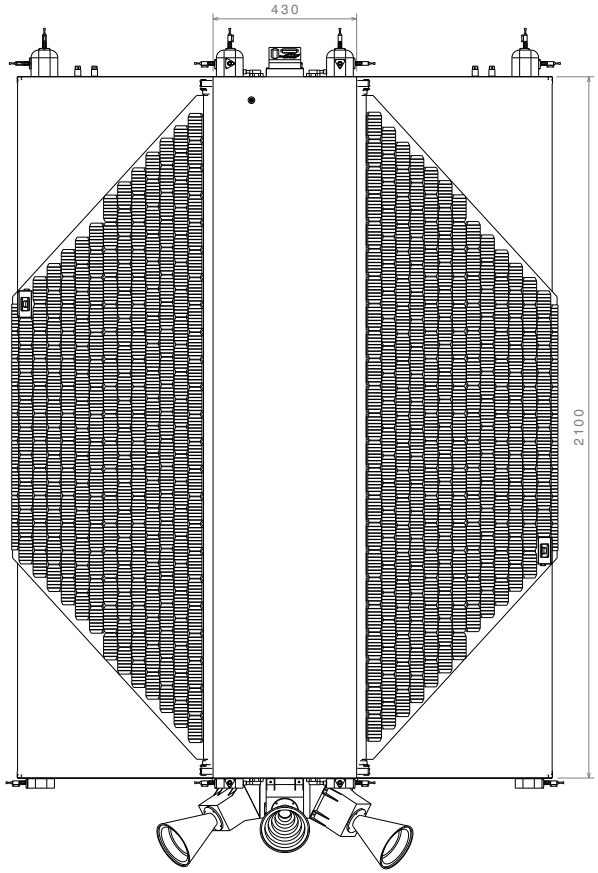

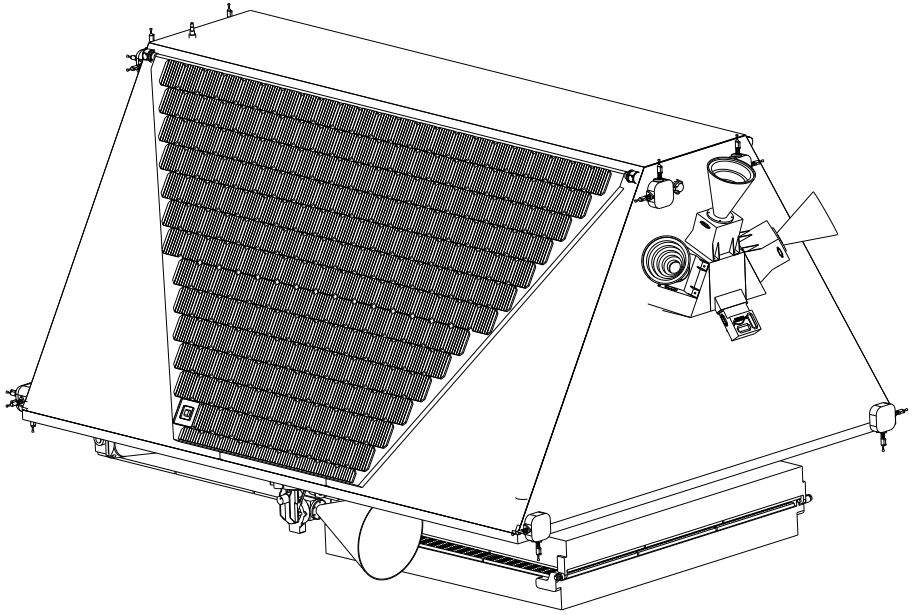

Isometric view
Scale: 1:8

DRAWN BY: Antanas Melaika	DATE: 2014-06-23	TU Delft: Aerospace Engineering Faculty
CHECKED BY	DATE	DRAWING TITLE: Receiver Satellite
DESIGNED BY: Antanas Melaika	DATE	SIZE: A1 / DRAWING NUMBER: 2 / REV
		SCALE 1:8 / WEIGHT(kg) / SHEET 1/1

Appendix B

Risk Maps

This appendix contains the risk maps for all the subsystems. The risks have been discussed in each respective chapter.

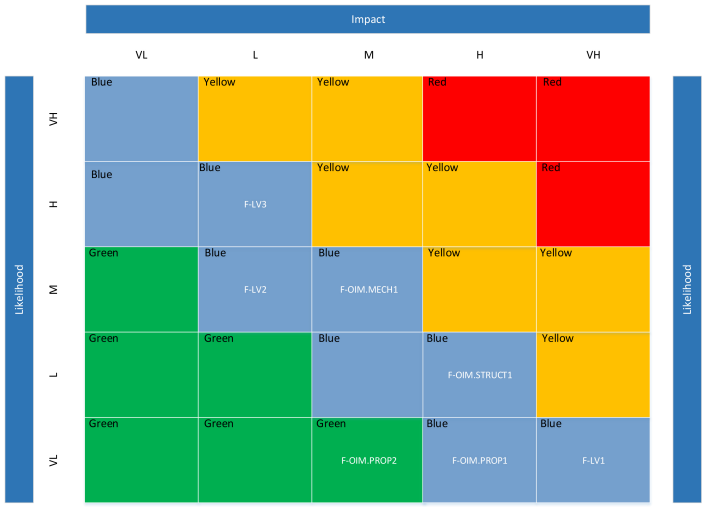

(a) OIM risk before mitigation

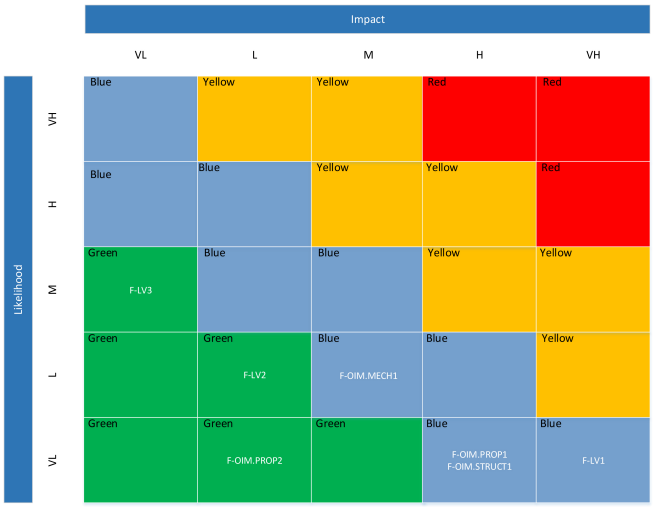

(b) OIM risk after mitigation

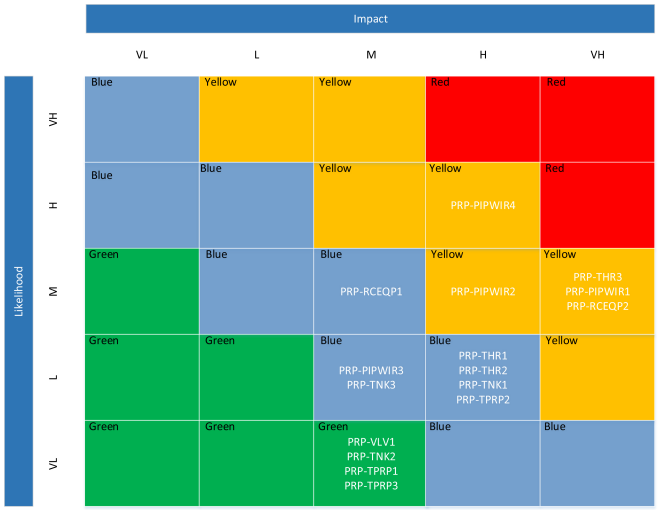

(a) Propulsion risk before mitigation

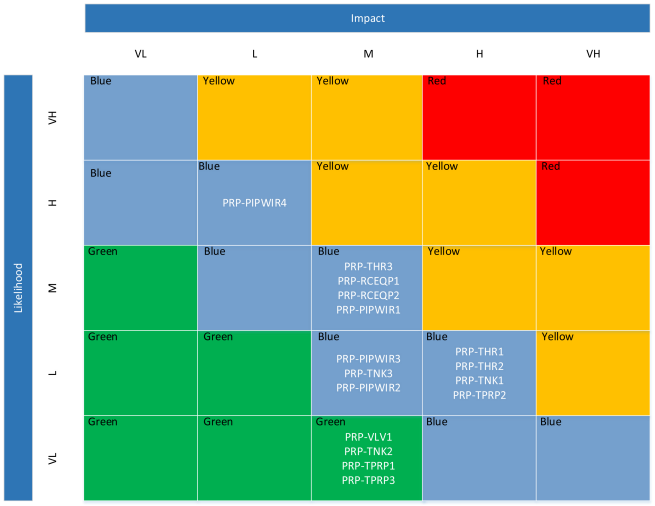

(b) Propulsion risk after mitigation

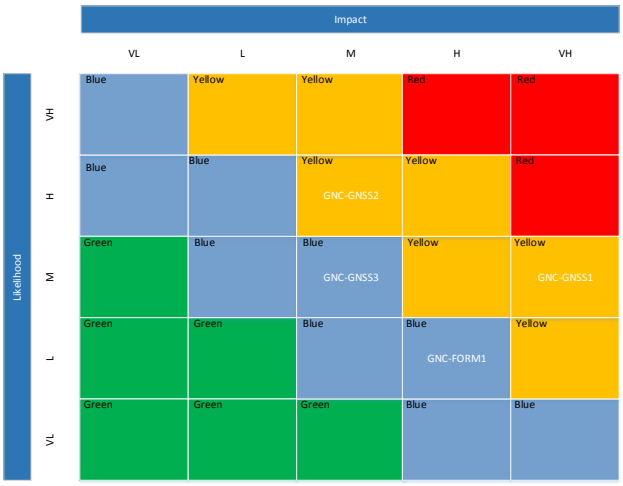

(a) GNC risk before mitigation

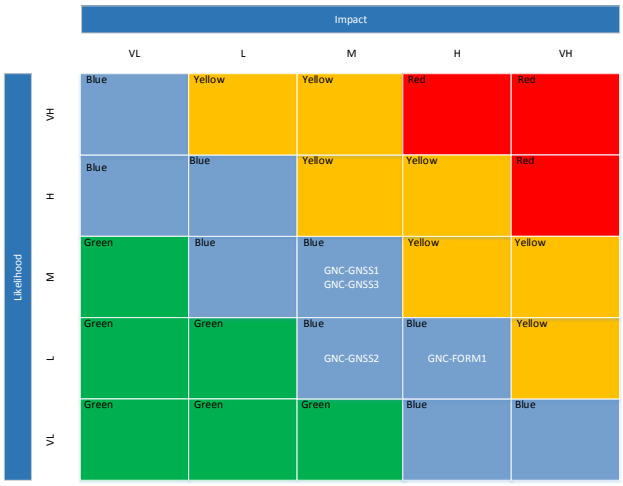

(b) GNC risk after mitigation

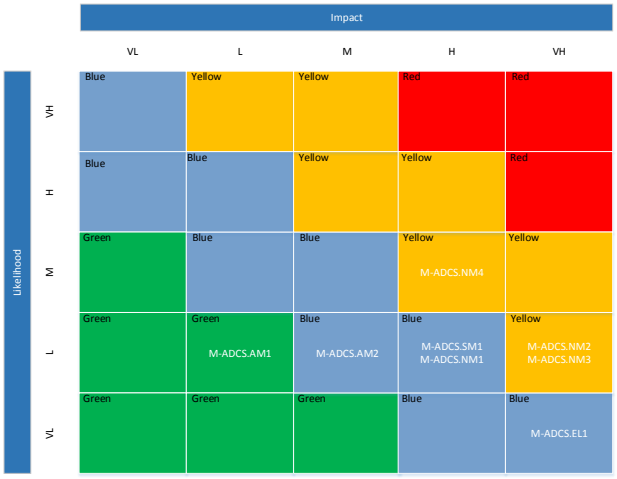

(a) ADCS risk before mitigation

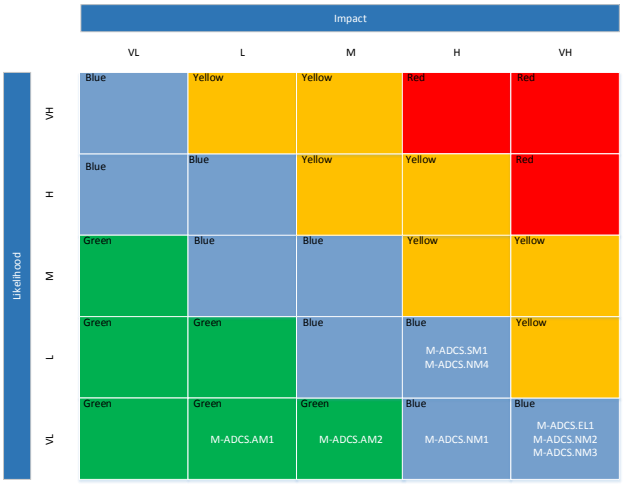

(b) ADCS risk after mitigation

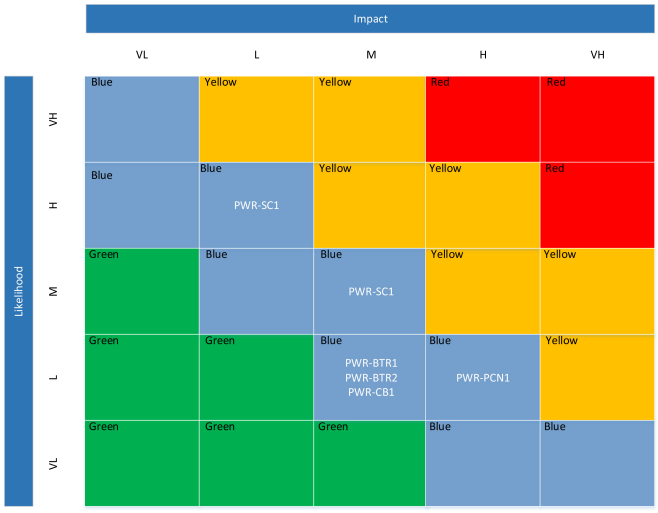

(a) Power risk before mitigation

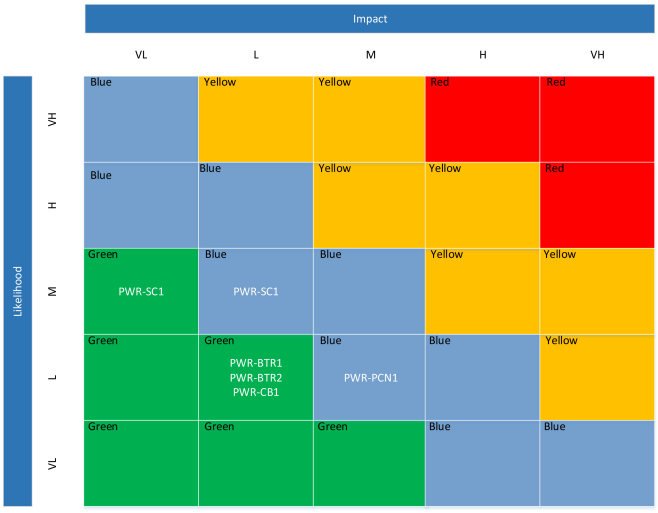

(b) Power risk after mitigation

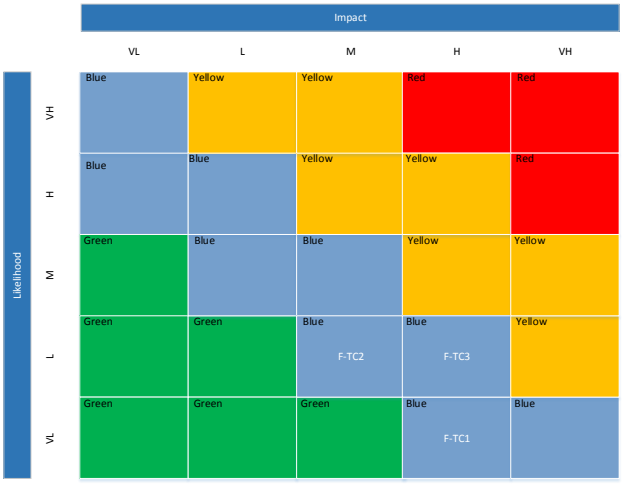

(a) Thermal risk before mitigation

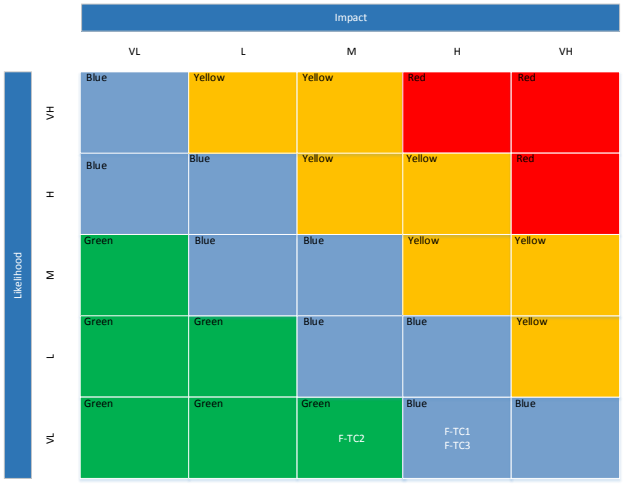

(b) Thermal risk after mitigation

(a) Structural risk before mitigation

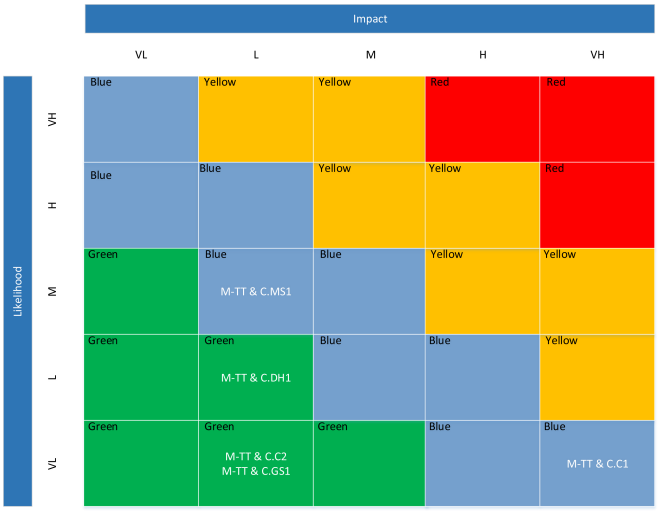

(b) TT& C risk before mitigation

Appendix C

Compliance Tables

Code	Requirements				Compliance	
	Item	Requirement	Value	Margin	Compliant	Comment
BSAR	Mission	The system shall continuously monitor the North Sea with a network of bistatic SAR satellites	Yes	-	Yes	-
BSAR-1	Mission	The system shall continuously monitor the North Sea with a network of bistatic SAR satellites in a technically feasible manner	Yes	-	Yes	-
BSAR-2	Mission	The system shall continuously monitor the North Sea with a network of bistatic SAR satellites within constrains	Yes	-	Yes	-
BSAR-1a	Stakeholder	At least 90% of the total ship traffic shall be detected	Yes	-	Yes	-
BSAR-1b	Stakeholder	Continuous monitoring shall be performed	Yes	- Yes	100 [min]	resolution
BSAR-1c	Stakeholder	The North Sea area shall be monitored	Yes	-	Yes	-
BSAR-1d	Stakeholder	The bistatic SAR instrument designed by SSBV shall be used	Yes	-	Yes	-
BSAR-1e	Stakeholder	The mission shall have a minimum lifetime of 5 years	Yes	-	Yes	-
BSAR-1f	Stakeholder	The mission shall be put in the correct orbit	Yes	-	Yes	-
BSAR-2a	Stakeholder	The mission shall be profitable	No	-	No	Not whole project can be funded but a start can be made
BSAR-2b	Stakeholder	The mission shall comply with the designated deadlines	Yes	-	Yes	-
BSAR-2c	Stakeholder	The mission shall comply with all laws and regulations	Yes	-	Yes	-
BSAR-1a-Sys1	System	The payload shall have a minimum pixel size of 230 [m2]	-	-	-	Dropped
BSAR-1b-Sys1	System	he system shall have a maximum temporal resolution of 100 min	71, 118 min	29, -18 min	Partly	Norwegian coast has 355 min
BSAR-1bc-Sys1	System	The spacecraft shall have an orbital period of 100 min	94 min	6 min	Yes	-
BSAR-1bc-Sys2	System	The constellation shall consist of 17 satellite pairs	20	3	Yes	-
BSAR-1bc-Sys3	System	The bistatic SAR instrument shall have a swath width of 100 km	128 [km]	28 [km]	Yes	-
BSAR-1c-Sys1	System	The orbital planes shall have a minimum inclination of 58 [deg]	58,63 [deg]	0,5 [deg]	Yes	-
BSAR-1d-Sys1	System	The spacecraft shall be able to perform formation flying	Yes	-	Yes	-
BSAR-1d-Sys2	System	The payload shall operate at an incidence angle of 28 [deg] +/- 8 [deg]	Yes	-	Yes	-
BSAR-1e-Sys1	System	The spacecraft shall maintain an operational orbit during the mission life	Yes	-	Yes	-
BSAR-1e-Sys2	System	The spacecraft shall have a minimum reliability of TBD	-	-	-	Dropped
BSAR-1e-Sys3	System	The spacecraft shall have a mission life of at least 5 years	5 [years]	0 [years]	Yes	-
BSAR-1f-Sys1	System	The spacecraft shall be launched with the Soyuz-2 launcher	Yes	-	Yes	-
BSAR-1f-Sys2	System	The spacecraft shall be able to correct the launch trajectory	Possible	-	Possible	Must be checked

Code	Requirements				Compliance	
	Item	Requirement	Value	Margin	Compliant	Comment
BSAR-1f-Sys3	System	The spacecraft shall be able to fit in the launcher	Yes	-	Yes	-
BSAR-1f-Sys4	System	The spacecraft shall have a maximum mass of 1330.7 [kg]	482.93 [kg]	847.77 [kg]	Yes	-
BSAR-2b-Sys1	System	The project definition shall be determined before 8th of May, 2014	Yes	-	Yes	-
BSAR-2b-Sys2	System	The preliminary design shall be determined before 28th of May, 2014	Yes	-	Yes	-
BSAR-2b-Sys3	System	The final design shall be finished before 28th of June, 2014	Yes	-	Yes	-
BSAR-2b-Sys4	System	The V & V procedures shall be finalized before 28 June, 2014	Yes	-	Yes	-
BSAR-2b-Sys5	System	The mission shall be launched before <TBD>	-	-	-	Has to be determined
BSAR-2c-Sys1	System	The payload shall operate at X-band frequency	Yes	-	Yes	-
BSAR-2c-Sys2	System	The orbit shall adhere to altitude restrictions	Yes	-	Yes	-
BSAR-2c-Sys3	System	The spacecraft shall have all necessary emergency subsystems	Yes	-	Yes	-
BSAR-2c-Sys4	System	The spacecraft shall be able to de-orbit in a controlled manner	Yes	-	Yes	-
BSAR-2c-Sys5	System	The spacecraft shall communicate using the X- or S-band frequency	Yes	-	Yes	-
ADCSAa	ADCS-Acquisition mode	The ADCS shall provide an initial determination time of one orbital period	Yes	-	Yes	-
ADCSAb	ADCS-Acquisition mode	The ADCS shall be able to provide the initialization during an ecplipse	Yes	-	Yes	-
ADCSAc	ADCS-Acquisition mode	The ADCS shall provide an initial determination range within the minimal normal attitude determination sensor range	Yes	-	Yes	-
ADCSAd	ADCS-Acquisition mode	The ADCS shall provide an initial control accuracy of 1 [deg]	Yes	-	Yes	-
ADCSAe	ADCS-Acquisition mode	The ADCS shall provide an initial attitude control range of 180 [deg]	-	-	N/A	N/A
ADCSSa	ADCS - Slew mode	The ADCS shall provide a slewing rate of at least 72 [deg] in half an orbital time during payload inoperative time.	Yes	-	Yes	-
ADCSSb	ADCS - Slew mode	The ADCS shall provide a slewing rate of at least 10 [deg] in 10 [s]during payload operative time	Yes	-	Yes	-
ADCS1a	ADCS - Normal mode	The ADCS shall provide a pointing accuracy of at least 13.5 [arcsec] per axis	Yes	-	Yes	-
ADCS1b	ADCS - Normal mode	The ADCS shall provide an attitude determination range of 28 [deg] of nadir +/- 8 [deg]	Yes	-	Yes	-

Code	Requirements				Compliance	
	Item	Requirement	Value	Margin	Compliant	Comment
ADCS1c	ADCS - Normal mode	The ADCS shall provide an attitude control accuracy of at least 26.9 [arcsec] per axis	Yes	-	Yes	-
ADCS1d	ADCS - Normal mode	The ADCS shall provide an attitude control range of 28 [deg] of nadir +/- 8 [deg]	Yes	-	Yes	-
ADCS1e1	ADCS - Normal mode	The ADCS shall maintain a maximum jitter of 0.0087" over $1.64 \cdot 10^{-4}$ [s] in x-direction	Yes	-	Yes	-
ADCS1e2	ADCS - Normal mode	The ADCS shall maintain a maximum jitter of 0.0033" over $6.25 \cdot 10^{-5}$ [s] in y-direction	Yes	-	Yes	-
ADCSEa	ADCS - Eclipse mode	The ADCS shall provide the same attitude requirements during a solar eclipse	Yes	-	Yes	-
ADCSCSa	ADCS - Contingency/Safe mode	The ADCS shall have a safe mode	Yes	-	Yes	-
ADCS4b	ADCS - constraints	The ADCS shall have a minimum lifetime of 5 [yr]	Yes	-	Yes	-
ADCS4d	ADCS - constraints	The ADCS shall have a maximum mass of 26.8 [kg]	37.95 [kg]	-	No	Will be compensated with other systems
ADCS4e	ADCS - constraints	The ADCS shall have a maximum power consumption of 97.8 [W]	Yes	-	Yes	-
GNC1a	GNC	The GNC system shall be able to provide guidance and navigation during formation flying	Yes	-	Yes	-
GNC2a	GNC	The GNC system shall have a minimum reliability of <TBD>	-	-	-	Dropped
GNC2b	GNC	The GNC system shall have a minimum lifetime of 5 years	-	-	yes	-
GNC2c	GNC	The GNC system shall have dimensions <TBD>	-	-	-	Dropped
GNC2d	GNC	The GNC system shall have a maximum mass of <TBD>	-	-	-	Dropped
GNC2e	GNC	The GNC shall determine the velocity of the spacecraft with an accuracy of 1 [cm/s]	1.9 [mm/s]	8.1 [mm/s]	yes	-
GNC2f	GNC	The GNC shall maintain a separation of 200 [m] to 2 [km] between spacecraft within a formation	200 [m] < separation < 2000[m]	0	yes	-
TT&C1a	TT&C	The TT&C system shall be able to process 2.4 Gb/s during observations	Yes	-	Yes	-
TT&C1b	TT&C	The TT&C system shall be able to communicate the data to ground stations with a maximum delay of 10 minutes	15 minutes	-5	No	Not possible due to large data amount
TT&C1c	TT&C	The TT&C system shall be able to transmit data to Earth with a maximum bit error rate of $1e^{-8}$	Yes	-	Yes	-

Code	Requirements				Compliance	
	Item	Requirement	Value	Margin	Compliant	Comment
TT&C1d	TT&C	The TT&C system shall be able to receive uplink commands from the ground station with a data rate of 256 kb/s	Yes	-	Yes	-
TT&C2a	TT&C	The TT&C system shall record housekeeping and position data	5 mb/orbit	-	Yes	-
TT&C3a	TT&C	The TT&C system shall be able to store 50 GB of data	85 [GB]	35 [GB]	Yes	-
TT&C4b	TT&C	The TT&C system shall have a minimum lifetime of 5 years	Yes	-	Yes	-
TT&C4d	TT&C	The TT&C system shall have a maximum mass of 20.2 [kg]	17.3	2.9	Yes	-
TT&C4e	TT&C	The TT&C system shall have a maximum power consumption of 117.4 [W]	265	-157.6	No	Double transmitter costs a lot of power
TT&C4f	TT&C	The TT&C system shall use existing ground stations during operational lifetime	-	-	Yes	-
POWER1a	Power	The power system shall provide a minimum power to the payload of 150 [W] per panel	Yes	-	Yes	-
POWER2b	Power	The power system shall have a minimum lifetime of 5 years	Yes	-	Yes	-
POWER2c	Power	The solar array shall have a maximum dimension of 6.84 [m^2]	4 m^2	2.84 [m^2]	Yes	-
POWER2d	Power	The power system shall have a maximum mass of 121.02 [kg]	43.3 [kg]	77.72 [kg]	Yes	-
POWER2e	Power	The power system shall have a maximum power consumption of 88 [W]	82 [W]	6 [W]	Yes	-
POWERpc	Power	The power system shall be able to shut down power for each component that needs power	Yes	-	Yes	-
TC1a	Thermal control	The thermal control system shall keep all components within operating temperature range during operations.	Yes	-	Yes	-
TC1b	Thermal control	The thermal control system shall keep all components within survival temperature temperature range at all times.	Yes	-	Yes	-
TC2b	Thermal control	The thermal control system shall have a minimum lifetime of 5 years	Yes	-	Yes	-
TC2d	Thermal control	The thermal control system shall have a maximum mass of 12.5 kg	3.7$[kg]$	8.8$[kg]$	Yes	-
TC2e	Thermal control	The thermal control system shall have a maximum power consumption of 97.8 [W]	50$[W]$	47.8$[W]$	Yes	-
STR1a	Structure	The structure shall provide attachment points for all components	Yes	-	Yes	-
STR2a	Structure	The structure shall withstand a comprehensive load factor of 5 during launch	Yes	-	Yes	-

Code	Requirements				Compliance	
	Item	Requirement	Value	Margin	Compliant	Comment
STR2b	Structure	The structure shall withstand a load tensile factor of 3 during launch	Yes	-	Yes	-
STR2c	Structure	The structure shall withstand a side load factor of 0.5 during launch	Yes	-	Yes	-
STR3a	Structure	The structure shall comply with the vibrations of the launcher	-	-	-	Must be tested
STR3b	Structure	The structure shall comply with the acoustic vibrations of the launcher	-	-	-	Must be tested
STR4b	Structure	The structure shall have a minimum lifetime of 5 years	Yes	-	Yes	-
STR5	Structure	The structure shall have dimensions <1.60 x 1.05 x 2.10$[m]$ >	Yes	-	Yes	-
STR6	Structure	The structure shall have a maximum mass of 112.5 [kg]	100$[kg]$	12.5$[kg]$	Yes	-
STR7	Structure	The structure shall have a maximum power consumption of 9.8 [W]	Yes	-	Yes	-
STR8	Structure	The solar panels shall be able to rotate 150 degrees	Yes	-	Yes	-
PROP1A	Propulsion	3.15 [m/s] of ΔV over the lifetime of the mission shall be provided for the formation keeping due to the disturbances	3.15	-	Yes	-
PROP2A	Propulsion	9.97 [m/s] of ΔV over the lifetime of the mission shall be provided for the differential drag maintenance	9.97	-	Yes	-
PROP3A	Propulsion	99.72 [m/s] of ΔV over the lifetime of the mission shall be provided for the altitude maintenance	99.72	-	Yes	-
PROP5A	Propulsion	20 [m/s] of ΔV over the lifetime of the mission shall be provided for the attitude maintenance	20	-	Yes	-
PROP6A	Propulsion	2.42 [m/s] of ΔV shall be provided for the insertion of the spacecraft into orbit	2.42	-	Yes	-
PROP7A	Propulsion	3-axis control shall have a 2 [s] pulse expulsion of the propellant during ΔV	2	-	Yes	-
PROP8A	Propulsion	Attitude control shall have a 1 [s] pulse expulsion of the propellant during ΔV	1	-	Yes	-
PROP9A	Propulsion	The propulsion system shall have a minimum lifetime of 5 years	5	-	-	Need to be tested
PROP10A	Propulsion	The orbit control thrusters' reaction force shall act through the center of gravity of the satellite	Yes	-	Yes	-
PROP11A	Propulsion	The attitude thrusters shall provide 3 DOFs to a satellite's attitude control	Yes	-	Yes	-
PROP12A	Propulsion	The propulsion system's attitude and orbit control thrusters shall have a maximum impulse of 213 [s]	213	-	Yes	-
PROP12B	Propulsion	The propulsion system shall use off the shelf components and have minimum modifications	Yes	-	Yes	-

Code	Requirements				Compliance	
	Item	Requirement	Value	Margin	Compliant	Comment
PROP13A	Propulsion	The de-orbiting phase shall not take longer than 25 years	25	14.9	Yes	-
LVa	Launch vehicle	The launch vehicle shall be able to reach an altitude of 516 [km]	Yes	-	Yes	-
LVb	Launch vehicle	The launch vehicle shall be able to reach an inclination of 64.3 [deg]	Yes	-	Yes	-
LVc	Launch vehicle	The launch vehicle shall reach its target orbit with a payload mass consisting of 5 pairs of satellites and a module	Yes	-	Yes	-
LVd	Launch vehicle	The launch vehicle shall provide a volume for at least 5 pairs of satellites and a module	Yes	-	Yes	-
LVe	Launch vehicle	The launch vehicle shall provide protection of the spacecrafts against external environment during the launch phase	Yes	-	Yes	-
OIMa	Launch vehicle	The OIM shall provide multistage orbital injection of the satellite pairs	Yes	-	Yes	-
OIMb	Launch vehicle	The OIM shall provide an end-of-life maneuver	Yes	-	Yes	-
OIMc	Launch vehicle	The OIM shall fit in the fairing of the Soyuz 2-1A/Fregat launcher	Yes	-	Yes	-
OIMd	Launch vehicle	The OIM shall provide a structural support for the satellites	Yes	-	Yes	-
OIMPROPa	Launch vehicle	The OIM's propulsion subsystem shall provide at least 5 pulses	Yes	-	Yes	-
OIMPROPb	Launch vehicle	The OIM's propulsion subsystem shall provide a maximal burn time of 60 [s]	Yes	-	Yes	-
OIMPROPc	Launch vehicle	The OIM's propulsion subsystem shall provide a delta V of 166 [m/s] for each stage	Yes	-	Yes	-
OIMPROPd	Launch vehicle	The OIM's propulsion subsystem shall provide a delta V of 10 [m/s] for the de-orbit phase	Yes	-	Yes	-
OIMPROPe	Launch vehicle	The OIM's propulsion subsystem shall provide a fuel storage system	Yes	-	Yes	-
OIMSTRUCTa	Launch vehicle	The OIM's structural subsystem shall be able to withstand the loads during the launch phase	Yes	-	Yes	-
OIMSTRUCTb	Launch vehicle	The OIM's structural subsystem shall have a diameter smaller than 930 [mm]	Yes	-	Yes	-
OIMSTRUCTc	Launch vehicle	The OIM's structural subsystem shall be lighter than 200 [kg]	Yes	-	Yes	-

Appendix D

Functional Flow Block Diagram

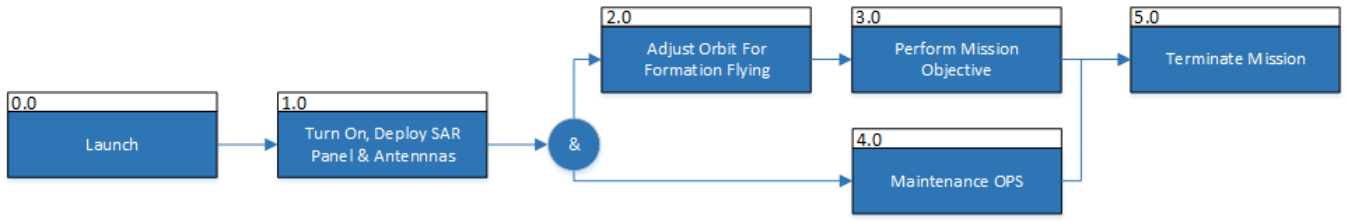

Figure D.1: Top Level Mission FFBD

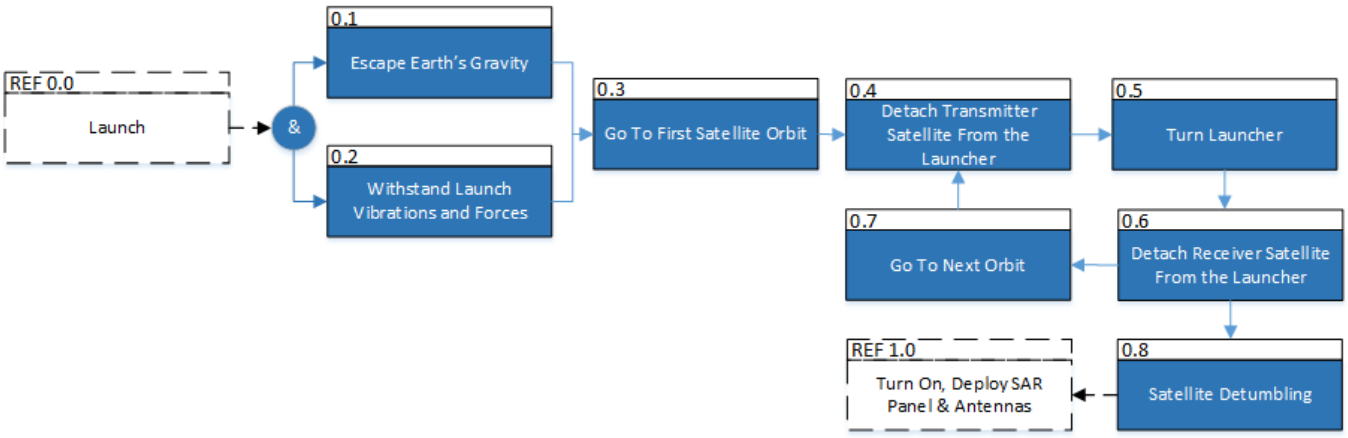

Figure D.2: Second Level Launch FFBD

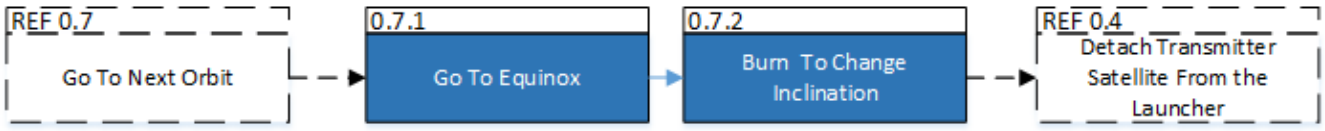

Figure D.3: Third Level Launch FFBD

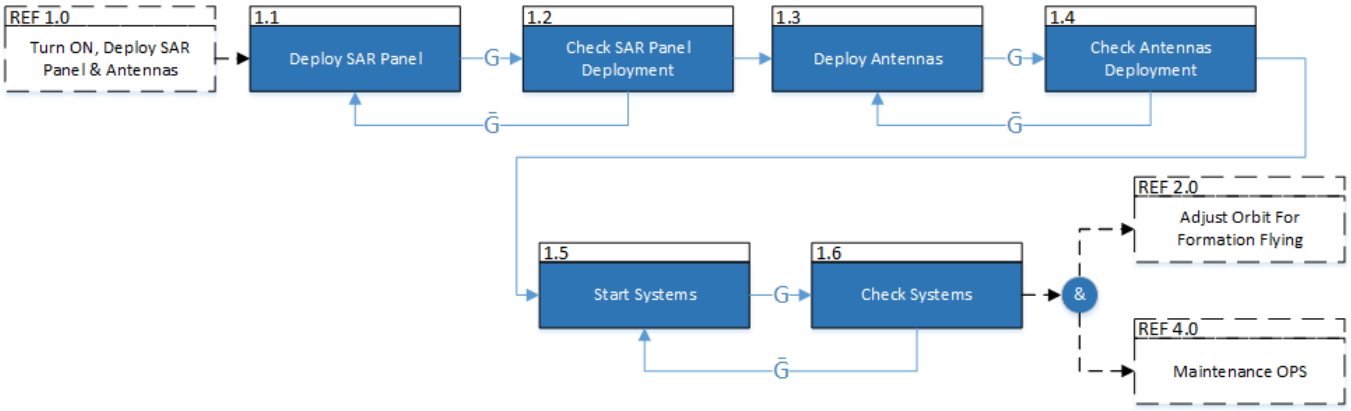

Figure D.4: Second Level Turn On FFBD

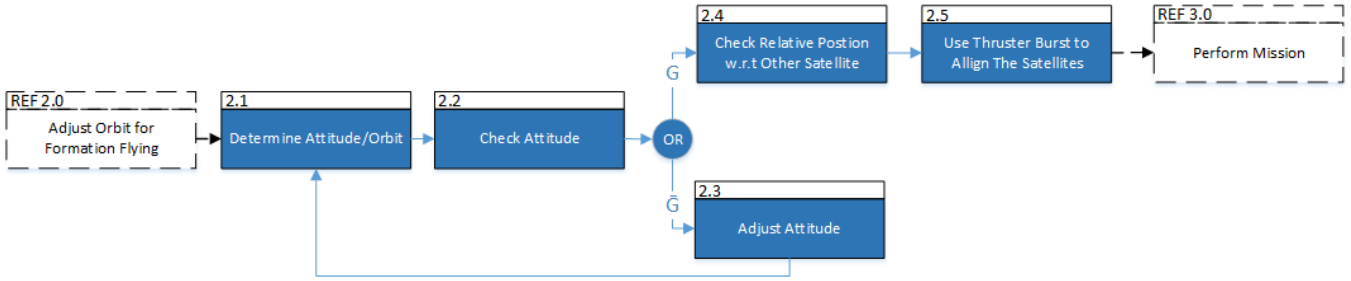

Figure D.5: Second Level Formation Flying FFBD

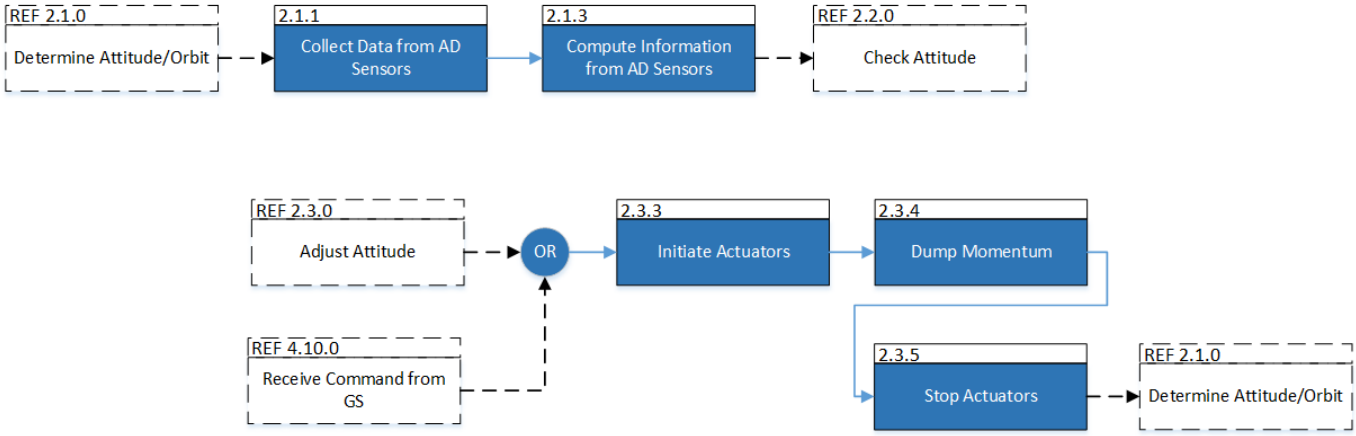

Figure D.6: Third Level Determine Attitude/Orbit and Adjust Attitude FFBD

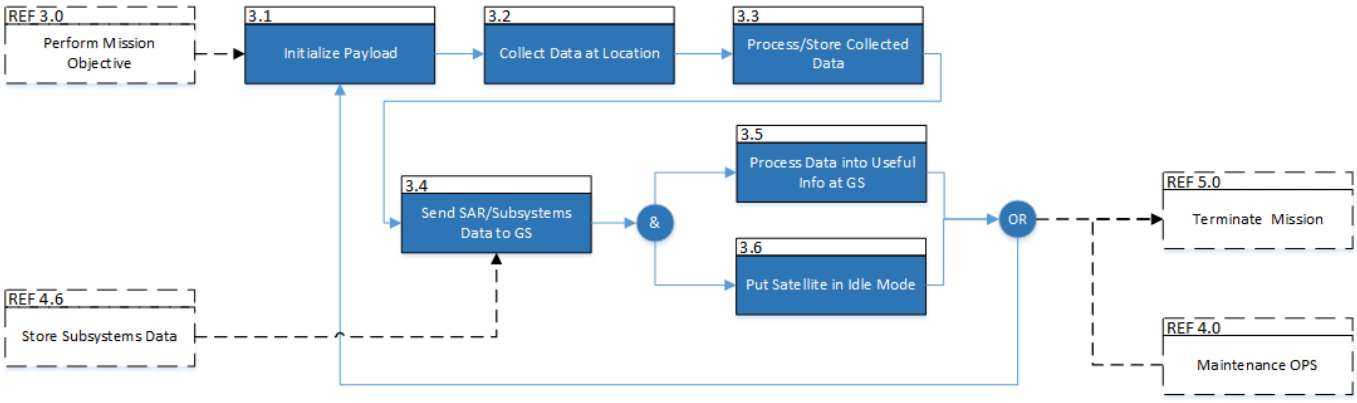

Figure D.7: Second Level Perform Mission FFBD

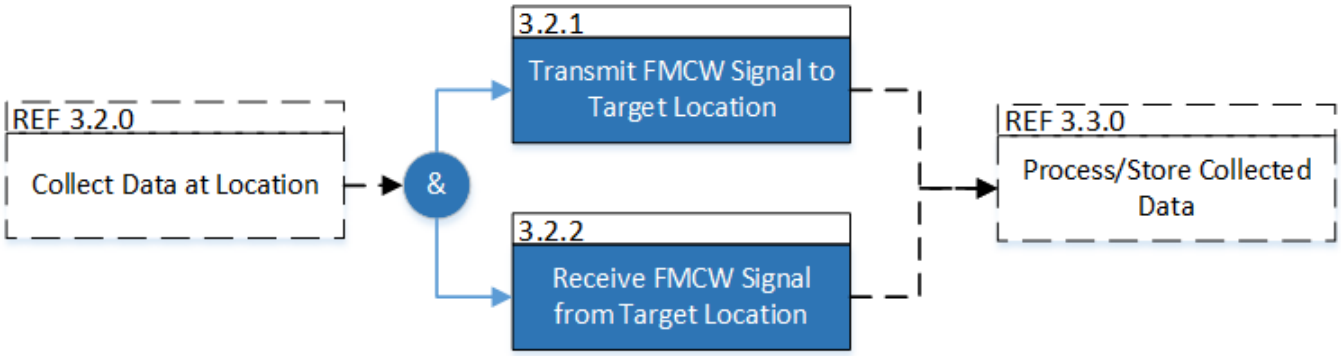

Figure D.8: Third Level Collect Data at Location FFBD

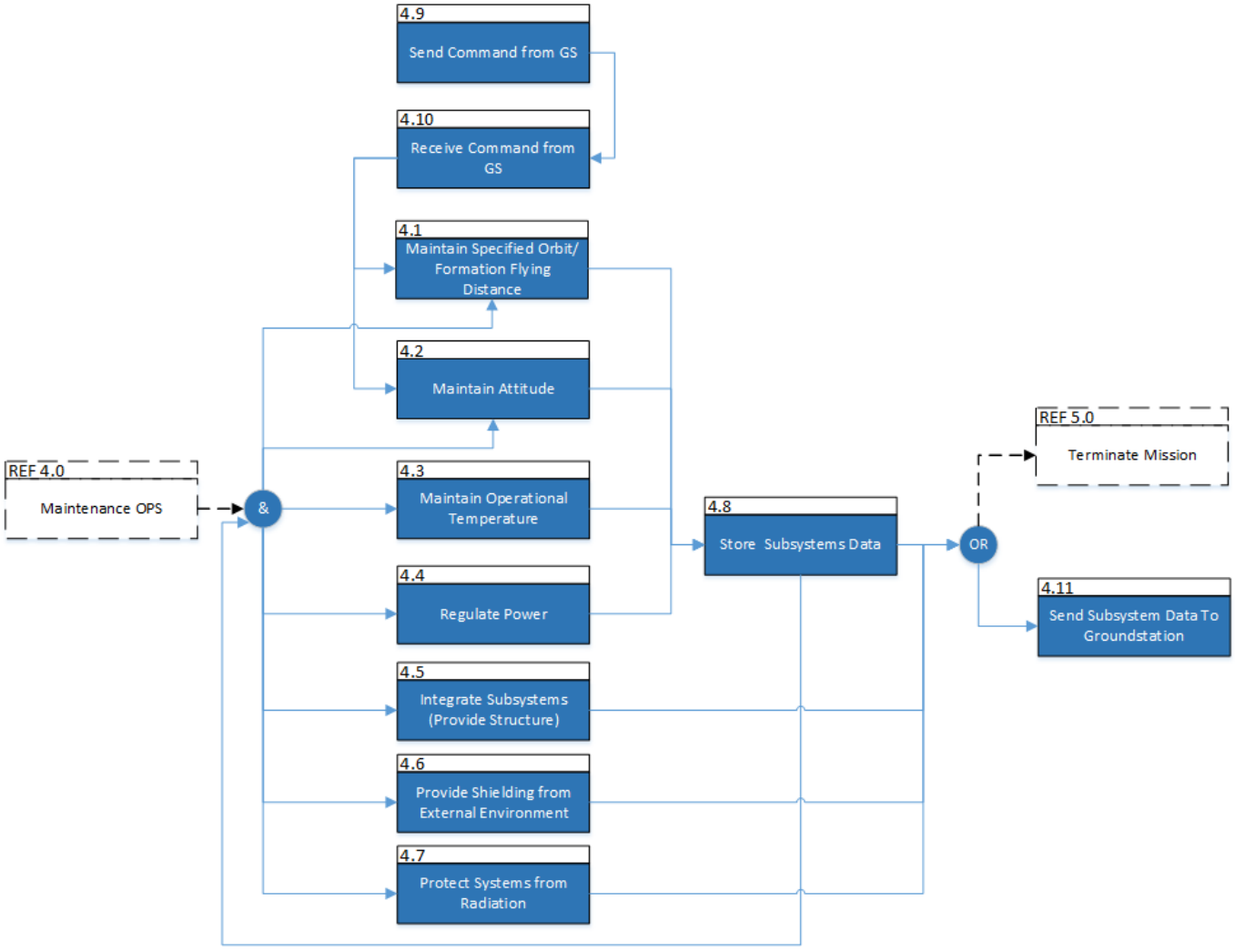

Figure D.9: Second Level Maintenance Ops FFBD

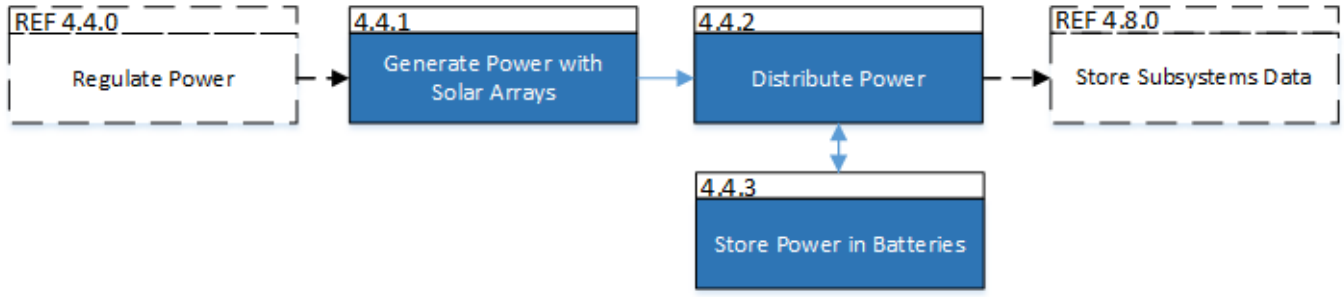

Figure D.10: Third Level Regulate Power FFBD

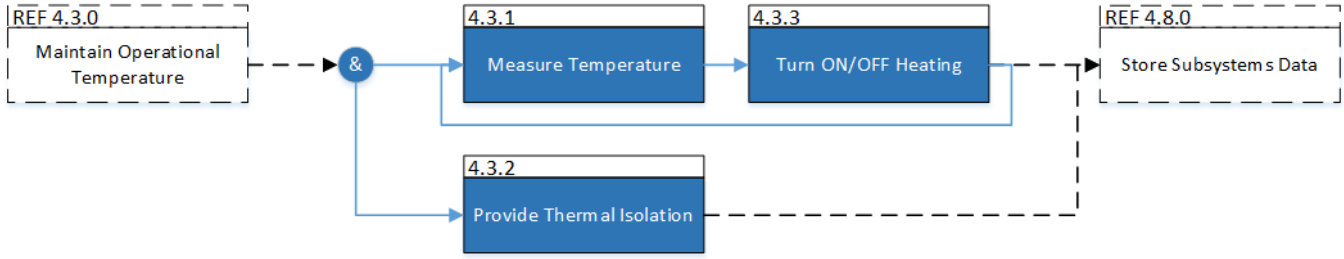

Figure D.11: Third Level Maintain Operational Temperature FFBD

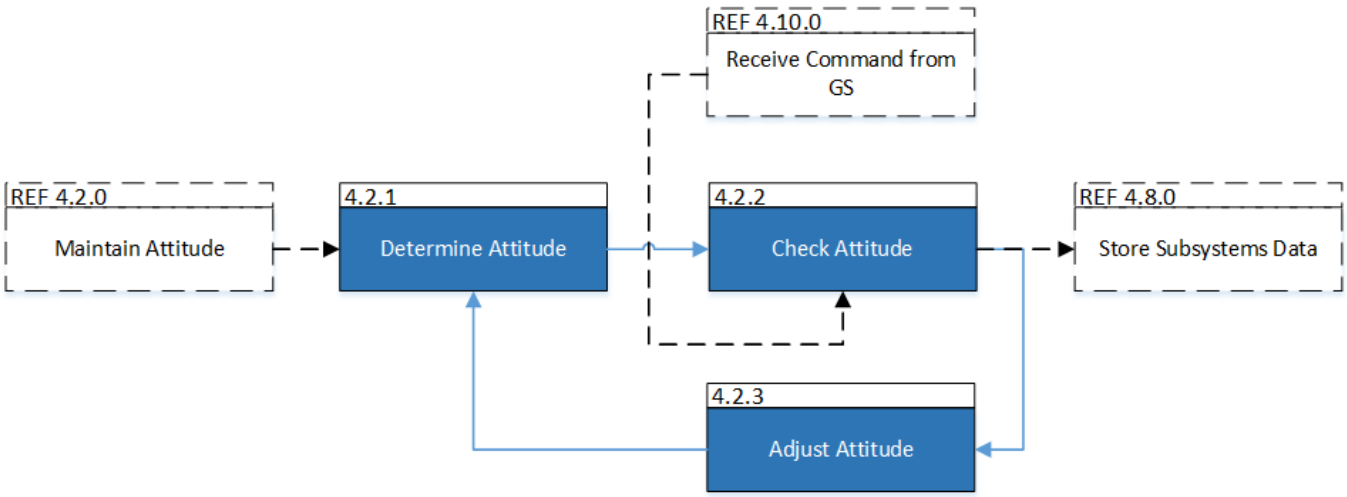

Figure D.12: Third Level Maintain Attitude FFBD

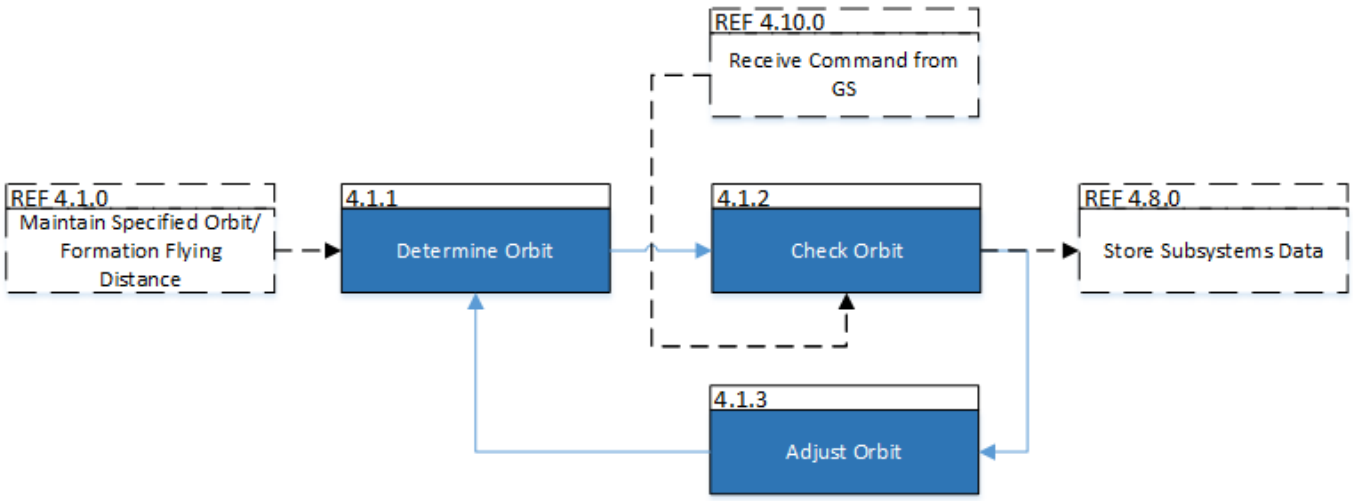

Figure D.13: Third Level Maintain Specified Orbit/Formation Flying Distance FFBD

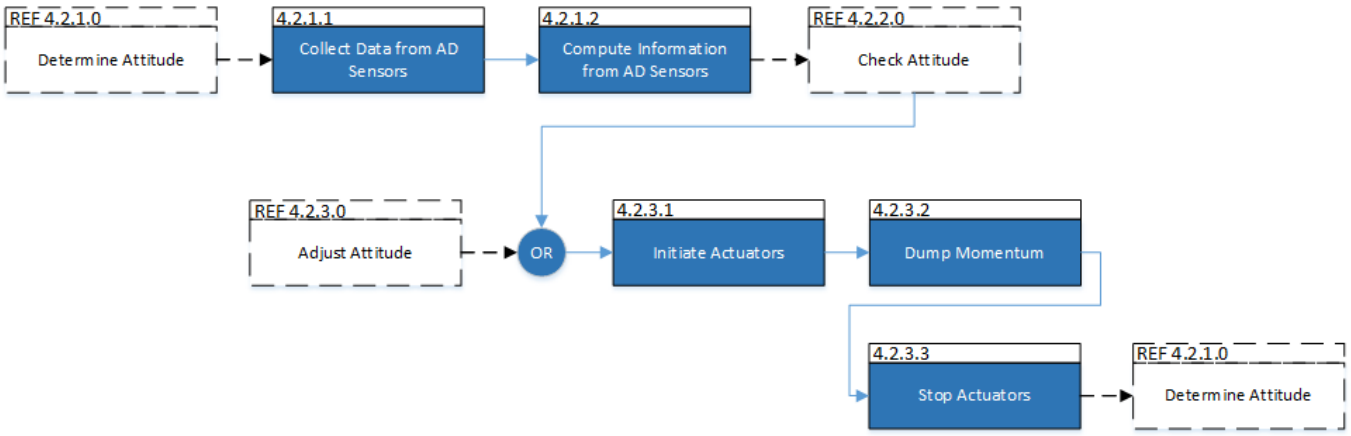

Figure D.14: Fourth Level Determine Attitude and Adjust Attitude FFBD

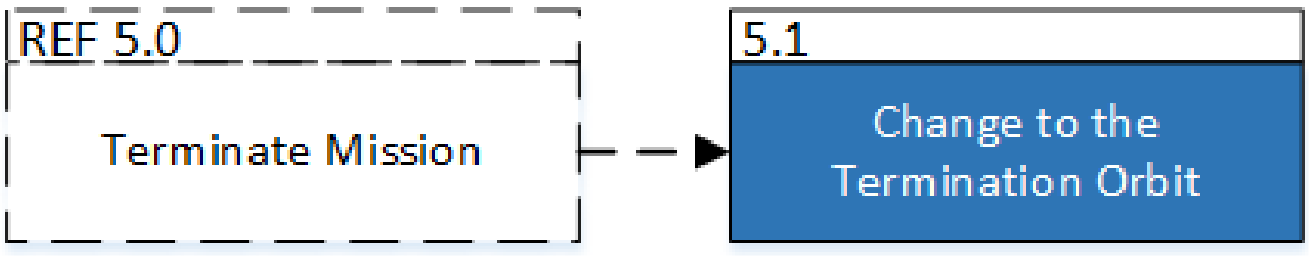

Figure D.15: Second Level Terminate Mission FFBD

Appendix E

Project Gantt Chart

The next page contains the Gantt chart estimating the amount of time spent in each main phase of the design and mission after the end of the DSE project. Furthermore, an estimation is made on the amount of time spent for each sub-phase. More details may be found in chapter 16.

ID	WBS	Task Name	Duration	Start	Finish
1	**1**	**Develop Business**	**26 wks**	**Sat 21-6-14**	**Thu 18-12-14**
2	1.1	Write Business Pla	4 wks	Sat 21-6-14	Thu 17-7-14
3	1.2	Setup Financials	1 wk	Fri 18-7-14	Thu 24-7-14
4	1.3	Find Office	4 wks	Fri 18-7-14	Thu 14-8-14
5	1.4	Acquire Staff	12 wks	Fri 15-8-14	Thu 6-11-14
6	1.5	Contact Investors and Customers	21 wks	Fri 25-7-14	Thu 18-12-14
7	1.6	Contact Manufacturers	21 wks	Fri 25-7-14	Thu 18-12-14
8	**2**	**Research**	**52 wks**	**Fri 19-12-14**	**Thu 17-12-15**
9	2.1	Verify Previous Work	12 wks	Fri 19-12-14	Thu 12-3-15
10	2.2	Finish Full Detailed Design	25 wks	Fri 13-3-15	Thu 3-9-15
11	2.3	Create Drawings for Production	15 wks	Fri 4-9-15	Thu 17-12-15
12	**3**	**On-Ground Validation**	**26 wks**	**Fri 18-12-15**	**Thu 16-6-16**
13	3.1	Create Test Plan	8 wks	Fri 18-12-15	Thu 11-2-16
14	3.2	Find Test Facilities	6 wks	Fri 12-2-16	Thu 24-3-16
15	3.3	Validation	12 wks	Fri 25-3-16	Thu 16-6-16
16	**4**	**Production and Launch**	**160 wks**	**Fri 17-6-16**	**Thu 11-7-19**
17	4.1	Set up Production Plan	10 wks	Fri 17-6-16	Thu 25-8-16
18	4.2	Buy Parts	52 wks	Fri 26-8-16	Thu 24-8-17
19	4.3	Line Production	76 wks	Fri 25-8-17	Thu 7-2-19
20	4.4	Production Testing	12 wks	Fri 8-2-19	Thu 2-5-19
21	4.5	Shipping to Launch Site	4 wks	Fri 3-5-19	Thu 30-5-19
22	4.6	Combining with Launcher	5 wks	Fri 31-5-19	Thu 4-7-19
23	4.7	Launch	1 wk	Fri 5-7-19	Thu 11-7-19
24	**5**	**On-Orbit Validation**	**5 wks**	**Fri 12-7-19**	**Thu 15-8-19**
25	**6**	**Perform Mission Objectives**	**260 wks**	**Fri 16-8-19**	**Thu 8-8-24**
26	**7**	**End-of-Life and Decommissioning**	**4 wks**	**Fri 9-8-24**	**Thu 5-9-24**

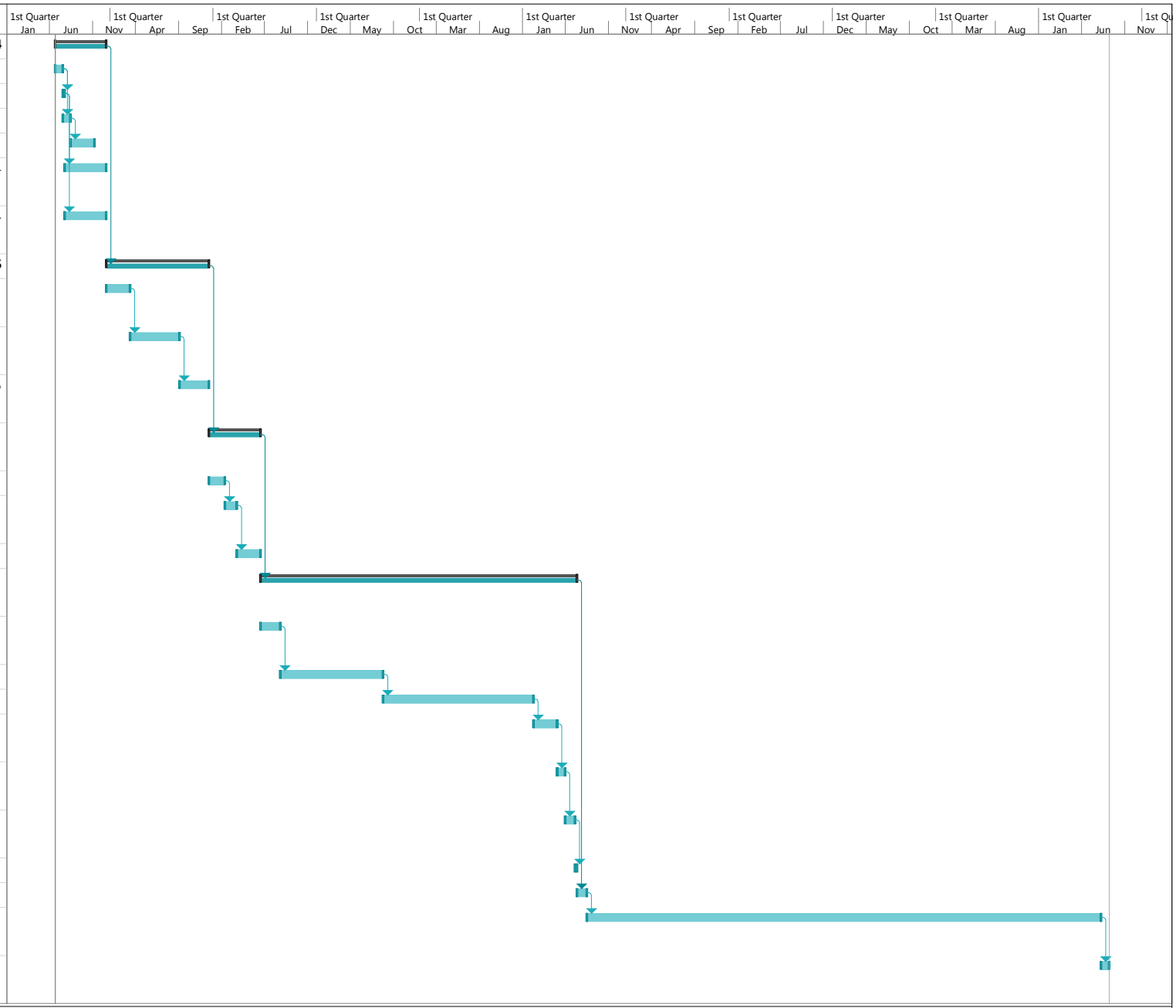

Project: gantt
Date: Sun 22-6-14

Task	Project Summary	Manual Task	Start-only	Deadline
Split	Inactive Task	Duration-only	Finish-only	Progress
Milestone	Inactive Milestone	Manual Summary Rollup	External Tasks	Manual Progress
Summary	Inactive Summary	Manual Summary	External Milestone	

Appendix F

Authors

Section	Author
Summary	Boris, Tom
Introduction	Stefan, Corné
1.1, 1.4	Stefan
1.2, 1.3	Tim
2.1-2.9	Tom
3.1 - 3.3	Thijs
3.1	Tom
4.1, 4.2	Stefan
4.3	Tim
5.1 - 5.3	David
6.1 - 6.6	Stefan
7.1 - 7.9	Antanas
8.1 - 8.8	David, Dimitrije
9.1 - 9.4, 9.7	Thijs
9.5, 9.6, 9.8	Corné
10.1 - 10.6	Boris
11.1 - 11.6	Tim
12.1 - 12.7	Boris
13.1 - 13.4	Tim, Tom
14.1 - 14.5	Corné, Tim
15.1 - 15.3	Stefan, Tom
16	Stefan
17.1, 17.2	Thijs
Appendix A, B, D	Antanas
Appendix C	Tim
Appendix E	Stefan
Catia Drawings	Antanas